NANYANG TECHNOLOGICAL UNIVERSITY

Superabsorbent Cryogels Decorated with Silver Nanoparticles as a Novel Technology for Emergency Point-of-Use Water Treatment

Loo Siew Leng

School of Civil and Environmental Engineering

2016

Superabsorbent Cryogels Decorated with Silver Nanoparticles as a Novel Technology for Emergency Point-of-Use Water Treatment

Loo Siew Leng

School of Civil and Environmental Engineering

Report submitted to
Nanyang Technological University
in partial fulfillment of the requirements for the degree of
Doctor of Philosophy (Environmental Engineering)

2016

To my dearest father

ABSTRACT

There has been an increase in the frequency and intensity of global natural disasters in recent decades. Contaminated water is a major problem in the aftermath of natural disasters. Providing potable water to the affected population (AP) is one of the first priorities after a disaster. However, the process in providing potable water to the AP is often constrained by the absence of an adequate power supply and limited means of transportation. As such, compact and easily-deployable emergency water technologies with simple and relatively low-energy operation are desirable. The aim of this research was to develop a novel approach for point-of-use (POU) water treatment through the fabrication of hydrogel materials.

Hydrogels offer promise for providing potable water in disaster-relief applications because they are capable of absorbing a large quantity of water that subsequently can be released by the application of pressure, temperature change, or other external stimuli. However, their application is limited by their inferior swelling and mechanical properties. Macroporous cryogels, which are formed by conducting a polymerization reaction in a semifrozen system in which the ice crystals (for aqueous systems) act as the porogens, display exceptional mechanical and swelling properties in comparison to conventional hydrogels. These cryogels can be further functionalized with silver nanoparticles (AgNPs) to impart antimicrobial properties. Inspired by the remarkable mechanical and swelling-deswelling properties of cryogels, a novel approach was proposed in which the cryogels can be used as a sorbent to treat water. The method developed in this research offers the simplicity of allowing the cryogel to swell in contaminated water after which the treated water can be recovered by a simple squeezing step. By using the proposed approach, the cryogels are envisioned to remove particulates via size exclusion, and inactivate bacteria through the action of AgNPs.

In this study poly(sodium acrylate) (PSA) cryogels with a superfast swelling rate and a high degree of swelling that can withstand large compressive strains were synthesized by conducting copolymerization reactions between *N,N'*-methylenebis(acrylamide) and sodium acrylate under subzero temperature

conditions. It was found that a lower freezing temperature and reduced initial monomer concentrations formed PSA cryogels with smaller but more interconnected pores. A higher initiator concentration in the "freezing before gelation" mode resulted in smaller pores of lower interconnectivity. PSA cryogels with open interconnected pores had both a higher rate and degree of swelling, and also a high elasticity in response to compression. Well-prepared PSA cryogels could undergo twenty swelling/deswelling cycles without showing any deterioration in network integrity. The particulate separation efficiency of PSA cryogels was evaluated by determining the turbidity removal over five operating cycles. The turbidity removal efficiency of the PSA cryogel having the highest swelling degree increased to 90% towards the fifth cycle. The water recovery during the five operating cycles ranged from 71 to 77% under a vacuum suction of 70 kPa (absolute pressure) for one minute. These results suggest that PSA cryogels can be used as integral membranes for turbidity removal.

The PSA cryogels were further functionalized with AgNPs in order to be applied for water disinfection. The properties of the resulting nanocomposites can be substantially different depending on the method used to incorporate the AgNPs into PSA cryogels. Therefore, the effects of three different synthesis approaches on the properties and bactericidal activity of the resulting AgNP-incorporated cryogels prepared were compared: (i) incorporation of pre-synthesized AgNPs during cryogelation, (ii) ice-mediated coating of pre-synthesized AgNPs on pre-formed PSA cryogels, and (iii) *in situ* reduction of PSA cryogels loaded with Ag^+ were compared. AgNP-incorporated cryogels prepared using the three different synthesis approaches resulted in distinctly different spatial distribution of the AgNPs i.e., only on the pore surface or embedded throughout the polymer matrix or a mixture of both. Furthermore, the AgNP-incorporated cryogels prepared via the different methods have varying AgNP size, pore morphology, swelling and mechanical behavior. The three types of cryogel nanocomposites were found to be effective in disinfecting *E. coli* to different extents. Specifically, synthesis routes that formed more AgNPs on the pore surface of the cryogels display enhanced bactericidal

efficacy that underscores the importance of considering the location of the AgNPs in the design of effective bactericidal materials.

The intermatrix synthesis method was employed to prepare PSA cryogels decorated with AgNPs (or PSA/AgNP cryogels) because of the ease and scalability of the method. Most importantly, this method forms AgNPs that are mainly located on the pore surface that leads to excellent bactericidal activity. Indeed, the as-prepared PSA/AgNP cryogels could achieve over 5-log reduction of viable bacteria with minimal Ag release (< 100 μg/L). In addition, the cryogels are also effective in disinfecting natural water samples whereby over 2 logs reduction could be achieved. They were highly reusable since there was no significant difference in the disinfection efficacies over five cycles of operation and they can be repeatedly compressed for over 1000 cycles.

The PSA/AgNP cryogels were also found to display rapid water disinfection whereby close to 3 logs of bacteria were inactivated immediately during a 15-s contact time. Increasing the contact time to 5 min allows irreversible inactivation of close to 6 logs of bacteria. Direct contact between the PSA/AgNP cryogel interface and the bacterial cells is required to effect disinfection. Specifically, the disinfection efficacy is closely correlated to the cell-bound Ag concentration, which constitutes >90% of the Ag released. Cells exposed to the PSA/AgNP cryogels show a significant depletion of intracellular adenosine triphosphate (ATP) content and cell-membrane lesions. A positive ROS (reactive oxygen species) scavenging test and enhanced level of TBARS (thiobarbituric acid reactive substances) in exposed cells implicate the occurrence of cell-membrane peroxidation mediated by ROS. Significantly, bacterial cells exposed to PSA/Ag^+ cryogels did not show any cell-membrane damage even though the former had a higher cell-bound Ag concentration than that of the PSA/AgNP cryogels, thus indicating the differential action of Ag^+ and Ag^0. Although both Ag^+ and Ag^0 have a different mode of action, both are involved in the bactericidal mechanism of AgNPs. The rapid disinfection ability of PSA/AgNP cryogels may be attributed to the exposure of a high surface-area of AgNPs to bacteria in the microchannels. In addition, the rapid swelling of

the cryogels provides the driving force for the bacterial cells to approach the AgNPs within a confined environment that ensures effective disinfection.

The effects of isolated environmental constituents – namely, Suwannee River humic acid as a surrogate for dissolved organic matter (DOM) and various electrolytes commonly found in environmental matrices (i.e., Cl^-, HCO_3^-, SO_4^{2-}, Na^+, K^+, Ca^{2+}, Mg^{2+}) – on the properties of PSA/AgNP cryogels were also studied. PSA/AgNP cryogels exposed to solutions of various chemistries show changes in the amount of oxidized Ag species and display some physical transformations in the AgNP morphology. The AgNPs in exposed samples generally have larger mean sizes. In particular, samples exposed to a DOM-containing solution show the formation of fine AgNPs surrounding larger clusters, while those exposed to electrolytes transformed into truncated and hexagonally shaped particles. The presence of DOM and electrolytes generally increased the Ag leaching. However, the biological uptake of Ag species is increased in the presence of DOM, but decreased in the presence of electrolytes. The presence of electrolytes did not result in any significant reduction in the bactericidal activity. Although the initial increase of DOM to 2.5 mg-C/L attenuated the toxicity of AgNP, a further increase in the DOM concentration beyond 5 mg-C/L led to toxicity enhancement. Apparently, the toxicity of AgNPs anchored on cryogels is less sensitive to changes in solution chemistry. As such, this could be a good strategy to preserve their efficacy for disinfection in various solution matrices.

In conclusion, the cryogels synthesized in this research offer excellent potential for applications requiring potable water production in response to emergencies or disasters. Furthermore, these cryogels are lightweight and highly portable allowing them to be easily deployed for emergency response.

ACKNOWLEDGMENTS

Firstly I would like to express my gratitude to my research supervisors, namely Professors Anthony Gordon Fane, Hu Xiao, Lim Teik Thye, and William Bernard Krantz. I appreciate their guidance and encouragement in completing this research. It is an honor to have the opportunity to learn from them.

Next, I thank Prof. Huang Yizhong for his help and entrusting me with his final year project students. I am also grateful to Dr. Adrian Yeo and Dr. Richard Hung for their help and support in this project. Also, I would like to thank my students: Cassandra See, Daren Cheong, Eunice Ho, Fan Hao, Gai Yi, Jessica Oh, Joycelyn Lim, Goh Kwan Chien, Ong Li Ting, Sim Zhi Yang, and Wang Fei for their cooperation, diligence, and enthusiasm during their involvement in this project.

This research would not have been completed without the help rendered by Chew Wang, Han Khiang, Maria Chong, Pearlyn Shee, Ton Ong, and Zan Ong; my sincere thanks go to them for their co-operation and for going the extra mile whenever I needed their help. Next, I would like to thank all my friends from CEE, MSE, and SMTC for their help, support, and camaraderie that have provided me a friendly working environment. A special mention goes to Liao Yuan, Tian Miao, Wong Mee Teng and Wu Bing for their friendship and company that have brought me great joy. I also wish to extend my thanks to Mr. Kong Poh Tah and family for their warmth and hospitality throughout my stay with them.

I would like to express my deep appreciation to my boyfriend, Kwok Yii for being a loyal companion, and for his genuine love and care for me. Most importantly, his optimism and unwavering support have given me the strength to keep going during tough times. Above all, I would like to extend my heartiest gratitude to my father, who is the inspiration and motivation to complete this thesis. My mere expression of thanks does not suffice for the unconditional love and unequivocal support he has given me — I would like to dedicate this thesis especially to him.

LIST OF PUBLICATIONS

A. Journal articles

1. **S.-L. Loo**, W.B. Krantz, X. Hu, A.G. Fane, T.-T. Lim, 2016. Impact of solution chemistry on the properties and bactericidal activity of silver nanoparticles decorated on superabsorbent cryogels, **Journal of Colloids and Interface Science**, 461 104-113.
2. **S.-L. Loo**, W.B. Krantz, A.G. Fane, X. Hu, T.-T. Lim, 2015. Effect of synthesis routes on the properties and bactericidal activity of cryogels incorporated with silver nanoparticles, **RSC Advances**, 5 44626-44635.
3. **S.-L. Loo**, W.B. Krantz, A.G. Fane, Y. Gao, T.-T. Lim, X. Hu, 2015. Bactericidal Mechanisms Revealed for Rapid Water Disinfection by Superabsorbent Cryogels Decorated with Silver Nanoparticles, **Environmental Science and Technology**, 49 (4) 2310–2318.
4. **S.-L. Loo**, T.-T. Lim, W.B. Krantz, A.G. Fane, X. Hu, 2015. Potential evaluation and perspectives on using sponge-like superabsorbent cryogels for onsite water treatment in emergencies, **Desalination and Water Treatment**, 53 (6) 1506-1515.
5. **S.-L. Loo**, A.G. Fane, T.-T. Lim, W.B. Krantz, Y.-N. Liang, X. Liu, X. Hu, 2013. Superabsorbent cryogels decorated with silver nanoparticles as a novel water technology for point-of-use disinfection, **Environmental Science and Technology**, 47 (16) 9363-9371.
6. **S.-L. Loo**, W.B. Krantz, T.-T. Lim, A.G. Fane, X. Hu, 2013. Design and synthesis of ice-templated PSA cryogels for water purification: Towards tailored morphology and properties, **Soft Matter**, 9 224-234.
7. **S.-L. Loo**, A.G. Fane, W.B. Krantz, T.-T. Lim, 2012. Emergency water supply: A review of potential technologies and selection criteria, **Water Research**, 46 (10) 3125-3151.
8. T.-H. Chong, **S.-L. Loo**, A.G. Fane, W.B. Krantz, 2015. Energy-Efficient Reverse Osmosis Desalination: Effect of Retentate Recycle and Pump and Energy Recovery Device Efficiencies, **Desalination**, 366 15-31.
9. T.-H. Chong, **S.-L. Loo**, W.B. Krantz, 2015. Energy-efficient reverse osmosis desalination process, **Journal of Membrane Science**, 473 177-188.
10. Y. Cai, W. Shen, **S.-L. Loo**, W.B. Krantz, R. Wang, A.G. Fane, X. Hu, 2013. Towards temperature driven forward osmosis using semi-IPNs as reversible draw agents, **Water Research**, 47 (11) 3773-3781.

B. Conference contributions

1. **S.-L. Loo**, A.G. Fane, T.-T. Lim, W.B. Krantz, X. Hu**,** Superabsorbent cryogels decorated with silver nanoparticles for emergency point-of-use water disinfection, Poster Presentation, **International Conference on Materials for Advanced Technologies (ICMAT)**, Suntec Singapore, 28 June to 3 July 2015, Singapore.
2. **S.-L. Loo**, A.G. Fane, T.-T. Lim, W.B. Krantz, X. Hu, Emergency potable-water disinfection using sponge-like superabsorbent cryogels, accepted for Platform Presentation (Paper ID: 2477437), **IWA World Water Congress**, 21-26 September 2014, Lisbon, Portugal.
3. **S.-L. Loo**, A.G. Fane, T.-T. Lim, W.B. Krantz, X. Hu, Development of novel superabsorbent cryogels for emergency potable-water production, Poster Presentation, **Water Convention 2014, Singapore International Water Week**, 1-5 June 2014, Singapore.
4. **S.-L. Loo**, A.G. Fane, T.-T. Lim, W.B. Krantz, X. Hu, Cryogel/silver nanoparticle hybrid for rapid disinfection of drinking water: Materials, mechanisms, and applications, Oral Presentation, **MRS Spring Meeting**, 21-25 April 2014, San Franscisco, California, USA.
5. **S.-L. Loo**, A.G. Fane, T.-T. Lim, W.B. Krantz, X. Hu, Rapid water disinfection using silver nanoparticles decorated cryogels: A mechanistic study**,** Poster Presentation, **MRS Spring Meeting**, 21-25 April 2014, San Franscisco, California, USA.
6. **S.-L. Loo**, A.G. Fane, T.-T. Lim, W.B. Krantz, X. Hu, Drinking-water disinfection in emergencies using superabsorbent cryogel membranes incorporated with silver nanoparticles, Oral Presentation, **International Membrane Science and Technology Conference 2013**, 25th to 29th November 2013, Melbourne, Australia.
7. X. Hu, **S.-L. Loo**, A.G. Fane, T.-T. Lim, W.B. Krantz, Superabsorbent cryogels decorated with silver nanoparticles for point-of-use water disinfection in disaster relief, Oral Presentation, **ACS Fall Meeting 2013**, 8th to 12th September 2013, Indianapolis, USA.
8. **S.-L. Loo**, A.G. Fane, T.-T. Lim, W.B. Krantz, X. Hu, Integral membranes from superabsorbent cryogels decorated with silver nanoparticles for point-of-use water disinfection in disaster relief, Oral Presentation, **Engineering With Membranes 2013: Towards a Sustainable Future**, 3rd to 9th September 2013, Saint-Pierre-d'Oleron, France.
9. **S.-L. Loo**, W.B. Krantz, T.-T. Lim, A.G. Fane, X. Hu, Preparation of superabsorbent cryogels with tailored properties as integral membranes for emergency water treatment, Poster Presentation, **Engineering With Membranes 2013: Towards a Sustainable Future**, 3rd to 9th September 2013, Saint-Pierre-d'Oleron, France.

10. **S.-L. Loo**, W.B. Krantz, T.-T. Lim, A.G. Fane, X. Hu, Novel superabsorbent cryogels for potable-water production in emergencies, Oral Presentation, **4th International Conference for Young Chemists**, 30th January to 1st February 2013, Penang, Malaysia.
11. **S.-L. Loo**, A.G. Fane, W.B. Krantz, T.-T. Lim, X. Hu, Drinking Water Supply for Developing Communities: Challenges, Technologies, and Selection Criteria, Oral Presentation, **2nd EE2 Seminar: Water and Environment in Asia's Developing Countries, Singapore International Water Week**, 1st July 2012, Singapore.
12. **S.-L. Loo**, A.G. Fane, W.B. Krantz, T.-T. Lim, Decision Tree for Water Technology Selection in Difficult Circumstances, Oral Presentation, Workshop II: Water for Difficult Circumstances: Building Capacities and Capabilities, **International Symposium and Workshop on Membrane Science and Technology**, 23rd Aug 2011, Singapore.
13. W.B. Krantz, T.-H. Chong, **S.-L. Loo**, Energy-efficient reverse osmosis desalination process, Oral Presentation, **AICHE 2014 Annual Meeting**, 16-21 November 2014, Atlanta, USA.
14. W.B. Krantz, Chong, T.H., **S.-L. Loo**, Novel Energy-Efficient Reverse Osmosis Desalination Process, Oral Presentation, **International Desalination Confererence**, 30th August - 4th September 2015, San Diego, California, USA.

C. Intellectual property

1. X. Hu, **S.-L. Loo**, A.G. Fane, T.-T. Lim, W.B. Krantz, Antibacterial Cryogel And Porous Hydrogel, Their Preparation Method, And Their Use For Disinfecting Water. PCT Application No: PCT/SG2014/000273. International Filing Date: 12 June 2014.
2. T.-H. Chong, W.B. Krantz, **S.-L. Loo**, Energy-efficient reverse osmosis process, US Provisional Patent (Application number 61/972,718; filed 31st March 2014). NTU Ref: PAT/059/14/14/US PRV.

TABLE OF CONTENTS

LIST OF TABLES

LIST OF FIGURES

LIST OF ABBREVIATIONS

2',7'-dichlorodihydrofluorescein	DCFH
2',7'-dichlorodihydrofluorescein diacetate	DCFH-DA
2',7'-dichlorofluorescein	DCF
2-acrylamido-2-methylpropanesulfonic acid	AMPS
Acrylamide	AAM
Acrylic acid	AA
Activated carbon	AC
Adenosine triphosphate	ATP
Affected population	AP
Ammonium persulphate	APS
Atomic force microscope	AFM
Bacillus subtilis	*B. subtilis*
Biosand filter	BSF
Ceramic filter	CF
Confocal laser scanning microscopy/microscope	CLSM
Critical concentration of gelation	CCG
Cryo scanning electron microscopy/microscope	Cryo-SEM
Deoxyribose nucleic acid	DNA
Dimethylacrylamide	DMA
Dimethylsulfoxide	DMSO
Disinfection byproduct	DBP
Dissolved organic carbon	DOC
Dissolved organic matter	DOM
Environmental scanning electron microscopy/microscope	ESEM
Fecal coliform	FC
Field-emission scanning electron microscopy/microscope	FESEM
Fluorescein isothiocyanate	FITC
Forward osmosis	FO
Granulated activated carbon	GAC
Graphene oxide	GO
Ice-mediated coating	IMC
Ice-segregation-induced-self-assembly	ISISA
Intermatrix synthesis	IMS
Log removal value	LRV
Magnetic resonance imaging	MRI
Membrane distillation	MD
Microfiltration	MF
Multi-walled carbon nanotube	MWCNT
N-(3-dimethylaminopropyl)-N'-ethylcarbodiimide hydrochloride	EDC-HCl
N,N,N',N'-tetramethylethylenediamine	TEMED
N,N'-methylenebis(acrylamide)	MBA
N-acetylcysteine	NAC
Nanofiltration	NF
Nanoparticle incorporation	NI
Natural organic matter	NOM

Nephelometric Turbidity Unit	NTU
n-isopropylacrylamide	NIPAM
Nuclear magnetic resonance	NMR
Outer membrane protein	Omp
Phosphate buffered saline	PBS
Photovoltaic	PV
Point-of-use	POU
Poly(acrylamide)	PAAM
Poly(acrylic acid)	PAA
Poly(ethylene glycol)	PEG
Poly(ethylene terephthalate)	PET
Poly(hydroxymethacrylate)	PHEMA
Poly(*n*-isopropylacrylamide)	PNIPAM
Poly(propylene glycol)	PPG
Poly(sodium acrylate)	PSA
Poly(vinyl alcohol)	PVA
polyunsaturated fatty acid	PUFA
Powdered activated carbon	PAC
Preparation temperature	T_{prep}
Propidium iodide	PI
Reactive oxygen species	ROS
Reverse osmosis	RO
Salmonella typhimurium	*S. Typhimurium*
Scanning electron microscopy/microscope	SEM
Selected area electron diffraction	SAED
Silver nanoparticle	AgNP
Single-walled carbon nanotube	SWCNT
Sodium acrylate	SA
Sodium diisocyanurate	NaDCC
Solar disinfection	SODIS
Staphylococcus aureus	*S. aureus*
Superoxide dismutase	SOD
Suwannee River humic acid	SRHA
Thermotolerant coliforms	TTC
Thiobarbituric acid reactive substances	TBARS
Three-dimensional	3D
Total coliform	TC
Transmembrane pressure	TMP
Transmission electron microscopy/microscope	TEM
Two-dimensional	2D
Two-photon fluorescence microscopy/microscope	TPFM
Ultrafiltration	UF
Ultraviolet	UV
Unfrozen liquid microphase	UFLP
Water technology	WT
X-ray microcomputed tomography	X-ray micro-CT
X-ray photoelectron spectroscopy/spectroscope	XPS

LIST OF SYMBOLS

C	Polymer concentration after gelation
D	Diameter of pore
E	Young's modulus
F	Force per unit cross-sectional area of the undeformed gel
R	Molar gas constant
f_i	Weighting factor for i^{th} water technology
C_o	Initial monomer concentration
h_o	Height of the gel sample during compression
K_f	Cryoscopic constant
m_B	Molality
$m_{de\text{-}swollen}$	Mass of de-swollen gel
m_{dried}	Mass of dried gel
m_o	Mass of dried gel
$m_{swollen}$	Mass of swollen gel
m_t	Mass of swollen gel at time t
v_{eff}	Effective crosslink density of a polymer network
v_{gel}	Volume fraction of polymer in gel
P	Intrusion pressure of liquid mercury
f	Effective charge density
f_{ice}	Volume fraction of ice
r	Radius of swollen gel used for compression tests
S_i	Total weighted score of i^{th} water technology
T_f	Freezing point of a solution
T_f^0	Freezing point of a pure solvent
V_p	Specific pore volume
x_{ij}	Score assigned to the i^{th} water technology for the j^{th} criterion
γ	Surface tension of mercury
χ	Polymer-solvent interaction parameter
Δh	Change in the height of the gel sample during compression tests
ΔH_m	Molar enthalpy of fusion for pure crystallized solvent
ΔT_f	Freezing point depression
θ	Contact angle of mercury with material
λ	Deformation ratio
ρ	Polymer density
$\rho_{cyclohexane}$	Density of cyclohexane

CHAPTER 1 Introduction

1.1 Background

In recent decades, there has been an increase in the frequency and intensity of global natural disasters due to climate change phenomena and a considerable growth of population in regions vulnerable to disaster (McCarthy et al., 2001; EMDAT, 2009). One of the first priorities after a disaster is to provide drinking water of sufficient quantity and quality to the affected population (AP). This along with shelter, medication, and food is crucial to prevent the spread of waterborne diseases due to consumption of unsafe water and as a means for near-term survival (Toole and Waldman, 1990; Clasen and Cairncross, 2004; Frist, 2005).

Treating drinking-water during emergencies is challenging due to inadequate access to infrastructure and variable water quality. Hence, emergency water technologies (WTs) must possess certain characteristics to permit their applications in disaster relief. Emergency WTs should preferably be (i) compact and easy to deploy, (ii) easy to use, (iii) able to produce treated water in good quantity and quality, and (iv) operable without access to energy from the power grid. A judicious choice of the WT to be deployed is crucial because there is no panacea. Hence, there is a need for a decision tool to help in the selection of an appropriate WT in a given situation. This project addresses this need and then focuses on the development of a potential point-of-use (POU) water treatment unit for disaster applications based on novel hydrogel membranes.

Hydrogels are three-dimensional (3D) polymer networks that are capable of absorbing a large amount of water. Hence, they provide a means for absorbing water that subsequently can be released via compression (under high-pressure application), temperature change, or other external stimuli. Hydrogels have been gaining increasing interest for water treatment applications (Höpfner et al., 2010; Li et al., 2011a; 2011b). However, the absorption and mechanical properties of hydrogels need to be improved for practical applications (Calvert, 2009).

It is thought that porous hydrogels can improve the swelling and mechanical properties of conventional hydrogels. Conventional hydrogels swell slowly because the water influx is limited by diffusion through the nonporous gel matrix. The presence of a large number of pores effectively increases the surface/volume ratio and could allow faster water absorption and desorption by osmotically driven bulk flow, which is a much faster process than diffusion (Omidian et al., 2005; Liu et al., 2009a). Various methods have been used to produce macroporous hydrogels such as gas foaming (Kabiri et al., 2003), micro-emulsification (Bennett et al., 1995), phase separation (Bennett et al., 1995), freeze-drying (Deng et al., 2012) and porogen leaching (Kemal et al., 2011). Although these methods improved the swelling properties of hydrogels, the mechanical properties were not significantly enhanced.

Cryogelation is a unique technique used to synthesize macroporous hydrogels having tissue-like elasticity that can withstand extensive deformation without irreversible deformation (Plieva et al., 2008c). This technique is based on the formation of a polymeric network in a semi-frozen system in which solvent crystals act as porogens (Lozinsky, 2002; 2003; 2008). Besides superior mechanical properties, cryogels have been reported to exhibit a superfast swelling rate in comparison to conventional hydrogels (Ozmen and Okay, 2005; Plieva et al., 2006; Dinu et al., 2007; Topuz and Okay, 2009; Orakdogen et al., 2011). Due to their high porosity, most of the absorbed water exists as free water that can be released via manual compression (Plieva et al., 2004; 2005; 2008a; Savina et al., 2007).

Microbial contamination is one of the major contaminants in water after disasters. As such, the cryogels should be further functionalized with antimicrobial agents to ensure that the treated water is microbiologically safe for potable use. Various antimicrobial agents have been developed to combat microbiological contamination. Among them, silver in the form of a nanoscale material has been widely recognized as an excellent antimicrobial agent because of its broad-spectrum antimicrobial activity and low-toxicity to human cells (Balogh et al., 2000; Liu et al., 2012; Alonso et al., 2013). Cryogels can be effective support materials for AgNPs to minimize particle aggregation and loss, whilst allowing maximum accessibility to the bacterial cells because of their interconnected micrometer-sized pores.

Furthermore, the lifespan of the supported AgNPs can be enhanced due to controlled release of dissolved Ag^+ that enables long-term applications. Therefore, cryogels incorporated with AgNPs offer the potential to be developed into efficient, affordable, and energy-efficient point-of-use (POU) devices for water disinfection to increase the availability of clean water, especially in regions without access to improved water or recovering from natural disasters. In addition, these cryogels are lightweight allowing them to be rapidly deployed for emergency drinking water response.

1.2 Motivation and knowledge gap

The motivation and unifying basis for the different projects presented in this thesis was to develop an infrastructure-independent technology to produce potable water in emergencies. Inspired by the remarkable mechanical and swelling-deswelling properties of the cryogels, a novel process, as shown in Fig. 1.1, is proposed in which the cryogels can be used as a sorbent to treat water. The present method offers the simplicity of allowing the cryogel to swell in contaminated water after which the treated water can be recovered by a simple squeezing step. As depicted in Fig. 1.1, the cryogels are designed to remove particulates via size exclusion, and inactivate bacteria through the action of AgNPs.

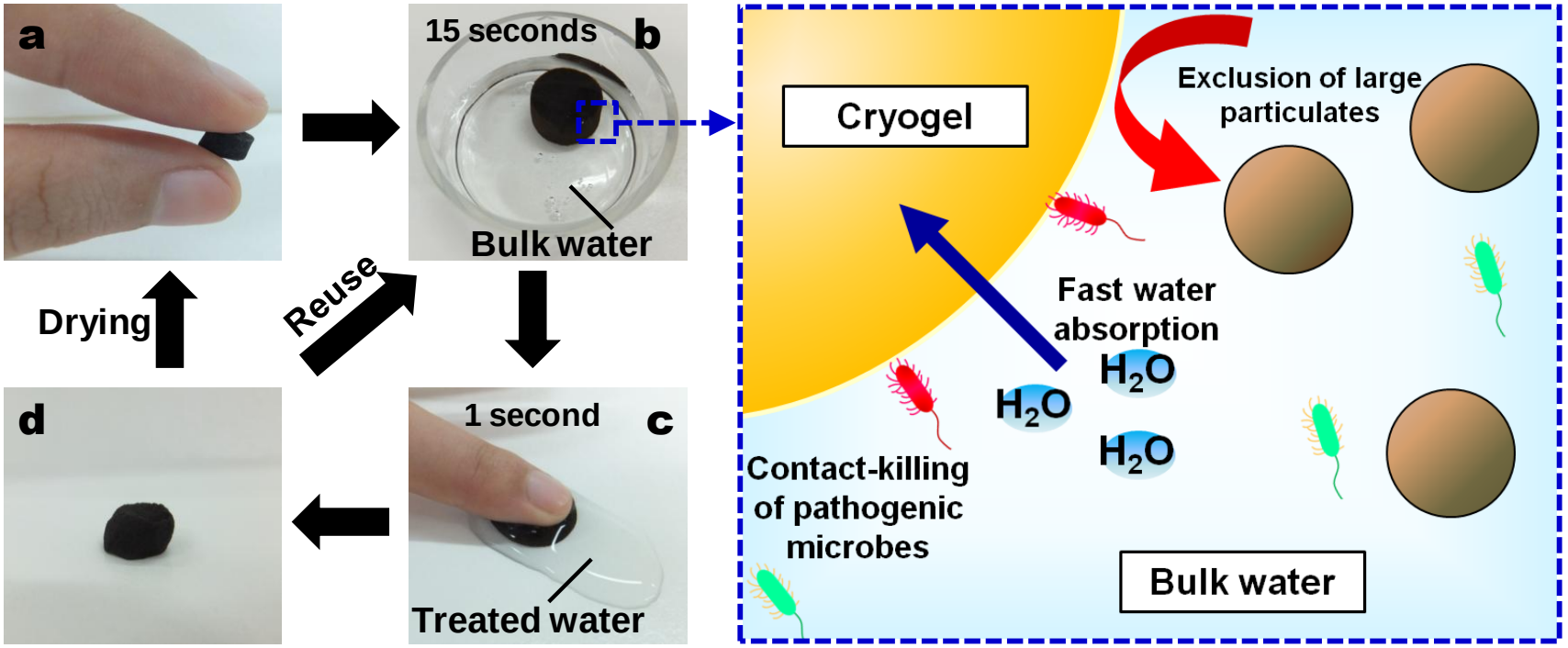

Figure 1.1 Photographs depicting the novel approach of using cryogels for point-of-use water treatment. (a) Dried cryogel, (b) swelling of cryogel in contaminated water, (c) recovery of treated (or squeezed) water via hand compression, and (d) deswollen cryogel that can be reused. The illustration on the right panel depicts the envisioned mechanism by which the cryogels remove particulates and inactivate pathogens.

Since this is the first study to explore the feasibility of using cryogels for emergency water treatment, there is a lack of understanding of the structure-activity relationship for cryogels as well as those incorporated with AgNPs. This understanding will provide insights into structural properties that will lead to desired performance characteristics. For example, there is uncertainty associated with the type of pore structures that will result in robust cryogels with fast and substantial swelling as well as effective particulates removal. As such, this requires a study that correlates the pore structure of the cryogel with its properties and performance. In addition, there is a need to develop design strategies in order to synthesize cryogels with tailored structure and properties. To achieve this, a systematic study that investigates the effects of synthesis conditions such as freezing temperature, initial concentrations of monomer and initiator, and crosslinker ratio needs to be conducted.

A variety of different synthesis methods have been developed to incorporate nanoparticles in polymeric materials (Dallas et al., 2011). However, employing different synthesis methods is anticipated to result in a variation of structures that would affect the performance of the resultant nanocomposites. Therefore, the selection of an appropriate synthesis approach is crucial to fabricate materials with tailored properties to meet the requirements of a particular application. AgNPs-incorporated cryogels prepared via different methods are anticipated to have varying AgNP size, pore morphology, swelling and mechanical behavior. The choice of the optimal synthesis route should also consider other factors such as the ease of synthesis and scalability among others. Therefore, a detailed comparative study of different synthesis routes for preparation of AgNP-incorporated cryogels is required.

The application of AgNP-functionalized activated carbon, ceramic filters, hydrogels, cellulosic papers, polyurethane foams, resins, and rice husks as bioactive components in flow-through or column systems for point-of-use water disinfection have been tested (Jain and Pradeep, 2005; Oyanedel-Craver and Smith, 2007; Gangadharan et al., 2010; Dankovich and Gray, 2011; Alonso et al., 2013; He et al., 2013; Lin et al., 2013). These studies have demonstrated the effectiveness of Ag

nanocomposites in terms of bacterial inactivation but little attention was given to elucidate their bactericidal mechanisms. On the other hand, the bactericidal mechanism of free AgNPs has been studied more intensely, but controversy still exists concerning the exact mechanism. In general, the bactericidal effectiveness of free AgNPs has been ascribed to the toxicity of the dissolved Ag^+ ions (Lok et al., 2007; Navarro et al., 2008; Kittler et al., 2010; Xiu et al., 2012; Bondarenko et al., 2013) and the nanoparticle-specific physicochemical effects (Sondi and Salopek-Sondi, 2004; Morones et al., 2005; Fabrega et al., 2009; Yin et al., 2011; Agnihotri et al., 2013; Park et al., 2013) that impair biological functions of functional biomolecules such as enzymes, DNA, and membrane proteins (Nel et al., 2006; Eckhardt et al., 2013; Lemire et al., 2013; Suresh et al., 2013; Rizzello and Pompa, 2014; Xiu et al., 2014). It is challenging to gain an unequivocal understanding of the mechanism because of the involvement of multiple pathways and Ag domains in the multifaceted bactericidal action of AgNPs. Hence, a systematic and comprehensive study is required to elucidate the bactericidal mechanisms of AgNPs, both generally and in the specific context of cryogels. This would lead to a deeper understanding of factors contributing to improved disinfection and can provide a guide for future design of effective Ag-based disinfectants.

There is still debate as to whether the bactericidal mechanism of nanosilver is attributed to Ag^+ or to a nanoparticle effect (Levard et al., 2012). Nonetheless, there is growing evidence that suggests localized interfacial interaction between silver nanoparticles (AgNPs) and bacteria plays a key role in their toxicity mechanism; this is particularly the case for immobilized AgNPs (Agnihotri et al., 2013; Alonso et al., 2013). The composition of the exposure media can alter the surface chemistry of the native particles by influencing the species surrounding the cell-AgNP interface (Nel et al., 2009; Walczyk et al., 2010; Chen and Bothun, 2013). Therefore, the disinfection efficacies of the composites may be susceptible to changes in the solution chemistry. Solution parameters such as dissolved oxygen (Xiu et al., 2011; 2012), pH (Fabrega et al., 2009; Xiu et al., 2012; Fauss et al., 2014), and the presence of dissolved organic matter (e.g., humic acids, fulvic acids, alginate, albumin, etc) (Fabrega et al., 2009; Gao et al., 2009; Kennedy et al., 2012;

Wirth et al., 2012; Zhang et al., 2012; Ostermeyer et al., 2013; Pokhrel et al., 2013; Fauss et al., 2014; Liu et al., 2014; Yang et al., 2014) and electrolytes (e.g., Na^+, K^+, Ca^{2+}, Mg^{2+}, Cl^-, HCO_3^-, NO_3^-, SO_4^{2-}) (Gao et al., 2009; Badawy et al., 2010; Jin et al., 2010; Zhang et al., 2012; Chambers et al., 2013; Levard et al., 2013; Fauss et al., 2014) have been found to significantly affect the bactericidal efficacy of free AgNPs. The discussion in the aforementioned studies is limited to the phenomenological level in which changes in bactericidal activity of free AgNPs are solely attributed to the physical behavior of the particles (e.g., particle shielding or aggregation induced by matrix species) in the bulk solution, while neglecting the potentially bactericidal biochemical effects of the reactions that might occur at the cell-matrix species-AgNP interface. In addition, most prior studies on the impact of solution chemistry were conducted using free AgNP suspensions despite the fact that AgNPs are usually applied in the immobilized form to prevent their release into the treated water. The few studies that investigated the impact of solution chemistry on immobilized AgNPs have obtained results that contradict findings drawn from studies using free AgNPs.[24,25] However, no discussion was offered to consolidate the discrepancies. Thus, the understanding on the impact of solution chemistry on AgNPs remains vague. As such, a systematic study of the effects of isolated environmental constituents (e.g., dissolved organic matter and electrolytes) on the properties and bactericidal activity of AgNPs immobilized on cryogels is required. A fundamental understanding of the effects of isolated constituents can help rationalize changes in the performance of the cryogels when applied for treatment of natural water samples with complex solution chemistry.

1.3 Objectives and scope of research

The objective of this research was to develop a new generation of emergency water technologies that can be easily deployed to disaster sites for rapid water production from contaminated sources with no additional energy requirement. To achieve this, the research is focused on preparing robust cryogels that permit a high degree of water absorption, water recovery, and water-treatment efficiency. To address the

aforementioned knowledge gaps, the specific objectives and scope of the research are as follows:

i. To fabricate robust superabsorbent cryogels with superfast swelling rates:
   - Study the dependence of the properties of cryogels on the synthesis parameters such as the preparation temperature, initial monomer concentration, crosslinker ratio, and initiator content;
   - Evaluate the potential of cryogels as integral membranes for particulates removal;
   - Correlate the structure and morphology of cryogels to their properties and performance;
   - Develop design strategies for synthesis of high-performance cryogels.

ii. To compare different approaches to incorporate AgNPs in cryogels:
   - Employ three methods to prepare AgNP-incorporated cryogels with different spatial distribution of AgNPs, i.e., on the outer surface of pore wall or within the pore wall or a combination of both;
   - Evaluate the effects of the synthesis approaches on the resultant cryogel nanocomposites in terms of their pore structure, AgNP morphology, swelling/deswelling and mechanical behavior;
   - Compare the bactericidal efficacies of three different nanocomposites;
   - Establish the relationship between bulk or surface Ag content to the observed disinfection efficacy;
   - Highlight the advantages and disadvantages for each synthesis approach.

iii. To evaluate the potential of superabsorbent cryogels decorated with AgNPs for point-of-use water disinfection:
   - Detailed characterization of the properties of as-synthesized cryogel nanocomposites;
   - Test the reusability of the cryogels by evaluating the changes in their swelling and mechanical behavior after 1000 compression cycles;

- Show that the proposed approach depicted in Fig. 1.1 whereby the cryogels are used as sorbents can result in enhanced disinfection;
- Demonstrate the bactericidal effectiveness of the cryogels using artificially prepared bacterial suspension and natural water samples.

iv. To elucidate the toxicity pathways involved in the bactericidal mechanism of cryogels decorated with AgNPs:
- Profile the kinetics of bactericidal action of the cryogel nanocomposites;
- Ascertain the fate of AgNPs after exposing the cryogels to a bacterial suspension through a detailed Ag speciation study;
- Compare the differential mode of action of Ag^{+} and AgNPs;
- Reveal the role of reactive oxygen species (ROS) in mediating cell lesions;
- Propose a mechanism to explain the bactericidal action of the AgNPs decorated on cryogels.

v. To investigate the effects of environmentally relevant solution chemistry on the disinfection efficacies of the cryogels decorated with AgNPs:
- Investigate the changes in the morphology and chemical states of AgNPs decorated on cryogels after exposure to solutions containing either electrolytes or dissolved organic matter (DOM);
- Study the effect of electrolytes and DOM on the Ag leaching behavior and uptake by bacteria;
- Fundamentally understand the effects of electrolytes and DOM on the toxicity of AgNPs decorated on cryogels.

1.4 Organization of thesis

This thesis comprises 9 chapters, which are structured as follows:

Chapter 1 provides a general introduction of background issues and the motivation for this research. The objectives and scope of this study are also outlined in this chapter. A summary of the thesis organization is also included.

Chapter 2 can be divided into three principal parts. The first part serves to provide the context for the novel technology developed in this research wherein an overview of the challenges and the available water technologies that offer potential for applications in emergency drinking water response is given. Furthermore, a methodology for emergency water-technology selection and a set of evaluation criteria are briefly described. In the second part a critical review of existing Ag-modified composite materials for point-of-use water disinfection is provided. The last part of this chapter constitutes an overview of the methods of synthesis and characterization of cryogels, which are the base materials used in this research. Current applications of cryogels are also highlighted.

Chapter 3 details the materials, general methods and experimental procedures used in the studies.

Chapter 4 discusses the effects of various synthesis parameters on the characteristics and particulate removal efficiency of the resulting cryogels.

Chapter 5 describes the exploration of different synthesis methods to prepare cryogels incorporated with AgNPs. The effects of various synthesis approaches on the characteristics and bactericidal activity of the cryogels are also presented.

Chapter 6 highlights properties and bactericidal effectiveness of the as-synthesized cryogels decorated with AgNPs.

Chapter 7 presents the major findings in elucidating the bactericidal mechanisms of AgNPs decorated on cryogels.

Chapter 8 discusses the effects of solution chemistry on the properties and bactericidal activity of cryogels decorated with AgNPs.

Chapter 9 outlines the major conclusions emanating from this study and recommendations for future work.

CHAPTER 2 Literature Review[†]

This chapter provides the context for the novel water technology (WT) developed in this report. Firstly, an overview of the challenges and water technologies that offer potential for drinking water emergency response is presented in this chapter. A methodology for emergency water-technology evaluation and selection is also briefly described here. This chapter also includes a critical review of existing Ag-modified composite materials for point-of-use water disinfection. The last part of this chapter provides a comprehensive overview of the methods of synthesis and characterization of cryogels, which are the base materials used in this research. Current applications of cryogels are also highlighted.

2.1 Challenges of drinking-water emergency response

One of the major goals in responding to some emergencies, in particular natural disasters, is to provide potable water in sufficient quantity and quality for the survival of the AP (affected population). The minimum standard for drinking-water quality for emergency response as stipulated by the Sphere Handbook of Humanitarian Charter and Minimum Standards in Disaster Response (Sphere, 2004) includes: no fecal coliform (FC) per 100 mL; chlorine residual < 0.5 mg/L; turbidity < 5 NTU (Nephelometric Turbidity Unit); and no negative impact on health due to short-term consumption. However, note that this stringent requirement can be compromised because water quantity is usually prioritized over water quality in emergencies. Providing potable water of adequate quantity and quality in emergencies is challenging due to various constraints. This section provides an overview of these challenges.

[†]A major part of this chapter has been published as 'Emergency Water Supply: A Review of Potential Technologies and Selection Criteria' in *Water Research* (46) 3125-3151. Please see Appendix A for reuse permission.

2.1.1 Water-quality problems

Natural disasters such as flooding can considerably increase microbial contamination of surface water (Faruque et al., 2005). Other water-quality problems following a disaster include salinization and water contamination by hazardous materials release (Young et al., 2004; Srinivas and Nakagawa, 2008; Violette et al., 2009). Hazardous materials such as radionuclides were detected in water bodies following the 2011 Japanese earthquake (Matsumoto and Inoue, 2011). Moreover, debris contamination and water turbidity up to 10,000 NTU have been observed (Garsadi et al., 2009). These show the complexity of water composition in the aftermath of a disaster.

Overloading of microbial and chemical pollutants in water increases the potential for failure of conventional water-treatment systems (Roig et al., 2011). These hazardous materials need to be removed if the water is to be drinkable. This adds to the complexity of the WT. A drastic increase in dissolved organic carbon (DOC) in surface water is also possible after an intense rain (Roig et al., 2011). An increase in the amount of DOC can lead to resolubilization of heavy metals (Remoundaki et al., 2007; Schwab et al., 2007), accelerated membrane fouling (Schäfer et al., 1998; Schäfer et al., 2000; Aoustin et al., 2001; Lee et al., 2008), disinfection byproducts (DBPs) formation (Krasner and Wright, 2005) and taste problems when treated with chlorine-based disinfectants. Due to the altered solution chemistry, the WT may fail to perform as expected. This is especially true for WTs such as coagulation/flocculation, adsorption, and high-pressure membrane filtration. Other problems are water-quality variability and the absence of onsite tool-kits for rapid contaminant screening in emergencies.

2.1.2 Limited access to infrastructure and resources

Limited access to the infrastructure and resources further complicates the process of providing water to the affected population (AP). One probable consequence of disasters is power breakdown that prevents using energy-dependent WTs. WTs that do not require energy from the power grid or can be powered by renewable energy

harnessed onsite are an option. Alternatively, a mobile electric generator can be used. Disasters such as earthquakes will result in infrastructure damage and limit access to the impacted regions. Hence, other means of access such as air transportation are required in which case the size and weight of the WT can be limiting. These considerations also limit manually transported devices (Frechen et al., 2011). In addition, during emergencies, trained operators for the WT might not be available that can result in improper process control and failure. Furthermore, unhygienic conditions in relief camps might result in post-contamination of treated water. Most WTs other than chlorination provide only interim disinfection due to the absence of any residual disinfectant. Hence, it is better to treat water at the point-of-use (POU) for WTs that cannot provide secondary disinfection.

2.2 A review of water technologies with potential for use in disaster relief

This section provides an overview of potential WTs, broadly classified into membrane- and non-membrane-based technologies. Tables 2.1 and 2.2 provide detailed information on these WTs. The following terms used in this chapter are defined:

- Modular units: Immobile WTs packaged as unit segments and assembled on-site;
- Mobile units: WTs mounted onto a self-contained vehicle or ship;
- Portable units: WTs carried by individual users.

2.2.1 Non-membrane-based water technologies

In general, non-membrane-based WTs can be classified as follows:

- Methods involving physical treatment – filtration;
- Methods employing chemicals – coagulation/flocculation, chlorination, combined coagulation/disinfection, and adsorption;

- Methods involving thermal or light-based treatment – boiling, pasteurization, SODIS (solar disinfection), UV (ultraviolet) disinfection and solar distillation;
- Methods involving integrated treatment – small-scale water-treatment plants that combine treatment methods.

Examples of these WTs are discussed in the following section.

Table 2.1 Summary of key characteristics of non-membrane-based water technologies

Name	Functional parts/filter type	Production rate	Capacity/life span	Cost[a] (US$)	Performance[b]	Maintenance	Pre-treatment	Post-treatment	Energy requirement	References
AC+UV	AC pressed filter block	~2.7 L/min	1800 L	N.R.	6 LRV bacteria; 3 LRV protozoa; 4 LRV virus	None	N.R.	UV	¾ hp centrifugal water pump (60 psi)	(Abbaszadegan et al., 1997)
Biosand filter	Crushed granite, gravels or sand	30-40 L/h (for a filter with 95 cm height and 36 cm width)	Can last up to 8 y or more	One time cost of 25-100	0.3-4 LRV bacteria; 3.8-5 LRV protozoa; 0-1.3 LRV virus; 96 % turbidity removal	Resuspension of the top 5-10 cm of sand	N.R.	N.R.	Gravity filtration	(Burch and Thomas, 1998; Palmateer et al., 1999; Duke et al., 2006; Jill et al., 2007; Elliott et al., 2008; Sobsey et al., 2008; Stauber et al., 2009; Murphy et al., 2010)
Boiling	N.A.	Varies	N.A.	0.272-1.68 /mth; ~ 0.003 /L[c]	86-99 % removal of bacteria	Cleaning of heating vessels	N.A.	N.A.	Fuel	(Clasen et al., 2008a; Clasen et al., 2008b; Rosa et al., 2010; Psutka et al., 2011)
Chlorination tablets	N.A.	Varies	N.A.	0.08-0.015 /L	1-2.8 LRV of bacteria	Cleaning of treatment vessel and storage container	May require filtration	None	None	(Schlosser et al., 2001; Clasen et al., 2007; Lantagne and Clasen, 2009; Jain et al., 2010)
Chulli purifier	*Chulli* and Al coil	0.5 L/min[d]	N.R.	6 /unit	> 5 LRV bacteria	N.R.	Sand filtration	N.R.	No additional fuel requirement	(Islam and Johnston, 2006; Gupta et al., 2008)

Table 2.1 Summary of key characteristics of non-membrane-based water technologies (continued)

Name	Functional parts/filter type	Production rate/flux	Capacity/life span	Cost[a] (US$)	Performance[b]	Maintenance	Pre-treatment	Post-treatment	Energy requirement	References
Combined flocculation-disinfection sachet (PUR®)	N.A.	0.3 L/min	N.A.	0.003-0.035/L	4 to >8 LRV bacteria; >2.5 LRV protozoa; 1-4 LRV virus	Cleaning of vessels and ladle	None	Cloth filtration	None	(Rangel et al., 2003; Sobsey et al., 2008; Lantagne and Clasen, 2009; McLennan et al., 2009)
MHMWTP	N.A.	15-20 000 L/ h	400 m^3/ d	N.R.	Effluent: <1 NTU, residual of 0.5-1 mg/L	N.R.	Coagulation/ flocculation, sedimentation, rapid filtration and optionally AC	Chlorine disinfection	5 kW generator	(Garsadi et al., 2009)
Portable Solar stills	0.2 or 0.6 m^2 PVC pyramidal or prism still	0.5-0.9 L/d	N.R.	0.046-0.063 /L	>3 LRV of bacteria; distillate < 3 NTU; remove nonvolatile contaminant and radionuclides	Cleaning of sludge layer in solar stills	N.R.	N.R.	Solar radiation	(Hanson et al., 2004; Wassouf et al., 2011)
SODIS	PET bottles	Varies	N.A.	PET bottles	3-5.5 LRV bacteria; 1-3 LRV protozoa; 2-4 LRV virus	Cleaning of PET bottles	May require filtration to remove turbidity	N.A.	Solar irradiation	(Wegelin et al., 1994; Meyer and Reed, 2001; Sobsey, 2002; Mendez-Hermida et al., 2005; Sobsey et al., 2008)
Solar water heater	Commercial solar water heater	125 L/d	N.R.	0.01 /L; 220 /unit	>4 LRV bacteria	Cleaning of PET bottles	May need filtration	N.A.	Solar irradiation	(Kang et al., 2006)

Name	Functional parts/filter type	Production rate/flux	Capacity/life span	Cost[a] (US$)	Performance[b]	Maintenance	Pre-treatment	Post-treatment	Energy requirement	References
Upflow clarifier	Oxfam tank + clarifier cone + nonwoven fabric polishing filter; coagulant dose: 10-60 mg/L alum	5 m^3/h	> 2 y	N.R.	97.6 to 98.6% turbidity removal (effluent <5 NTU); ~ 2 LRV bacteria	Manual cleaning of the polishing fabric filter	N.R.	May need chlorination	Diesel generator	(Dorea et al., 2006; Dorea and Clarke, 2006)
UV007	UV lamp	20-25 L /batch; ~8L/min	N.R.	~ 100-300 /unit	>2.3 LRV virus	N.R.	May require filtration	N.R.	Powered by hand crank, bicycle or electric	(Berg, 2010)
WADIS	Lorena stove	1-2 L/min[d]	N.R.	6 /unit	~ 4 LRV bacteria	N.R.	N.R.	N.R.	No additional fuel requirement	(Christen et al., 2009)

Note: N.R. = Not reported; N.A.= Not applicable
[a] Cost is as reported in the reference
[b] Performance may vary due to differences in the quality of water
[c] Cost may vary depending on the price of fuel for a given location
[d] Depends on cooking frequency

Table 2.2 Summary of key characteristics of membrane-based water technologies

Name	Filter type	Production rate/ flux[a]	Capacity /life span	Cost[b] (US$)	Performance[c]	Maintenance	Pre-treatment	Post-treatment	Energy requirement	References
Household ceramic filter	Varied pore size depending on production method	0.04-0.3 L/min	Depends on breakage	8 -10 /unit; 4-5 /unit of filter replaced	2 to >4 LRV bacteria; 2-6 LRV protozoa; 1-2.3 LRV virus	Scrubbing	N.R.	N.R.	Gravity filtration	(van Halem et al., 2007; Sobsey et al., 2008; Murphy et al., 2009; van Halem et al., 2009; Berg, 2010; Brown and Sobsey, 2010)
Katadyn Mini Ceramic	0.2 µm ceramic Ag-impregnated	0.5 L/min	7000	~ 2/L	1.7-4.9 LRV of bacteria	Cleaning of filter	Prefilter	None	Handpump	(Schlosser et al., 2001; Katadyn, 2011)
Bicycle-powered ceramic filter	Potters for Peace ceramic filter (MF)	4 L/min (50 psi)	N.R.	N.R.	67% TC; 89% FC; permeate < 1 NTU	N.R.	Upflow rapid sand filter	N.R.	Pedal-powered pumps	(McBean, 2009)
WaterBack-Pack	0.04 µm membrane (deadend)	50 L/h	10 y	0.0047 €/L	1 to >3 LRV bacteria	No maintenance or cleaning (for < 2 mth operation	Mesh sieve	N.R.	Gravity feed	(Frechen et al., 2011)
Bicycle-powered UF	UF membrane	800 L/h	N.R.	N.R.	Permeate: <1 cfu/100 mL and <1 bacteria /mL; < 1NTU	Backwashing by permeate and/or CIP	N.R.	N.R.	Pedal-powered	(He, 2009)
Lifestraw®	UF hollow-fiber membrane of 20 nm; cylinder cartridge (26 cm × 30 cm)	8.6-12 L/h	~18000 L	0.001/L	6-7 LRV bacteria; 2-4.7 LRV virus; 3.6 LRV protozoa	Periodic cleaning and backwashing	27 µm prefilter and halogen chamber (not included during microbial assessment)	N.R.	Gravity feed or mouth suction	(Vestergaard; LifeStraw, 2007; Clasen et al., 2009)

Table 2.2 Summary of key characteristics of membrane-based water technologies (continued)

Name	Filter type	Production rate/ flux[a]	Capacity/ life span	Cost[b] (US$)	Performance[c]	Maintenance	Pre-treatment	Post-treatment	Energy requirement	References
Mobile water maker	40 nm tubular ceramic membrane (UF)	~0.35 L/min	N.R.	N.R.	> 5 LRV bacteria; effluent < 1 NTU ; 0.2 mg/L of chlorine residual	Simple flushing without chemicals once daily	N.R.	Anodic oxidation	Solar panel (6 V) to power anodic oxidation and hand-powered bicycle pump to pressurize feed water to 4-6 bar	(Groendijk and de Vries, 2009)
Low pressure UF	PS UF capillary membrane (MWCO: 50 000 Da)	30-40 L/m^2.h (100-150 kPa)	> 5 y	N.R.	85 % NOM removal; > 90% color removal; no FC in effluent; 5 LRV bacteria; 3-4 LRV virus	Backwashing for 60s for 10 min cycle time; CIP when TMP is 80-100 kPa using detergent and complexing agent at high pH	Sand filter	Contact column	100-150 kPa provided by feed pump or use water head; recycle pump powered by electricity	(Pryor et al., 1998)
AQUAPOT	Hollow fiber PES membrane, MWCO 150 kDa or PS spiral wound module of 100 kDa (6.5 m^2)	1000-2000 L/h (0.3-0.4 MPa); Operated at 2h/d	Capital cost of 28, 000	N.R.	53. 6% turbidity reduction; 100% TC and TTC removal	Microfilter cleaned daily, sand filter once a week, UF CIP once a week using 100 mg/L NaOCl	Sand filter and 25-50 µm microfilter	Addition of NaOCl (1-2 mg/L)	0.3-0.4 MPa pressure pump driven by diesel engine	(Arnal et al., 2001; 2004; 2007; 2008; 2009; 2010)
Ultralow pressure UF	Flatsheet PES with MWCO 100 kDa (deadend)	4-10 L/m^2.h	N.R.	N.R.	N.R.	None	None	None	40-66 mbar	(Peter-Varbanets et al., 2010; 2012)

Table 2.2 Summary of key characteristics of membrane-based water technologies (continued)

Name	Filter type	Production rate/ flux[a]	Capacity/ life span	Cost[b] (US$)	Performance[c]	Maintenance	Pre-treatment	Post-treatment	Energy requirement	References
Transport-able UF system	Hollow fiber UF (outside-in) with MWCO 100 kDa; 4 modules (18 m^2)	1000L/h (0.3-1 bar)	N.R.	N.R.	N.R.	Backwashing pressure at 2 bar at every 30 s and a dose of 5 mg/L of chlorine; CIP use 200 mg/L chlorine, 4 g/L NaOH and 5 g/L citric acid	200 µm prefilter	Chlorination and post-filtered by 1 µm filter	0.6 kW powered by electricity generator	(Barbot et al., 2009)
Sky-Hydrant™	0.04 µm PVDF membrane	400 -1000 L/h	5-8 y	3500 /unit; 0.35-0.50 /capita / annum	Permeate < 0.1NTU and > 4 LRV particles of size 2-5 µm	CIP use 40 mL of 10 % hypochlorite + 300 g citric acid powder	N.R.	Chlorine dosage	Gravity feed or suction	(Butler, 2009)
Bicycle powered NF	60 cm^2 polyaromatic flatsheet NF (nominal salt rejection of 99.6 %)	0.2-0.3 L/min (2-6 % recovery)	N.R	N.R.	90% of total As	N.R.	Need pre-oxidation methods for enhanced As(III) removal	N.R.	Pedal-powered (0.2-0.7 MPa)	(Oh et al., 2000)
Small-scale RO system	RO module for brackish water desalination	~4L/min (6 bar); 25-37 % recovery	N.R.	0.01 / L	Permeate < 100 mg/L TDS	N.R.	Three-step filtration (cartridge prefilter, GAC filter and 5 µm cartridge) (SDI of feed water reduced to 0.8-1.5)	UV and AC treatment	N.R.	(Elfil et al., 2007)
PV-RO I	Two spiral-wound seawater membrane modules in parallel	0.8-3 m^3/d (15 % recovery)	N.R.	0.016 /L	Seawater desalination	Flushing using permeate water	Two 1 µm cartridge filters, antiscalant (SDI of feed water <1)	N.R.	4.8 kWp PV with additional battery storage of 60 kWh	(Herold et al.; Herold and Neskakis, 2001)

Table 2.2 Summary of key characteristics of membrane-based water technologies (continued)

Name	Filter type	Production rate/ flux[a]	Capacity/ life span	Cost[b] (US$)	Performance[c]	Maintenance	Pre-treatment	Post-treatment	Energy requirement	References
PV-RO II	Seawater RO membrane module	500 L/h (65 bar); 23 % recovery	20 years	0.04 /L	Permeate <500 mg/L of TDS	N.R.	N.R.	N.R.	68.5 kWh powered by PV and back-up diesel generator	(Tzen et al., 1998)
Mobile RO demo plant installed in bus	~ 73 m^2 spiral-wound modules for brackish water desalination	7-14 L/min (27 bar); 50 % recovery	N.R.	N.R.	Permeate: 250-450 mg/L	N.R.	Sand filter and acid and antiscalant addition	Decarbonation (neutralization)	Diesel generator or electric power supply	(Shah et al., 1988)
Skid-mounted Brackish RO plant	8 in. spiral-wound TFC low pressure membrane (nominal salt rejection 98 %)	0.05 L/h (15-25 bar); 60 % recover y	N.R.	0.2 /L	<100 mg/L TDS	Backwashing using permeate	Dual media filter (hydroanthracite and fine sand) ,5 µm cartridge filter, H_2SO_4 (5 mg/L) and antiscalant (6 mg/L) and sodium bisulfate (2 mg/L)	Chlorination (1 mg/L)	Diesel generator or electric power supply	(Malik et al., 1989)
Wind-powered RO system	Brackish water RO	~9 L/h (600-1100 kPa); 10 % recovery	N.R.	10,000 (capital); 250-490 (expenditure)	~83% observed salt rejection	N.R.	5- 10µm cartridge filter, AC cartridge (if organics are present in feed)	N.R.	150 W powered by wind pump and back-up diesel/gasoline pump	(Robinson et al., 1992)
ROWPU	Deadend RO single pass or double pass (depending on the quality of feed water)	5000 L/h (single pass); 2400 L/h (double pass)	N.R.	N.R.	Treats seawater, brackish, NBC contaminated water	4 h maintenance	50 µm self-cleaning filter followed by 5 µm cartridge filter	Chlorination, AC adsorption, ion exchange	Diesel generator or electric power supply (3.2 kWh/m^3)	(Bagwell et al., 1994; Downing et al., 1994; Harris, 2000)

Table 2.2 Summary of key characteristics of membrane-based water technologies (continued)

Name	Filter type	Production rate/ flux[a]	Capacity/ life span	Cost[b] (US$)	Performance[c]	Maintenance	Pre-treatment	Post-treatment	Energy requirement	References
Mobile floating desalination plant (PCS®)	Seawater RO membrane	~2000 L/h; 35 -45 % recovery	N.R.	N.R.	Effluent < 500 mg/L salt	Backwashing of media filters with filtrate or brine and air scouring	Disinfectant, acid, coagulant, polyelectrolyte, dual media filter, fine filter, dechlorination	Disinfection and lime addition	7 kWh/m^3 powered by 3 electric generators of 800 kW; energy recovery turbine	(Lampe et al., 1997)
FO filter pouch[d]	FO membrane; draw solute: mixture minerals and sugar	1.6 L/d (single charge)	10 d (filter life)	~ 4 /L; 64[e]	Claimed to be able to reach 6-4-3 standards	Recharge using oral rehydration syrup	N.R.	N.R.	N.R.	(Atkinson, 2006; Wallace et al., 2008)
Small scale desalination (compact SMADES)	PTFE spiral-wound MD module with 0.2 µm pore size, 80 % porosity with effective area 10 m^2	150 L/d-10 m^3/d	N.R.	0.015 /L	99.5% salt removal	N.R.	N.R.	N.R.	Equipped with internal heat recovery; PV panel to run feed pump and 5.73 m^2 solar collector to heat up the feed water(solar thermal and solar PV); 200-300 kWh/m^3	(Banat et al., 2007; Banat and Jwaied, 2008; Fath et al., 2008)

Note: N.R. = Not reported; N.A.= Not applicable; NBC= Nuclear, biological and chemical contaminants; PES= Polyethersulfone; PS= Polysulfone; TFC = Thin film composite; CIP= Clean in place; MWCO= Molecular weight cut-off; SDI= Silt density index

[a] Water throughput may vary due to differences in the feed water quality and the frequency of maintenance employed

[b] Cost is as reported in the reference

[c] Performance may vary due to differences in the quality of water

[d] Information cited is based on the reusable pouch (single-use pouch is also available)

[e] Price for one unit of the filter pouch and ten charges of fresh draw solution

2.2.1.1 Methods involving physical treatment

Biosand filter

A biosand filter (BSF), commonly used at the household level, can be constructed by filling a container with sand and/or gravel and allowing a bioactive layer responsible for removing pathogens to form (Mahmood et al., 2011). Laboratory determination of microbial removal by a BSF has shown that it is capable of removing > 95% of turbidity, ~ 1 log removal value (LRV) of viruses, ~ 2 LRV of bacteria, and > 3 LRV of protozoa (Palmateer et al., 1999; Duke et al., 2006; Stauber et al., 2006; Elliott et al., 2008; Murphy et al., 2010) (Note: 1 LRV is 90% removal; 2 LRV is 99%, etc.). A modular BSF was used after the 2005 Pakistan earthquake (Mahmood et al., 2011). Despite the modest microbial removal by BSF, a considerable reduction of pathogens was observed in the aforementioned studies. Stauber et al. (2009) and Tiwari et al. (2009) have shown that BSF reduced diarrheal occurrences by 47-54%. Recently, Ahammed and Davra (2011) improved BSF performance by using iron-oxide-coated sand that showed better removal of total coliform (TC) and *E. coli* by > 1 LRV throughout the operation. The enhanced removal was attributed to bacterial adhesion on iron oxide. Since a BSF requires regular maintenance and a long start-up time, it is more suitable for the later rather than the immediate acute stage of an emergency.

Pressure filter

A pressure filter consists of a small vessel with a system to distribute the incoming water over the surface of the filter bed and a drainage system to collect the filtrate (Clarke and Steele, 2009). Pressure filters are usually compact and easy to deploy with high productivity. Hence, they are suitable for use at the community level in acute emergencies. Pressure filter systems are available in both mobile and modular forms. Mobile media filtration includes sand pressure filters and precoat filters (with diatomaceous earth) (Dorea et al., 2006). Precoat filters were deployed during emergency relief in some Tsunami-affected areas in Acheh in 2005 (Clarke and

Steele, 2009). It is believed that the diatomaceous earth improved the filtration efficiency.

2.2.1.2 Methods employing chemicals

Clarification

Modular clarifiers can be operated in either continuous or batch mode (Dorea, 2009). Clarification is often assisted by coagulants for turbidity reduction such as alum or natural coagulants such as powder from *Moringa oleifera* seeds, *Jatropha curcas* and Guar gum (Ndabigengesere and Subba Narasiah, 1998; Pritchard et al., 2009; 2010). Batch coagulation can be carried out by adding coagulants to the contaminated water flowing into a large modular tank that permits settling and decanting of the purified water (Dorea, 2009). Continuous mode operation is generally restricted to the modular Oxfam upflow clarifier (Fig. 2.1) developed by Ives (1968).

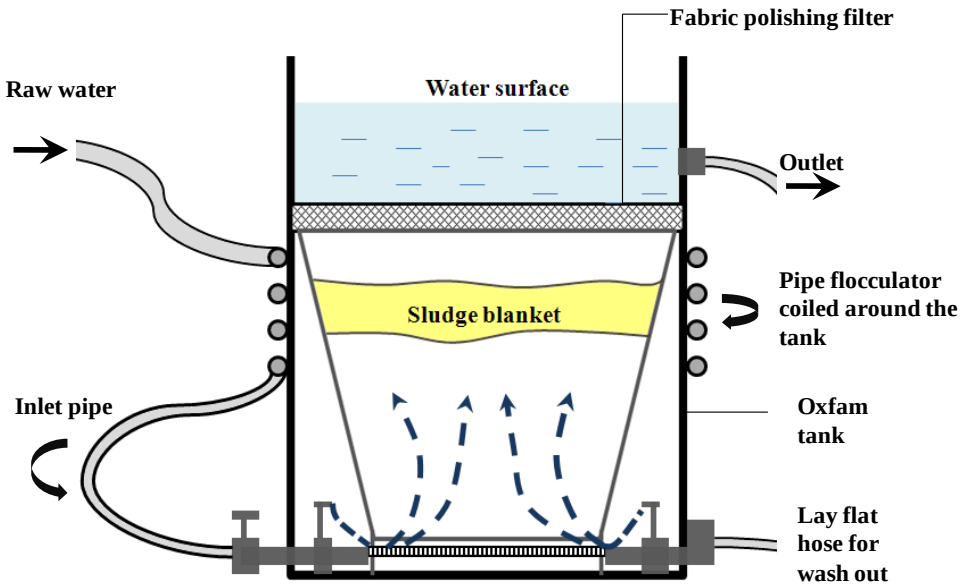

Figure 2.1 Schematic diagram of the upflow clarifier (modified from Dorea et al., 2009).

Clarifers have high productivity (up to 10 m^3/h) and can be used for treating high turbidity water. In addition, a clarifier is capable of ~2 LRV of fecal coliform (FC) reduction (Dorea et al., 2006). Hence, clarifiers can be used for safe drinking-water production at the community level. After the 2004 Asian tsunami, two Oxfam clarifiers were deployed in the affected Indonesian villages of Lamno and Meulaboh (Dorea, 2008). Their performance demonstrated that the system was robust and capable of producing drinking water with acceptable turbidity for prolonged periods (Dorea, 2009). However, these clarifiers are more suitable for application in the later stage of emergencies due to the long start-up time required to assemble the whole system.

Chlorination

Halogens such as chlorine are inexpensive, easily available in several forms, and can treat large volumes of water (Backer, 2008). They can be used at both the community and household levels. Chlorination using sodium hypochlorite (NaOCl) has been found to improve stored water quality after the Indonesian tsunami (Gupta et al., 2007). Chlorine in tablet form such as sodium dichloroisocyanurate ($NaC_3N_3O_3Cl_2$ abbreviated as NaDCC) is widely used in emergencies and offers advantages such as better stability, safety, low capital investment, convenience due to its single-use packaging and lightweight when compared to NaOCl (Clasen and Edmondson, 2006; Lantagne et al., 2010a). Tablets also have longer shelf-life and lower transportation cost than chlorine solutions (Berg, 2010). McLennan et al. (2009) compared four types of POUs for emergency disinfection and found that only NaDCC tablets could provide sufficient residuals for safe storage.

Innovative technologies using water insoluble polymeric beads that release halogen when in contact with microbes are available (Chen et al., 2003; Mazumdar et al., 2010). The disinfection mechanism is probably a diffusion-induced release of halogen. These biocidal beads can be integrated into filtration trains for controlled flow rates and predictable performance. Nevertheless, NaDCC tablets might be the

preferred chlorination technology because they are easier to handle and allow rapid deployment in acute emergencies.

Chlorine dose depends on factors such as temperature, turbidity, presence of NOM (natural organic matter), and the type of bacteria/viruses (LeChevallier et al., 1981; Feachem et al., 1983; Abbaszadegan et al., 1997). The disinfectant capability of NaDCC tablets has been demonstrated (Clasen et al., 2007; Jain et al., 2010). They were reported to reduce diarrheal risks by 48% in Zambia. However in a recent epidemiological study in Ghana, no significant reduction in diarrheal risk was associated with using NaDCC tablets (Jain et al., 2010). These conflicting findings regarding diarrheal reduction could be attributed to different levels of water contamination. A disadvantage of using chlorination is the formation of harmful disinfection byproducts (DBPs). Chloroform levels as high as 84 µg/L and 90 µg/L were detected when river water was subjected to chlorination by NaOCl and NaDCC tablets, respectively (Lantagne et al., 2008; 2010).

Combined coagulant-disinfectant powder

An example of a portable coagulation-based WT is the PuR® sachet (Lougheed, 2006) that was reverse-engineered based on a municipal water treatment plant. PuR® sachet combines ferric sulfate, bentonite, sodium carbonate, poly(acrylamide), chitosan (flocculating aids), potassium permanganate (oxidizing agent), and calcium hypochlorite (disinfectant) into a sachet for treating 10 L of water (Reller et al., 2003). The sachet contents are mixed with turbid water. Clean water is obtained by screening the resulting solution via a cotton cloth (Souter et al., 2003). It is suitable for household level intervention.

PuR® is capable of producing microbiologically safe drinking water (Rangel et al., 2003; Souter et al., 2003; Crump, 2005; Doocy and Burnham, 2006; McLennan et al., 2009). The use of PuR® has been associated with diarrhea reductions of 90%, 24% and 19% in Liberia, Guatemala and Kenya, respectively (Reller et al., 2003; Crump, 2005; Doocy and Burnham, 2006). The significantly higher diarrheal reduction in Liberia was attributed to the extremely high level of compliance among users (95%

versus < 44%) and a high incidence of diarrhea in the control households (29% versus < 5% of the weeks).

PuR® has the added advantage of removing arsenic by 99.8% down to a mean level of 1.2 µg/L, which is safe for consumption (Souter et al., 2003). Arsenic removal might be due to its co-precipitation or adsorption on the ferric hydroxide formed. PuR® has been used following the 2004 Tropical Storm Jeanne in Haiti. Significantly, 81% of the users reported that PuR® was easy to use and 97% reported that the product appears and tastes better than raw water (Colindres et al., 2007). Furthermore, PuR® can be applied in acute emergencies due to its compact packaging that allows easy distribution.

Adsorption

Adsorbents can be used to remove toxic substances such as chlorine-disinfectant residuals, organics and particulates (Tobin et al., 1981; Bell et al., 1984). However, their microbial removal efficiency is generally low (Snyder et al., 1995). Activated carbon (AC) is the most widely used adsorbent. It is available in powdered (PAC) or granulated (GAC) forms and is commonly incorporated into household filters (Snyder et al., 1995).

Although virgin AC could adsorb microbes in water, NOMs would rapidly occupy the adsorption sites and promote biofilm growth (Caroli et al., 1985). Several studies have shown that the microbiological quality of treated water was worse than the feed due to biofilm formation that prevented further bacterial colonization on the AC (Wallis et al., 1974; Tobin et al., 1981; Su et al., 2009). Operating conditions such as high flow rate, low filter temperature and short residence time can retard biofilm formation (Su et al., 2009).

Tsarik et al. (1993) found that AC could remove ^{131}I and ^{106}Ru. However, the performance declines as the AC becomes saturated. Tagami and Uchida (2011) reported that AC caused no substantial reduction of ^{131}I in water. AC can also remove objectionable taste and odorous compounds such as iodine and chlorine by

adsorption and chemical reduction (Backer, 2008). Detailed reviews on the removal of organic and inorganic contaminants are available (Dabrowski et al., 2005; Mohan and Pittman Jr, 2006; Foo and Hameed, 2009; 2010). AC adsorption is not suitable for long-term application because it requires continuous replacement owing to saturation. However, it is suitable for acute emergencies when coupled with other disinfection techniques.

2.2.1.3 Methods involving thermal or light-based treatment

Boiling

Boiling can inactivate some waterborne pathogens including viruses and protozoan cysts that are resistant to chlorination (Sobsey, 2002) and is an effective intervention at the household level. It has been shown to produce microbiologically safe drinking water based on the reduction of thermo-tolerant coliforms (TTC) (Clasen et al., 2008b; Rosa et al., 2010) and fecal coliform (FC) (Clasen et al., 2008a). Several studies conducted in Peru (Oswald et al., 2007), Indonesia (Gupta et al., 2007), and Zambia (Psutka et al., 2011) found that boiling did not always improve water quality. In addition, the quality of stored boiled water was worse than the source water, presumably due to the lack of residual protection, and unsafe handling and storage (Psutka et al., 2011). Boiling cannot remove chemicals and radionuclides. For example, it could not remove the ^{131}I found in the drinking water supply following the 2011 Japanese earthquake (Tagami and Uchida, 2011). In fact, boiling increased the concentration of the nonvolatile ^{131}I owing to evaporation of water (Tagami and Uchida, 2011). Another limitation of boiling is the need for fuel that might not be available after a disaster. Nevertheless, boiling can be used in all stages of emergency relief if fuel were available and affordable.

Thermal pasteurization

Pasteurization employs heat as does boiling but requires only moderate temperatures (~ 75 ^{o}C). It is suitable for household level intervention in the late-

emergency stage. It is a simple flow-through system using waste heat to pasteurize raw water. Normal cooking heats water that passes through an aluminum-coiled tube built into the *Chulli* (a traditional clay cooking stove) (Islam and Johnston, 2006; Gupta et al., 2008). *Chulli*-pasteurized water does not have detectable TTC and has more than 5 LRV of *E. coli* (Islam and Johnston, 2006; Gupta et al., 2008) . However, a study in Bangladesh found that 80 out of 101 persons discontinued its use due to mechanical problems, inconvenience and perceived high cost (Gupta et al., 2008).

The water disinfection stove (WADIS) is a flow-through boiling system similar to the *Chulli* but uses the Lorena-stove that features one combustion chamber with three pot holes and chimney ventilation (Christen et al., 2009). It uses galvanized iron water pipe wound into three helical coils (Christen et al., 2009).

Solar water heaters can be used to thermally inactivate pathogens (Kang et al., 2006). A commercial modular solar water heater was shown to be capable of 4 LRV of fecal coliforms (FCs) and viruses after 2 h during sunny days and 4 h on rainy days. It was able to inactivate the Hepathitis A virus after 4 h.

Solar disinfection

Solar disinfection (SODIS) is effective for disinfecting water under severely limited conditions (Reed, 2004). Using SODIS involves filling a PET (polyethylene terephthalate) container with low-turbidity water, shaking it to ensure saturation with oxygen, and then exposing it to direct sunlight for at least 6 h or 2 d during cloudy periods (CDC, 2008). PET is preferred over other clear plastics for the bottles because it is resistant to leaching of harmful materials into the water (Sobsey, 2002; Schmid et al., 2008). SODIS inactivates bacteria based on the synergistic effects of the UV rays and increased water temperature (Murinda and Kraemer, 2008). Because SODIS is simple, it can be applied by individuals, households, and small communities during emergencies (Reed, 2004; Hindiyeh and Ali, 2010).

SODIS has been shown to produce microbiologically-safe drinking water (Meyer and Reed, 2001; Mendez-Hermida et al., 2005; Berney et al., 2006; McGuigan et al.,

2006). Epidemiological studies conducted on Kenyan children aged 5-16 (Conroy et al., 1996) and under the age of 5 (Conroy et al., 1999) showed a 16% and 10% reduction of diarrhea, respectively. Rose et al. (2006) found a 40% reduction in diarrhea among Indian children under the age of 5 with the use of SODIS. However, a significant reduction of dysentery and diarrheal diseases cannot be achieved unless there is a high level of motivation and compliance among the users (Mäusezahl et al., 2009; Du Preez et al., 2010). It is believed that motivation can be promoted through educational campaigns, training and marketing (Meierhofer and Landolt, 2009).

SODIS is applicable only when the impacted region has intense solar radiation. However, good disinfection during low solar radiation is achievable by using homemade solar collector disinfection (Amin and Han, 2009; Gelover et al., 2006; Hindiyeh and Ali, 2010) and the addition of lemon juice and vinegar (Amin and Han, 2009). Sunlight-assisted photocatalysis with suspended TiO_2 (Wei et al., 1994) or as a coating on a flat PET sheet (Duffy et al., 2004) has been shown to be more effective for disinfection than SODIS alone.

UV disinfection

UV disinfection of water uses ultraviolet light in the germicidal wavelength range on a batch basis (Berg, 2010). Berg et al. (2010) discuss a portable POU UV unit (called UV007) for disinfecting 2.5-20 L of water using either a handcrank, bicycle or electrical power. It can be used at the household level. It was capable of inactivating >2.3 LRV of MS-2 coliphage under 60-75% transmittance within a minute depending on the penetration depth. The main challenge with UV systems is that their performance is affected by turbidity. However, they can be coupled to pre-filters to improve light transmittance and enhance their performance (Gadgil, 1998). They are appropriate for acute applications when coupled to other WTs.

Solar distillation

The simplest most commonly used solar distillation technology is the single effect still (Aboabboud et al., 1997). It uses direct solar radiation for desalination (Bouchekima et al., 1998). It is ideal for applications in remote areas such as refugee camps where the water demand is less than 50 m^3/d (Bouchekima et al., 1998). The cost for desalination using a solar still is 0.0024-0.02 US$/L (Madani and Zaki, 1995; Ghoneyem and Ileri, 1997), which is less than all other WTs at this scale (Hanson et al., 2004). Fig. 2.2 shows the typical design and summarizes the processes that take place in a solar still.

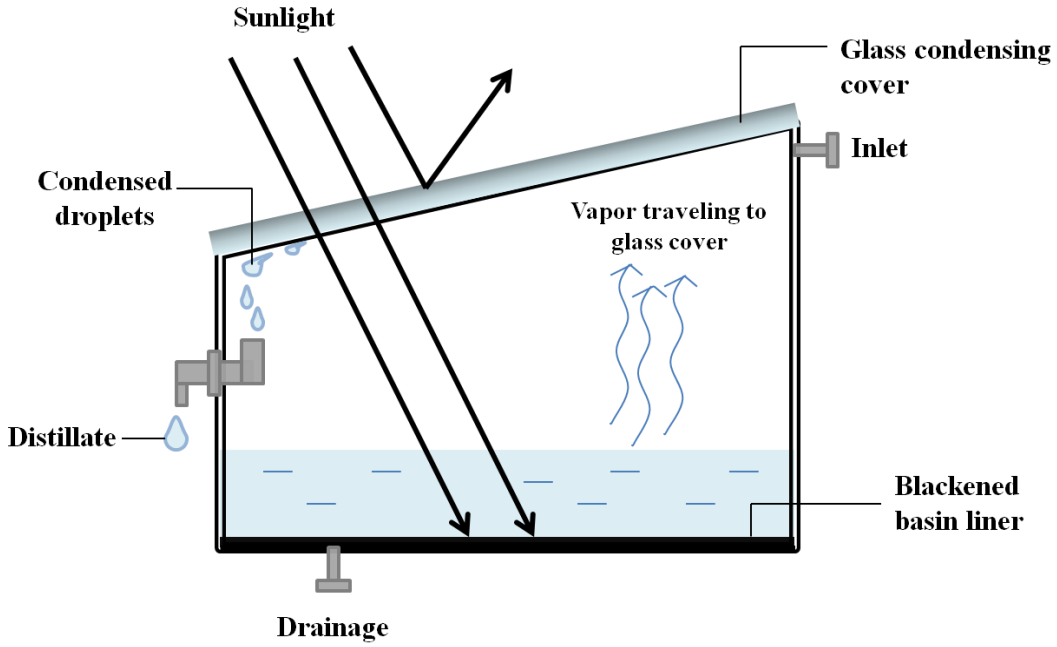

Figure 2.2 Summary of processes taking place in a solar still (modified from Tiwari et al., 2003).

Solar stills are reported to be successful in removing non-volatile contaminants and bacteria if care is taken to avoid contamination from the raw water source (Qiblawey and Banat, 2008). However, solar stills had mixed success insofar as the removal of volatile organic compounds such as pesticides (Hanson et al., 2004). Detailed reviews of solar stills and factors affecting their performance are available

(Tiwari et al., 2003; Kaushal and Varun, 2010; Sampathkumar et al., 2010; Kabeel and El-Agouz, 2011; Velmurugan and Srithar, 2011).

A *portable* pyramidal still made from poly(vinyl chloride) has been designed that is capable of delivering 0.5 L/d at a cost of 0.046/L (Wassouf et al., 2011). However, due to their low productivity, solar stills are suitable for individual use only. Hence, they are practical only for applications when the affected area has intense solar radiation and no fresh water supply.

2.2.1.4 Methods involving integrated treatment

Water can often be contaminated by multiple species, such as dissolved inorganics, organics and particulates including pathogens. To handle this, some integrated systems with several separation steps have been used. These systems usually have a high production rate making them appropriate for community-level intervention. For instance, Garsadi et al. (2009) reported a water-treatment plant installed in a truck known as the micro-hydraulic mobile water-treatment plant (MHMWTP). It includes hydraulically driven coagulation/flocculation, plate sedimentation, rapid filtration, optional GAC filtration and chlorination. It was used following the 2004 Tsunami in Aceh and a modified version was used for disaster relief in Indonesia. A similar mobile system was developed that incorporates coagulation, flocculation and a separator for particulate and turbidity removal, and an ion exchanger for post-treatment (Northcott et al., 2007).

2.2.2 Membrane-based water technologies

Membrane processes are classified based on the driving force for separation such as pressure, temperature and osmotic differences across the membrane (Mulder, 2000; Fane et al., 2011). Pressure-driven membrane processes are subclassified based on the membrane pore size into microfiltration (MF), ultrafiltration (UF), nanofiltration (NF) and reverse osmosis (RO) (Mulder, 2000; Fane et al., 2011). An emerging

membrane technology is forward osmosis (FO) whose driving force is an osmotic gradient (Cath et al., 2006).

The main advantages of membrane processes are the production of clean water in a single step, a small footprint, and modularity that enables easy scale-up and shipment. Thus, membrane-based WTs can be applied at all stages of an emergency and any intervention level. However, they are plagued by membrane fouling and usually have a higher energy requirement than conventional WTs. Nevertheless, some membrane-based systems are superior with respect to cost and permeate quality (Fane, 1996; Madaeni, 1999). These advantages in addition to their lightweight, simplicity, and scalability underlie the current trend to deploy membrane-based WTs for disaster relief. Membrane companies such as Norit, Kächer Futuretech, Berkefeld, HTI, Siemens, Veolia, GE Zenon, and others now deploy membrane systems for disaster relief.

2.2.2.1 Pressure-driven membrane processes

Microfiltration (MF)

The most widely used small-scale MF system is the ceramic filter (CF). CFs can be made locally by firing a mixture of clay and a combustible filler such as rice husk or sawdust that after burning creates pores (Murphy et al., 2009; van Halem et al., 2009; Archer and Elmore, 2010). CFs are also available as candle filters. Some commercial candle filters have a hollow core filled with GAC such as that deployed by Oxfam GB after the flooding in the Dominican Republic (Clasen and Boisson, 2006).

The microbiological removal efficiency of CFs determined from the decrease in *E. coli* (Bielefeldt et al., 2010; Brown and Sobsey, 2010) and thermotolerant coliforms (TTC) (Clasen et al., 2004b) was considerable. However, viruses are removed to a lesser extent (Bielefeldt et al., 2010; Brown and Sobsey, 2010). CFs resulted in 49% reduction of diarrheal cases in Cambodia (Brown et al., 2008) and 70% in Bolivia (Clasen et al., 2004a). CFs impregnated with silver to improve their bactericidal

effects led to mixed results. van Halem et al. (2007) found that the silver particles significantly enhanced the biocidal effect. Others found no significant difference in microbial reduction in the effluent of silver-augmented receptacles (Murphy et al., 2009) or filters (Bielefeldt et al., 2010; Brown and Sobsey, 2010).

A major drawback of CFs is the low water throughput. An option to increase throughput is to use a bicycle-powered system with a sand filter and CF (McBean, 2009). Konieczny and Klomfas (2002) reported that adding 100 mg/L of PAC or GAC in the raw water prior to ceramic MF resulted in a stabilized flux 15% to 30% higher than using MF alone. Portable MF technology is also available commercially such as the Katadyn Mini (2011) that uses a ceramic MF membrane impregnated with silver. Independent laboratory testing of the system with respect to *E. coli* removal showed 3 and 1.7-4.9 LRV in clear and turbid waters, respectively, making it among the best portable filters (Schlosser et al., 2001). Recently, CFs were reported to have sustained arsenic levels above the World Health Organization (WHO) standard of 0.01 mg/L (van Halem et al., 2007). This arsenic came from contaminated clay used in preparing the ceramic filters (Archer and Elmore, 2010).

Ultrafiltration (UF)

UF systems are commonly used in disaster relief because of their excellent rejection of bacteria and viruses as well as turbidity (Laîné et al., 2000). The LifeStraw® filter (Vestergaard) is a portable straw-like POU UF technology. Clean water is produced as raw water is sucked through the UF membrane embedded in the straw. Independent laboratory testing showed that the LifeStraw® was effective in producing microbiologically safe water (LifeStraw, 2007; Clasen et al., 2009; Boisson et al., 2010).

A randomized, placebo-controlled field assessment of the LifeStraw® conducted in the Congo showed that it reduced diarrheal lapses by 15%, which was not statistically significant when compared to the placebo (Boisson et al., 2010). However, these results may underestimate its performance because the placebo removed more than 1 LRV of the TTC in the field, but was microbiologically

ineffective in the laboratory testing (Boisson et al., 2010). It is believed that the placebo's microbiological effectiveness in the field was due to biofilm formation on the placebo cartridge under longer term operation. Other portable UF systems are also available (Peter-Varbanets et al. 2012; Pryor et al., 1998; Groendijk and de Vries, 2009; Peter-Varbanets et al., 2010; Frechen et al., 2011).

He (2009) designed a mobile UF system that can be transported and powered by a bicycle. Raw water is pumped into the module by pedaling the bicycle. Another mobile UF system using membrane modules housed on a fire engine was reported (Barbot et al., 2009). Examples of modular UF systems are the Skyhydrant^{TM} (Butler, 2009) by the Skyjuice Foundation and a UF pilot plant designed by the University of Valencia through the AQUAPOT project (Arnal 2001; 2004; 2007; 2008; 2009; 2010).

Nanofiltration (NF)

NF membranes are typically used to reject multivalent ions as well as dissolved organics (Fane et al., 2011), but cannot be used alone to desalinate water (Greenlee et al., 2009). Oh et al. (2000) developed a membrane process that uses an NF module coupled to a stationary bicycle to generate energy required for pressurizing the feed.

Reverse osmosis (RO)

In general, RO membranes have high rejection for a wide range of contaminants including radionuclides. Consequently, they have better versatility in cases when the water quality is uncertain. The effectiveness of RO in rejecting radionuclides such as ^{238}U, ^{234} U, ^{137}Cs and Ra has been documented (Hsiue et al., 1989; Huikuri et al., 1998; Arnal et al., 2003a; 2003b; Arnal et al., 2005). Tagami and Uchida (2011) reported that an RO filter reduced ^{131}I by more than 95% following the 2011 Japanese earthquake. However, RO systems are not always the best choice due to their high energy consumption and the absence of a power supply after disasters. Thus, RO is practical only when there is no fresh water supply or the water quality is uncertain and when an adequate power source is available.

Solar energy can be harnessed onsite to power RO systems using photovoltaic (PV) panels. Several modular PV-RO systems have been reported (Herold et al.; Tzen et al., 1998; Herold and Neskakis, 2001; Richards and Schäfer, 2002; 2003; Masson et al., 2005). Wind energy can also be harnessed onsite for RO desalination. Robinson et al. (1992) reported a modular RO system for brackish water desalination powered by a wind pump.

Small-scale RO systems that do not use renewable energy are usually powered by an electric generator (Malik et al., 1989; Bagwell et al., 1994; Downing et al., 1994; Harris, 2000; Elfil et al., 2007). A mobile RO demonstration plant for brackish-water desalination has also been reported (Shah et al., 1988). An innovative mobile floating seawater desalination plant known as the PCS® was reported by Lampe et al. (1997).

2.2.2.2 Osmotically driven membrane processes

Forward osmosis (FO)

FO technology is attractive because it can achieve a rejection as high as that of RO for a wide range of contaminants with no applied pressure (Holloway et al., 2007). FO technology in the form of a filter pouch is commercially available (HTI, 2010a; b). It consists of double-lined FO membrane filled with a concentrated sugar-based draw solution. It is reusable after recharging with fresh draw solution. The outer compartment is filled with contaminated water while the inner compartment is allowed to swell as water diffuses across the FO membrane owing to the osmotic pressure difference. This dilutes the initial draw solution that can then be consumed as a sweet drink for nutrients and minerals. The filter pouch has been used successfully for disaster relief after the Haiti earthquake (HTI, 2010a) as well as for military applications (Cohen and Ross, 2004). The potential of the filter pouch for emergency purification of a small amount of brackish water has been demonstrated in the laboratory (Wallace et al., 2008). However, Cath et al. (2006) pointed out that it may have limited application since it does not produce water *per se* but a sweetened drink. Furthermore, it may be prone to rapid bacterial re-growth.

Nevertheless, due to its compact packaging, it is suitable for acute emergencies when there is no fresh water source. Note that due to the low productivity, it is only suitable for individual use.

2.2.2.3 Thermally driven membrane processes

Membrane distillation (MD)

MD is a hybrid separation process consisting of three steps: (i) evaporation of water on the feed side; (ii) migration of water vapor to the permeate side via membrane pores; and (iii) condensation of water vapor on the permeate side (Bouguecha et al., 2005; Susanto, 2011). The driving force for MD is the vapor pressure difference due to a temperature gradient between the feed and permeate sides (Susanto, 2011). Therefore, it requires only a moderate working temperature that can be achieved using a solar thermal collector (50°C to 90°C) (Banat et al., 2002; Blanco Gálvez et al., 2009). By coupling MD with a solar thermal collector as the energy source, MD might find potential use for disaster relief in areas with intense solar radiation and only seawater or brackish water as the available source. One example of small-scale MD is the compact SMADES WT (Banat et al., 2007; Fath et al., 2008). The energy required for heating the feed water for desalination in SMADES is supplied entirely by solar thermal collectors, while a photovoltaic (PV) panel supplies electrical auxiliary energy.

2.3 Comparison of technologies: appropriateness for specific scenario

This section discusses the limitations and strengths of the technologies reviewed in Section 2.2 with regards to their application for disaster relief. It is important to understand the strengths and weaknesses of the WTs available so that a judicious choice of WT can be made for a given disaster scenario.

BSF has a reasonable removal of pathogens and is documented to be effective in reducing diarrheal risks. In addition, no additional cost is required. However, the major drawback of BSF is its low throughput. Hence, it is only suitable for use at the household level. Since it requires regular maintenance to achieve a reasonable flux, it is not suitable for use during the acute emergency stage when the AP may not have the resources to do this. It can be more appropriate for application in the later stage of emergency.

Pressure filters are effective in reducing turbidity and have high water throughput. However, poor maintenance and loss of filter media can result in substandard performance and reduced efficiency (Pryor et al., 1998). In addition, pressure filters are also prone to clogging when used to treat high turbidity water. Pressure filters are not suitable for rapid response because they require a long start-up time.

Alternatively, clarifiers can be used to treat raw water with high turbidity. However, the use of a clarifier requires operational control and accurate determination of coagulant dosage. This can be done only by a qualified operator who might not be available in relief camps. In addition, the disposal of metal-hydroxide wastes can result in some disposal problems.

The disinfection efficacy of chlorination has been well-documented. However, a major issue with the use of chlorination for emergencies is the difficulty in determining the correct dose for disinfection. The taste problem is another challenge, especially if the raw water has a high organic content. This could lead to reduced social acceptance of the WT. Formation of DBPs is also a problem with chlorination.

PuR® sachets can be distributed easily during emergency due to their compact packaging. In addition, their disinfection efficiency is not affected by turbidity. Hence, they are suitable for application in the acute stage when the surface water is highly contaminated. However, they involve the formation of a chemical precipitate that gives rise to a disposal problem. In addition, PuR® requires the presence of a

supply chain for continued use. Hence, this WT is not suitable for long-term use unless a supply chain is established.

AC adsorption can remove certain chemicals and organics. However, its adsorption capacity is exhausted quickly. Hence, frequent replacement is needed. This will result in an increased ongoing cost and the need for a supply chain. Another drawback of AC is its ineffectiveness for microbial removal. AC adsorption is not suitable for long-term use. It can be suitable for use in the acute emergency stage if used in combination with other WTs.

Boiling has a high potential acceptance by users since it coincides with the practice of most cultures. In addition, its disinfection efficiency has been well-documented although there are some controversial results on its health impact. Boiling is suitable for use in the acute or later stage of an emergency if the price of fuel at the area of interest is reasonably low.

The *Chulli* water purifier and WADIS do not require additional time or operating cost to treat water. Their use in the acute stage is not possible due to their long start-up time. However, they are suitable for use in the later stage of an emergency. Proper storage of the treated water is required to prevent post-contamination.

SODIS is simple to use and requires essentially no maintenance. However, its disinfection efficiency is affected by turbidity and weather. Therefore, it is only suitable for use in areas with high solar radiation. In places where there is no access to PET bottles, a supply chain needs to be established for continued use of the WT. East Lombok is a successful example of a bottle-supply scheme through the creation of a microenterprise (Meierhofer and Landolt, 2009).

UV can disinfect water rapidly with high throughput. However, it is expensive and has an efficiency that is affected by turbidity. In addition, it does not provide residual protection. It is not suitable for long-term use because it requires

specialized parts replacement (UV lamps). Hence, it needs to be used in combination with another WT to be appropriate for acute applications.

A solar still system is easy to operate and maintain. It can produce very pure water even from saline sources. The main problem with this technology is its low thermal efficiency that results in the need to use a large solar collector area and a very low production rate. Hence, it is only practical for use when the affected area is located in a region with solar irradiation and does not have access to fresh water supply.

Household CFs can be used to treat turbid water and provide reasonable microbial removal. However, they have a low water throughput and are prone to breakage. In addition, CFs have a variable quality due to differences in the firing process. Since CFs require regular maintenance, they are not suitable for use in the acute stage. They can be more suitable for long-term use.

In general, membrane processes are compact and have a low aerial and chemical footprint. In addition, they can remove a wide range of contaminants and provide disinfection at the same time. Hence, membrane filters qualify as a rapid response technology for disaster relief. They also can be used for long-term applications. However, replacement of the membranes that requires the presence of a supply chain can be a problem.

Membrane desalination processes such as RO and MD are relatively energy-intensive. Renewable energies can be harnessed by using solar panels and wind turbines to supply the energy required for desalination. Although renewable energy is essentially free, the equipment used to convert it to a useful form is not free (Abraham and Luthra, 2011). PV panels come with high capital cost and the need for battery replacement (Lacayo and Mauzerall, 2006). These might not be available locally. Hence, they are appropriate only when there is no available fresh water supply.

Membrane desalination by FO is attractive because essentially no hydraulic pressure is required. However, a major challenge with the use of FO is the use of an

appropriate draw solution. Cath et al. (2006) pointed out that the FO filter pouch may have limited application since it does not produce water *per se* but a sweetened drink. In addition, the water throughput is very low. However, due to its compact packaging, it is suitable for use in the acute stage of an emergency when there is no fresh water source.

In conclusion, each WT has its strengths and limitations, thus, there is no panacea for emergency drinking-water response. Table 2.3 provides a summary of the merits and drawbacks of each WT. Due to the vastly varying scenarios for different disasters, it is impractical to adopt a singular solution for every disaster. The WT selection process is not straightforward. It depends on the characteristics of the emergency, nature of the water source and the technical aspects of the WT. As such, Appendix B details a methodology for selection of an emergency WT based on compensatory multi-criteria analysis. Furthermore, the critical analysis of the review presented in Section 2.2 indicates the lack of early-stage emergency WTs that are effective, robust, easily deployable, and infrastructure-independent. Therefore, there is a need for new and innovative technologies that are directed to applications in this neglected area.

Table 2.3 Comparison of the strengths and limitations of key water technologies

Major WTs	Strengths	Weaknesses
Biosand filter	No chemicals required; simple to use; can be constructed using local materials; documented reduction of protozoa and bacteria; one-time cost only; documented reduction of diarrheal risks	Disinfection efficiency affected by turbidity; long start-up time (filter ripening); low throughput; require regular maintenance; poor virus removal; no residual protection
Pressure filter	Effective in reducing turbidity; high throughput; compact and easy to deploy	Requires regular maintenance; needs replacement of filter media; prone to clogging; not suitable for treatment of high turbidity water
Clarifier	Can treat highly turbid water; high throughput; removes NOMs	Long start-up time; need to use chemicals; need skilled personnel to determine proper coagulant dosage; potential disposal problem
Chlorination	Provides residual protection; inexpensive; documented reduction of most bacteria, protozoa and viruses; documented health improvement	No visible improvement in water quality; potential taste problem; formation of DBPs; disinfection efficacy affected by turbidity; *cryptosporidium* unaffected by chlorination; difficult to determine proper dosage
Combined coagulant-disinfectant powder	Long shelf life; easy to transport; can be used to treat highly turbid water; visible improvement in water quality; removes some chemical contaminants (arsenic); removes DBP precursors	Need supply chain; multiple steps required for treatment; may not have sufficient residual protection; potential disposable problem
Adsorption	Can remove chemicals, radionuclides and organics	Needs frequent replacement; not effective for microbial removal; expensive
Boiling	Disinfection efficiency not affected by turbidity; possible high social acceptance; simple to use; documented inactivation of bacteria, viruses and protozoa	No residual protection; costly due to use of fuel; lack of epidemiological confirmed health impact; incomplete treatment if users do not bring it to a boil
Thermal pasteurization	Takes place at lower temperature than boiling; no additional time and operating cost; high water throughput	No residual protection; *Chulli* tends to break
SODIS	Easy to use; essentially no maintenance and ongoing cost; documented reduction in diarrheal diseases	Need supply chain for PET bottles; disinfection efficiency affected by many factors; long treatment time; low yield; cannot treat turbid water
UV disinfection	Rapid disinfection; high throughput	No residual protection; cannot treat turbid water; expensive; need replacement of specialized parts
Solar stills	Can disinfect and desalinate; simple; low-cost operation and construction; simple maintenance	Low yield; need larger land area than indirect solar desalination; only suitable for arid regions; low thermal efficiency; productivity affected by weather
Household ceramic filters	Can be made using locally available materials; simple; documented reduction of protozoa and bacteria; potential long life of CFs if not broken; visual improvement in treated water	No residual protection; leaching of some metals including arsenic; low throughput; prone to breakage; requires regular maintenance; variable quality of CFs produced; not effective in virus removal
Low Pressure Membrane	Can disinfect without the use of chemicals; performance not affected by feed water quality; potential simple automation; removes DBP precursor; compact and small footprint	Fouling; requires operation control; frequent backwashing required
High Pressure membrane	Versatile; low energy consumption for desalination; compact and small footprint	Requires proper storage of membrane for intermittent use; potential brine disposal problem; extensive pretreatment required; prone to operational failure due to the use of high pressure parts; treatment limited by osmotic pressure
FO filtration bags	No pressure requirement; versatile; less prone to clogging/fouling; no maintenance	Low yield; expensive; does not produce pure water but sweetened drink; may be prone to bacterial re-growth
Membrane distillation	Can use low grade heat; compact and small footprint; less pretreatment requirement compared to RO; not limited by osmotic pressure; intermittent operation possible with no danger of membrane damage in dry conditions	High energy requirement; no commercial MD membrane; requires handling of hot water; membrane wetting problem

2.4 Application of silver nanocomposites for water disinfection

As mentioned earlier, microbial contamination of potable water sources is one of the major threats to public health in the aftermath of disaster. Various antimicrobial agents have been developed to combat microbiological contamination of potable water sources that threatens public health. Among them, silver in the form of a nanoscale material has been widely recognized as an excellent antimicrobial agent because of its broad-spectrum antimicrobial activity and low-toxicity to human cells (Balogh et al., 2000; Liu et al., 2012; Alonso et al., 2013).

The bactericidal effects of AgNPs include impairment of functional biomolecules such as enzymes, DNA, and membrane proteins through the action of dissolved Ag^+ ions and the physicochemical effects specific to the nanoparticles (Nel et al., 2006; Eckhardt et al., 2013; Lemire et al., 2013; Suresh et al., 2013; Rizzello and Pompa, 2014). Due to the excellent antimicrobial properties of AgNPs, they are now widely used in various consumer products. The increased exposure of Ag in the environment has raised concerns regarding the emergence of resistant bacteria that are able to reproduce even in the presence of a high concentration of Ag species.

Ag-resistant bacteria was first isolated from a burn wound that was treated with $AgNO_3$ (Jelenko, 1969). Thereafter, there have been increasing reports documenting the isolation of Ag-resistant bacteria from various environments that have been exposed to Ag (Summers, 1978; Charley and Bull, 1979; Haefeli et al., 1984; Pumpel and Schinner, 1986; Chouhury and Kumar, 1998; Silver, 2003; Davis, 2005; Holland et al., 2011; Kremer and Hoffmann, 2012; Gunawan et al., 2013). The mechanisms of Ag resistance bacteria have been proposed to involve (i) the transcriptional downregulation of porins (ie., outer membrane protein, Omp in the cell wall of Gram-negative bacteria), which allow the passage of antimicrobial agents (along with substances required for cell metabolism) resulting in a lowered intracellular concentration of the antimicrobial agent (Livermore, 1992), and/or (ii) activation of efflux pumps that actively transport the toxic agents out from the cell (Nikaido and Takatsuka, 2009). Chopra (2007) suggested that the risk of Ag resistance can be minimized by using composite materials that can release a high

dose of Ag^+ ion with a rapid bactericidal activity because microbes are more likely to be disinfected, thereby reducing the possibilities for enrichment of the resistant population through growth and division, especially in the context of mutational development of resistance.

For enhanced bactericidal activity, fine AgNPs are preferred due to their with higher specific surface area (Morones et al., 2005; Panáček et al., 2006; Pal et al., 2007; Choi and Hu, 2008; Zhang and Oyanedel-Craver, 2012). However, fine AgNPs tend to aggregate with a consequent decrease in their disinfection performance. Another practical issue to be addressed is the recovery and separation of the AgNPs from the treated water that may be time- and energy-consuming, and limit their reusability. As summarized in Table 2.4, to address the aforementioned issues, a wide range of materials such as activated carbon, ceramic filters, hydrogels, cellulosic papers, polyurethane foams, resins, and rice husks have been employed to support AgNPs for water disinfection applications (Jain and Pradeep, 2005; Oyanedel-Craver and Smith, 2007; Gangadharan et al., 2010; Dankovich and Gray, 2011; Alonso et al., 2013; He et al., 2013; Lin et al., 2013). This strategy minimizes aggregation of the AgNPs and allows simultaneous separation from the treated water since the AgNPs are retained in the support material. Furthermore, the lifespan of the supported AgNPs can be enhanced due to controlled release of dissolved Ag^+ that enables long-term applications.

Table 2.4 Summary of the performance of Ag-modified materials for point-of-use water disinfection

Material	Operation mode	Bacterial inactivation efficiency (LRV/min)	Advantages	Disadvantages	Reference
Polymeric spheres containing AgNPs	Batch	0.04	Easy to deploy due to its lightweight	Need filtration to recover the polymeric spheres after treatment; low antibacterial efficiency	(Gangadharan et al., 2010)
Ceramic filers impregnated with AgNPs	Filtration	0.04	Ceramic filter is inexpensive and robust	Low water throughput; filter prone to clogging; low antibacterial efficiency	(Oyanedel-Craver and Smith, 2007)
Magnetized nanoscavengers containing AgNPs	Batch (recovery using magnetic trapping)	0.2	Capping layer can be functionalized to degrade organics or adsorb heavy metal ions	Need magnetic field and additional time to recover nanoscavengers after treatment; relatively low antibacterial efficiency	(Zhang et al., 2013)
Fibrous ion-exchange polymer containing AgNPs	Column	0.5	Easy to deploy due to its lightweight; can have high Ag-content due to its high ion-exchange capacity	Need pumping system and good operational control; relatively low antibacterial efficiency - several recirculation cycles may be required to achieve the desired disinfection level	(Alonso et al., 2011a; Alonso et al., 2011b; Alonso et al., 2013)
AgNPs coated resin gel beads	Column	0.5	Good antibacterial activity during initial use; easy to deploy due to its lightweight	Need pumping system and good operational control; antibacterial properties deteriorate substantively after breakthrough	(Mthombeni et al., 2012)
Activated carbon impregnated with AgNPs	Batch	0.7	Easy to deploy due to its lightweight	Activated carbon is expensive; need filtration to recover the activated carbon after treatment	(Srinivasan et al., 2013)
AgNPs-impregnated paper	Filtration	0.8	Low-cost support material; easy to deploy and highly portable	Relatively long treatment time (10 min of average percolation time); reusability may be limited by the durability of the papers used	(Dankovich and Gray, 2011)
AgNPs-coated polyurethane foam	Batch and column	1.2	High water throughput; robust support material; easy to deploy and highly portable	Stability of the AgNPs incorporated unclear	(Jain and Pradeep, 2005)

Table 2.4 Summary of the performance of Ag-modified materials for point-of-use water disinfection (continued)

Material	Operation mode	Bacterial inactivation efficiency (LRV/min)	Advantages	Disadvantages	Reference
Silica beads	Column	1.2	Easy to deploy due to its lightweight	Need pumping system and good operational control	(Quang et al., 2011; Quang et al., 2013)
Alginate beads containing AgNPs	Column	6	Simple synthesis of alginate beads; high water throughput; can be easy to deploy due to the lightweight of dried gels; rapid bacterial disinfection	Need pumping system and good operational control; washing of excess reagent may be difficult due to the nonporous structure; dried gel beads may take a long time to re-swell to equilibrium for column operation	(Lin et al.)
Polyurethane sponge or cotton textile coated with carbon nanotubes and Ag nanowires	Filtration (with electric field)	360	Low-cost support materials; rapid bacterial disinfection; easy to deploy due to its lightweight	Need electricity to achieve high rate of disinfection; need pumping system and good operational control; relatively low water throughput	(Schoen et al., 2010; Liu et al., 2013)

Note: the bacterial inactivation efficiency was calculated by normalizing the highest bacterial (E. coli) inactivation reported in the papers with respect to their average contact times or time taken to achieve the log reduction value (the longer time was used for calculation).

Nonetheless, one disadvantage of incorporating AgNPs in a dense support material is the possibility of reducing the accessibility of the AgNPs for interaction with the target bacteria. Furthermore, their applications may be limited due to some operational drawbacks. For example, composites being applied in the form of suspensions require an additional energy-demanding separation step such as filtration and magnetization. On the other hand, filtration-based systems (e.g., papers or membranes) usually have low water throughputs because of the long treatment and percolation times). In particular, operation in the column mode requires the use of sophisticated pumping systems for operational control that may be challenging under limited conditions. Therefore, in addition to being low-cost and robust, an ideal support material should have high porosity with micrometer-size pores to allow enhanced cell-AgNP interaction. Furthermore, the disinfection rate can be accelerated if the support material could provide some driving force for the bacterial cells to approach the AgNPs. From an operational perspective, it is also crucial if the selected support material could enable a simple approach to recover the treated water while retaining AgNPs within its matrix.

The support material chosen in this study is macroporous hydrogels prepared via cryogelation (or also known as cryogels). They can be effective support materials for AgNPs because the interconnected micrometer-sized pores allow maximum accessibility to the bacterial cells. They have been shown to have fast and substantial swelling as well as excellent mechanical properties. Because of their ability to rapidly imbibe water, this would drive the bacteria to flow into the cryogels whereby the latter can be exposed to the AgNPs supported on their pore surface. In addition, the remarkable elasticity of cryogels enable them to be used as antibacterial sorbents whereby the disinfected water can be readily recovered via a simple squeezing step (Fig. 1.1). In fact, polymeric cryogels such as alginate, chitosan, polyacrylamide, and poly(2-hydroxyethyl methacrylate) have been successfully used to support various nanomaterials (Yao et al., 2006b; Yao et al., 2007; Suwanchawalit et al., 2009; Savina et al., 2011a). Section 2.6 provides a comprehensive review on the synthesis, characterization and current applications of cryogels.

2.5 Classification of hydrogels

This section provides a brief introduction to hydrogels as background information for cryogels. A comprehensive overview on cryogels will be provided in Sections 2.6 to 2.8. Hydrogels are three-dimensional (3D) hydrophilic polymer networks that are capable of absorbing a large amount of water. They can be classified into chemical or physical hydrogels on the basis of the intermolecular bonds that crosslink the polymer network. Table 2.5 classifies hydrogels based on the mechanism used for gelation (Lozinsky et al., 2003).

Table 2.5 Classification of hydrogels and synthesis methods (Lozinsky et al., 2003)

Type	Mechanism of gel formation	Examples
Chemotropic hydrogels	Intermolecular chemical bonds resulting in a 3D covalent network	Hydrogels synthesized using monomers containing double bonds (e.g., acrylates, styrene, etc.), or specific functional groups that can be crosslinked (carboxylic acids, amines, etc.)
Ionotropic hydrogels	Ion-exchange reactions resulting in intermolecular ionic bonds	Hydrogels based on polyelectrolyte complexes such alginate-poly(lysine) and chitosan polyphosphate mixed matrices, etc.
Chelatotropic hydrogels	Chelating reactions giving rise to intermolecular coordination bonds	Hydrogels formed on addition of multivalent strongly-coordinating metal ions (e.g., Cu(II) or Co(II) to chitosan solutions or Cr(III) ions to carboxymethyl cellulose, or Ca to alginate solutions)
Solvotropic hydrogels	Gelation due to the changes of solvent composition – a result of a coacervation phenomenon	Cellulose nitrates and cellulose acetates
Thermotropic hydrogels	Gelation due to heating of an initial polymer system	Ovalbumin and egg-white gels
Psychrotopic hydrogels	Gelation caused by chilling (without freezing) of the initial polymer system	Gelatine, starch, agarose, and carrageenan hydrogels
Cryotropic hydrogels (cryogels)	Gelation conducted in a semi-frozen polymer system	These hydrogels constitute the topic of the present review

2.5.1 Hydrogels used for water and wastewater treatment

Hydrogels are traditionally used for biotechnological applications. However, there has been a recent increase in interest for applications in water- and wastewater-treatment processes. Table 2.6 summarizes the current applications of hydrogels in water- and wastewater-treatment processes.

Table 2.6 Summary of hydrogel applications in water and wastewater treatment

Application	Description	Hydrogel used	References
Disinfection			
Base materials for antimicrobial agents	Hydrogels immobilized with antimicrobial agents such as silver nanoparticles and chlorine-releasing compounds	Poly(acrylamide-*co*-acrylic acid) hydrogel-silver nanocomposite	(Thomas et al., 2007)
		Poly(acrylamide) hydrogel-silver nanocomposite	(Uygun et al., 2009)
		Poly(methacrylic acid) hydrogel-silver nanocomposite	(Gangadharan et al., 2010)
		Poly(sodium acrylate-*co*-1-vinyl-2-pyrrolidone) hydrogel-silver nanocomposite	(Lee and Huang, 2007)
		Poly(acrylamide) and poly(vinyl pyrrolidone) semi-IPN hydrogel-silver nanocomposite	(Murthy et al., 2008)
		Poly(acrylic acid) hydrogel containing hexamethylenetetramine	(Ahmed, 2011)
Wastewater treatment			
Adsorbent	The presence of various functional groups that can chelate heavy metals and dyes	Poly(pyrrolidone-co-acrylic acid)	(Shawky et al., 2006)
		Cellulose hydrogels grafted with acrylamide or acrylic acid	(Chauhan and Lal, 2003)
		Chitosan-coacervated calcium alginate hydrogel beads	(Vijaya et al., 2008)
		Chitosan/SiO_2 and chitin/SiO_2 hydrogels	(Copello et al., 2011)
		Poly(*n*-isopropylamide)/tributyl phosphate hydrogels	(Pan et al., 2008)
		Hyperbranched poly(etheramine) hybrid hydrogels	(Deng et al., 2012)
Immobilization agent of microorganisms in bioreactors	Immobilized microorganisms have greater tolerance to the toxicity of heavy metals /organics in the wastewater, and allow the retention of slow-growers	Gelatin hydrogels	(Liu et al., 2010b)
		Poly(*n*-vinyl pyrrolidone)-calcium alginate hydrogels	(Doria-Serrano et al., 2002)

Table 2.6 Summary of hydrogel applications in water and wastewater treatment (continued)

Application	Description	Hydrogel used	References
Desalination			
Forward osmosis draw solute	The swelling pressure of a dried (or de-swollen) hydrogel drives the permeation of water across the FO membrane. Absorbed water can be recovered by a combination of thermal-mechanical compression or solar heating	Poly(acrylamide), poly(sodium acrylate), poly(*n*-isopropylamide), and poly(sodium acrylate-*co*- *n*-isopropylamide) hydrogels	(Li et al., 2011a)
		Carbon composites of poly(acrylamide), poly(sodium acrylate), poly(*n*-isopropylamide), and poly(sodium acrylate-*co*- *n*-isopropylamide) hydrogels	(Li et al., 2011b)
Thermoreversible ion-exchange resin	Hydrogel comprising weakly-basic and –acidic components. Salt removal occurs at ambient temperature while desorption occurs at a higher temperature	Poly(acrylic acid) hydrogel coated with ethoxylated polyethyleneimine resin	(Chanda et al., 2009)
		Interpenetrating network of poly(acrylic acid) hydrogel and with ethoxylated polyethyleneimine	(Chanda et al., 2010)
Integral desalination membrane	During swelling, salt-depleted water was absorbed into hydrogel. Absorbed (desalinated) water was recovered by compression	Poly(acrylic acid) hydrogel	(Höpfner et al., 2010)
Liquid/liquid separation			
Oil/water mixture separation	The hydrogel-coated mesh acted as a filter for an oil/water mixture. The hydrated hydrogel had low oil-adhesion and this allowed water to selectively permeate through the mesh	Polyacrylamide hydrogel layer coated on stainless steel mesh	(Xue et al., 2011)

However, the applications of hydrogels have been limited due to their relatively poor mass-transfer efficiencies and mechanical properties. Porous hydrogels are thought to have improved mass-transfer properties. The presence of a large number of pores could allow faster water absorption and desorption by osmotically driven bulk flow due to the higher surface/volume ratio (Omidian et al., 2005; Liu et al., 2009a). Gas foaming (Kabiri et al., 2003), micro-emulsification (Bennett et al., 1995), phase separation (Gopishetty et al., 2012), freeze-drying (Deng et al., 2012), and porogen leaching (Kemal et al., 2011) have been used to produce macroporous hydrogels. Although these methods improved the swelling properties of hydrogels, the mechanical properties were not significantly enhanced.

Cryogelation is a unique technique used to synthesize macroporous hydrogels having tissue-like elasticity that can withstand extensive deformation without mechanical degradation (Plieva et al., 2008c). This technique involves the formation of a polymeric network in a semi-frozen system in which the solvent crystals act as porogens (Arvidsson et al., 2002; Lozinsky et al., 2003; Lozinsky, 2008). Cryogels have been reported to exhibit remarkable mechanical properties and superfast swelling ability (Ozmen and Okay, 2005; Dinu et al., 2007; Topuz and Okay, 2009; Orakdogen et al., 2011). The following sections will provide an overview of the synthesis and characterization of cryogels. In the later section, current applications of cryogels will be highlighted.

2.6 Fabrication of cryogels and synthesis factors affecting their properties

This section provides some fundamental background on the formation of cryogels. The effects of synthesis conditions on the properties of cryogels will be discussed in the later part of this section.

The processes involved in the formation of cryogels are summarized in Fig. 2.3. Cryogels are synthesized by conducting crosslinking reactions at a subzero temperature in a semi-frozen condition (Lozinsky, 2002; Lozinsky et al., 2003; Lozinsky, 2008). As shown in Fig. 2.3, the semi-frozen system is heterogenous and contains an unfrozen liquid microphase (UFLP) along with ice crystals.

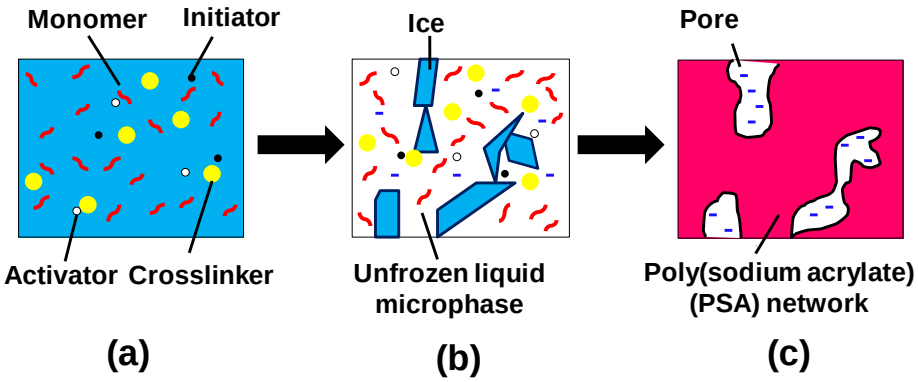

Figure 2.3 Conceptual diagram of the formation of a polymeric cryogel: (a) inital system, (b) frozen system in which crosslinking reactions take place in the UFLP, and (c) thawed cryogel (modified from Lozinsky et al., 2003). Note: the illustration was not drawn to scale.

According to Lozinsky (2014), the three key requirements for the preparation of cryogels include: (i) the solvent used must undergo crystallization rather than vitrification under the conditions used for cryogelation; else, the UFLP cannot form and hence no cryo-concentration effect; (ii) the solubility of the precursors used (especially for the case of monomers) should be sufficiently high in the UFLP (i.e., at subzero temperature) to ensure that the critical concentration of gelation can be reached; and (iii) the redox initiating systems used must be able to generate radicals at subzero temperatures.

During cryogenic treatment, water starts to freeze whereas the dissolved solutes accumulate in the UFLP. This phenomenon is commonly known as cryo-concentration. At temperatures above the eutectic point, the solute concentration in UFLP increases until it reaches the equilibrium concentration, which is governed by the freezing-point depression (Ozmen and Okay, 2005; Kirsebom et al., 2008). The extent of the freezing-point depression, ΔT_f is defined as the difference between the freezing points of the pure solvent and solution:

$$\Delta T_f = T_f^0 - T_f \quad (2.1)$$

whereby T_f^0 and T_f are the freezing points of the pure solvent and solution, respectively. By assuming that (i) only pure water freezes out of the reaction mixture when cooled to its freezing temperature and (ii) the gel phase, which is formed from the UFLP, is in thermodynamic equilibrium with the ice crystals, the following relationship is obtained (Ozmen and Okay, 2005):

$$\frac{1}{T_f} = \frac{1}{T_f^0} - \frac{R}{\Delta H_m}\left[\ln(1 - v_{gel}) + v_{gel} + \chi v_{gel}^2 + 0.5 v_{eff} V_m v_{gel} - f v_{gel}\right] \quad (2.2)$$

whereby R is the molar gas constant, ΔH_m is the molar enthalpy of fusion for pure crystallized solvent, v_{gel} is the volume fraction of polymer in the gel or the UFLP, χ is the polymer-solvent interaction parameter, v_{eff} is the effective crosslink density of the UFLP or the polymer network after polymerization, V_m is the molar volume of solvent, and f is the effective charge density (i.e., the fraction of charged units in the network chains that are effective in gel swelling). The polymer concentration, C, which is defined as the polymer mass in 100 mL of solution is related to v_{gel} in the following equation (Ozmen and Okay, 2005):

$$C = 100 v_{gel} \rho \quad (2.3)$$

whereby ρ is the polymer density. Therefore, the equilibrium concentration in the UFLP is independent of the initial monomer concentration. However, the amount of UFLP is determined by the initial monomer concentration (Ozmen and Okay, 2005; Kirsebom et al., 2009). By assuming complete monomer conversion, the volume fraction of ice, f_{ice} can be computed according to the following equation:

$$f_{ice} = 1 - \frac{C_0}{C} \quad (2.4)$$

whereby C_0 is the initial monomer concentration. Polymerization reactions take place in the UFLP that give rise to a macroporous polymer network after thawing. It has been shown that some water is not frozen below the bulk freezing point due to the freezing-point depression as the reaction precursors are concentrated in the UFLP (Wolfe et al., 2002).

The essential feature of cryogelation is the crystallization of solvent (Plieva et al., 2009b). The growing ice crystals (for aqueous systems) function as the porogen, which dictates the shape and size of the pores that develop after thawing the sample (Plieva et al., 2008c). Cryogels usually have an interconnected pore structure because the ice crystals grow until they impinge upon one another to reduce the surface tension during cryogelation. However, crystallization of the solvent should take place prior to polymerization to obtain interconnected pores (Kirsebom and

Mattiasson, 2011). It has been shown that post-freezing of preformed hydrogels did not produce properties unique to cryogels (Xue et al., 2004). Thus, macroporous hydrogels obtained by post-freezing (such as those porous hydrogels reported by (Zhang and Zhuo, 1999a; b; Zhang et al., 2002; Suwanchawalit et al., 2009; Nieto et al., 2010) are not considered to be true cryogels.

Polymers, monomers and crosslinkers can be crosslinked to form physically-, ionically-, or covalently-crosslinked cryogels. Physically crosslinked cryogels, whose formation is driven by noncovalent interactions at subzero temperatures, have been synthesized from various materials including poly(vinyl alcohol) (PVA) (Domotenko et al., 1988; Lozinsky et al., 1996; Lozinsky, 1998; Lozinsky and Damshkaln, 2003; Hernández et al., 2004; Podorozhko et al., 2010), β-glucan (Lazaridou and Biliaderis, 2004; Lazaridou et al., 2008), galactomannans (Doyle et al., 2006), xanthan (Giannouli and Morris, 2003), and collagen (Podorozhko et al., 2000). These cryogels can be synthesized via a freeze-and-thaw strategy due to their thermal reversibility.

The major obstacle in the formation of ionically crosslinked cryogels is the high rate of gelation that proceeds even during component mixing (Lozinsky, 2002). Consequently, it is virtually impossible to freeze the system while it is still in the liquid state. A typical example is the synthesis of calcium alginate cryogels. Two approaches can be used to overcome this problem. The first approach was suggested by Lozinsky (2002) that involved the use of a salt having a negative solubility dependence on temperature (solubility of the salt increases with decreasing temperature) to conduct the crosslinking reaction. Examples of such salts are calcium butyrate, pentanoate, succinate, glycerophosphate, etc., (Seidel, 1953). Another strategy that can be employed to synthesize ionic cryogels is freeze-gelation. This technique involves two steps: (i) freezing of the polymer precursor, and (ii) crosslinking with a counter-ion dissolved in a nonsolvent. The nonsolvent is chosen such that the counter-ion has a high solubility in it and does not freeze at the temperature at which the synthesis is being conducted. An example is $CaCl_2$ dissolved in ethanol. Several researchers have used this technique to synthesize calcium alginate cryogels (Ho et al., 2004; Yuan et al., 2009). Chitosan and

carboxymethyl cellulose cryogels have been synthesized using freeze-gelation by replacing $CaCl_2$ with NaOH and HCl, respectively (Ho et al., 2004; Hsieh et al., 2007; Yuan et al., 2009).

Covalently crosslinked cryogels are produced via two main approaches, namely through a crosslinking reaction with an appropriate crosslinker or via a radical-initiated polymerization reaction using suitable initiators (Plieva et al., 2009a). For the first approach, polymers such as chitosan, gelatin, agarose, and alginate can be crosslinked using glutaraldehyde, tripolyphosphate or N-(3-dimethylaminopropyl)-N'-ethylcarbodiimide hydrochloride (EDC-HCl) (Hsieh et al., 2007; Kirsebom et al., 2007; Tripathi et al., 2008; Kathuria et al., 2009; Savina et al., 2011b; Tripathi and Kumar, 2011).

Free-radical polymerization reactions have been among the most widely used techniques to prepare cryostructured materials from various monomers. They are often initiated by ammonium persulfate (APS) and *N,N,N',N'*-tetramethylethylenediamine (TEMED) to polymerize monomers such as acrylamide (AAM), 2-acrylamido-2-methylpropane sulfonic acid (AMPS), dimethylacrylamide (DMAAM) and *n*-isopropylacrylamide (NIPAM) with the crosslinker *N,N'*-methylenebis(acrylamide) (MBA) in a partially-frozen condition (Ozmen and Okay, 2005; 2006; Dinu et al., 2007; He et al., 2007; Ozmen et al., 2007; Srivastava et al., 2007; Plieva et al., 2008c). An alternative to the APS/TEMED system is the use of water-insoluble dodecyldimethylbenzylammonium persulfate aggregates developed by (Zhao et al., 2011).

In free radical cryopolymerization, two possible situations may occur: (i) freezing before gelation or (ii) freezing after gelation (Plieva et al., 2006). The second case precludes the formation of a true cryogel. This issue can be overcome by proper control of the synthesis conditions. Another alternative is to employ photo-initiated free radical cryopolymerization that could prevent premature polymerization (Petrov et al., 2006; Petrov et al., 2007; Petrov et al., 2009; Kahveci et al., 2010; Petrov et al., 2011). Among the drawbacks of this technique are the limited penetration depth of the radiation through the frozen system and possible melting of the ice crystals due to the heat liberated from inefficient radiation. Reversible

addition fragmentation chain transfer (RAFT) polymerization can also be employed to form cryogels (Sun et al., 2010). The properties of cryogels can be modulated by changing synthesis parameters such as the preparation temperature (T_{prep}), initial monomer concentration, and the composition of the reaction mixture. Table 2.7 provides a detailed summary of the effects of various synthesis parameters on the properties of cryogels.

Table 3.7 A summary of papers reporting the effects of the synthesis conditions on cryogel properties

References	Cryogel material	Synthesis conditions varied	Findings
(Caykara et al., 2006)	PDEAEMA	X = 61:39, 66:34, 70:30, 75:25, and 79:21 (DMEAEMA:DMAAM); Polymerize at 22 °C for 0, 15, 30, and 45 min followed by –30 °C for 24 h; solvent: ethanol/water mixture	Swelling degree increased with DMAAM content; cryogels have lower swelling degree than hydrogels due to polymer entanglement in highly concentrated UFLP
(Dinu et al., 2007)	PAAM	T_{prep} = 25 and –25 °C; 2 to 30% monomer content; X = 1:5 to 1:100	Cryogels have higher elastic moduli than those of hydrogels; decreasing the T_{prep} decreased the elastic moduli of cryogels; increasing monomer concentration increased the elastic moduli of cryogels; crosslinker ratio did not have substantive effect on mechanical properties; higher mass swelling degree was obtained by decreasing T_{prep}, monomer concentration, and crosslinker ratio; decreasing T_{prep} reduced the pore size but the pore wall thickness was unaffected; increasing monomer concentration decreased the pore size and increased the pore wall thickness; crosslinker ratio had negligible effect on the pore structure
(Dinu et al., 2011a; Dinu et al., 2011b)	PAAM-dextran	T_{prep} = 22, 5, and –18 °C; X = 1:40 or 1:80 (MBA:AAM)	Porosity and swelling rate of cryogels increased with decreasing T_{prep}; a high crosslinker ratio formed a more stable composite; pore size and swelling degree decreased with increasing crosslinker ratio
(He et al., 2007)	PAAM	1 to 10% monomer concentration ; freezing rate = 0.06, 0.07, 0.08, 0.11, 0.17, and 0.33 °C min^{-1}	T_{prep} must be lower than – 9 to – 14.5 °C for a 7% monomer solution to form cryogels; freezing point of a system decreased with increase in monomer content
(Hwang et al., 2010)	PEG	T_{prep} = –14 and –20 °C; [APS] = 0.5% and [TEMED] = 0.05 or 0.1%;	The top and bottom layers of the cryogels synthesized using a high TEMED concentration had different porosities (cryogel-like and hydrogel-like layers); low TEMED concentration formed cryogels with more homogenous interconnected pores; pore connectivity increased with decreasing T_{prep}; cryogels with homogenous and interconnected pores had higher swelling degree than cryogels with heterogenous porosity although the latter swelled more than hydrogels; decreasing T_{prep} decreased the elastic modulus; compression failure occurred at the hydrogel-like layer but not cryogel-like layer

Table 3.7 A summary of papers reporting the effects of the synthesis conditions on cryogel properties (continued)

References	Cryogel material	Synthesis conditions varied	Findings
(Kirsebom et al., 2009)	PDAAM	3, 6, and 12% monomers; T_{prep} = 4, –10, and –20 °C	The solute concentration in a semi-frozen system was significantly higher than that of a supercooled system; concentration of UFLP not affected by the initial monomer concentration but the T_{prep}, increasing the monomer concentration and T_{prep} increased the amount of nonfrozen water during cryopolymerization; higher monomer concentration formed thicker pore walls but smaller pore size; cryogels prepared at –20 °C were weaker than those prepared at –10 °C; decreasing T_{prep} formed cryogels with smaller pores and greater resistance
(Kirsebom et al., 2010)	PAAM	T_{prep} = –12 °C; Additives: NaCl or $CaCl_2$; Solvent: Acetone/water or methanol/water; Note: Freezing points of acetone and methanol are –94 and –98 °C, respectively.	Cryogels prepared with the addition of solutes have smaller pores and thicker pore walls due to larger amount of UFLP; Adding NaCl and $CaCl_2$ formed cryogels with uneven surfaces and smaller pore volume but increased elastic moduli; methanol and acetone addition formed porous pore walls that weakened the mechanical properties but the pore volume was not affected; thin and smooth pore walls were formed for cryogels fabricated without solute addition
(Ozmen and Okay, 2005)	PAMPS	T_{prep} = 25 to –22 °C; 5% of monomer	Macroporous cryogels with high swelling rate and elasticity that can undergo reversible swelling-de-swelling cycles in acetone were obtained when T_{prep} was below –8 °C; increasing AMPS (with fixed charges) content (at constant monomer concentration) increased the volume fraction of ice and swelling degree, and formed smaller pores; addition of NaCl formed cryogels with smaller pores
(Ozmen and Okay, 2006)	PAMPS	T_{prep} = 25 and –22 °C; 0.1 to 10% monomer concentration	Cryogels have a lower CCG (critical concentration of gelation) than hydrogels and can undergo reversible swelling-de-swelling; increasing the monomer concentration increased the elastic moduli but decreased the swelling degree; increasing the monomer content increased the pore size, porosity, and thickness of the pore wall
(Ozmen and Okay, 2008)	PAAM	T_{prep} = 22 and –18 °C; solvent system: DMSO/water mixture	Elastic moduli, swelling degree, and average pore size of cryogels decreased with decreasing T_{prep}; presence of DMSO reduced the pore size of cryogels by two orders of magnitude
(Ozmen et al., 2007)	PAMPS	T_{prep} = 25 and –22 °C (with and without precooling in liquid N_2; 0.1 to 10% monomer concentration; additive: hydroquinone as inhibitor	Precooling allowed the formation of macroporus network to occur at a higher T_{prep} and formed cryogels with less regular pores, slightly higher swelling degree, and lower elastic moduli; adding inhibitor decreased the rigidity of cryogels and formed more regular pores but did not have significant effects on the pore size and swelling properties

Table 3.7 A summary of papers reporting the effects of the synthesis conditions on cryogel properties (continued)

References	Cryogel material	Synthesis conditions varied	Findings
(Plieva et al., 2004)	PAAM	T_{prep} = –12, and –18 °C	Cryogels prepared at –12 °C had large interconnected pores while those prepared at –18 °C had a bimodal pore-size distribution of hundred micron and submicron sizes; cryogels prepared using lower T_{prep} had a lower permeability; more than 70% of water can be squeezed out
(Plieva et al., 2005)	PAAM	6, 10, 15, 18, and 22% monomer; DATAAM (more hydrophilic than MBA) and MBA as crosslinkers	Swelling degree, permeability, pore size, and free water content decreased while polymer-bound water content and pore wall thickness increased with increasing monomer concentration; swelling rate decreased with increasing monomer content; replacement of MBA by DATAAM resulted in spongy, elastic cryogels with higher swelling degree and flow resistance; the degree of pore size shrinkage during dehydration experiment (using environmental scanning electron microscopy) decreased with increasing monomer concentration; larger pore size resulted in higher dehydration rate
(Plieva et al., 2006)	PAAM	T_{prep} = –12, –20, and –30 °C; [TEMED] = [APS] = 1.2, 5% (for aqueous system) and 0.5, 1.4% (when the solvent is formamide, 95% (freezing point = 2 °C) or dioxane, 95% (freezing point = 11 °C). Note: order of solvent polarity: formamide>water>dioxane	Cryogels formed in the "freezing before gelation" mode had a spongy and elastic structure and could reswell in seconds; cryogels formed from "freezing after gelation" had large unconnected pores, high flow resistance, and high rigidity; less overcooling was observed for systems with higher initiator content and faster ice nucleation due to less severe freezing-point depression as the solutes were depleted faster; smaller pore size and lower permeability with decreasing T_{prep}; formation of cryogels below their eutectic point (~ –20 °C) resulted in lower gel yield and inferior mechanical properties; cryogels synthesized in dioxane had microporous structure and bimodal pore size distribution (large macropores and microporous pore walls) due to segregation of polymeric phase (immiscible in dioxane) during gelation
(Plieva et al., 2008)	Combination of PAAM, PDMAAM, dextran-MA, PHEMA, PVA, Agarose, PEG	T_{prep} = 22, –12, –14, –18, and –35 °C; 5-7 % total monomer concentration; X = 1:5 to 1:10	Pore size of the secondary network was smaller than that of the first; compressive strength increased with increasing number of network while the swelling and pore volume decreased; cryogels prepared with a lower crosslinker ratio had thicker but less mechanically strong pore walls with high swelling degree; use of poorly-crosslinked cryogel as primary network does not improve the mechanical properties of the resultant double network; the primary network needs to be stiff while the secondary network should be soft and ductile to produce tough double network cryogels

Table 3.7 A summary of papers reporting the effects of the synthesis conditions on the cryogel properties (continued)

References	Cryogel material	Synthesis conditions varied	Findings
(Savina et al., 2007)	P(HEMA-co-DMAAM)	6, 10, 12, and 20% monomers; T_{prep} = –12 °C	Increasing monomer content decreased pore size but increased the pore surface area; increasing DMAA content in P(HEMA-co-DMAA) cryogels increased the compressive strength but decreased the failure strain;
(Savina et al., 2011b)	PHEMA	8 and 12% monomers; T_{prep} = –12 °C	The mean thickness of pore wall decreased from 11.2 to 9.6 µm during drying; most of the water was in the macropores rather than in the swollen walls; thin pore walls gave rise to elasticity of cryogels; pore size decreased with increasing monomer concentration; "freezing after gelation" resulted in cryogels with aligned polymer walls and smaller pores;
(Srivastava et al., 2007)	PNIPAM	X = 1:20, 1:15, 1:10, and 1:5; 6, 7, and 8% monomer; T_{prep} = –12 °C and room temperature	Cryogels became more rigid, less spongy and elastic, and showed a lower thermal shrinkage with increasing monomer content; swelling degree and response rate of cryogels were significantly higher than those of hydrogels; swelling degree decreased with increasing monomer content due to thicker pore walls, more rigid and less porous cryogels
(Topuz and Okay, 2009)	P(AAM-co-AMPS)	T_{prep} = 19, –15, –18, and –20 °C for a concentration of 9.5% monomer	Hydrogels have higher swelling degree but a lower swelling rate than that of cryogels; cryogels prepared at lower T_{prep} had a lower elastic moduli; cryogels were very elastic and were not damaged after compression of 100% strain while hydrogels broke at 40% strain
(Yao et al., 2006a)	PAAM	0.1, 0.5, 0.8, and 1.2 w/w% (TEMED: AGE + MBA +AAM); Tprep = –20 °C	Cryogels with sponge-like structure were formed under relatively low TEMED concentrations; cryogels formed using high TEMED content were not elastic and could not reswell; a high freezing rate formed cryogels with irregular and less interconnected pores; pore interconnectivity was better in cryogels synthesized using a container with smaller diameter;
(Zhang and Chu, 2003b; a)	PNIPAM	T_{prep} = 37, 22, 0.5, and –20 °C (Note: Freezing point of DMSO = 18 °C); 5 and 10% monomer; Solvent: Anhydrous DMSO	CCG and swelling degree decreased with the T_{prep} but increased again when T_{prep} was too low; cryogels have regular and well-oriented pores while hydrogels have irregular pores; the change in the degree of swelling due to temperature-induced shrinkage of cryogels decreased with increasing monomer concentration; cryogels exhibited more rapid, sharp, and larger magnitude hydration/dehydration changes than those of hydrogels.

Table 3.7 A summary of papers reporting the effects of the synthesis conditions on the cryogel properties (continued)

References	Cryogel material	Synthesis conditions varied	Findings
(Zhang and Zhuo, 1999a; b)	PNIPAM	T_{prep} = 20 and –18 °C; 5% monomer	Swelling degree and response rate of cryogels were significantly higher than that of hydrogels; more hydrogen bonds among amide groups of cryogels than those of hydrogels; the PNIPAM cryogel network was regularly arranged and had a spiral structure due to the extensive hydrogen bonding between water molecules and the amide group

Note: Deionized water was the solvent used unless otherwise stated; DMEAEMA = 2-(diethylamino)ethyl methacrylate; DMAAM = dimethylacrylamide; CCG = critical concentration of gelation: PAMPS = poly(2-acrylamidepropanesulfonic acid); DATAAM = diallyltartaramide; MA = methacrylic acid; PEG = poly(ethylene glycol); AGE = allyl glycidyl ether; X = crosslinker ratio (mol crosslinker/mol monomer).

For example, the reaction temperature has effects on the reaction rate and the structure by influencing the amount of nonfrozen microphase and the size of the ice crystals formed. A lower T_{prep} (which also corresponds to a faster freezing rate) results in a smaller UFLP and a greater number of small pores (Lozinsky et al., 2001; Plieva et al., 2004; Ozmen et al., 2007; Kirsebom and Mattiasson, 2011). The T_{prep} should be sufficiently low to avoid overcooling the reaction mixture in which case neither gelation nor freezing would occur. However, the T_{prep} should not be too low because a cryogel could not form when the freezing temperature is below the eutectic point of the given system as there will be no UFLP in which cryopolymerization could proceed.

The initial monomer concentration affects the volume of UFLP (Kirsebom et al., 2010; Kirsebom and Mattiasson, 2011). A higher initial monomer concentration results in a smaller amount of solvent to be frozen, thereby resulting in a reduced pore volume due to a higher volume of UFLP. Thus, increasing the monomer concentration increases the polymer concentration in the pore walls but decreases the pore interconnectivity and size as well as the degree of equilibrium swelling (Plieva et al., 2005; Dinu et al., 2007; Savina et al., 2007; Srivastava et al., 2007; Johnson et al., 2011). In contrast, Ozmen and Okay (2006) found that by increasing the monomer AMPS concentration from 2.5 to 10%, cryogels with larger and thicker pore walls were obtained. In addition, the pores became more regular as the monomer concentration was increased.

The concentration of the initiating system also has a significant influence on the polymerization rate and the molecular weight of the resulting polymer (Plieva et al., 2007). By changing the amount of the initiating system in the reaction mixture, the pore structure of the cryogels can be tuned accordingly (Plieva et al., 2006; Yao et al., 2006a). For example, when the polymerization rate was much higher than the rate of ice nucleation, closed rather than interconnected pores were formed (Plieva et al., 2006).

Cryostructuration can also be conducted using organic solvents. Dioxane (Plieva et al., 2006; Sun et al., 2010), formamide (Plieva et al., 2006), dimethylsulfoxide

(DMSO) (Zhang and Chu, 2003b; a; Ozmen and Okay, 2008), and ethanol (Caykara et al., 2006) have been shown to be suitable solvent systems. However, this may alter the temperature region used for the cryogelation process (depending on the freezing point of the solvent). In addition, the presence of organic solvents has an effect on the pore structure by affecting the solubility of the polymer and monomer as well as the shape and size of the solvent crystals formed. For example, water gave an irregular complex 3D honeycomb structure while DMSO yielded regular pores aligned in a specific direction (Zhang and Chu, 2003a; 2003b). On the other hand, formamide formed long and oriented needle-like crystals (Plieva et al., 2006).

Kirsebom et al. (2010) studied the effects of the addition of NaCl, $CaCl_2$, acetone and ethanol in the reaction mixture on the properties of the cryogels obtained. It was found that the addition of the aforementioned salts and solvents caused an increased UFLP volume resulting in cryogels with smaller pore sizes and thicker pore walls. In addition, the pore walls of cryogels with salts added had an uneven surface while those with solvents added had a porous wall. The secondary porosity resulting from the addition of ethanol or acetone was most likely a result of reaction-induced phase separation (Okay, 2000; Ozmen and Okay, 2008). As expected, the presence of secondary porosity weakened the mechanical strength due to presence of pores in the pore walls. In contrast, the addition of salt resulted in an increase in the elastic modulus, E, of the cryogels due to increase in the gel fraction.

Hydroquinone inhibits polymerization of acrylamide-based monomers. The addition of hydroquinone prolonged the gel point to longer times as the hydroquinone content was increased (Ozmen et al., 2007). The addition of 0.2 % hydroquinone during cryopolymerization of a PAAM gel resulted in a smaller pore diameter (12 ± 4 μm) than that without hydroquinone addition (35 ± 11 μm). The addition of hydroquinone could have provided a more homogenous nucleation that increased the number of small-sized ice crystals leading to the formation of small pores in the final materials.

2.7 Cryogel properties and characterization

This section highlights some unique properties and techniques that can be used to characterize the pore structure of cryogels along with their advantages and disadvantages. Table 3.8 summarizes the techniques that have been used to characterize cryogels.

Table 3.8 A summary of techniques that have been used to characterize porous hydrogels

Property	Characterization technique	References
Cryopolymerization mechanism and UFLP concentration	Proton nuclear magnetic resonance	(Kirsebom et al., 2008; 2009; Kirsebom et al., 2010)
Pore volume Pore volume	Theoretical calculation based on volume and mass swelling degrees	(Ozmen and Okay, 2006; Dinu et al., 2007; Topuz and Okay, 2009; Dinu et al., 2011a; Dinu et al., 2011b)
	Density measurement method	(Dinu et al., 2007; Dinu et al., 2011a; Dinu et al., 2011b)
	Nonsolvent uptake	(Plieva et al., 2005; Savina et al., 2005; Ceylan and Okay, 2007; Topuz and Okay, 2009; Kirsebom et al., 2010; Orakdogen et al., 2011)
	Water-vapor adsorption and swelling studies	(Savina et al., 2005; Plieva et al., 2008b)
	Proton nuclear magnetic resonance	(Savina et al., 2011b)
	Confocal laser scanning microscopy	(Savina et al., 2011b)
	Scanning electron microscopy	(Mather et al., 2008)
	Multiphoton microscopy	(Savina et al., 2011b)
	X-ray microcomputed tomography	(Lin et al., 2003; Darling and Sun, 2004; Savina et al., 2007)
	Magnetic resonance imaging	(Mather et al., 2008)
	Mercury intrusion porosimetry	(Zhao et al., 2011)
Pore interconnectivity	Permeability studies to measure flow resistance	(Plieva et al., 2005; Plieva et al., 2008a)
	X-ray microcomputed tomography	(Darling and Sun, 2004a; Savina et al., 2007)
	Confocal laser scanning microscopy	(Savina et al., 2011b)
	Magnetic resonance imaging	(Mather et al., 2008)
	Multiphoton microscopy	(Savina et al., 2011b)

Table 3.8 A summary of techniques that have been used to characterize porous hydrogels (continued)

Property	Characterization technique	References
Pore-size distribution	Two-photon fluorescence microscopy	(Chalal et al., 2009)
	Scanning electron microscopy	(Ozmen and Okay, 2005; Mather et al., 2008)
	X-ray microcomputerized tomography	(Mather et al., 2008)
	Magnetic resonance imaging	(Mather et al., 2008)
	Confocal laser scanning microscopy	(Kirsebom et al., 2010; Savina et al., 2011b)
	Differential scanning calorimetry	(Savina et al., 2011b)
	Proton nuclear magnetic resonance (cryoporometry)	(Savina et al., 2011b)
	Optical microscopy	(Dinu et al., 2011a; Dinu et al., 2011b)
Water states	Water-vapor adsorption studies	(Plieva et al., 2004; Plieva et al., 2008a)
	Differential scanning calorimetry	(Plieva et al., 2005; Dinu et al., 2007)
Morphology	Confocal laser scanning microscopy	(Plieva et al., 2008a; Savina et al., 2011b)
	Environmental scanning electron microscopy	(Plieva et al., 2005; Dinu et al., 2011a; Dinu et al., 2011b)
	Scanning electron microscopy	(Zhang and Chu, 2003b; a; Ozmen and Okay, 2005; Plieva et al., 2006; Savina et al., 2007; Kirsebom et al., 2008; Plieva et al., 2008a; Kirsebom et al., 2009; Topuz and Okay, 2009; Hwang et al., 2010; Kirsebom et al., 2010; Savina et al., 2011b; Zhao et al., 2011)
	Optical microscopy	(Dinu et al., 2007; Ozmen et al., 2007; Dinu et al., 2011a; Dinu et al., 2011b)
	Multiphoton microscopy	(Savina et al., 2011b)
	Two-photon fluorescence microscopy	(Chalal et al., 2009)
	X-ray microcomputed tomography	(Lin et al., 2003; Darling and Sun, 2004; Savina et al., 2007)
	Magnetic resonance imaging	(Mather et al., 2008)
	Cryo scanning electron microscopy	(Savina et al., 2011b)

The principal difference between cryogels and other macroporous materials is the tissue-like elasticity and their ability to withstand extensive deformation without being destroyed/collapsed (Plieva et al., 2008c). The superior mechanical properties of cryogels are attributable to the cryoconcentration phenomenon that forms dense pore walls. Cryogels synthesized from various materials have been reported to withstand compression strains of 80-100% of their initial lengths without any crack development (Plieva et al., 2006; Topuz and Okay, 2009; Dinu et al., 2011a; Orakdogen et al., 2011).

Cryogels were found to attain their equilibrium swelling state in less than 30 s while those formed at higher temperatures took more than 1 h to reach equilibrium (Ozmen and Okay, 2005; Ceylan et al., 2006). The enhanced swelling kinetics of cryogels is attributed to the interconnected structure of the pores. Despite the fast swelling kinetics of cryogels, some researchers found that they swelled to a lesser extent than the conventional hydrogels (Arvidsson et al., 2002; Ozmen and Okay, 2005; Plieva et al., 2005). This could be due to polymer chain entanglement resulting from cryo-concentration. In contrast, Srivastava et al. (2007) found that PNIPAM cryogels swelled twice as much as PNIPAM hydrogels. The authors attributed the higher swelling to the high porosity of the cryogels that allowed a larger amount of water to permeate into the porous network. Swelling of porous networks such as cryogels is governed by two separate processes, namely (i) hydration of network chains and (ii) pores filling by the water (Okay, 2000). This results in three different water states in swollen cryogels, namely (i) water that is hydrogen-bonded to the polymer (nonfreezable at –15 ^{o}C), (ii) water that is weakly interacting with the polymer (freezable), and (iii) free water that does not interact with the polymer (essentially pure water) (Savina et al., 2011b).

These remarkable properties of cryogels stem from their highly interconnected porous network. Thus, the properties of cryogels are largely defined by their pore structure (i.e., pore size, volume, interconnectivity, and wall thickness). It should be noted that the cryogels may contain three different types of pores, namely closed pores, open- or through pores, and blind pores that are defined based on the degree of interconnectivity as shown in Fig. 2.4.

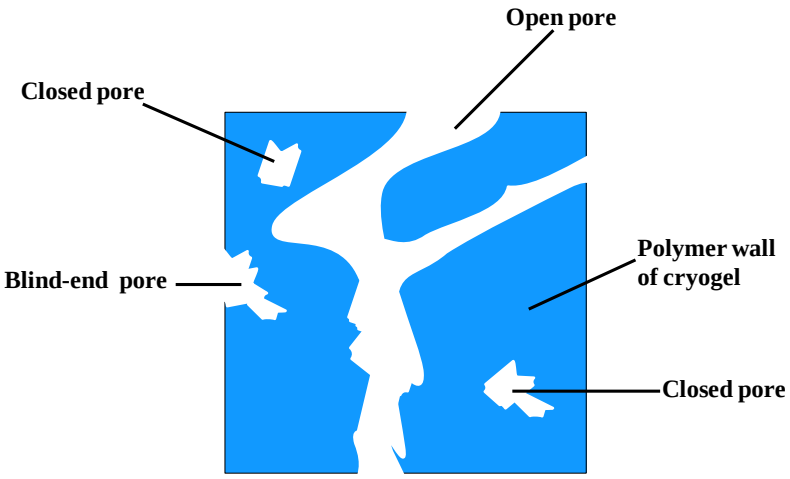

Figure 2.4 Schematic depicting the various types of pores than may exist in porous materials (modified from Savina et al., 2009)

In contrast to dry and rigid systems, the study of pore structure in cryogels is challenging since there is no standard method to determine the pore structure of soft and highly hydrated systems. Porosimetric techniques such as mercury porosimetry is an established method to determine porosity and pore-size distribution of porous materials. This technique is based on pressurized penetration of liquid into the sample. The total pore volume is measured at maximum pressure. The pore diameters and pore volume distribution by pore sizes can be determined using the Washburn equation:

$$D = -\frac{4\gamma\cos\theta}{P} \qquad (2.6)$$

Where D is the pore diameter at pressure P, θ is the contact angle of mercury with the material (140°), and γ is the surface tension of mercury (480 dyne cm^{-1}). This equation assumes perfectly cylindrical pores but this is not usually the case for cryogels. Parameters such as the ratio of cumulative surface area to pore size, pore tortuosity, sample compressibility, permeability and densities can be derived from the extrusion profile. However, this technique does not measure the pore interconnectivity, strut thickness, anisotropy and cross-sectional area (Ho and Hutmacher, 2006). In addition, this technique is limited to pore sizes in the range of 7.5 nm to 75 µm, and may lead to incorrect pore-size determination due

compression of the cryogels resulting from penetration of mercury under high pressure (Blacher et al., 2001; Ho and Hutmacher, 2006).

Imaging has been among the popular techniques used for studying the morphology of porous materials. A variety of methods can be used to image cryogels such as optical microscopy (OM), scanning electron microscopy (SEM), Cryo-SEM, environmental scanning electron microscopy (ESEM), X-ray microcomputed tomography (X-ray micro-CT), and confocal laser scanning electron microscopy (CLSM). The reliability and quality of the information obtained using these techniques may be affected by the instrument resolution and contrast as well as the sample preparation procedure that may result in structural distortion.

Conventional SEM involves scanning a focused beam of electrons across a specimen surface under vacuum resulting in the emission of different types of electrons and electromagnetic waves. The secondary electrons ejected are collected by the detector to generate an image. SEM has a good resolution for imaging of fine structures and is commonly used for analysis of cryogel morphology (Plieva et al., 2007). However, SEM sample preparation is relatively tedious as it usually includes fixing, drying, and coating the sample with about 20-30 nm of an electron-dense metal film before imaging that could alter the structure of the cryogels. For example, sample processing techniques such as freeze-drying at a relatively high temperature (above –70°C) may induce large pores even for nonporous materials. Nevertheless, there is general consensus that cryogels can withstand the drying process due to their dense pore wall that can be preserved if proper sample preparation such as supercritical point drying after immersion in ethanol or freeze-drying at low temperatures (i.e., below –70°C) is employed (Savina et al., 2007).

Alternative techniques such as Cryo-SEM and ESEM require less-demanding sample preparation and the hydrated sample can be studied during dehydration (Savina et al., 2009). Samples for Cryo-SEM are cryo-fixed by flash-freezing in semi-solid nitrogen (slush nitrogen) close to its freezing point (–210°C) to minimize damage from ice-crystal formation and inhibit ice sublimation. The sample is then transferred to the cold-stage of the cryo-preparation chamber (where fracturing can

be performed, if needed). Then the pore structure at the surface of the sample is revealed as the temperature is raised and the free water begins to sublime. The sample is examined at subzero temperature (usually between –100 to –175°C). Images can be captured during the sublimation process (Savina et al., 2009).

On the other hand, ESEM images are captured by exposing the samples to a low-pressure gaseous environment (1-50 Torr) and high relative humidity (up to 100%). The internal pressure in the sample chamber can be controlled within fine limits. This allows monitoring of the changes in the structures of the cryogels as they dehydrate (Rizzieri et al., 2003; Savina et al., 2009). No pores are visible in the fully hydrated cryogel since they are fully filled with water but the surface details become more visible as water evaporates (Plieva et al., 2005).

SEM, Cryo-SEM, and ESEM images are 2D representations of 3D systems that can be difficult to interpret as they can only provide qualitative information limited to the surface of the material. In addition, the extraction of quantitative data can be difficult as the image of the plane of interest may be interfered by that of the planes below and above it (Mather et al., 2008). Thinly sectioned samples may improve the quality of the results but drying of thinly-sliced cryogels may result in a more significant alteration of the structure and edge effects. Thus, imaging techniques that allow visualization of the 3D structure of cryogels have significant advantages. Such techniques include confocal laser scanning microscopy (CLSM), two-photon fluorescence microscopy (TPFM), X-ray micro-computed tomography (X-ray micro-CT), and magnetic resonance imaging (MRI).

CLSM permits the observation of the pore structure of swollen cryogels. However, the cryogel samples need to be made fluorescent by immersing in a solution of Lucifer yellow (Přádnýa et al., 2003), fluorescein isothiocyanate (FITC) (Plieva et al., 2008a; Kirsebom et al., 2010; Savina et al., 2011b; Berillo et al., 2012), or Rhodamine B (Plieva and Mattiasson, 2008; Zhao et al., 2011) prior to imaging. CLSM can reduce out-of-focus-blur (Hamthamrongwit et al., 1996) and provides a 3D image of the sample but it does not have sufficient resolution to observe the structure of the pore walls (Berillo et al., 2012). The penetration depth of CLSM is

limited to 50-500 μm depending on losses due to scattering. In addition, the fluorescent probes should be uniformly distributed on the cryogel network in order to obtain a reliable representation of the pore structure.

Two-photon fluorescence microscopy (TPFM) is a nonintrusive technique that allows a 3D imaging of the structure (Chalal et al., 2009). It can also be used to probe the changes in the pore structure of a PNIPAM cryogel as the temperature changes. This technique has a maximum observable depth of 200 μm. TPFM is a nonlinear optical microscopy technique that uses a femto-second pulsed laser. A localized absorption results from the simultaneous absorption of two photons in a quantum event. This technique allows deeper penetration for opaque samples because of lower Rayleigh scattering resulting from the use of the excitation wavelength that is almost twice the absorption wavelength. Samples need to be made fluorescent prior to analysis. A suitable fluorophore should: (i) absorb the excitation light following a two-photon absorption process leading to a fluorescence localized at the focal region, (ii) it must be soluble in water, and (iii) should adsorb on the gel backbone in order to stain the macropore walls (Chalal et al., 2009). For example, Sulforhodamine B is a suitable dye to stain PNIPAM cryogels (Chalal et al., 2009).

Micro-CT scans image of the sample by exposing the sample to small quantities of ionizing radiation (usually X-rays). X-rays are attenuated upon transversing the 2D slices; the emergent X-rays with reduced intensity are captured by the detector. The resultant grayscale images depict the density map of the scanned sample. 3D images can then be reconstructed from the 2D slices. This method has recently been employed to analyze the pore structure of poly(hydroxymethacrylate) (PHEMA) cryogels (Savina et al., 2007). Dried samples would give better images than those of hydrated samples. However, the quality of the images obtained may still be limited as the contrast between hydrogels (which comprised low electron-density elements such as C, H, N, O, etc.) and air is low. This can be overcome by pretreating the sample with an X-ray contrasting agent (that contains either iodine or a heavy metal) to enhance absorption by the radio-transparent polymer (Muller et al., 1997; Darling

and Sun, 2004). $FeCl_3$ has been used as an X-ray contrasting agent to visualize the 3D structure of PHEMA cryogels.

In MRI a magnetic field is used to align the nuclear magnetization of hydrogen atoms of the water in the sample. The alignment of this magnetization is adjusted by a radio-frequency field. This produces a signal (i.e., a strong rotating magnetic field) detectable by a scanner that can be further manipulated by an additional magnetic field to construct an image of the sample (Savina et al., 2009). MRI can be used to obtain 3D images of relatively large and hydrated samples (Mather et al., 2008). However, it has a relatively low resolution. Thus, it is not suitable for imaging fine structures. Note that it is important to remove air pockets in the samples prior to analysis as they will result in image artifacts due to microscopic gradients in the magnetic field strength at the interface between substances of different magnetic susceptibility (i.e., air, and polymer/water). Ultrasound can be employed to remove the majority of air bubbles from the samples (Mather et al., 2008).

A set of quantifiable data can be obtained from the images to represent the pore structure by using image-analysis software (Savina et al., 2009). 3D images would allow the extraction of more information on the pore structure such as the pore volume, tortuosity, and interconnectivity than 2D images (Lin et al., 2003; Darling and Sun, 2004; Wang et al., 2004; Savina et al., 2007; Mather et al., 2008). Image analysis is based on the interpretation of differences in grayscale intensities or hues. Typically 256 greyscale monochrome images have tonalities ranging from pure black (grayscale value of 0) to pure white (grayscale value 255). In an ideal situation, dark level 0 regions correspond to the pores while the light gray regions approach 255. However, in reality, images show a range of tonalities that require the image contrast to be enhanced prior to analysis. This can be done via thresholding after which the data are converted into a binary file where the pores are pure black and pore walls are pure white. Depending on the quality of the images obtained, segmenting them into regions associated with pores and walls can be challenging. It has been found that the threshold value selected has a substantive effect on the calculated porosity value (Mather et al., 2008). Thus, the values obtained should not be treated as absolute. Nevertheless, image analysis gives a

good estimation of the pore structure and is a good technique that allows comparison of the relative values for different samples.

2.8 Applications of cryogels

Cryogels provide a versatile platform for various modifications to impart desired properties for specific applications. For example, grafting of polymer brushes has been employed to modify the surface energies of cryogels (Savina et al., 2005; 2006; Su et al., 2012). In addition, various nanomaterials can be incorporated either onto the surface or in the cryogel matrix. For example, single-walled and multi-walled carbon nanotubes (SWCNTs and MWCNTs) have been successfully incorporated into several types of polymeric cryogels (Petrov and Georgiev, 2011; 2012). This allowed the fabrication of foam-like materials having high conductivities (1-6 S m^{-1}) using low CNT content (0.012-0.015 wt%) (Petrov and Georgiev, 2011). Other nanomaterials such as ferric oxide (Savina et al., 2011a) and silica nanoparticles (Xu et al., 2010) have also been incorporated into cryogels.

In certain applications, cryogels with oriented pores are preferred. This can be achieved by employing directional freezing also known as ice-segregation-induced self-assembly (ISISA) prior to cryogelation. This permits greater control in creating desired morphologies and achieving sophisticated structures exhibiting organization at different scales (Zhang et al., 2005; Zhang and Cooper, 2007; Gutiérrez et al., 2008). Cryogels with microtubular pores aligned along the freezing direction have been synthesized using PEG (Wu et al., 2012), PVA (Gutiérrez et al., 2007), cellulose microfibrils (Lee and Deng, 2011), and conductive PEDOT-PSS (Zhang et al., 2010) via the ISISA technique. Cryogels with aligned pores can be further made conductive by incorporating CNTs (Kwon et al., 2009), silver nanowires (Romeo et al., 2012), and graphenes (Barrow et al., 2012) by employing ISISA.

This literature review provides some examples on the possible modifications that can be employed to functionalize cryogels. This allows the fabrication of cryogels with tailored properties. Cryogels are currently used as carriers in drug delivery,

scaffolds in regenerative medicine, support materials for bioseparations, adsorbents for pollutants as well as other applications (Table 2.9). In this research it is proposed to prepare cryogels with antimicrobial properties that have the potential to be developed into portable POU water-treatment units for application in emergencies such as disaster relief. The cryogels fabricated should preferably be robust, and have rapid and significant swelling. Chapter 4 describes the preparation and characterization of such cryogels. Chapters 5 to 8 describe studies conducted to develop antibacterial cryogels via functionalization with AgNPs of the cryogels prepared in Chapter 4.

Table 2.9 Current applications of cryogels

Cryogel materials	Method of synthesis	Application	References
Drug delivery applications			
Aligned PVA cryogels	Physical crosslinking of PVA by unidirectional freezing	For controlled release of drugs (ciprofloxacin)	(Gutiérrez et al., 2007)
Drug-loaded alginate and chitosan cryogels	Polyelectrolyte complexation between alginate and chitosan at subzero temperatures	For controlled drug release	(Lai et al., 2003)
Drug-loaded PETEGA cryogels	Photo-initated radical cryopolymerization of ETEGA in the presence of a drug (verapamil hydrochloride)	For controlled release of drugs	(Kostova et al., 2011)
PAA cryogel	Free-radical cryopolymerization of AA, SA, and MBA	As self-oscillating gel when subjected to a pH oscillator creating dynamic rhythms of sufficient mechanical energy for applications such as self-walking microactuators or micropumps with peristaltic motion, pacemakers, timers, and oscillatory drug-release systems	(Yoshida et al., 1997; Bilici et al., 2010)
Regenerative medicine applications			
Agarose-alginate cryogels	Crosslinking of a mixture of agarose and alginate with EDC at subzero temperatures	As cell scaffolds for fibroblast cell adhesion and proliferation	(Tripathi and Kumar, 2011)
Agarose-gelatin cryogels	Crosslinking of a mixture of agarose and gelatin at subzero temperatures	As cell scaffolds for fibroblast cell adhesion and proliferation	(Tripathi et al., 2008)
Aligned MWCNT/silk fibroin cryogels	Physical crosslinking of silk fibroin by unidirectional freezing in the presence of MWCNTs	Have potential to be used as electrodes in capacitors, catalysts in chemical reactions, or scaffolds for electrically-responsive cell such as neuron cells	(Kwon et al., 2009)
Chitosan cryogels	Freeze-gelation approach. Frozen chitosan samples were precipitated in NaOH/ethanol at subzero temperatures followed by crosslinking reaction.	Intended to be used as scaffolds for tissue engineering	(Hsieh et al., 2007)
Chitosan-gelatin cryogels	Crossling a mixture of chitosan and gelatin with glutaraldehyde at subzero temperatures	As scaffolds for fibroblast cell adhesion, proliferation, and extracellular matrix secretion	(Kathuria et al., 2009)

Table 2.9 Current applications of cryogels (continued)

Cryogel materials	Method of synthesis	Application	References
PAN/gelatin full-IPN cryogels	Free-radical cryopolymerization of PAN and simultaneous gelation with MBA and glutaraldehyde as crosslinkers for PAN and gelatin, respectively	As scaffolds for cell immobilization	(Jain et al., 2009)
PEG cryogels	Free-radical cryopolymerization of PEGDA	As scaffolds for cartilage tissue engineering	(Hwang et al., 2010a)
Peptide-incorporated chitosan cryogels	Chitosan cryogels were synthesized by crosslinking with glutaraldehyde at subzero temperatures. Peptide attachment on cryogels was facilitated by amino group activation in acetic acid followed by Schiff-base reduction.	The peptide attached to the cryogel surface improves cell adhesion properties of the bioactive scaffolds	(Kirsebom et al., 2007)
P(NIPAM-co-Alm) particle-structured cyrogels containing bacteria	Crosslinking reaction between PNIPAM nanoparticles, glutraldehyse and bacteria under subzero temperatures	Have potential to be used for tissue engineering, drug delivery, or as immobilized cells in bioreactors	(Kirsebom et al., 2009a)
Bioanalytical chemistry/bioseparation/biocatalysis applications			
Agarose/chitosan cryogels containing agarose beads	Crosslinking of agarose/chitosan cryogels with glutaraldehyde at subzero temperature conditions. The resultant cyrogels were functionalized by divinyl sulfone activation followed by covalent attachment of 2-mercaptopyridine	For purification of immunoglobulin from human plasma	(Sun et al., 2012)
P(MA-co-PEGDA) cryogels	Free-radical cryopolymerization of MA and PEGDA	As stationary phase in high-performance liquid chromatography of lysozyme and PNIPAM-based nanoparticles	(Chen et al., 2008)
Enzyme immobilized albumin/chitosan cryogels	Cryogelation of a mixture of albumin, chitosan, gutaraldehyde, and functional protein	For bioanalytical chemistry applications in quantitative detection of glucose in a flow-injection-analysis set-up	(Hedström et al., 2008)
Hydroxyethylcellulose cryogels entrapped with yeast cells	UV-initiated cryopolymerization of hydroxyethylcellulose solution containing yeast cells	The yeast cells immobilized in the cryogels function as biocatalyst for ethanol fermentation process	(Velickova et al., 2009)

Table 2.9 Current applications of cryogels (continued)

Cryogel materials	Method of synthesis	Application	References
MWCNT/PVA cryogels	Crosslinking of PVA with glutaraldehyde in the presence of MWCNTs at subzero temperatures	As sorbents for extraction and preconcentration of trace PAHs in water samples prior to HPLC (high performance liquid chromatography) analyses	(Kueseng et al., 2010)
PAAM cryogels grafted with ion exchange polymer brushes	Anion-exchange polymer chains (PDMAEMA and PMETA) and cation-exchange polymer chain (PAA) were grafted on the PAAM cryogel surface using potassium diperiodatocuprate as the initiator	The grafted polymer chains could function as the tenacles that are capable of multipoint interaction with protein molecules for enhanced binding capacities	(Savina et al., 2005b; 2006)
PAAM cryogels loaded with ferric oxide nanoparticles	Free-radical cryopolymerization of AAM, MBA, AGE, and surfactant-stabilized Fe_3O_4 nanoparticles	Fe_3O_4 nanoparticles provide protein binding sites in the cryogel matrix, which is used as a chromatographic medium	(Yao et al., 2007)
PVA cryogels loaded with anion-exchange particles	Freeze-gelation of a suspension of PVA solution containing Amberlite resin particles	To capture negatively-charged solutes (i.e., benzoate and lactate) from a yeast suspension in ion-exchange chromatography	(Savina et al., 2005a)
Water and environmental/cleanup/remediation applications			
Agarose-alginate cryogels	Crosslinking of a mixture of agarose and alginate with EDC at subzero temperatures	As filter materials for adsorption and recovery of heavy metals such as copper and nickel	(Tripathi and Kumar, 2011)
Anammox sludge entrapped in PVA cryog	Freeze-thawing a suspension of PVA solution containing anammox sludge	PVA cryogels immobilized the slow-growing bacteria for de-ammonification treatment of wastewater	(Magrí et al., 2012)
PAAM and chitosan IPN cryogels	Crosslinking of preformed PAAM/chitosan semi-IPN cryogels with epichlorohydrin under alkaline conditions	For selective sorption of cationic dyes (methylene blue)	(Dragan et al., 2012)
PAAM-based cryogels formed inside a plastic core (Kaldnes carriers)	Free-radical cryopolymerization of AAM, MBA, and AGE in Kaldnes carrier. IDA (iminodiacetate) ligands were then incorporated into the cryogels.	To be incorporated into processes involving well-stirred reactors such as Cu(II) ions adsorption or capture of yeast cells	(Plieva and Mattiasson, 2008)
PAAM and potato starch semi-IPN cryogels	Free-radical cryopolymerization of a AAM and MBA in the presence of potato starch	For sorption of cationic dyes (methylene blue)	(Dragan et al., 2011)

Table 2.9 Current applications of cryogels (continued)

Cryogel materials	Method of synthesis	Application	References
PAAM and potato starch semi-IPN cryogels	Free-radical cryopolymerization of a AAM and MBA in the presence of potato starch	For adsorption of heavy metals (Cu^{2+}, Cd^{2+}, Ni^{2+}, and Zn^{2+})	(Apopei et al., 2012)
PAAM cryogels containing molecularly-imprinted polymers (of arsenic) or aluminium oxide nanoparticles	Free-radical cryopolymerization of a AAM and MBA in the presence of molecularly-imprinted polymers (of arsenic) or aluminium oxide nanoparticles	For arsenic adsorption	(Önnby et al., 2012)
PHEMA cryogels containing iron nanoparticles	Free-radical cryopolymerization of a suspension of HEMA, PEGDA, and α-Fe_2O_3 or Fe_3O_4	Iron oxide nanoparticles embedded in cryogels provide enhanced As(III) adsorption	(Savina et al., 2011a)
P(NIPAM-co-Alm)	Free-radical cryopolymerization of a monomer suspension containing activated carbon	For phenol adsorption	(Hajizadeh et al., 2010)
PVA, PAAM, and chitosan cryogels containing polymeric particles imprinted with target molecules	Free-radical cryopolymerization of AAM and MBA for PAAM cryogels containing MIP (molecularly-imprinted polymer) particles while PVA and chitosan cryogels were formed by crosslinking PVA or chitosan with glutaraldehyde in the presence of MIP particles	To absorb endocrine disrupting trace contaminants (17β-estradiol) for water cleanup	(Le Noir et al., 2007)
Rubber-based cryogels	Crosslinking various types of rubber (butyl rubber, cis-polybutadiene, styrene-butadiene, etc.) using sulfur monochloride at subzero temperature	To selectively adsorb oil and polycyclic aromatic hydrocarbons from surface- and seawater – they are reusable after squeezing	(Ceylan et al., 2009; Karakutuk and Okay, 2010)
Antibacterial cryogels with significant and fast swelling, good separation efficiency, robust, good water recovery, and antibacterial properties		**Portable water treatment unit for emergencies**	**To be explored in this project**

Note: Alm = allylamine; PETEGA= poly(ethoxytriethyleneglycol acrylate); MA = methacrylic acid; PEGDA = poly(ethyleneglycol diacrylate); PDMAEMA = poly(2-(diethylamino)ethyl methacrylate); PMETA = poly([2-(methacryloyloxy)ethyl]-trimethylammonium chloride); AGE = allyl glycidyl ether; PAN = poly(acrylonitrile).

CHAPTER 3 Materials and methods

This chapter describes the general materials and methods for testing and characterization employed in this study. Detailed descriptions on the specific experimental conditions and materials syntheses can be found in the respective chapters.

3.1 Materials

3.1.1 Chemicals and reagents

The base material of this project, namely poly(sodium acrylate) (PSA) cryogel was prepared using monomer, sodium acrylate (SA, 97%), crosslinker, *N,N'*-methylenebis(acrylamide) (MBA, 99%), initiator, ammonium persulfate (APS, 98%), and activator, *N,N,N',N'*-tetramethylethylenediamine (TEMED, ≥99%). All other chemicals and reagents used in this study were of analytical grade with over 99% purity, unless otherwise specified. Ultrapure or deionized (DI) water with a resistivity of 18.2 MΩ·cm (at 25 °C) was used to prepare all working solutions.

3.1.2 Synthesis of poly(sodium acrylate cryogel)

The reaction mixture of SA and MBA was degassed with oxygen-free nitrogen for 20 min and chilled in an ice bath for another 20 min. Then APS and TEMED were added and mixed for 10-15 s. Three mL of the reaction mixture was transferred into a poly(propylene) syringe (3 mL and 9 mm ID); the syringe was placed into the liquid cooling chamber of a chiller (Polyscience 9012) for 24 h. In Chapter 5 onwards, the syringes were placed in a bath fluid incubated in an ultra-low temperature freezer (Eutra ED-FU4100) instead to increase the production of the cryogels. The bath fluid used was a 1:1 mixture of ethylene glycol/DI water. Detailed synthesis conditions used to optimize the PSA cryogel synthesis can be found in Chapter 4. Based on the findings in Chapter 4, the synthesis conditions selected to fabricate PSA cryogels for use in the subsequent chapters were as

summarized in Table 3.1. The resultant PSA gels were thoroughly washed with DI water and were dehydrated in a series of aqueous ethanol solutions (25-99.5%) followed by drying in a freeze-dryer (Alpha 1-4LD) before they were fractured into smaller disk samples. The yield of the syntheses was calculated by taking the ratio of the mass of dried gel to the mass of monomers used for the synthesis.

Table 3.1 Synthesis condition used to prepare PSA cryogels

Synthesis parameter	Conditions
Bath temperature	–20°C
Total monomers concentration† (SA + MBA)	8%
Crosslinker ratio† (mol MBA/mol SA)	0.05
APS concentration†	1.75 mM
TEMED†	8.4 µm

Note: † The concentrations reported are those in the final reaction mixture.

3.1.3 Preparation of PSA cryogels decorated with silver nanoparticles

Chapter 5 describes the exploration of various approaches to incorporate silver nanoparticle (AgNPs) in PSA cryogels. Based on the results, the intermatrix synthesis method was selected to prepare PSA cryogels decorated with silver nanoparticles (or PSA/AgNP cryogels) for further development detailed in Chapters 6 to 8. Typically, 1 g of the dried PSA cryogels was allowed to swell in a 250 mL solution of 1, 5, or 10 mM of $AgNO_3$ (≥98%, Merck). The suspension was shaken at 120 rpm on an orbital shaker for 24 h in the dark. The cryogels were immersed in a 250 mL solution of $NaBH_4$ (Alfa Aesar, 10:1 molar ratio of $NaBH_4$ to $AgNO_3$) to form silver nanoparticles (AgNPs). The resultant nanocomposites were thoroughly washed by immersion in DI water followed by vacuum filtration. After three repetitions of the washing step, the nanocomposites were dried using the same procedure that was used for the PSA cryogels. Note that in Chapters 6 to 8, the as-synthesized PSA/AgNP cryogel nanocomposites were denoted as AgNC-x, where x (x = 20, 90, and 170) represents the Ag content (mg/g) in the nanocomposites.

3.2 Materials characterization

3.2.1 Characterization of pore structure

The morphology of dried gels was characterized with either a scanning electron microscope (SEM; Zeiss EVO50) or a field-emission scanning microscope (FESEM; JEOL JSM-7600F). The specimens were coated with Pt for 30 s (20 mA) using an auto-fine coater (JEOL JFC-1600) prior to imaging. The SEM and FESEM images were analyzed using image-analysis software (ImageJ) to determine the pore-size distribution of the cryogels. At least 5 images taken at different regions of the fractured gel cross-section were used for the pore-size determination.

A confocal laser scanning microscope (CLSM; Nikon A1R) was used to obtain images of the swollen gels. The gel samples (1 mm thickness) were stained by incubation in 1 mL of 0.1 M carbonate buffer (pH 9.45) and 40 µL of FITC (fluorescein isothiocyanate isomer I 90%; 1 mg/mL in DMSO). After 24 h of incubation the gels were washed with carbonate buffer and DI water. They were then examined with a CLSM at excitation and emission wavelengths of 488 and 530 nm, respectively. The 3D images were reconstructed from 2D images obtained by performing optical sectioning in the lateral-planes along the vertical axis.

The 3D pore structure of the dried cryogel was also visualized using a high-resolution X-ray tomography scanner (SkyScanner 1172) to obtain raw data of the cryogels. The 2D images were then reconstructed into 3D images using the software Avizo Fire. To quantify the pore structure of the cryogel, **t**hresholded 2D and 3D images were analyzed using ImageJ software. 2D images were used for the determination of the mean pore size of PSA cryogel. Pore interconnectivity, porosity, surface area, and strut thickness were quantified using the 3D image from reconstruction of the optical slices obtained from X-ray micro-CT. To determine the pore interconnectivity, the thresholded 3D image was inverted to measure the volume of all pore spaces using the Object Counter3D plugin (Cordelires and Jackson, 2007). The same (inverted) thresholded image was then "purified" to contain only of the interconnected pore using the command, purify in BoneJ plugin (Doube et al., 2010). The volume of this region-grown mask that represents the

volume of interconnected pore was also determined. Pore interconnectivity was computed by taking the ratio of the volume of interconnected pore to that of the total pore volume (Lin et al., 2003; Darling and Sun, 2004). The porosity was determined by subtracting the volume fraction (of the cryogel) from 1 (Darling and Sun, 2004). The volume fraction was determined using BoneJ (Doube et al., 2010). The surface area of the pores were obtained using the Object Counter3D plugin (Cordelires and Jackson). The value of the pore surface area obtained was normalized with respect to the total volume of cryogel used for the image analysis (Savina et al., 2011b). The strut thickness was determined by measuring the thickness of the trabeculae (pore walls) using BoneJ (Doube et al., 2010).

The specific pore volume of the dried gels was estimated by the uptake of cyclohexane after 3 h of immersion (Topuz and Okay, 2009). The specific pore volume, V_p (cm^3/g) was calculated as follows:

$$V_p = \frac{m_{swollen} - m_{dried}}{\rho_{cyclohexane} \times m_{dried}} \tag{4.1}$$

where $m_{swollen}$ and m_{dried} are the masses of the gel sample after and before immersion in cyclohexane, respectively, and $\rho_{cyclohexane}$ is the mass density of cyclohexane (0.779 g/mL). Strictly speaking, the pore volume estimated using this technique represents the "accessible" pore volume and is affected by the interconnectivity of pores. Gels having closed pores may have a lower "accessible" pore volume than their actual pore volume.

The water states in the swollen gel samples were characterized according to the method described by Plieva et al. (2005; 2008a) with slight modifications to obtain more reproducible results. The polymer-bound water was quantified by water-vapor adsorption in which the dried gel was placed in a chamber saturated with water vapor (but not in contact with liquid water) until its mass became constant. The mass increase due to water-vapor adsorption is the mass of polymer-bound water. The amount of free water in the swollen gel was estimated by the mass decrease in the swollen gel after being subjected to vacuum suction on a microfilter unit at an absolute pressure of 70 kPa (differential pressure of 30 kPa) for 15 min. A microfiltration membrane (Advantec, 0.45 μm) was used to prevent weak gel

samples from being destroyed by the suction. The mass of capillary water was determined by taking the difference between the mass of the deswollen gel after vacuum suction and the mass of the gel at the end of the water-vapor adsorption experiment. The determination of specific pore volume and characterization of the water states were conducted in triplicate.

3.2.2 Characterization of cryogel nanocomposites

UV-Vis absorption spectra of the nanocomposite solutions were obtained using a UV-Vis absorption spectrophotometer (Shimadzu UV-1700).

The topography of the nanocomposites was characterized using an atomic force microscopy (AFM, XE-100, Park Systems, Korea) via tapping mode in air at 26 °C. Note that thin hydrogel (nanocomposite) films were used for AFM studies.

The morphology of the cryogel nanocomposites was visualized using FESEM (JEOL JSM-7600F) while the elemental composition was determined using an energy-dispersive X-ray spectroscopy detector (EDX) attached to the FESEM.

X-ray diffraction (XRD) spectra were acquired using a powder X-ray diffractometer (Shimadzu 6000 or Bruker Advanced D8) with a monochromatic intensity Cu Kα radiation (λ = 1.5418 Å) in a 2θ range of 5-80° at a scan rate of 1.5°/min.

X-ray photoelectron spectroscopy (XPS) studies were conducted on a Kratos Axis Ultra or Theta Probe spectrometer with a monochromatic Kα excitation source ($h\nu$ = 1486.71 eV). The binding energies were calibrated using a C 1s core level at 284.8 eV as a reference.

The morphology and size of the AgNPs were studied using a transmission electron miscroscope (TEM, Carl Zeiss Libra 120) at an accelerating voltage of 120 kV. TEM images were analyzed using image-analysis software (ImageJ) to determine the particle-size distribution of the AgNPs. High-resolution TEM images of the AgNPs were obtained at an accelerating voltage of 200 kV (JEOL JEM-2010). TEM samples were prepared by grinding the nanocomposites into fine particles before they were dispersed in absolute ethanol. A few drops of the suspension were

added to a carbon-coated Cu grid (300 mesh) and were left to dry in a fume hood prior to imaging.

3.2.3 Uniaxial compression measurements

Fully-swollen gel samples of 10 mm thickness were tested under an unconfined compression condition using a computer-controlled mechanical testing system (Instron 5567). A 5 kN load cell at a ramp rate of 10 mm/min was used to compress the sample up to 95% strain of its initial total length at room temperature. The experiments were conducted in triplicate. The Young's modulus, E, was determined from the initial linear slope of the stress-strain curves plotted according to the following equation:

$$\frac{F}{\pi \times r^2} = E \frac{\Delta h}{h_o} \tag{4.2}$$

where F is the force applied to cylindrically-shaped gels with a cross-sectional area of πr^2, h_o is the height of the hydrogel during compression, and Δh is the change in the height of the sample during compression.

3.2.4 Determination of swelling and de-swelling properties

The swelling properties were determined by gravimetric analysis. For the determination of the swelling profile, a dried gel sample with 5 mm diameter and a 5 mm height was allowed to swell in an excess of MilliQ water. Water uptake by the gel sample was determined by measuring the cumulative mass increase at a pre-determined time interval. Excess surface water was gently wiped off using a damp paper towel before measuring the mass of the swollen gel. The degree of swelling at time t was calculated as follows:

$$\text{Degree of swelling} = \frac{m_t}{m_o} \tag{3.3}$$

where m_t and m_o are the masses of the swollen gel at time t and dried gel, respectively. The experiment was conducted in triplicate.

For the deswelling studies the fully swollen gel was placed on a microfilter unit (with a support membrane) connected to a vacuum suction at a pressure of 70 kPa for 1 min. Note that vacuum suction rather than mechanical compression was employed due to better experimental reproducibility. In practice, the absorbed water can be efficiently recovered by manual compression. Water recovery from the swollen gels was computed according to the following equation:

$$\text{Water recovery} = \frac{m_{swollen} - m_{deswollen}}{m_{swollen} - m_{dried}} \times 100\% \quad (3.4)$$

where m_{dried}, $m_{swollen}$, and $m_{unswollen}$ are the masses of the dried, swollen and de-swollen gels, respectively. Duplicate experiments involving twenty swelling-de-swelling cycles were conducted.

3.3 Protocols for microbiological assays

This section details the procedure employed to characterize the bactericidal efficacy of the materials developed and measurements of cellular-level changes of exposed cells. Unless otherwise mentioned, the control experiments for all microbiological assays were conducted using PSA cryogels. Also, note that for colorimetric-based assays outlined in Sections 3.3.3 to 3.3.7 (i.e., assays for determination of leakage of cytoplasmic contents, membrane integrity, intracellular ROS and ATP level, and TBARS level), abiotic control samples exposed to Ag-containing cryogel samples were also studied to account for possible interference due to the optical properties of Ag species.

3.3.1 Quantification of disinfection efficacy via plate-count assay

The antibacterial activity of the cryogels was tested against 4 types of bacteria: Gram-negative, *Escherichia coli* (ATCC25922) and *Salmonella Typhimurium* (NCTC 13348), and Gram-positive bacteria, *Bacillus subtilis* (ATCC6633) and *Staphylococcus aureus* (ATCC6538). Bacterial cells were harvested after reaching their mid-exponential growth phase. The harvested cells were washed by

centrifugation followed by resuspension in phosphate buffered saline (PBS, 0.01 M, pH = 7.45). Unless otherwise stated, the disinfection efficacy of the cryogels were determined by adding a 0.02 g cryogel sample into a 10 mL bacterial suspension of cell density 10^8 colony-forming units per mL (cfu/mL); manual shaking was provided during cryogel swelling in bacterial suspension. Control experiments were conducted without adding any cryogel into the bacterial suspension. After 15 s of swelling in the bacterial suspension, the swollen cryogels were quickly removed and squeezed to recover the absorbed water; hereafter this will be referred to as "squeezed water", while the term "bulk water" will refer to the excess bacterial suspension outside the cryogel (see Fig. 1.1). The spread-plate method was used for enumeration of the number of viable cells.

The kinetics of the bactericidal action was studied by using Universal Quenching Agent (UQA, 0.1% peptone + 0.1% $Na_2S_2O_3$ + 0.5% Tween 80 + 0.07% lecithin) to quench the disinfection reaction (Lambert et al., 1998; Johnston et al., 2002). Aliquots of squeezed water, which were contacted with the cryogels at various contact times, were diluted 10 times in UQA. The resultant mixture was allowed to react for 60 min before it was diluted in PBS and spread on agar plates. At least 6 replicate experiments were conducted.

Various ROS scavengers such as *N*-acetyl-*L*-cysteine (0.1 mM), superoxide dismutase (10 U/mL), catalase (10 U/mL), and DMSO (0.1 mM) were added to the bacterial suspension (15 min before the antibacterial tests) to elucidate the role of the ROS in disinfection. Control samples spiked with the ROS scavengers were conducted. Note that all the aforementioned ROS scavengers added at the indicated concentrations did not result in the reduction of viable bacteria in the suspension.

3.3.2 Examination of re-growth damaged bacterial cells

2 mL of bacterial suspensions exposed to cryogels were centrifuged in order to separate the excess silver leachate in the squeezed water. The pellets then were re-suspended in 50 mL of nutrient-rich medium at 37 ºC for 5 h to examine the possibility of cell repair under favorable conditions. Sample aliquots were obtained

every 0.5 h to determine the OD_{600} (optical density at 600 nm) using a spectrophotometer (Shimadzu UV-1700).

3.3.3 Determination of intracellular ATP level

E. coli exposed to cryogels for various contact times were assayed for adenosine triphosphate (ATP) by a luciferin/luciferase assay using a BacTiter-Glo microbial cell viability assay kit (Promega). The luminescence signal was measured in a microplate reader (Biotek Synergy 2). Triplicate experiments were conducted.

3.3.4 Determination of intracellular ROS level

Intracellular reactive oxygen species (ROS) generation was assessed by monitoring the enhancement of the fluorescence intensity of the exposed cells relative to that of the control. Bacterial samples were incubated with 2 µg/mL of 2',7'-dichlorodihydrofluorescein diacetate (DCFH-DA) for 30 min before they were exposed to the cryogels for 2 h in the dark. The bacterial suspension then was squeezed out and its fluorescence intensity was measured using a microplate reader (Biotek Synergy 2) at excitation and emission wavelengths of 485 and 535 nm, respectively. DCFH-DA is a non-fluorescent dye that is cell-permeable. DCFH-DA hydrolyzes to the non-fluorescent DCFH (2',7'-dichlorodihydrofluorescein) by esterases in the cells. In the presence of ROS, DCFH oxidizes to the fluorescent DCF (2',7'-dichlorofluorescein). Thus, enhanced fluorescence is indicative of an elevated level of ROS in the cell.

3.3.5 Determination of lipid peroxidation of exposed cells

A thiobarbituric acid reactive substances (TBARS) assay was employed to determine the presence of byproducts of lipid peroxidation (i.e., malondialdehyde). A bacterial suspension of cell density 10^{10} cfu/mL was used for this assay. The cells were exposed to the cryogels for 15 min before the assay. 1 mL of the exposed cells was lysed in 0.5% sodium dodecyl sulfate. Then 2 mL of the TBA reagent (that

comprises 20% trichloroacetic acid; 0.5% thiobarbituric acid; and 2.5 N HCl) was added to the sample. The resultant mixture was incubated in a water bath at 95ºC for 1 h. After cooling, the mixtures were centrifuged at 10,000 rpm for 15 min. The absorbance of the supernatant was measured at 532 nm using a spectrophotometer (Shimadzu UV-1700).

3.3.6 Determination of the leakage of cytoplasmic contents

Bacterial cell membrane integrity was examined using UV spectrophotometry (Shimadzu UV-1700) at 260 nm. When the bacterial membrane damage is severe, the release of cytoplasmic contents can be detected. The amount of DNA and RNA released from the cytoplasm can be estimated by the detection of the absorbance at 260 nm (Chen and Cooper, 2002; Liu et al., 2009b). After a 5 min incubation with cryogels, the bacterial suspension was immediately squeezed out and filtered through a 0.20 μm syringe filter before measuring its absorbance at 260 nm.

3.3.7 Determination of bacterial membrane integrity

The morphological changes of the bacterial cells after exposure to the cryogels were observed using FESEM (JEOL JSM-7600F). Samples were prepared by fixation with 2% glutaraldehyde for 1 h followed by repeated washing in 0.1 M sodium cacodylate buffer. The samples were subsequently dehydrated in an ethanol series of increasing concentration for 15 min before they were left to dry in a freeze-dryer for at least 24 h. The dried samples were coated with Pt prior to imaging.

The integrity of the bacterial membranes was also evaluated by staining the cells with SYTO 9 (6 mM) and propidium iodide (PI, 30 mM) (Live/Dead Baclight kit, Molecular Probes). Stained samples were observed under an epifluorescence microscope (Olympus BX60) using a ×100 oil objective. Note that both dyes are excited at 470 nm but emit at different wavelengths, namely 630 nm (PI) and 530 nm (SYTO 9).

3.4 Analytical methods for quantification of Ag species

The procedure used for the Ag speciation study is summarized in Fig. 3.1. The cellular fraction was separated from the suspensions via centrifugation at 10,000 rpm for 15 min. The supernatant of the bacterial suspension was further filtered through a 0.2 µm membrane to obtain the extracellular phase. Also, Ag^0 was separated by filtration through a centrifugal ultrafilter (Amicon, MWCO 3 kDa) (Liu and Hurt, 2010; Kennedy et al., 2012). All samples were digested in concentrated HNO_3 (67%, Merck) prior to total Ag analyses. A catalytic amount of H_2O_2 (30% v/v) was also added to ensure complete digestion of samples with high organic content. Either an inductively coupled plasma-optical emission spectrophotometer (ICP-OES, Perkin Elmer Optima 2000DV) or an inductively coupled plasma-mass spectrometer (ICP-MS, Elan DRC-e) was used to determine the total Ag concentration in the samples. The method of standard addition (Skoog et al., 1998) was employed to determine the Ag^+ concentration in the squeezed water (before digestion) using a silver/sulfide solid-state ion selective electrode (ISE, Orion) connected to an ion meter (Orion Dualstar) to detect Ag as Ag^+; all standards and samples were buffered with ionic strength adjuster (Orion) before ISE measurements.

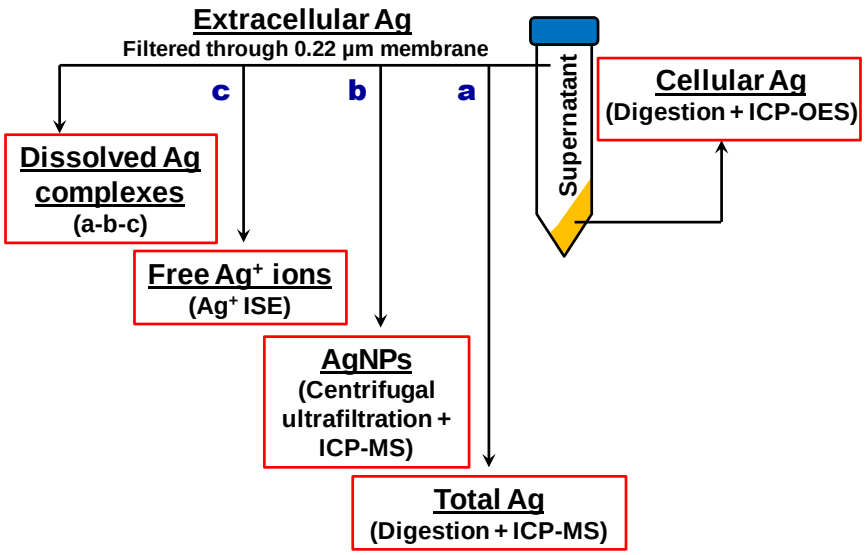

Figure 3.1 Schematic detailing the procedure employed for the Ag speciation.

3.5 Statistical treatment of data

The statistical significance of the difference between the obtained results was determined using the Student's *t* test; p-values smaller than 0.05 and 0.01 indicate a significant difference at a 95% and 99% confidence levels, respectively. All measurements are reported as the mean ± one standard deviation of at least three replicates.

CHAPTER 4 Design and synthesis of ice-templated PSA cryogels for water purification: towards tailored morphology and properties[†]

The objectives of the research reported in this chapter were (i) to study the effects of the synthesis conditions on the properties of poly(sodium acrylate) (PSA) cryogels, and (ii) to investigate the potential of PSA cryogels as an integral membrane for water purification during emergencies. PSA cryogels with a superfast swelling rate and a high degree of swelling that can withstand large compression strains were synthesized by modulating the synthesis conditions such as the freezing temperature, initial concentrations of monomer and initiator, and crosslinker ratio. In addition, the pore structure of the cryogels was correlated to their properties and performance. The results in this chapter will form the basis for the design strategies for the synthesis of cryogels with desired properties for emergency water treatment.

4.1 Experimental

The syntheses, characterization, and experimental procedure in this chapter can be found in Chapter 3. The detailed synthesis conditions used in this study are summarized in Table 4.1. In natural waters, most pathogens are attached to particulates in the water. Hence, the potential use of the PSA cryogels for water treatment was evaluated based on the efficiency of turbidity removal and water recovery. Contaminated water was obtained from a freshwater pond on the campus of Nanyang Technological University to which bentonite was added to increase its turbidity. Turbidity was measured using a turbidimeter (Hach 2100N). The turbidity removal efficiency was determined by comparing the turbidity of the raw and treated (or recovered) water samples. The experiments were conducted in triplicate.

[†]This chapter has been published as 'Design and Synthesis of Ice-Templated PSA Cryogels for Water Purification: Towards Tailored Morphology and Properties' in *Soft Matter*, 9 (1), 224-234. Please see Appendix A for reuse permission.

Table 4.1 Gel yield and mechanical properties of PSA gels synthesized under various conditions

Experimental variables					Gel yield (%)	Mechanical properties			Remarks
Preparation temperature (°C)	TEMED (% v/v)	APS (mM)	Monomer (%)	Crosslinker ratio (mol/mol)		Young's modulus (kPa)	Failure stress (kPa)	Failure strain (%)	
25	0.125	1.75	8	0.15	90	24.6 (1.4)	2.12	18	X
0	0.125	1.75	8	0.15	0	N.D.	N.D.	N.D.	N.D.
-6	0.125	1.75	8	0.15	37	35.6 (1.9)	6.7	29.2 (1.2)	X
-9	0.125	1.75	8	0.15	80	12.2 (1.9)	8.4 (1.4)	65.9 (1.2)	X
-12	0.125	1.75	8	0.15	85	4.7 (0.25)	10.8 (1.7)	79.0 (5.9)	O[b]
-15	0.125	1.75	8	0.15	84	5.25 (0.25)	[a]	[a]	O[c]
-20	0.125	1.75	8	0.15	85	6.25 (0.25)	[a]	[a]	O[d]
-20	0.0625	0.875	8	0.15	0	N.D.	N.D.	N.D.	N.D.
-20	0.125	1.75	8	0.15	85.0	6.25 (0.25)	[a]	[a]	O[d]
-20	0.25	3.50	8	0.15	85.4	13.7 (5.6)	[a]	[a]	O[f]
-20	0.50	7.00	8	0.15	81.6	106.3	15.4	25.5	X
-20	0.125	1.75	1	0.05	0	N.D.	N.D.	N.D.	N.D.
-20	0.125	1.75	3	0.05	54.1	N.D.	N.D.	N.D.	N.D.
-20	0.125	1.75	5	0.05	52.2	N.D.	N.D.	N.D.	N.D.
-20	0.125	1.75	8	0.05	95.3	2.2 (0.1)	[a]	[a]	O[e]
-20	0.125	1.75	10	0.05	92.9	4.5 (0.5)	[a]	[a]	O
-20	0.125	1.75	12	0.05	81.7	8.0	12.9 (1.6)	95	O
-20	0.125	1.75	15	0.05	78.7	10	18.2 (0.1)	86.7 (1.7)	X
-20	0.125	1.75	20	0.05	40.5	N.D.	N.D.	N.D.	N.D.
-20	0.125	1.75	8	0.0125	89.0	3.2 (0.5)	[a]	[a]	O
-20	0.125	1.75	8	0.05	95.3	2.2 (0.1)	[a]	[a]	O[e]
-20	0.125	1.75	8	0.10	83.5	3.3 (0.6)	[a]	[a]	O
-20	0.125	1.75	8	0.15	85.0	6.25 (0.25)	[a]	[a]	O

Note: N.D. = not determinable because the reaction mixture did not gel or the as-synthesized gel was too weak for further characterization, X = the gel was unable to complete the twenty cycles of swelling-de-swelling, and O = the gel was able to complete twenty cycles of swelling-de-swelling. Standard deviations are shown in parentheses. [a] No failure was observed at the end of the compression test; [b] Cryogel A; [c] Cryogel B; [d] Cryogel C; [e] Cryogel D; [f]Cryogel E.

4.2 Results and discussion

Note that for the following sections, the term "cryogel" refers to porous PSA gels that were synthesized at a preparation temperature of –9 °C and below, while the term "hydrogel" is used for non-porous PSA gels synthesized at a temperature of –6 °C and above. This distinction is based on the morphological difference observed for PSA gels synthesized at different preparation temperatures in the present study. The term "gel" is used as a general term that includes both hydrogels and cryogels.

4.2.1 Syntheses and gel yields of PSA cryogels

PSA cryogels were synthesized by conducting crosslinking reactions at subzero temperatures in a semi-frozen state. The semi-frozen system was heterogeneous and contained an unfrozen liquid microphase (UFLP) along with ice crystals (Lozinsky,

2002; Lozinsky and Damshkaln, 2003; Lozinsky, 2008). When the reaction mixture containing SA, MBA, TEMED, and APS was cooled to a temperature below the nominal freezing temperature, the majority of water formed ice crystals, whereas the bound water and soluble substances accumulated in the UFLP as a result of the freezing-point depression (Wolfe et al., 2002). This phenomenon is commonly referred to as cryo-concentration. In the UFLP, TEMED catalyzes the decomposition of the persulfate ions to form sulfate-free radicals that initiate the copolymerization reaction between SA and MBA under subzero temperature conditions.

The gel yields for most of the PSA cryogels synthesized below a T_{pep} of –9 °C were 80-95% (Table 4.1). The relatively high gel yield was attributed to the cryo-concentration phenomenon that effectively increased the reaction mixture concentration. A portion (or all) of the reaction mixture cooled to either –6 or 0 °C was neither crosslinked nor frozen during the course of the reaction. This could be due to a decrease in the reaction rate constant (at lower temperatures) that was not accompanied by an increase in the reaction mixture concentration in the absence of cryo-concentration as the T_{prep} was thought to be higher than the initial ice crystallization temperature of the system.

The concentration of the initiator pair used also has a significant influence on the gel conversion. As shown in Table 4.1, when the concentrations of APS and TEMED were lower than 1.75 mM and 0.125%, respectively, no gelation was observed because the concentrations were too low such that the number of free radicals generated was insufficient to initiate the crosslinking reaction of SA and MBA.

The gel yield was found to increase with an increase in monomer concentration from 1 to 10% due to an increased polymerization rate (Table 4.1). However, a further increase in the initial monomer concentration resulted in a lower gel yield (Table 4.1). This may be the result of the increased viscosity of the UFLP that affected the reaction between the free radical and monomer owing to a corresponding decrease in their diffusivities. Note that the concentration of the reaction mixture can be significantly increased due to the cryo-concentration

phenomenon. Kirsebom et al. (2009b) have shown that the concentration of solute in the UFLP increased from an initial 6% monomer solution of dimethylacrylamide and poly(ethylene glycol) diacrylate to 33% and 46% at T_{prep} of –10 and –20 ^{o}C, respectively.

4.2.2 Morphological characterization of PSA gels

The study of pore structures in gel samples is challenging since there is no standard method for pore-structure determination of soft matter. Pore-structure characterization techniques such as mercury-intrusion porosimetry and gas adsorption/desorption among others are not suitable due to the compressibility of gels under high pressure. Microscopic techniques that allow examination of swollen gels can be used to reveal their actual structure (prior to drying). Examples of such techniques are optical microscopy, environmental scanning electron microscopy (ESEM), and confocal laser scanning microscopy (CLSM).

CLSM was used to obtain 3D images of swollen PSA gels. Fig. 4.1 shows a comparison of the 3D reconstructed images of PSA gels synthesized at 25 and –15 ^{o}C that were previously stained with a fluorescent probe. This figure shows that a highly porous network can be obtained when the polymerization is carried out at subzero temperatures in comparison to the nonporous network obtained at ambient temperature (Fig. 4.1). Although CLSM can be used to visualize the 3D pore structure of swollen gels, this technique did not have sufficient resolution to reveal the fine structure of the cryogels.

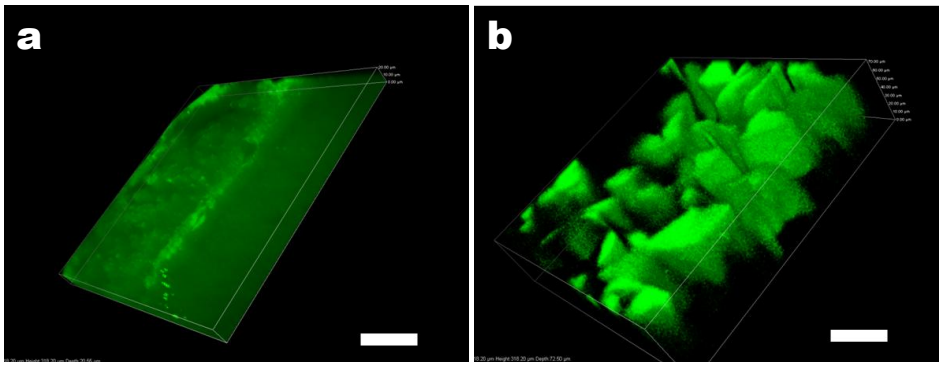

Figure 4.1 3D confocal images of PSA gels synthesized at (a) 25 °C and (b) –15 °C, respectively. Note that the green area is the gel matrix that was stained with fluorescent FITC dye. The scale bars represent 100 µm.

Fig. 4.2a shows selected SEM images of PSA cryogels synthesized at different T_{prep}. A highly porous network was obtained when T_{prep} was below –9 ^{o}C while those synthesized above –6 ^{o}C were essentially nonporous (Fig. 4.2a). The SEM images of PSA hydrogels showed some crack development because they could not withstand the internal volume changes during the solvent-exchange process used to prepare the samples for analysis (Fig. 4.2a). The SEM images show that the pore interconnectivity and porosity increased while the pore-size distribution became narrower as T_{prep} decreased from –9 to –20 ^{o}C (Fig. 4.2a). Indeed, the specific pore volume was found to increase from 2.43 to 2.92 cm^3/g as T_{prep} decreased. Similar observations were made by Hwang et al. (2010) who observed that poly(ethylene glycol) cryogels prepared at –14 and –20 ^{o}C had a closed and an interconnected structure, respectively. Furthermore, the average pore size decreased from 25 to 11 μm as T_{prep} decreased from –9 to –20 ^{o}C (Fig. 4.3a). Note that a lower T_{prep} corresponds to a faster freezing rate. Hence, this is consistent with the thermodynamics of ice nucleation that predicts the formation of a larger number of small ice crystals at a faster freezing rate (Lozinsky et al., 2001; Plieva et al., 2004; Kirsebom and Mattiasson, 2011). The concentration of the APS/TEMED initiator pair controls the polymerization rate and also has a significant effect on the gel morphology as shown in Fig. 4.2b. In order to discuss the effects of the initiator content on the gel morphology, two modes of gelation need to be distinguished, namely: (i) freezing before gelation, and (ii) freezing after gelation (Plieva et al., 2006). It was observed that cryogelation using an APS concentration between 1.75 and 3.50 mM for an 8% monomer concentration followed the first mode of gelation and gave rise to a well-interconnected structure (Fig. 4.2b). The specific pore volume decreased slightly from 2.92 to 2.70 cm^3/g on doubling the APS concentration from 1.75 mM (at a constant APS/TEMED ratio). The average pore size decreased as the initiator concentration increased from 1.75 to 3.50 mM (Fig. 4.3b). This may be due to a faster polymerization rate that leads to smaller ice crystals.

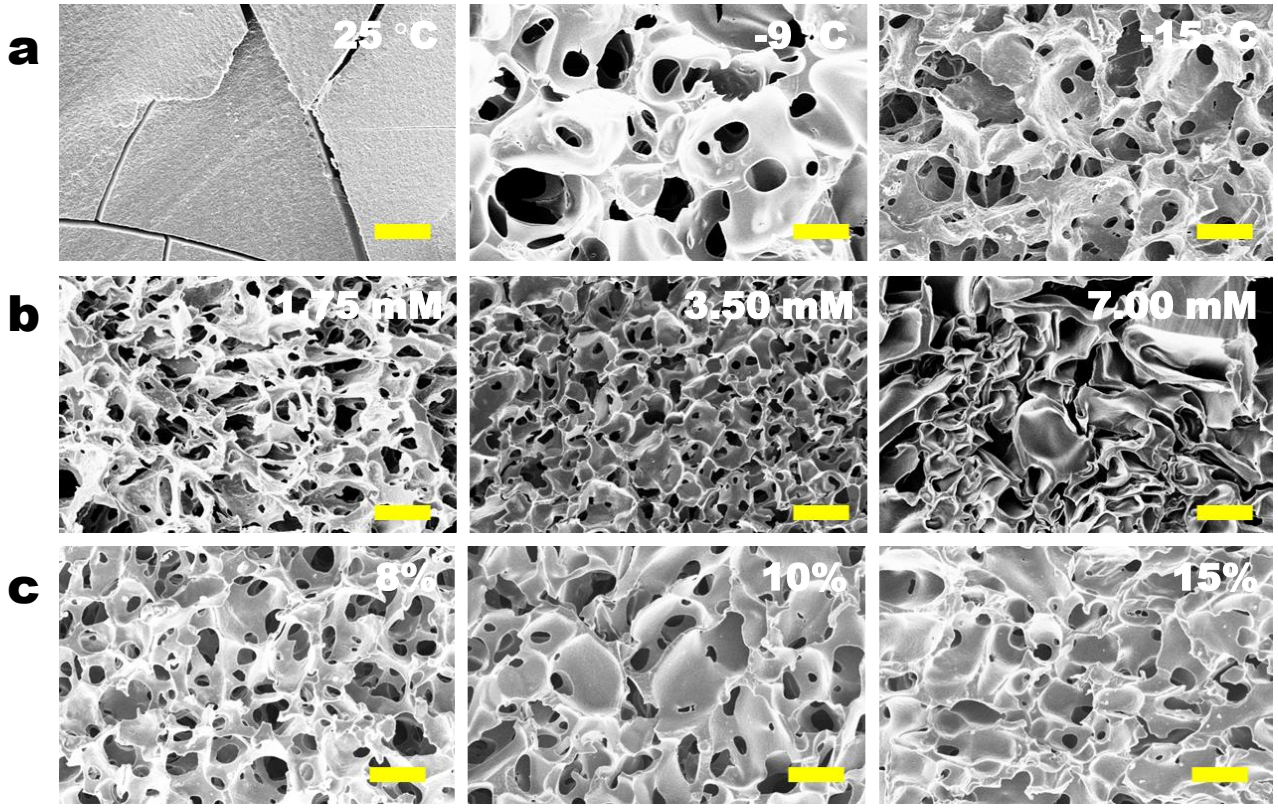

Figure 4.2 Selected SEM images of PSA gel cross-sections synthesized at various (a) preparation temperatures, (b) APS concentration (at constant TEMED to APS ratio), and (c) initial monomer concentration. Unless otherwise stated, the above PSA cryogels were synthesized at –20 °C for an 8% monomer concentration; the APS and TEMED concentrations used were 1.75 mM and 0.125%, respectively. The crosslinker ratio used for the cryogels shown in (a) was 0.15 mol MBA/mol SA while those in rows (b) and (c) employed a crosslinker ratio of 0.05 mol MBA/mol SA. Note: all the scale bars represent 50 µm.

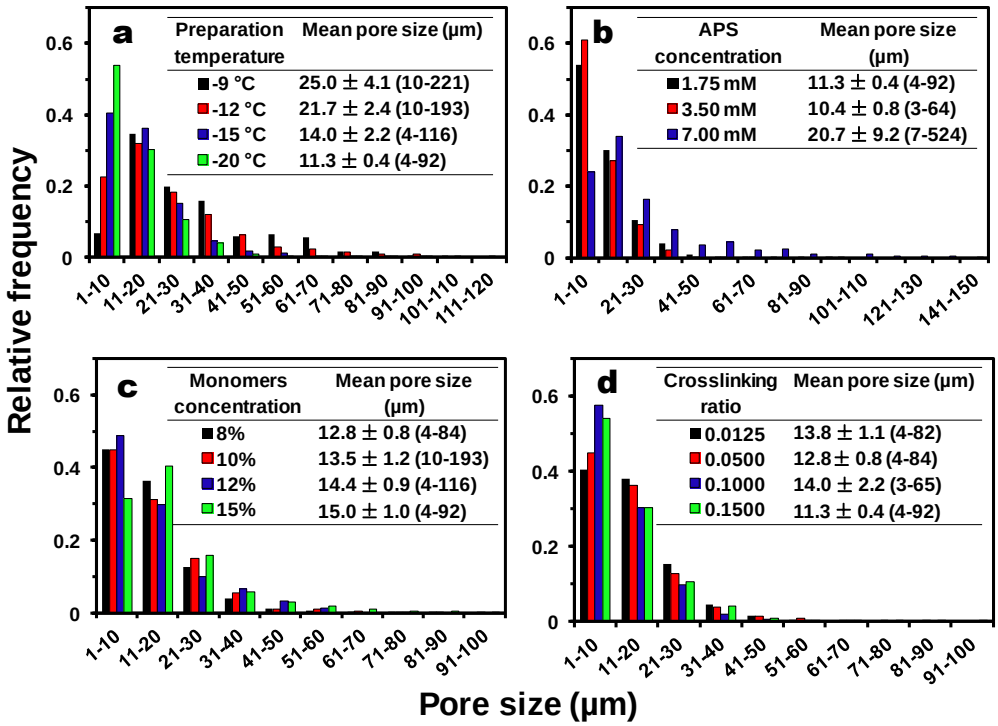

Figure 4.3 Effect of (a) preparation temperature, (b) APS concentration, (c) initial monomer concentration on the pore-size distribution, and (d) crosslinker ratio. Note: the figure shows only a limited range of pore sizes. The real range of pore sizes for a given PSA gel sample is shown in parentheses under the "average pore size" column.

A further increase in the APS concentration resulted in PSA cryogels with a larger average pore size. A mixture of open and closed pores was formed indicating that the gelation mode is "freezing after gelation" (Fig. 4.2b). The specific pore volume was significantly reduced to 0.19 cm^3/g. This can be attributed to the presence of numerous closed pores that could have prevented the absorption of cyclohexane. Closed rather than interconnected pores were formed because it was not possible for the ice crystals to merge in a reaction mixture that was already crosslinked. In addition, it is thought that larger pores are formed because the water in large voids is preferentially frozen relative to that in small capillaries due to a smaller freezing-point depression (Plieva et al., 2006). The smaller pores observed in the SEM image of the PSA cryogel obtained by the "freezing after gelation" mode were probably the result of collapsed pores due to weak pore walls that were not formed by cryo-concentration (Fig. 4.2b).

Fig. 4.2c shows that increasing the initial monomer concentration resulted in lower porosity, less pore interconnectivity, and thicker pore walls. In addition, the SEM images revealed that there were numerous large closed pores that were formed as the monomer concentration was increased (Fig. 4.2c). This resulted in a larger average pore size as the monomer concentration increased (Fig. 4.3c). The formation of large closed pores could be the result of (i) an increased viscosity of the UFLP that reduced the rate of ice crystallization and (ii) an enhanced rate of polymerization due to higher monomer concentration. This could have caused gelation to take place faster than freezing, thereby leading to the formation of large closed pores. Ozmen and Okay (2006) also found that increasing the 2-acrylamido-2-methylpropane sulfonic acid (monomer) concentration resulted in the formation of larger pores with thicker pore walls. They believed that the larger pore size resulted from a higher charge density in the network chain that increased the ice volume fraction (Ozmen and Okay, 2005). However, other researchers have reported that an increase in the initial monomer concentration led to cryogels with thicker pore walls but a smaller pore size due to a higher amount of UFLP (Plieva et al., 2005; Dinu et al., 2007). These conflicting findings might be attributed to the difference in the nature of the monomers (i.e., ionic or non-ionic) used.

The crosslinker ratio (mol MBA/mol SA) was found to have little effect on the PSA cryogel morphology (data not shown). The specific pore volume for various crosslinker ratios of 0.0125 to 0.1500 mol/mol ranged from 2.92 to 3.39 cm^3/g. PSA cryogels synthesized using crosslinking ratios of 0.0125 to 0.1500 (mol/mol) (for an 8% monomer solution at –20 °C, 0.125% TEMED, and 1.75 mM APS) all formed highly interconnected pores. However, it was noted that on increasing the crosslinker ratio, the average pore size decreased slightly (Fig. 4.3d). This could be attributed to a decrease in the network charge density with increasing crosslinker ratio (i.e., lower SA content) leading to a smaller pore size.

4.2.3 Mechanical properties of PSA gels

The stress-strain curve in Fig. 4.4a shows the typical elastic behavior of a PSA cryogel in contrast to a weak and fragile hydrogel. Digital photographs of a PSA hydrogel and cryogel during compression tests provide a visual comparison of their mechanical properties (Fig. 4.4b).

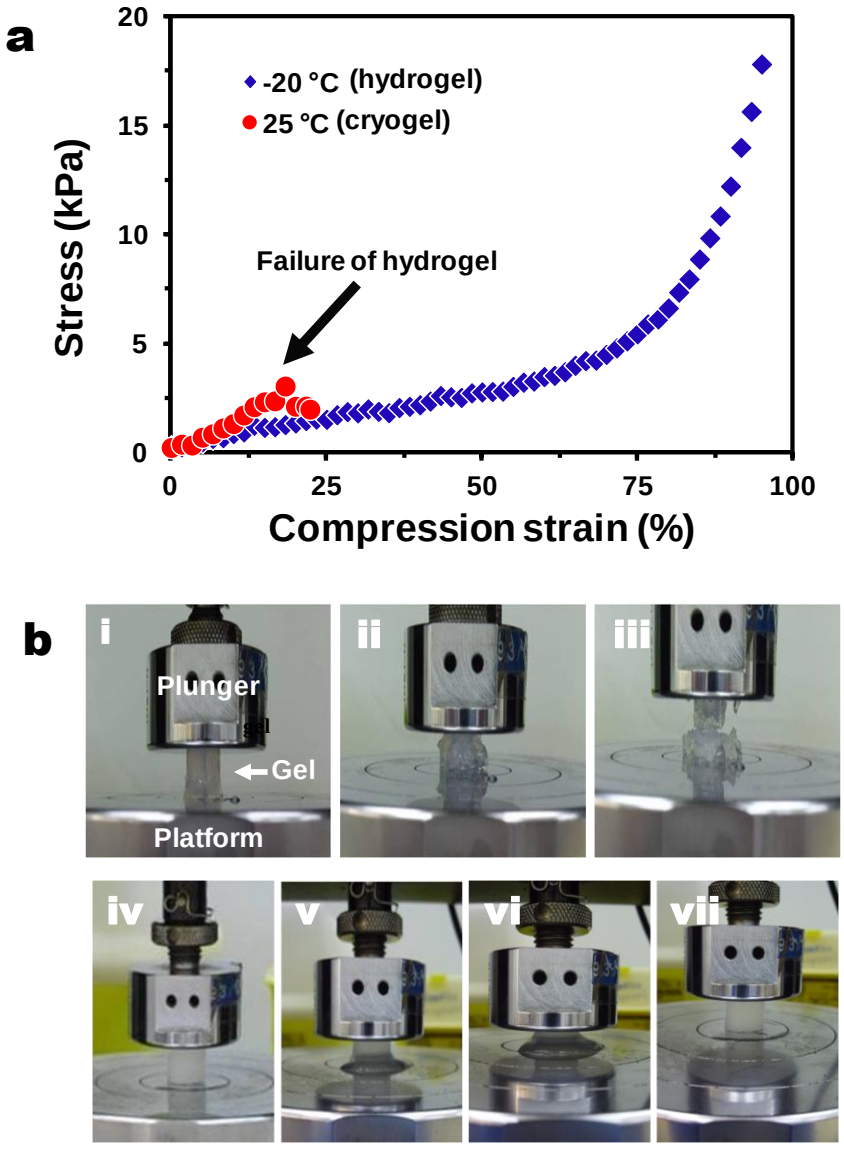

Figure 4.4 (a) Stress-strain curves for PSA hydrogels and cryogels. Note that the arrow shows the point at which the hydrogel started to fail/disintegrate. (b) Visual comparison of the mechanical properties of PSA hydrogels (insets: i-iii) and cryogels (insets: iv-vii).

The PSA hydrogel was completely broken when compressed to 18% strain (Fig. 4.4b i-iii). In contrast, the PSA cryogel did not show any crack development after being compressed to 95% strain (accompanied by a loss of water or deswelling) and re-swelled to its original shape after relieving the pressure (Fig. 4.4b iv-vii). Most PSA cryogels synthesized in this study did not break when compressed to 80% strain (Table 4.1). However, the PSA cryogel obtained by "freezing after gelation" had a very fragile network (Table 4.1). This may be attributed to the formation of ice crystals in the gelled reaction mixture that damaged the network because it could not withstand the stress exerted by the growing ice crystals.

In order to apply PSA cryogels for water purification, it is important that the cryogels have high elasticity to undergo oscillatory swelling-deswelling cycles while maintaining the network integrity. In addition, the network should not be too rigid so that water recovery can be conducted using mild pressure. The stiffness of a conventional hydrogel mainly depends on the network structure such as the crosslinking density of the material. In contrast, for porous materials such as cryogels, the stiffness is a function of the porosity (Savina et al., 2007). In addition, the swelling degree could have an effect on their stiffness since the compression of a cryogel involves the release of absorbed water.

Interestingly, it was observed that PSA cryogels with pore volumes greater than 2.7 cm^3/g did not fail at the end of the compression tests. A cross-examination of the morphology of these cryogels revealed that they have open interconnected pores with sufficiently small pores (average pore size: 10-14 μm) that confer them with impeccable mechanical properties. In contrast, cryogels that have the worst mechanical properties are those with very large open pores (average pore size >20μm) even though their pore volumes are quite high (2.5 cm^3/g). PSA cryogel with a mixture of closed and open pores that have a relatively lower pore volumes (0.2-2 cm^3/g) show intermediate mechanical properties.

4.2.4 Swelling behavior of PSA gels

From an application viewpoint, gels that can swell quickly are desirable since this reduces the treatment time. In this respect decreasing the T_{prep} drastically improved

the swelling rate of the PSA gels (Fig. 4.5). PSA cryogels reached their equilibrium degree of swelling within 15 s while the PSA hydrogels took about 30-90 min (Fig. 4.5). The swelling profiles of PSA cryogels indicate that those with large and open interconnected pores had a faster swelling rate than those having small or closed pores (data not shown).

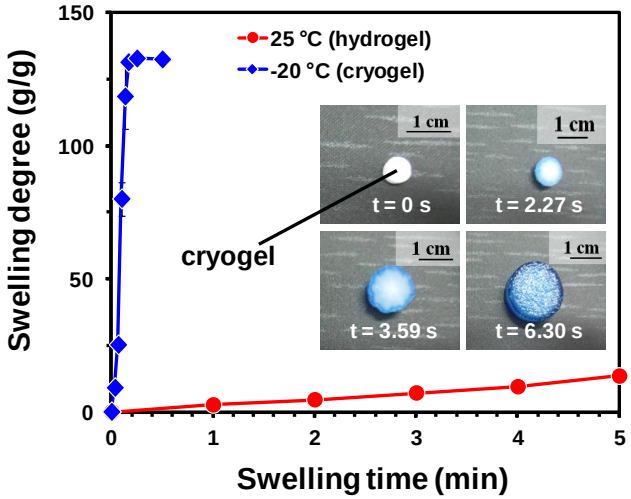

Figure 4.5 Dynamic swelling profiles of PSA hydrogels and cryogels. The inset shows the time-dependent swelling of a typical PSA cryogel.

Overall, a higher degree of swelling was observed for PSA cryogels having a larger pore volume although the correlation is not necessarily linear (Figs. 4.6a-d, inset). It is postulated that PSA cryogels with a higher pore volume could absorb more water due to the additional volume present in the cryogel matrix. This hypothesis is supported by the findings from the characterization of the water states in swollen cryogels, which indicated that the increase in the degree of swelling was due to a greater amount of free water in the pores (Fig. 4.7). The specific pore volumes of dried PSA cryogels synthesized in this study ranged from 1.9 to 3.4 cm^3/g. The relatively small difference in the specific pore volume among the dried PSA cryogels cannot explain the large increase in the degree of swelling. However, it is likely that the network expansion as the cryogel swelled led to an enlarged pore volume that allowed even more absorption of water. Indeed, the CLSM image of a swollen PSA cryogel showed an expanded network with a larger pore size in comparison to a dried PSA cryogel (Fig. 4.1).

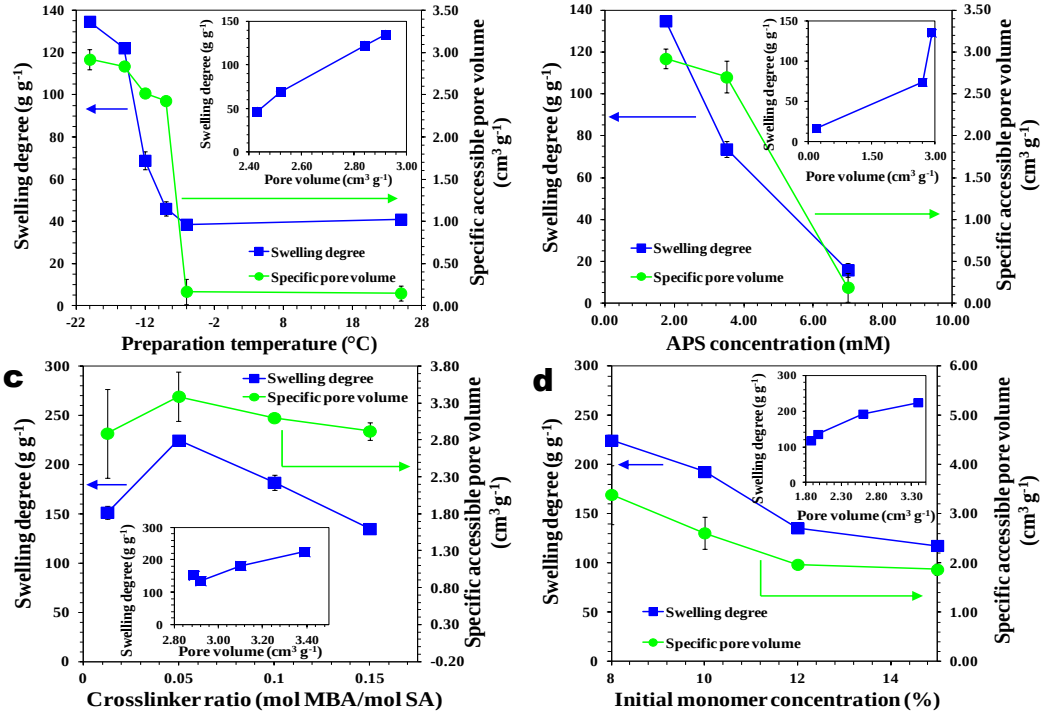

Figure 4.6 Effects of (a) preparation temperature, (b) APS concentration, (c) crosslinker ratio, and (d) initial monomer concentration on the equilibrium swelling degree and specific pore volume of PSA gels. The insets show the relationship between the swelling degree and pore volume.

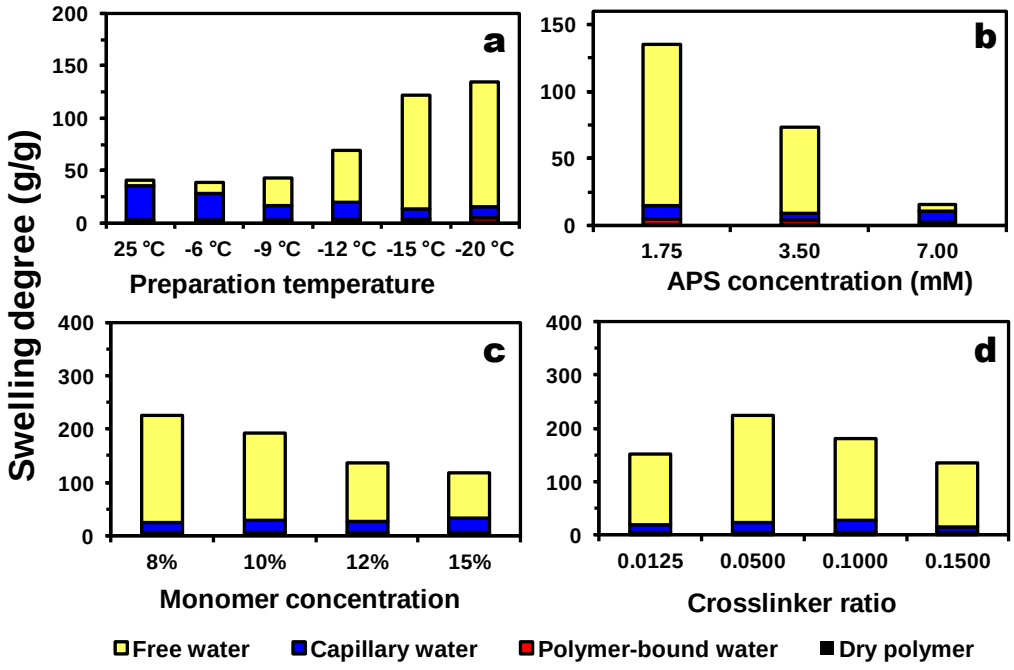

Figure 4.7 Effects of (a) preparation temperature, (b) initiator content, (c) crosslinker ratio, and (d) initial monomer concentration on the swelling degree and distribution of water states.

In addition to the pore volume, the network flexibility could also affect the swelling degree. It was found that the swelling degree increased with decreasing crosslinker ratio and reached a maximum at a crosslinker ratio of 0.05 (mol MBA/mol SA) (Fig. 4.7c). A lower crosslinking density would facilitate network expansion due to flexible polymer chains. However, a further decrease of the crosslinker ratio resulted in a lower degree of swelling (Fig. 4.7c). It is thought that at a low crosslinking density there could be a tradeoff between chain flexibility and the ability of the polymer chains to withstand elongation. It is believed that the latter factor predominated in this case causing less network expansion that resulted in a lower degree of swelling.

4.2.5 Oscillatory swelling-deswelling behavior of PSA cryogels

Another remarkable feature of cryogels is their ability to reversibly swell and de-swell without losing mechanical integrity (Mikhalovsky et al., 2011). As shown in Fig. 4.8, most of the PSA cryogels exhibited a superfast and stable oscillatory swelling-deswelling up to 20 cycles without any significant loss in the degree of swelling and recovery of water. In addition, the deswollen PSA cryogels re-swell instantaneously once in contact with water. The stable, rapid, and large oscillations of PSA cryogels indicate that they have the robustness to be reusable in emergency situations.

Cryogels that lacked elasticity could not withstand the swelling-deswelling cycles developed cracks and broke before the completion of the 20 cycles. The cryogels that broke before the completion of the swelling-deswelling test are indicated with a symbol “X” in the “Remarks” column of Table 4.1. A cross-examination of their morphologies indicate that PSA cryogels with closed and/or large pores could not survive the 20 swelling-deswelling cycles whereas those with small and open interconnected pores could survive the oscillatory swelling-deswelling without significant mechanical degradation.

In addition to reversible behavior, a large difference in the swelling-deswelling magnitude is also desired since it permits higher water recovery. Also, the absorbed

water should be recoverable using mild compression or vacuum suction because the use of high energy-consuming devices is usually not possible after a disaster due to power breakdown. Most of the water in swollen conventional hydrogels is polymer-bound and cannot be released easily. It has been reported that a 3 MPa pressure could recover only 5% of the absorbed water in a PSA hydrogel (Li et al., 2011a)

In contrast, there are three different water states in a swollen cryogel, namely (i) water that is hydrogen-bonded to the polymer (polymer-bound water), (ii) water that is weakly interacting with the polymer and is freezable (capillary water), and (iii) free water that does not interact with the polymer (free water) (Savina et al., 2011b). The majority of the water in a swollen cryogel exists as free water and can be recovered by low-pressure compression (Lozinsky, 2002; Plieva et al., 2004).

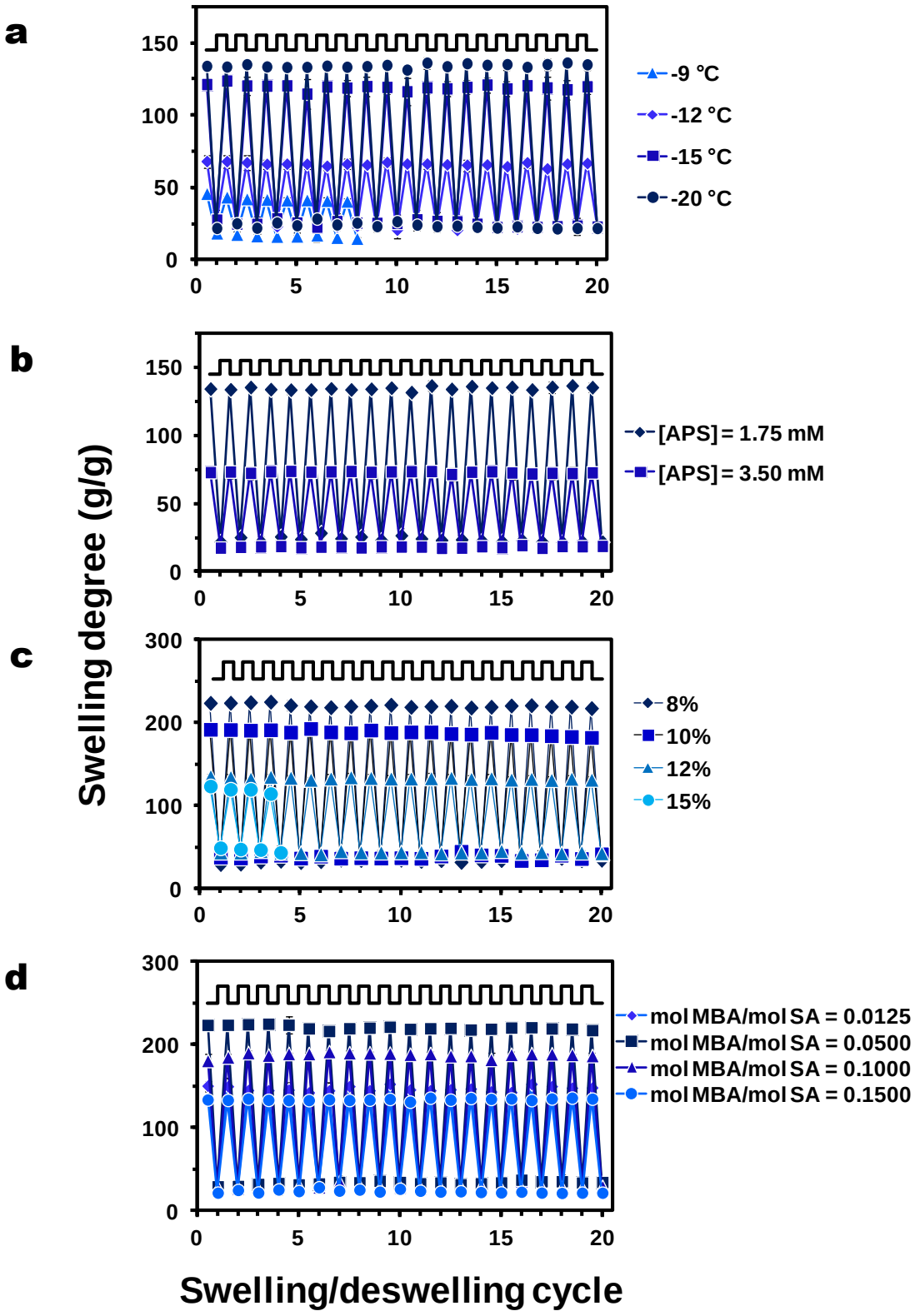

Figure 4.8 Effect of preparation temperature on the oscillatory swelling-deswelling behavior of PSA cryogels.

The water recoveries varied between 31-85% depending on the synthesis conditions of the PSA cryogels. It was found that the water recoveries were higher for cryogels synthesized with a lower T_{prep}, initiator content and initial monomer concentration, but were not significantly affected by the crosslinker ratio. This is because these conditions allowed the formation of a swollen network in which the proportion of free water was higher. This is supported by the fact that water recovery has a good correlation with the dry pore volume and free water content of swollen PSA cryogels (Fig. 4.9).

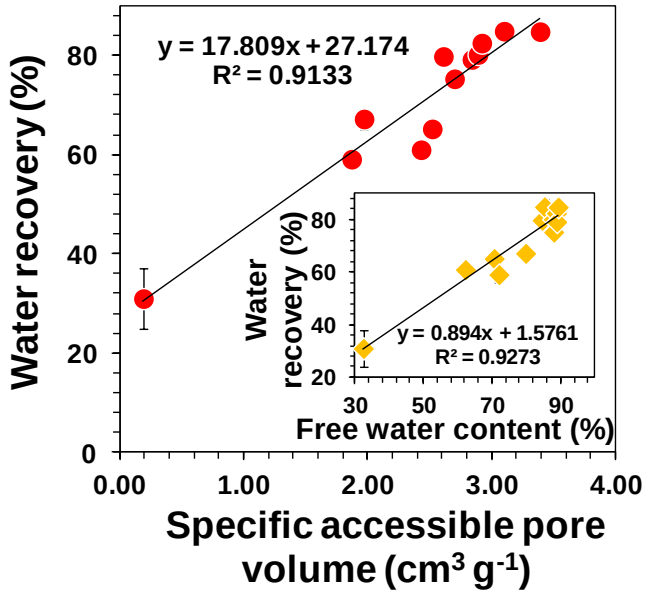

Figure 4.9 Correlation of water recoveries of PSA cryogels with their corresponding pore volumes. The inset shows the correlation between water recovery and free water content.

4.2.6 Potential of PSA cryogels for particulate removal

In order to be applied for water purification in emergency situations, PSA cryogels must exhibit the following properties: (i) fast swelling, (ii) significant swelling, (iii) high reusability, (iv) high water recovery, and (v) high rejection towards particulates. For example, the PSA cryogel with the highest degree of swelling could swell up to 220 grams of water per gram of cryogel of which 85% could be recovered. This means that about 190 mL of water can be treated by 1 g of the dried

PSA cryogel in one cycle. In addition, the rapid swelling kinetics that allowed the PSA cryogel to reach equilibrium within 15 s and the relatively high water recovery using mild vacuum suction for a short duration (1 min) showed that the PSA cryogel has met the first four criteria required for emergency drinking-water response applications. Note that the absorbed water can also be recovered via manual hand compression. Hence, to evaluate the potential of PSA cryogels for water purification in emergencies, the separation efficiency of PSA cryogels needs to be investigated.

Fig. 4.10 illustrates the concept of using a PSA cryogel as an integral membrane for water purification in disaster relief. The approach involves allowing the dried cryogels to fully swell in the manually-stirred contaminated water (~ 2 min) after which they were gently rinsed in DI water for 10 s to remove superficial contaminants (Fig. 4.10). The absorbed water was recovered by vacuum suction using a microfilter unit for 1 min (without using a membrane support) (Fig. 4.10).

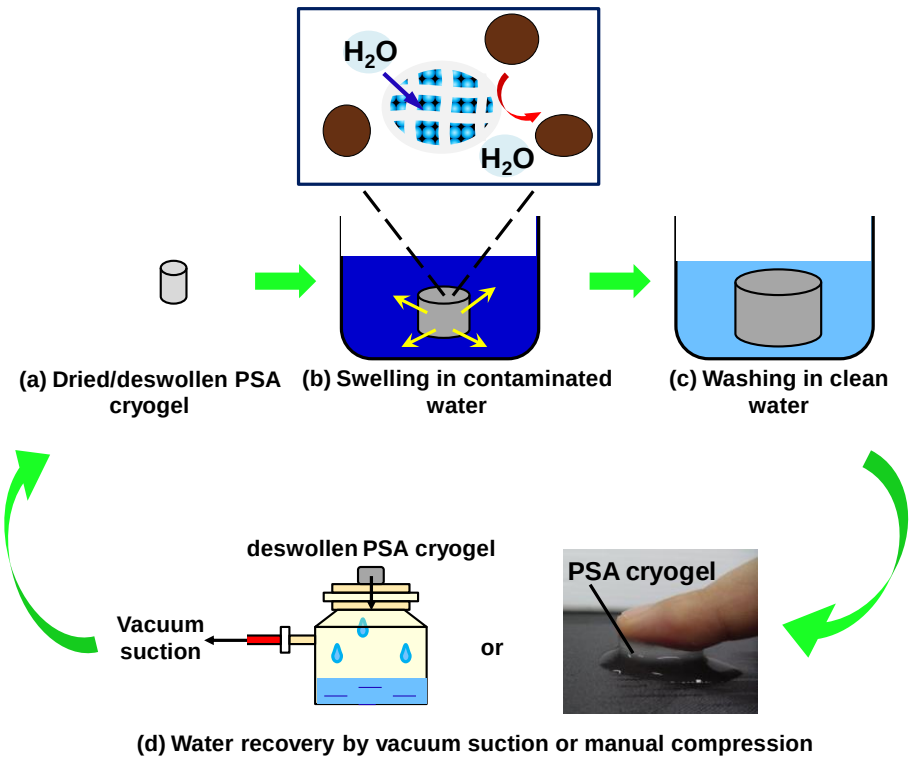

Figure 4.10 Conceptual diagram depicting the use of superabsorbent cryogels for emergency water treatment.

The separation efficiency of the PSA cryogels was evaluated by measuring the turbidity removal. A contaminated water sample with a turbidity of about 650 NTU (Nephelometric Turbidity Unit) was used as the raw water. The PSA cryogel having the highest swelling degree was tested for its separation efficiency (Cryogel C, Table 4.1). It was found that the PSA cryogel took a longer time to reach its equilibrium swollen state in the contaminated water (2 min versus 15 s). In addition, the water recovery decreased by 5-10% relative to the tests conducted using MilliQ water (Fig. 4.11a). This could be due to the partial clogging of the cryogel pores by the particulates present in the contaminated water.

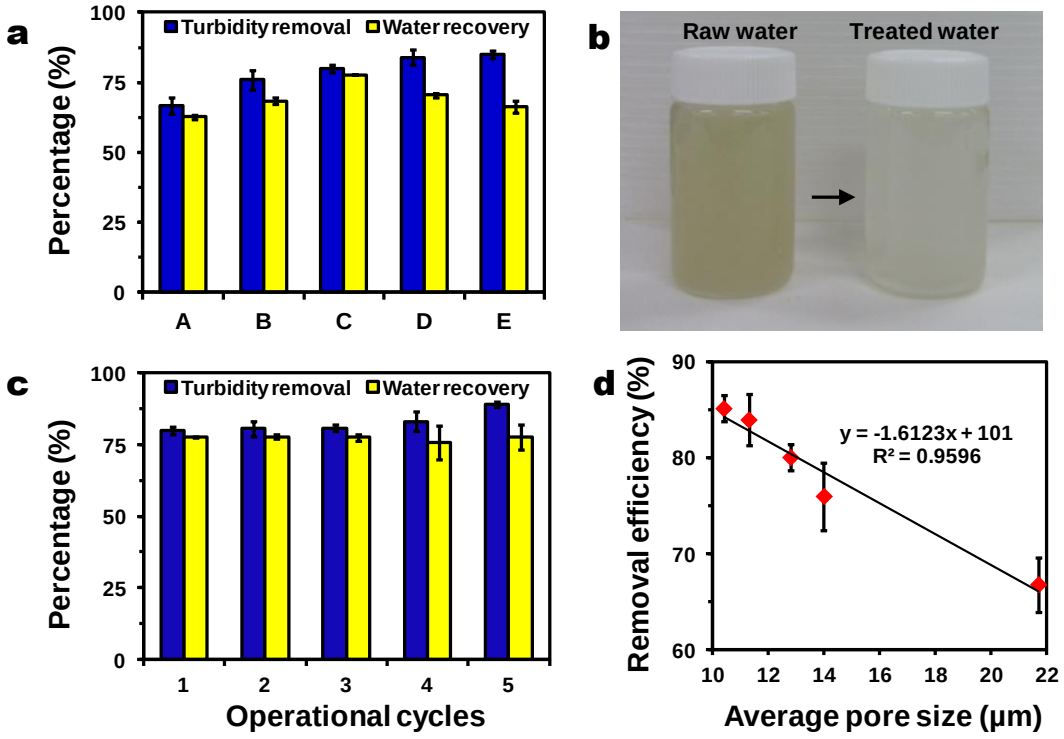

Figure 4.11 (a) Turbidity removal efficiencies and water recoveries of PSA cryogels with the highest swelling ratio over five operating cycles, (b) digital photograph of the raw and treated water, (c) turbidity removal efficiencies and water recoveries of five PSA cryogels having different average pore sizes, and (d) the correlation between the turbidity removal efficiency and average pore size. Note: synthesis conditions for cryogels A, B, C, D, and E can be found in Table 4.1.

Although the deposited particulates resulted in some reduction in the water recovery and a lower swelling rate, they enhanced the removal of turbidity (Fig. 4.11). The Fig. 4.12 shows the morphological differences between fresh and used cryogels. For the used PSA cryogel the SEM image shows a large number of foreign particles that were not present in the fresh PSA cryogel (Fig. 4.12). The particulates were distributed rather uniformly throughout the cross-section of the cryogel and were deposited mostly in the internal pore surface (Fig. 4.12b).

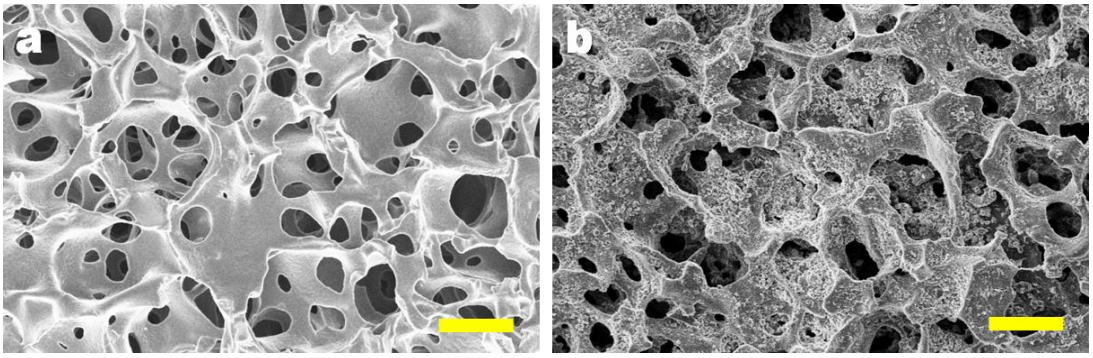

Figure 4.12 Comparison of the SEM images of (a) fresh and (b) used PSA cryogels. Note the scale bars represent 50 µm.

The PSA cryogel had an initial turbidity removal efficiency of 80% that increased to 90% towards the fifth cycle (Fig. 4.11a). This could be due to the decrease in the cryogel pore size as the particulates were deposited in the pores. Fig. 4.11b shows the visual improvement of the treated water samples. The turbidity removal efficiency and water recovery of a series of PSA cryogels having different average pore sizes (labeled A-E in the order of decreasing average pore size, Table 4.1) are shown in Fig. 4.11c. The turbidity removal efficiency was found to increase linearly with decreasing average pore size (Fig. 4.11d). The results indicated that PSA cryogels have a relatively good turbidity removal. Nevertheless, the separation properties of PSA cryogels can be improved by the inclusion of a fast freezing step to produce smaller pores that can be achieved by flash freezing in liquid nitrogen (Qian et al., 2009; Wu et al., 2012). The PSA cryogels can also be functionalized using agents such as silver nanoparticles to impart disinfection properties (Li et al., 2008; Qu et al., 2013). Chapters 5 to 8 elaborate the findings obtained from work performed on cryogels incorporated with AgNPs.

4.2.7 Design strategies of PSA cryogels

The findings in this study indicated that PSA cryogels with open interconnected pores and high porosity are desired for water-treatment applications because they had a higher rate and degree of swelling, and could withstand large deformation. In addition, the pore size of the PSA cryogels should be sufficiently small in order to achieve satisfactory separation and mechanical properties although there could be a compromise in the swelling rate. Controlling the T_{prep} is instrumental in achieving the desired pore morphology since pore formation results from ice crystallization. However, it is also important to control the initial monomer and initiator concentrations in order to tune the polymerization rate such that ice crystallization occurs prior to gelation. The crosslinker ratio can be varied to tune the swelling degree of PSA cryogels although it did not have a substantive effect on the morphology. Table 4.2 summarizes the design strategy that can be employed to fabricate cryogels with tailored properties.

Table 4.2 Summary of design strategies to achieve the desired properties of PSA cryogels

Criteria	Desired morphology	Design strategy
Fast swelling	Large and open interconnected pores	Moderate freezing rate; ensure "freezing before gelation" mode by minimizing monomer and initiator concentrations
Significant swelling	Open interconnected pores with high pore volume	Ensure "freezing before gelation" mode by minimizing monomer and initiator concentrations; use a lower freezing temperature; minimize crosslinker ratio to obtain a flexible network
High reusability/ robust	Small and open interconnected pores with high pore volume	Ensure "freezing before gelation" mode by minimizing monomer and initiator concentrations; use a lower freezing temperature and fast freezing rate
High water recovery	Open interconnected pores with high pore volume	Ensure "freezing before gelation" mode by minimizing monomer and initiator concentrations; use a lower freezing temperature.
Good separation	Small pores	Use a fast freezing rate; use high initiator content; minimize monomer concentration.

This study found a range of conditions for the synthesis of PSA cryogels with the desired morphologies and properties (T_{prep} of −15 to −20 °C; 8-10% monomer concentration; 0.125-0.250% APS and 1.75-3.50 mM TEMED; and 0.0125-0.150 mol MBA/mol SA). Further optimization based on the ranges identified may further improve the properties of PSA cryogels.

4.3 Concluding remarks

This study demonstrates that the pore structure and swelling properties of poly(sodium acrylate) (PSA) cryogels can be modulated by synthesis conditions such as the preparation temperature, initial monomer and initiator concentrations, and crosslinker ratio. By varying the synthesis conditions PSA cryogels were prepared that displayed a superfast swelling rate, high degree of swelling, and the ability to withstand large deformation. In addition, the predominant form of water in swollen PSA cryogels is free water that can be recovered easily by mild pressure. The use of PSA cryogels as integral membranes for turbidity removal was tested. A relatively high water recovery and particulate removal efficiency were achieved. In addition, the turbidity removal efficiency was found to increase with operating cycles due to pore-size reduction as the particulates in the raw water become deposited in the cryogel pores. These cryogels can also be used to absorb water to the exclusion of particulates in hybrid processes that employ other agents to remove the pathogens in contaminated sources. Hence, the PSA cryogels fabricated in this study have the potential to be developed into portable water filters for application in emergency response.

CHAPTER 5 Fabrication of PSA cryogels incorporated with silver nanoparticles via various synthesis routes[†]

The objective of this chapter was to compare the effects of employing different synthesis approaches on the properties and bactericidal activity of the resulting cryogels incorporated with silver nanoparticles (AgNPs) prepared via three synthesis routes: (i) incorporation of pre-synthesized AgNPs during cryogelation, (ii) ice-mediated coating of pre-synthesized AgNPs on pre-formed PSA cryogels, and (iii) *in situ* reduction of PSA cryogels loaded with Ag^+. The three synthesis methods are anticipated to result in cryogels with different different AgNP-size and -spatial distributions, pore morphology, swelling and mechanical behavior, and disinfection efficacy. The results in this chapter will guide the selection of the synthesis approach of AgNP-incorporated cryogels for development in the subsequent chapters.

5.1 Experimental details

The description on PSA cryogel synthesis and general material characterization techniques can be found in Chapter 3. The following describes some specific experimental details of the studies reported in this chapter.

5.1.1 Preparation of AgNP stock suspension

A citrate-stabilized AgNPs suspension was prepared following the method described by Jana et al. (2001) with slight modifications. A 490 mL solution of 0.3 mM trisodium citrate and 1 mM of $NaBH_4$ was prepared in an ice bath; 10 mL of a 10 mM $AgNO_3$ was then added into the reaction mixture and allowed to mix for 1 h. The hydrodynamic diameter of the citrate-stabilized AgNPs as determined by

[†]This chapter has been published as 'Effect of synthesis routes on the properties and bactericidal activity of cryogels incorporated with silver nanoparticles' in *RSC Advances* (5) 44626-44635. Please see Appendix A for reuse permission.

dynamic light scattering (Malvern Zetasizer) revealed that the particles were mostly smaller than 10 nm. The citrate-stabilized AgNPs had a Zeta potential of -48.5 mV. Fig. 5.1 shows a representative TEM image of the AgNPs with their corresponding diameter distribution; the mean diameter of the AgNPs was determined by TEM was 24.2 ± 8.5 nm.

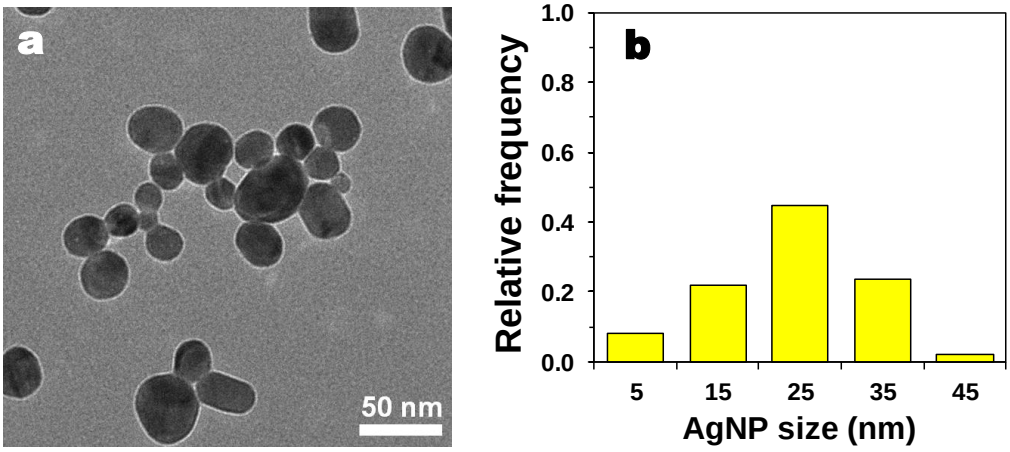

Figure 5.1 (a) A representative TEM image and (b) the corresponding particle-diameter distribution of the citrate-stabilized AgNP suspension.

5.1.2 Preparation of AgNP-incorporated cryogels

Three different methods were used to prepare AgNP-incorporated cryogels that resulted in a variation in the AgNP-size and -spatial distribution in the PSA cryogels.

In the first method, the nanocomposites were fabricated by cryopolymerization of SA and MBA in the presence of the pre-formed citrate-stabilized AgNPs. The cryogelation conditions used were the same as those for PSA cryogels with an Ag concentration in the mixture of 0.2 mM. These nanocomposites will be subsequently referred to as 'NI (nanoparticle incorporated) cryogels'.

The second method involves ice-mediated coating (IMC) of the pre-formed citrate-stabilized AgNPs on the PSA cryogels. 1 g of the dried PSA cryogels was allowed to swell in 250 mL of the AgNP suspension (0.2 mM) during which shaking was

provided. After 24 h the swollen cryogels were removed and placed in a freezer (–20 °C) for another 24 h. Care was taken to prevent accidental squeezing of the absorbed AgNPs solution from the swollen cryogel. Hereafter, these nanocomposites will be referred to as 'IMC cryogels'.

In the third method, PSA/AgNP cryogels were prepared using the intermatrix synthesis (IMS) method. 1 g of the dried PSA cryogels was allowed to swell in a 250 mL solution containing 0.2 mM of $AgNO_3$ (≥98%, Merck). The suspension was shaken at 120 rpm on an orbital shaker for 24 h. The cryogels were then immersed in a 250 mL solution of $NaBH_4$ (Alfa Aesar, 10:1 molar ratio of $NaBH_4$ to $AgNO_3$) for 1 h to form silver nanoparticles (AgNPs). The nanocomposites produced by this method are referred to as 'IMS cryogels'.

All the resultant nanocomposites were thoroughly washed by immersion in DI water followed by vacuum filtration. After three repetitions of the washing step, the nanocomposites were dried using the same procedure that was used for the PSA cryogels.

5. 3 Results and Discussion

5.3.1 Synthesis of PSA/AgNP cryogel nanocomposites

Fig. 5.2 summarizes the processes involved in the three synthesis routes used to fabricate PSA/AgNP cryogels with different Ag distributions. The fabrication of NI cryogels appears simple as it involves only one step, i.e., cryopolymerization of a physical mixture of monomer, crosslinker, and initiator in the presence of AgNPs. However, the formation of a PSA cryogel embedded with AgNPs is actually a complex process involving ice growth, nanoparticle embedding, and copolymerization occurring simultaneously (Fig. 5.2a). During freezing, the AgNPs were expelled from the growing ice crystals together with the monomer, crosslinker, and initiator in a confined space between adjacent ice crystals that remained unfrozen. The AgNPs were entrapped in the pore walls of the cryogel as copolymerization between SA and MBA proceeded in the unfrozen liquid

microphase (UFLP) while pores formed upon melting the ice crystals. The presence of the AgNPs might have affected the cryogelation process because the gel fraction yield was significantly reduced (30% versus 95% without AgNPs). Because the Ag concentration in the free water of the as-synthesized NI cryogel was very low (< 5 µg/L), it is reasonable to assume that most of the added AgNPs were embedded in the cryogels. Nonetheless, it should be noted that depending on the size of the AgNPs or their aggregates, they may be fully or partially embedded within the cryogel matrix as shown in the far-right panel of Fig. 5.2a. The Ag content of the NI cryogel was determined to be 0.8±0.3 mg/g (Table 5.1). Note that the Ag content in the NI cryogel is not only dictated by the Ag incorporation efficiency but also by the gel fraction yield.

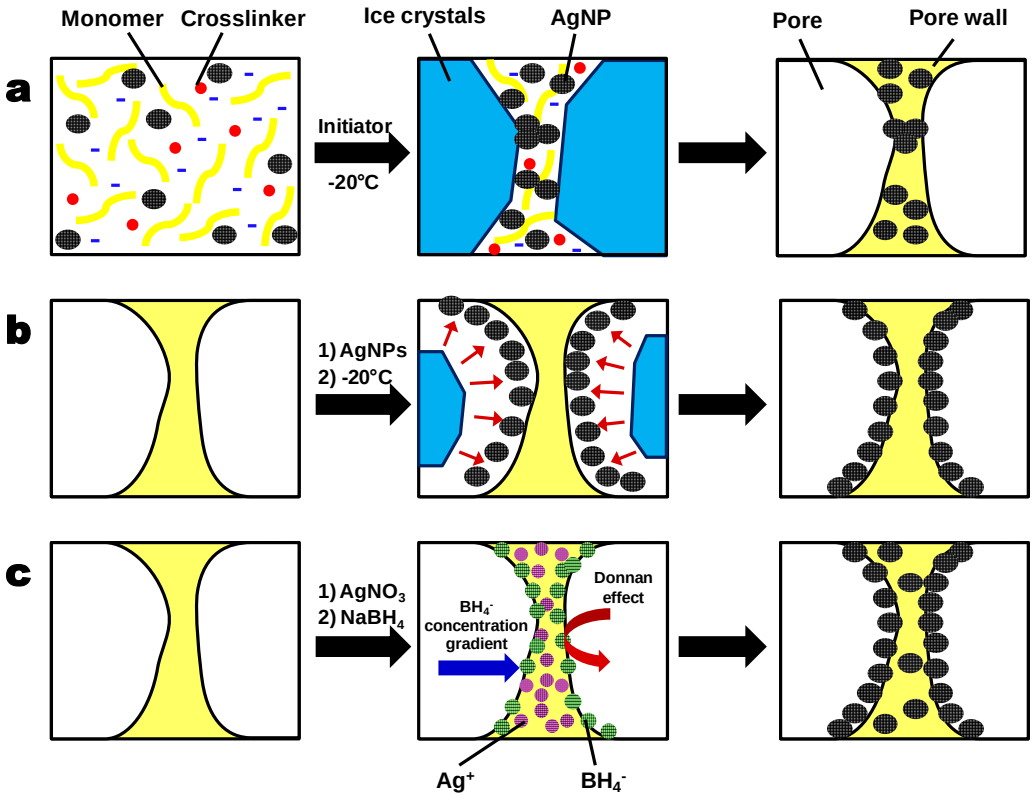

Figure 5.2 Schematic of the synthesis routes used to prepare (a) NI cryogel via cryogelation in the presence of pre-formed AgNPs, (b) IMC cryogels via ice-mediated coating of AgNPs on pre-formed PSA cryogels, and (c) IMS cryogels via *in situ* borohydride of pre-formed PSA cryogels loaded with Ag^{+}.

Table 5.1 Salient properties of the cryogels prepared via different methods

Samples	Ag incorporation[a] (%)	Ag content (mg/g)	Specific pore volume[b] (cm^3/g)	Total Ag in squeezed water (μg/L)	Mean AgNP size[c] (nm)	Surface roughness[d] R(a) (nm)
PSA cryogel	N.A.	N.A.	2.8 (0.2)	N.A.	N.A.	4.4 (1.2)
NI cryogel	> 99	0.8 (0.3)	1.6 (0.1)	33.7 (0.7)	25.1 (13.4)	7.2 (2.7)
IMC cryogel	26.0 (3.8)	1.4 (0.2)	3.6 (0.1)	42.8 (2.5)	12.2 (8.5)	13.8 (1.4)
IMS cryogel	74.8 (2.7)	4.0 (0.2)	2.9 (0.2)	102.2 (1.4)	5.1 (2.1)	7.0 (1.5)

Note: N.A. = not applicable; standard deviations are shown in parentheses.

[a] The Ag incorporation efficiency was determined by taking the ratio of the mass of Ag incorporated into the cryogel nanocomposites to the mass of Ag in the initial synthesis solution.

[b] The specific pore volume was computed by measuring the mass increase of a cryogel immersed in cyclohexane (0.779 g/cm^3) versus its initial dry mass.

[c] Determined from TEM images.

[f] Determined from AFM images.

On the other hand, the IMC and IMS cryogels were prepared using pre-formed PSA cryogels (with a gel yield of 95%) that allow a better control of the amount of Ag incorporated into the resulting composite. Because cryogels have heterogenous open porous structures that allow unhindered diffusion of solutes, their pores are easily filled with AgNPs upon immersion in the nanoparticle suspension. As depicted in Fig. 5.2b, the subsequent freezing step in the IMC method induced nucleation and growth of ice crystals that propels AgNPs away from the ice front to reduce the surface energy (Deville et al., 2006; Gutiérrez et al., 2008; Estevez et al., 2011; Petrov and Georgiev, 2011; 2012). This additional freezing step assists the deposition and assembly of AgNPs on the pore surface of PSA cryogels. Compared to PSA/AgNP cryogels prepared without the post-freezing step, the Ag incorporation efficiency was significantly enhanced; the Ag incorporation efficiency increased from 4.6±0.6% to 26.0±3.8% with the additional freezing step. Without the additional freezing step, most of the AgNPs absorbed were released back into solution during washing (Fig. 5.3). The Ag content of the as-synthesized IMC cryogel was 1.4±0.2 mg/g.

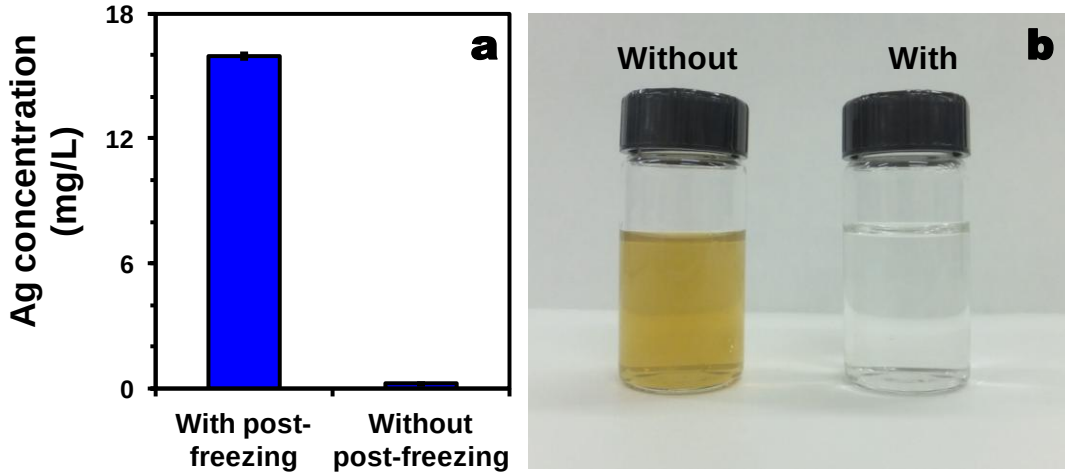

Figure 5.3 Ag concentration in the free water of AgNPs-incorporated cryogels prepared with and without a post-freezing step after immersion in a citrate-stabilized AgNPs suspension. The former method forms the IMC cryogels.

Fig. 5.2c illustrates that the fabrication of IMS cryogels involves (i) loading of the pre-formed PSA cryogels with Ag^+ ions via an ion-exchange reaction followed by (ii) reduction of the sorbed Ag^+ ions by $NaBH_4$ (Ruiz et al., 2010). The Ag incorporation efficiency was 74.8±2.7% due to release of some of the sorbed Ag during the second step. Because this method is not limited by the dipersibility of the AgNP suspension, the preparation of composites with a higher Ag content can be readily achieved by employing a higher concentration of precursor Ag^+. The IMS cryogels had an Ag content of 4.0±0.2 mg/g with a probable peripheral distribution of AgNPs as shown in Fig. 5.2c.

The following observations can be made concerning the three synthesis methods. NI and IMC cryogels that were prepared using pre-formed AgNPs allows the flexibility of using commercially available AgNPs. However, a key problem could be the limited dispersibility of the AgNPs, especially at high concentrations that might preclude the preparation of nanocomposites of high Ag contents. While the NI method has the highest Ag incorporation efficiency; however, the amount of Ag incorporated also depends on the gel fraction yield that makes the control and prediction of Ag content in the nanocomposite difficult. In contrast, the IMS

method requires *in situ* reduction to form AgNPs but it allows the preparation of high Ag content and better control of the amount of Ag incorporated.

5.2.2 Characteristics of AgNP-incorporated cryogels

The unmodified PSA cryogels are highly porous with well-interconnected open pores (Fig. 5.4a). For the IMS and IMC cryogels, the incorporation of AgNPs into the pre-formed PSA cryogels did not cause any significant change in the pore structure of the cryogel as evidenced by their SEM images (Fig. 5.4c and d). In fact, both the IMS and IMC cryogels show a slight increase in their specific pore volumes relative to the PSA cryogels (Table 5.1). The increased pore volumes for the IMS and IMC cryogels might be due to the repulsion between the electron-dense AgNPs that causes expansion of the network and/or pores of the cryogels. In contrast, the NI cryogels prepared by cryogelation in the presence of AgNPs show a significant reduction in porosity compared to the PSA cryogels (Table 5.1). Furthermore, the SEM image of an NI cryogel shows the presence of numerous closed pores (Fig. 5.4b). Note that to obtain cryogels with well-interconnected open pores, the conditions for cryogelation (i.e., reagent concentration and freezing temperature among others) must be precisely controlled to ensure that freezing occurs before gelation. As discussed in Chapter 4, closed pore formation in the case of NI cryogels might be due to an increased viscosity (in this case the viscosity increase is due to the presence of the additional AgNPs) in the unfrozen liquid microphase that reduced the freezing rate, thereby preventing the ice crystals to merge in the gelled mixture. Similar observation has also been made by Seo et al. (2012) when preparing cryogel nanocomposites via this method.

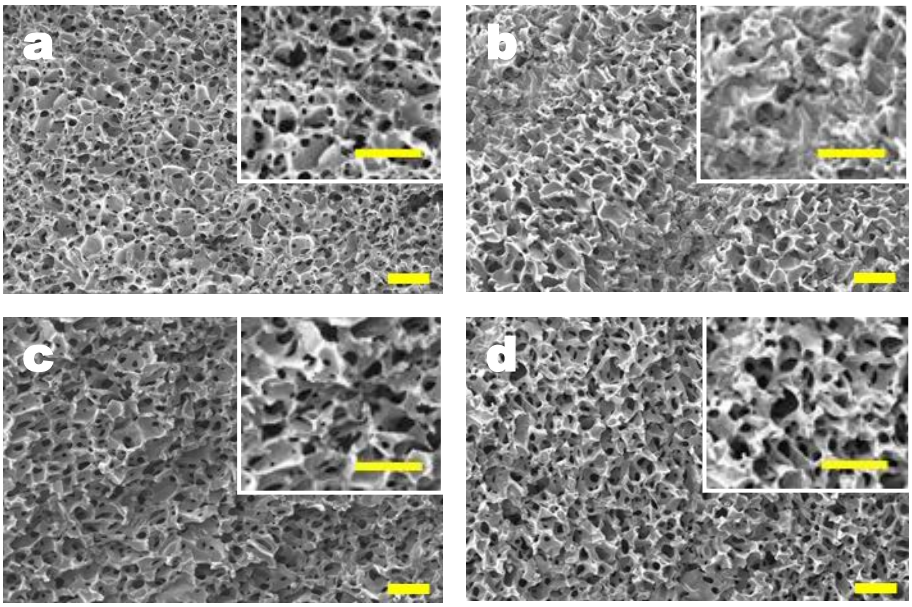

Figure 5.4 SEM images of (a) PSA cryogels, (b) NI cryogels, (c) IMC cryogels, and (d) IMS cryogels. Note scale bars represent 100 µm.

One of the main motivations for stabilizing AgNPs in the support materials was to prevent aggregation, thereby maintaining their small size. Note that smaller-sized particles have been found to display superior bactericidal efficacy (Morones et al., 2005; Pal et al., 2007; Choi and Hu, 2008). Interestingly, the AgNPs incorporated into cryogels via different methods have distinctly different sizes (Fig. 5.5). The mean AgNP sizes for NI, IMC, and IMS cryogels were determined to be 25.1±13.4, 12.2±8.5, and 5.7±2.1 nm, respectively (Table 5.1). Notably, the mean size of the AgNPs in the IMS cryogels is significantly smaller than those of the NI and IMC cryogels. This is mainly due to the *in situ* reduction of Ag^{+} stabilized on the PSA cryogel matrix that bypasses aggregation problems encountered when using nanoparticle suspensions for synthesis. Furthermore, the free volume in the highly crosslinked network of PSA can provide spatial confinement for the growing AgNPs resulting in the formation of ultrafine particles (Mohan et al., 2006; Murthy et al., 2008; Kozlovskaya et al., 2009; Agnihotri et al., 2012).

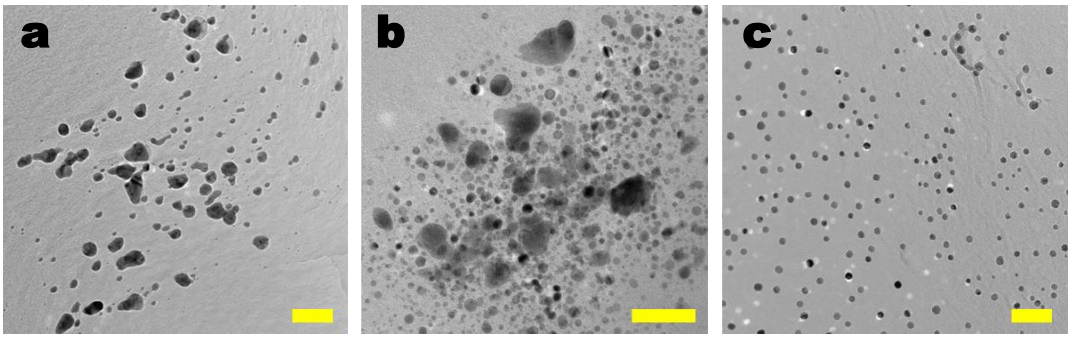

Figure 5.5 TEM images of the AgNPs incorporated in (a) NI, (b) IMC, and (c) IMC cryogels. Note that the scale bars represent 50 nm.

Besides AgNP size, the location of the AgNPs in the support material may also influence the bactericidal efficacy of the resultant nanocomposites. To verify the location of the AgNPs in the cryogel matrix, topographic studies using AFM were conducted along with EDX analyses of the cryogel surfaces (Fig. 5.6). The AFM image of the control (i.e., without AgNP incorporation) shows a smooth topography (data not shown). For NI cryogels the AgNPs are expected to be embedded throughout the polymer matrix of NI cryogels. This hypothesis is supported by the low surface Ag content and a relatively smooth topography (Fig. 5.6). Nevertheless, some large AgNP clusters protruding from the gel surface can be observed in the AFM image with a concurrent increase in surface roughness relative to the unmodified gel (Fig. 5.6a and Table 5.1). Note that although the AgNPs are generally located in the pore walls of the NI cryogel, some of them may only be partially embedded particularly for larger-sized AgNP clusters as illustrated in Fig. 5.2c. Therefore, the increase in surface roughness may be attributed to protrusion of partially embedded particles rather than a "real" surface distribution of AgNPs (Table 5.1). Note that scaffolds prepared in the presence of small particles (6 nm) has been found to form featureless pore walls with concealed particles, whereas the use of larger particles (25 nm) remained exposed at the surface of the channel walls (Suwanchawalit et al., 2009).

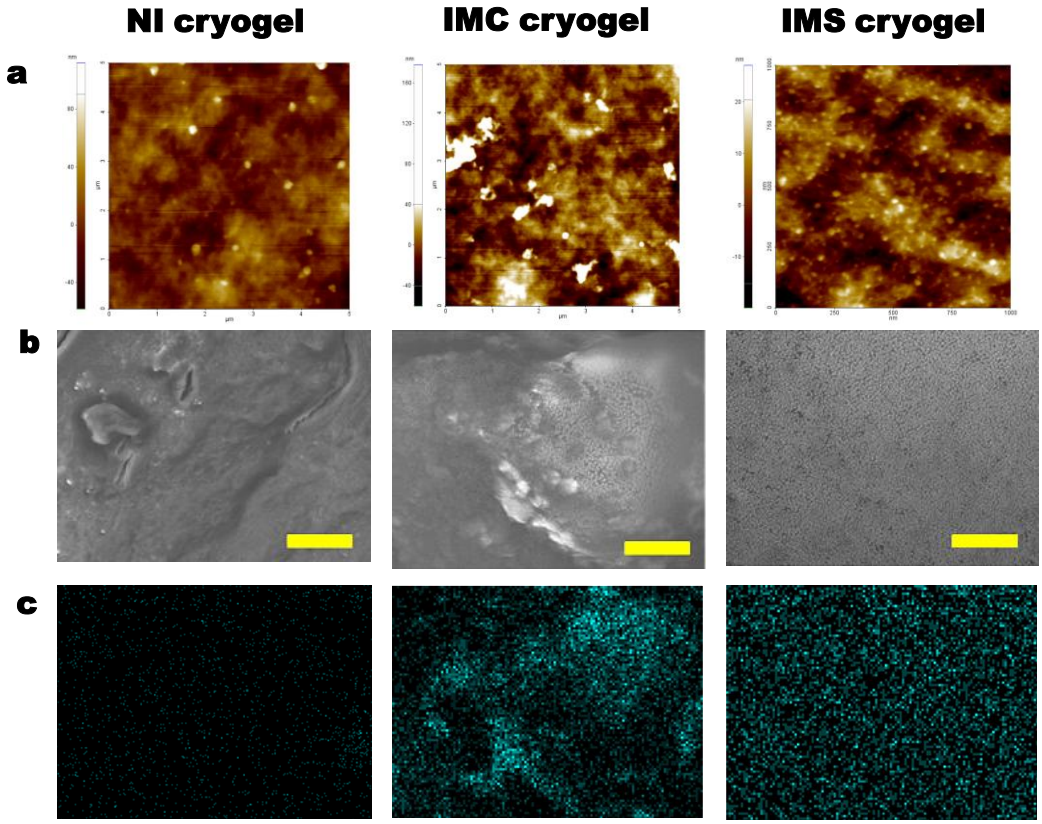

Figure 5.6 Representative images from (a) AFM, (b) FESEM, and (c) EDX elemental Ag mapping of NI, IMC, and IMS cryogels. Note that the scale bars in (b) represent 500 nm.

In contrast, the IMC cryogels have the AgNPs located only on their pore surfaces because the AgNPs could not penetrate the dense PSA matrix due to steric hindrance. This hypothesis is supported by the significant increase in surface roughness and the presence of AgNP clusters on the surface that are apparent in the both the AFM and FESEM images (Fig. 5.6a and b). Furthermore, EDX analyses revealed that the majority of the pore surfaces show an intense signal for surface-bound Ag (27-43 wt%).

However, the IMS cryogels show a combination of the Ag distribution observed in both the NI and IMC cryogels whereby the AgNPs are incorporated throughout the cryogel matrix, but with the majority of the AgNPs being located on the pore surfaces. As illustrated in Fig. 5.2c, this is the result of Donnan exclusion effect during the second step of IMS (i.e., reduction of the Ag^{+} sorbed on PSA cryogel)

whereby BH_4^- is unable to diffuse deeply into the PSA matrix due to electrostatic repulsion between the negatively charged surface cryogels and BH_4^- resulting in the formation of AgNPs primarily on the exposed pore surfaces (Alonso et al., 2010). As such, the pore walls of the IMS cryogels appear to be densely decorated with AgNPs as evidenced by their AFM and FESEM images (Fig. 5.6b and c). Despite the peripheral distribution and higher Ag content of the IMS cryogels, the surface-bound Ag was significantly lower than that of the IMC cryogels (6-15%). Although the majority of AgNPs were located on the surface, only a small increase in the surface roughness was observed that may be attributed to the small size of the AgNPs on the surface (Table 5.1 and Fig. 5.6a).

The difference in the morphology and Ag distribution among the NI, IMC, and IMS cryogels is expected to result in distinctly different bulk properties such as their swelling-deswelling and mechanical behavior. As discussed in Section 4.2.6, the cryogels should preferably have fast and high water absorption and desorption to be applied as sorbents for water disinfection. Furthermore, the cryogels should have a high elasticity and durability to allow repeated use. Similar to the PSA cryogels, both IMC and IMS cryogels can reach swelling degrees greater than 150 g/g within 15 s due to the highly interconnected open pores (Fig. 5.7a and b). Furthermore, 85% of their absorbed water can be recovered using mild pressure compression (Fig. 5.7c). However, due to the presence of closed pores and reduced porosity, the NI cryogels could only swell to 76.3±7.9 g/g (also within 15 s, but with a slight decrease in the swelling rate with respect to the PSA cryogel); moreover, the water recovery was reduced to 72% (Fig. 5.7c).

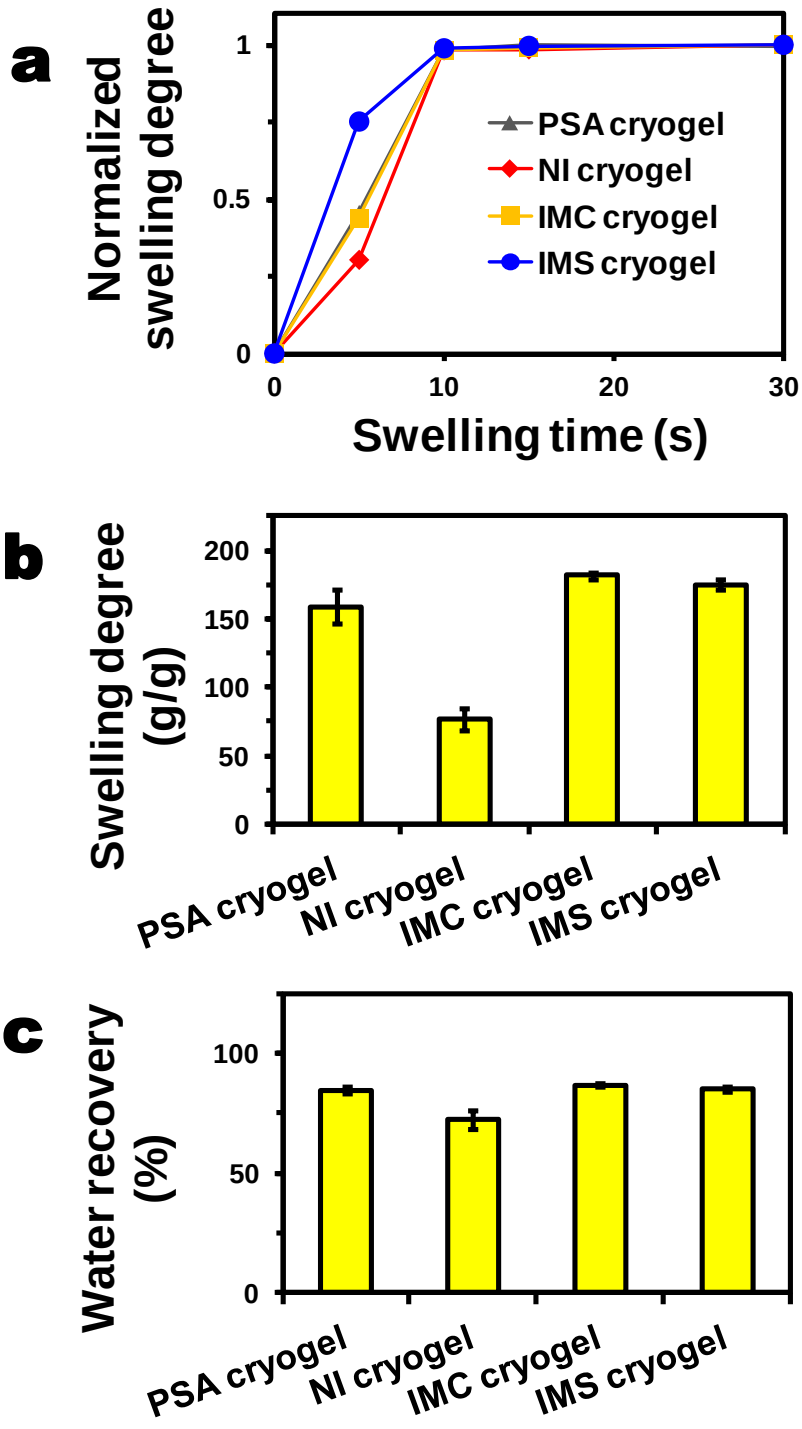

Figure 5.7 (a) Swelling profile, (b) equilibrium swelling degree, and (c) water recovery efficiency of cryogels prepared via different methods.

Nonetheless, the incorporation of AgNP has provided some form of reinforcement to the mechanical structure of the NI cryogels and to a lesser extent of the IMS cryogels as evidenced by their increased Young's modulus relative to the PSA cryogels (Fig. 5.8). The increased stiffness of the NI and IMS cryogels may be attributed to extensive integration of the AgNPs into the polymer matrix that could hinder buckling of the polymer chains when placed under compression (Suwanchawalit et al., 2009). Although the NI cryogels showed the highest enhancement in terms of the Young's modulus, the large hysterisis loop indicates a substantial loss of elasticity that may be undesirable for application as antibacterial sorbents (Fig. 5.8). This loss of elasticity may be attributed to the presence of closed pores and a reduced porosity of the NI cryogels. On the other hand, there is no mechanical reinforcement for the case of the IMC cryogels because the AgNPs are not incorporated within the matrix of the cryogels. In fact, there is a slight — but insignificant — reduction in the Young's modulus (compared to the PSA cryogels) that might be attributed to the additional freezing step that could have affected the structure of the polymer matrix due to the pressure exerted by the ice crystals against the pore walls (Fig. 5.8).

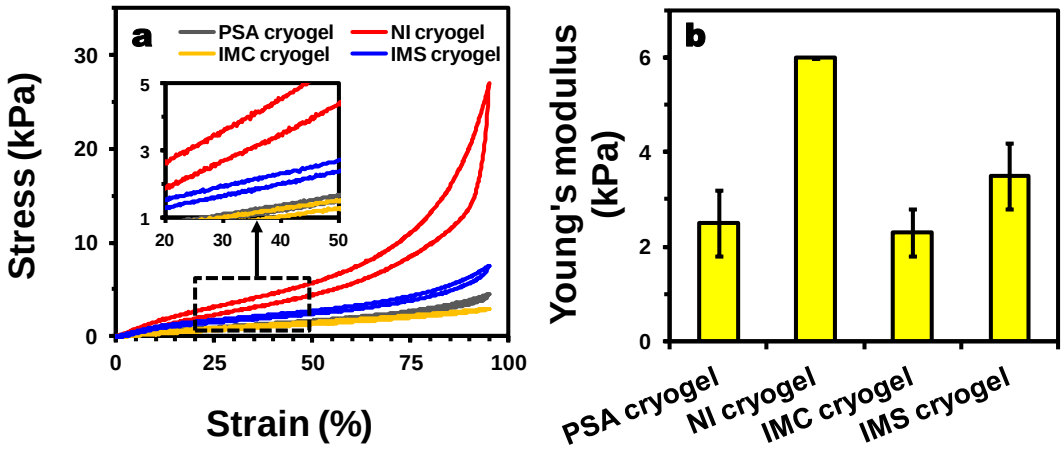

Figure 5.8 (a) Stress-strain curve and (b) Young's modulus of the AgNP-incorporated cryogels prepared via different synthesis methods. Note that the Young's modulus was determined by taking the initial slope of the stress-strain curves (n=3).

5.2.3 Application of the cryogel nanocomposites for POU water disinfection

The bactericidal efficacy of the as-synthesized NI, IMC, and IMS cryogels was determined by applying them as sorbents to disinfect water. In this approach, the cryogels were used to soak up a bacterial suspension during which the bacterial cells entered the pores of the cryogels to effect disinfection; the disinfected water could then be recovered by squeezing the cryogels (Fig. 5.9).

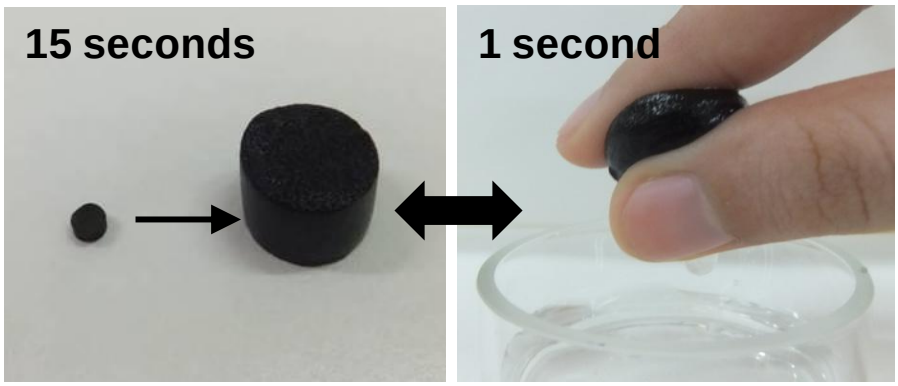

Figure 5.9 Photographs showing the approach whereby AgNP-incorporated cryogels were used for disinfection.

Fig. 5.10 shows a qualitative comparison of the disinfection efficacies of the NI, IMC, and IMS cryogels with respect to the unmodified PSA cryogel via fluorescence imaging of exposed cells stained with dyes. Note that SYTO 9 is a permeant dye that stains all bacterial cells while propidium iodide (PI) is a non-permeant dye that can only be taken up by cells whose membranes have been compromised. Therefore, viable cells fluoresce green while cells with compromised membranes fluoresce red (because more PI can enter damaged cells) due to fluorescence quenching of SYTO 9 by PI. In contrast to the PSA cryogels, bacterial cells exposed to the NI, IMS, and IMC cryogels show cell-membrane damage albeit to varying degrees of severity (Fig. 5.10); the extent of cell-membrane damage of cells exposed to the NI cryogels appears to be drastically less severe than those exposed to the IMC and IMS cryogels.

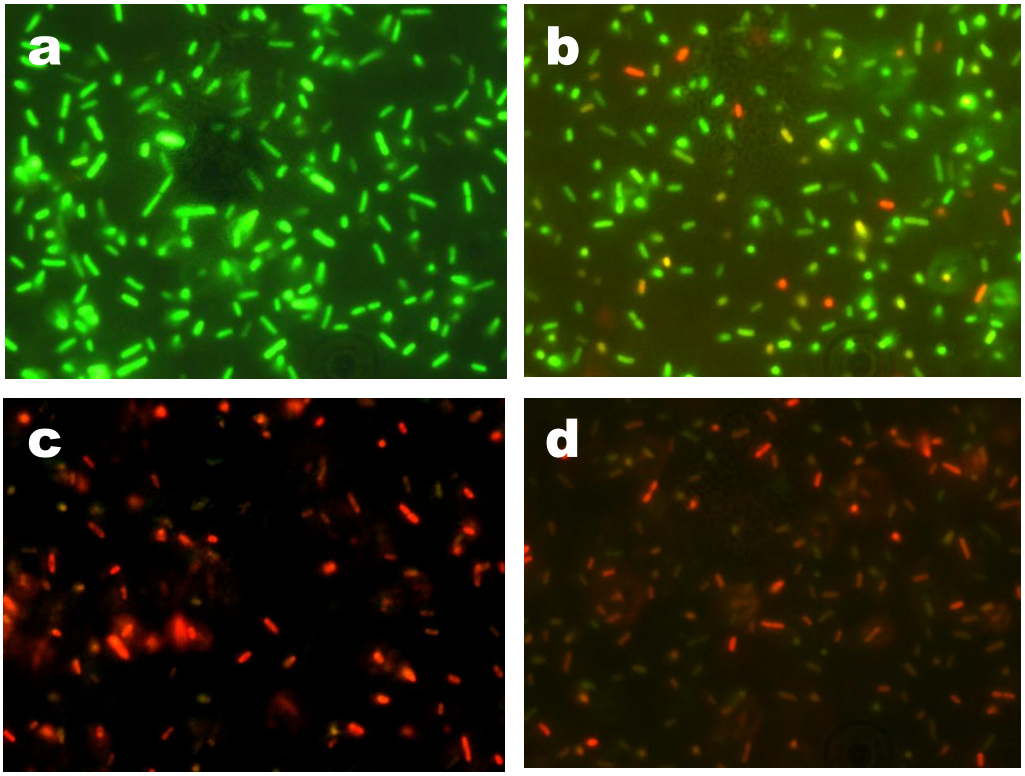

Figure 5.10 Representative fluorescence images of bacterial samples exposed to (a) PSA cryogels, (b) NI cryogel, (c) IMC cryogel, and (d) IMS cryogels. Note that live cells fluoresce green while cells whose membranes have been compromised fluoresce red.

To obtain a more quantitative comparison, the bacterial suspensions squeezed out from the different cryogels were plated and subsequently enumerated to determine the concentration of surviving cells. As shown in Fig. 5.11a, the results are consistent with the fluorescence images of the exposed cells. Both the PSA and NI cryogels result in a slight reduction in the viable cells (Fig. 5.11a). While true inactivation of the bacterial cells may apply for the case of the NI cryogels, the insignificant reduction in the number of viable cells for the case of the PSA cryogels is probably due to serendipitous removal via physical mechanisms: (i) bacterial exclusion by smaller pores, (ii) bacterial entrapment in blind pores, and/or (iii) deposition of bacterial cells on the interior surface of the cryogel during squeezing. In contrast, both the IMC and IMS cryogels show significant inactivation of the bacterial cells whereby they can achieve 4.1±0.2 and 3.2±0.1 log-reductions, respectively. Notably, the IMC cryogels show the highest

disinfection efficacy among the three nanocomposites. This is rather surprising because the IMC cryogels have a lower Ag release (42.8±2.5 µg/L versus 102.2±1.4 µg/L) and Ag content (1.4±0.2 mg/g versus 3.99±0.2 mg/g), and generally larger AgNPs than those of the IMS cryogels (Table 5.1).

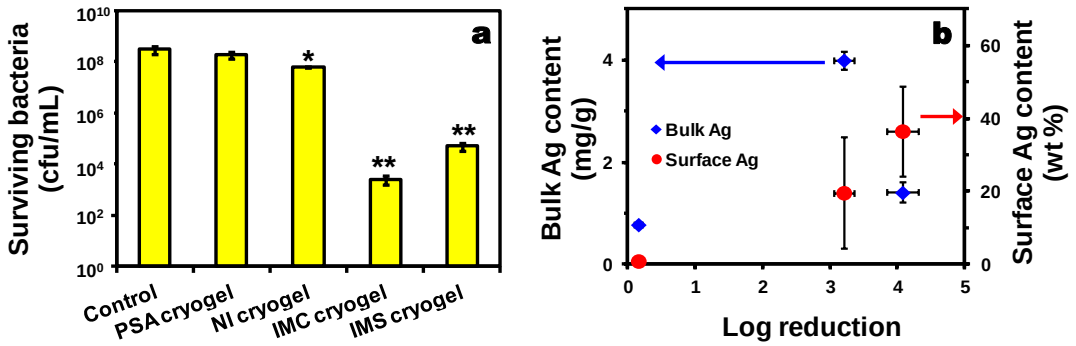

Figure 5.11 (a) Number of viable bacteria in water samples exposed to various AgNP-incorporated cryogels. Note that (*) and (**) denote significantly different results compared to the control at 95% and 99% confidence levels, respectively. (b) Relationship between the disinfection efficacies and bulk and surface Ag content. Note that the bulk Ag content was determined by ICP-OES analysis of acid-digestion of the cryogel nanocomposites, while the surface Ag content was estimated using EDX analysis of at least 3 sites for each cryogel sample.

As shown in Fig. 5.11b, the disinfection efficacy of the AgNP-incorporated cryogels shows a better correlation with the concentration of Ag on the cryogel surface rather than with the bulk concentration of the cryogel. These results suggest that the location of the AgNPs is an important, and possibly an overriding factor in dictating the bactericidal efficacy of Ag-based nanocomposites. Therefore, to attain superior bactericidal efficacy, AgNPs should be located on the surface of the support material to allow maximum exposure to the bacterial cells. This is in line with the observations that the bactericidal activity is enhanced by improved contact between cell and composite materials (Agnihotri et al., 2013; Bondarenko et al., 2013). These findings stress the importance of optimizing the synthesis approach to yield the desirable properties. However, the choice of the optimal synthesis method is usually not only determined by the performance of the resulting material, but by a trade-off with other factors such as the ease of synthesis and scalability among other

factors. Table 5.2 provides a summary of the merits and drawbacks of the synthesis methods used in this study.

Table 5.2 Summary of the advantages and disadvantages of the synthesis approaches employed in this study

Synthesis approach	Advantages	Disadvantages
Cryogelation in the presence of pre-synthesized nanoparticles	• Low AgNPs wastage due to high efficiency of Ag incorporation; • One-step synthesis; • Low Ag leaching; • Forms stronger cryogel nanocomposites;	• Difficult to control the Ag content in the resultant cryogel nanocomposite; • Need re-optimization of the cryogelation conditions for synthesis of cryogels with different Ag content; • The resulting nanocomposites have lower swelling rates and degree of swelling, elasticity, and water recovery; • Low bactericidal efficacy;
Ice-mediated coating of nanoparticles on pre-formed cryogels	• Can achieve high bactericidal efficacy at lower Ag content; • Low Ag leaching • Can use pre-formed cryogels with optimized swelling/deswelling and mechanical properties • Re-optimization of cryogelation conditions for synthesis of cryogels with different Ag content not required;	• High wastage of AgNPs due to low efficiency of Ag incorporation - especially in the first step; • Difficult to prepare nanocomposites with high Ag content due to dispersion problem;
In situ reduction of nanoparticles on pre-formed cryogels	• Can achieve good bactericidal efficacy; • Can use pre-formed cryogels with optimized swelling/deswelling and mechanical properties • Re-optimization of cryogelation conditions for synthesis of cryogels with different Ag content not required; • Can prepare cryogels with high and predictable Ag content;	• Ag leaching higher than the other two methods • Lower Ag wastage due to the higher Ag incorporation efficiency

The IMS method was selected to prepare PSA cryogels decorated with AgNPs (or PSA/AgNP cryogels) for subsequent studies that will be described in Chapters 6 to 8. This method is selected because of the ease, reproducibility, and scalability of the method. Furthermore, this method allows the preparation of PSA/AgNP cryogels with a high and predictable Ag concentration. Most importantly, this method forms AgNPs that are mainly located on the outer surface of the pore walls, thereby promoting excellent bactericidal activity.

5.4 Concluding remarks

PSA/AgNP cryogel nanocomposites were successfully prepared using three different synthesis approaches. The three synthesis methods resulted in PSA/AgNP cryogels with distinctly different Ag distributions whereby the AgNPs were located only on the pore surface or embedded throughout the polymer matrix or a mixture of both. Furthermore, the PSA/AgNP cryogels prepared via the different methods have varying AgNP size, pore morphology, swelling and mechanical behavior. The three types of PSA/AgNP cryogels were found to be effective in disinfecting the *E. coli* to different extents. Specifically, synthesis routes that formed more AgNPs on the exterior surface of the cryogels displayed enhanced bactericidal efficacy. These findings underscore the importance of optimizing the synthesis approach in yielding material structures that lead to the desired material properties involving multiple aspects.

CHAPTER 6 Application of superabsorbent cryogels decorated with silver nanoparticles for point-of-use water disinfection[†]

This chapter provides a detailed description on the synthesis and characterization of PSA cryogels decorated with AgNPs (or PSA/AgNP cryogels). The PSA/AgNP cryogels were employed as antibacterial sorbents for point-of-use (POU) water disinfection using the approach shown in Fig. 1.1. The bactericidal effectiveness of the PSA/AgNP cryogels were demonstrated against various types of bacteria. The PSA/AgNP cryogels were further tested for disinfection of natural water samples. The later part of this chapter also discusses the prospects of using the cryogels in disaster-relief applications and provides some insights into their end-of-life handling.

6.1 Experimental details

The description of the intermatrix synthesis of the PSA/AgNP cryogels and relevant material characterization techniques can be found in Chapter 3.

[†]This chapter has been published as 'Superabsorbent cryogels decorated with silver nanoparticles as a novel water technology for point-of-use disinfection' in *Environmental Science and Technology* (47) 9363-9371 and 'Potential evaluation and perspectives on using sponge-like superabsorbent cryogels for onsite water treatment in emergencies' in *Desalination and Water Treatment* (53) 1506-1515.. Please see Appendix A for reuse permission.

6.2 Results and discussion

6.2.1 Synthesis and properties of PSA/AgNP cryogel nanocomposites

As shown in Fig. 6.1, the PSA cryogels used to prepare the PSA/AgNP cryogels are highly porous with well-interconnected pores. This allows unhindered access to the solutes for AgNP formation to take place.

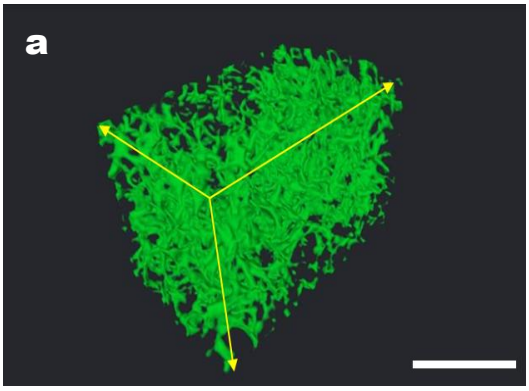

b

Pore architecture parameters	
Interconnectivity (%)	99.97
Porosity (%)	68.3 ± 1.5
Surface area (μm²/ μm³)	0.035 ± 0.002
Pore size (μm)	16.5 ± 2.7
Strut thickness (μm)	2.1 ± 0.5

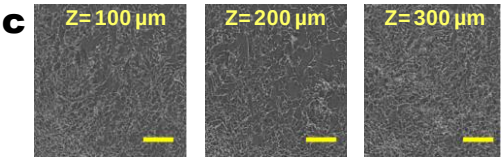

Figure 6.1 X-ray microcomputed tomographic characterization of a PSA cryogel. (a) 3D-reconstructed image of the cryogel. (b) Summary of quantitative pore parameters of PSA cryogels. (c) X-ray microtomography images of PSA cryogels taken at different sample depths (Z). Note: all the scale bars represent 50 μm length.

In Chapter 5, the intermatrix synthesis method was found to be a reproducible approach that also allows *in situ* formation of fine AgNPs in cryogels. As such, this method was selected to prepare PSA/AgNP cryogels for further development. The intermatrix synthesis of the PSA/AgNP cryogels involves (i) loading of the preformed PSA cryogels with Ag^+ ions via an ion-exchange reaction followed by (ii) reduction of the sorbed Ag^+ ions by $NaBH_4$ (Ruiz et al., 2010). Both reactions are represented as equations 6.1 and 6.2, respectively:

$$R–COO^- Na^+ + Ag^+ \rightarrow R–COO^- Ag^+ + Na^+ \quad (6.1)$$

$$R–COO^- Ag^+ + NaBH_4 + 3H_2O \rightarrow R–COO^- Na^+ + Ag^0 + 7/2H_2 + B(OH)_3 \quad (6.2)$$

Note that reaction (6.2) is a combination of reactions (6.3) and (6.4):

$$R–COO^- Ag^+ + Na^+ \rightarrow R–COO^- Na^+ + Ag^+ \quad (6.3)$$

$$Ag^+ + BH_4^- + 3H_2O \rightarrow 7/2H_2 + B(OH)_3 + Ag^0 \quad (6.4)$$

.

The first step is a simple ion-exchange between Ag^+ in solution and Na^+ in the PSA cryogel as indicated by the complementary trend in their concentration profiles shown in Fig. 6.2. Note that the PSA cryogels have an ion-exchange capacity of 9.0 ± 0.8 meq/g determined using the acid-base titration method described elsewhere (Fisher and Kunin, 1955). As such, the PSA cryogels could rapidly take up almost all the Ag^+ ions in the solution due to their high ion-exchange capacity and high affinity of the $–COO^-$ groups towards Ag^+. However, about 20% of the sorbed Ag^+ ions were released back into the solution during the second step. This is due to the flux of Ag^+ towards the cryogel surface as a consequence of the ion-exchange reaction between the sorbed Ag^+ and Na^+ (from $NaBH_4$) in the solution (Eq. 6.3) before they are reduced by BH_4^- ions to form AgNPs (Eq. 6.4). For this reason, the carboxylate groups of the polymer can be completely regenerated allowing reloading of Ag (Alonso et al., 2011b; 2012b). Nevertheless, this synthesis method formed PSA/Ag cryogels having high Ag content (20 to 170 mg/g, Table 6.1) and a predictable linear increase of the Ag content with the precursor Ag^+ concentration used (Table 6.1, $R^2 > 0.99$). Alonso et al. (Alonso et al., 2011a; 2012a) also employed the intermatrix synthesis method to prepare Ag nanocomposites with a high Ag content (> 200 mg/g) from fibrous ion-exchange materials. Hereafter, the as-synthesized PSA/Ag cryogel nanocomposites will be denoted as AgNC-x, where x (x = 20, 90, and 170) denotes the Ag content (mg/g) in the nanocomposites.

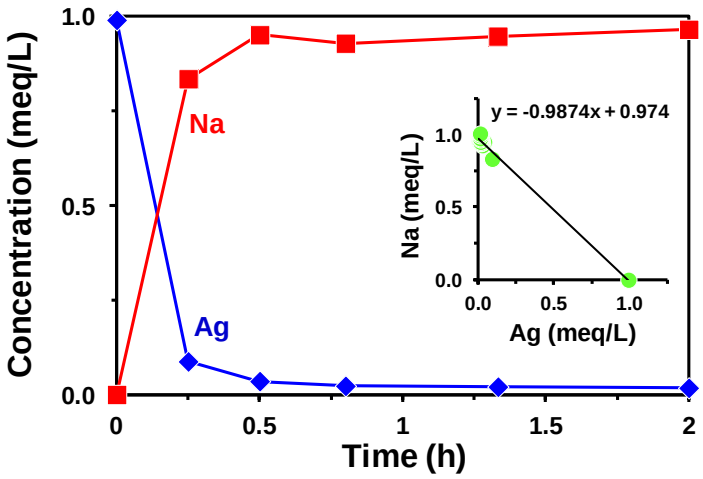

Figure 6.2 Concentration profiles of Ag and Na during the Ag-loading step of the intermatrix synthesis of AgNC-20.

.

Table 6.1 Nomenclature and summary of PSA/AgNP cryogel properties

Sample	Precursor Ag^+ (mM)	Ag content (mg/g)	Young's modulus[c] (kPa)	Mean AgNP size[e] (nm)	Mean Ag crystallite size[f] (nm)	Total Ag loss after 24 h[g] (%)	Total Ag in squeezed water (µg/L)
PSA gel	N.A.	N.A.	2.6 (0.5) [d]	N.A.	N.A.	N.A.	N.A.
AgNC-20	1.0	21.3 (0.3)	3.0 [d]	4.3 (1.3)	3.8	1.79 (0.02)	76.6 (0.7)
AgNC-90	5.0	88.7 (12.3)	3.2 (0.4)[d]	6.2 (1.7)	5.5	0.08	59.6 (0.8)
AgNC-170	10.0	166.7 (15.0)	3.2 (0.4) [d]	8.6 (3.8)	7.8	0.03	36.4 (1.5)

Note: N.A. = not applicable; standard deviations are shown in parentheses.

[a] The equilibrium swelling degree was computed by taking the ratio of swollen mass to that of the dried mass of cryogel.

[b] The water recovery efficiency of cryogel was computed by taking the ratio of the difference between the swollen and deswollen cryogel masses to the difference between the swollen and dried cryogel masses.

[c] The Young's modulus was determined from the initial linear slopes of the stress-strain curves.

[d] No failure was observed at the end of the uniaxial compression test.

[e] Determined from TEM images.

[f] Estimated from X-ray diffractograms using the Scherrer equation; full-width-at-half maximum of (111) reflection and a shape factor of 0.9 were used for computation.

Upon borohydride reduction, the cryogels changed color from white to dark brown (inset of Fig. 6.3). The dark brown color was due to the surface plasmon resonance of AgNPs as evidenced by the characteristic absorption peak in the vicinity of 420-430 nm (Fig. 6.3) (Zargar and Hatamie, 2012).

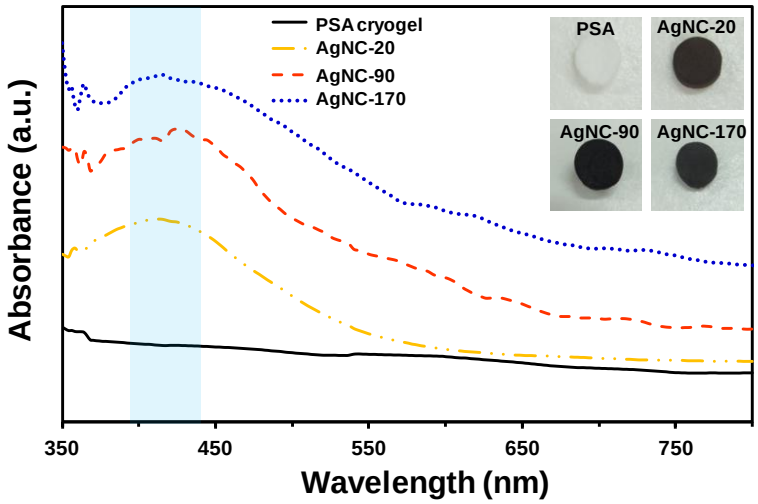

Figure 6.3 UV-visible absorption spectra of PSA/Ag cryogels with different Ag loadings. The inset shows photographs of the as-synthesized cryogel nanocomposites.

.

The FESEM image show that the pore size and interconnectivity of the cryogel was relatively unaffected after AgNPs decoration (Fig. 6.4a). This is because of the large difference in the scale of the cryogel pores (1-100 µm) and AgNPs (mostly <10 nm). Bright spots that appeared like studs on the surface of the cryogel pore walls were evident under a higher magnification (Fig. 6.4a), showing that the AgNPs, were very well dispersed in the cryogel network. The good dispersion may be attributed to electrosteric stabilization of the AgNPs in the PSA cryogels. Furthermore, the highly crosslinked network of the PSA provided random confinement of AgNP growth in the free volume between the polymer networks, thereby forming particles that are mostly <10 nm (Fig. 6.4b-d) (Balogh et al., 2000; Mohan et al., 2006).

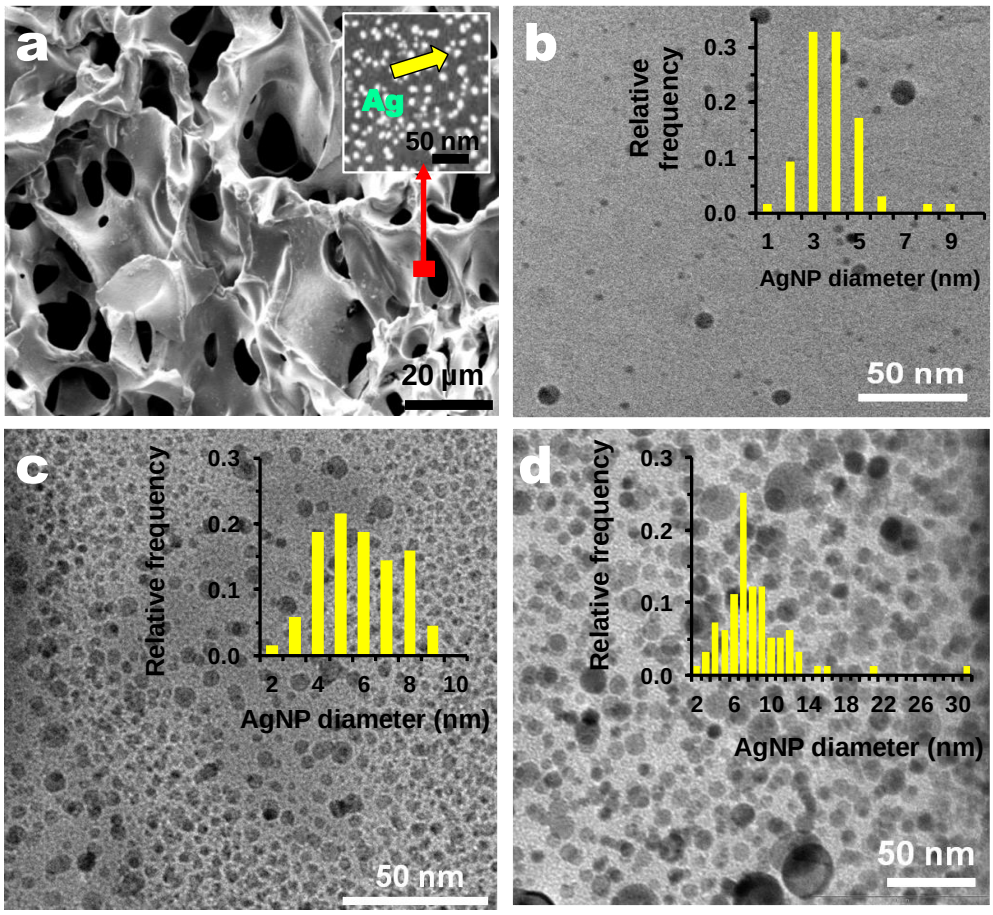

Figure 6.4 (a) FESEM image of AgNC-170 under a low magnification; the inset shows a high-magnification FESEM image of AgNPs dispersed on the pore surface of AgNC-170. The AgNP-size distribution and TEM images of the AgNPs in (b) AgNC-20, (c) AgNC-90, and (d) AgNC-170.

.

Also, the average AgNP size, and the size distribution were found to increase slightly with Ag content (Table 6.1, Fig. 6.4b-d). It should be noted that the AgNP sizes derived from TEM images are in good agreement with the average Ag crystallite sizes determined from XRD (Table 6.1). This synthesis method formed AgNPs that are mostly located near the surface of the cryogels as evidenced by the FESEM images that show the outer pore wall being densely decorated with AgNPs while the inner surface of the pore wall is smooth (Fig. 6.5a-c). Furthermore, the EDX line-scan profile and Ag elemental mapping of the cross-section of a pore strut show that the Ag peak has a significantly higher intensity on the outer surfaces of the pore walls (Fig. 6.5d and e). It is unlikely that such a distribution results from limited penetration of Ag^{+} or BH_4^{-} due to diffusional processes in view of the high porosity of the cryogel. A more likely explanation for this observation could be the Donnan exclusion effect; the presence of a large number of negative charges (due to carboxylate groups) on the PSA cryogels could have impeded a deep penetration of the negatively charged BH_4^{-} ions into the polymer matrix that preferentially form AgNPs on the surface of the cryogels (Alonso et al., 2010; 2012b; 2013). Impregnation of the AgNPs on the external surface is desirable because it allows maximum contact with the bacteria. This, in combination with the good dispersion of fine AgNPs combined with the highly interconnected porous network of PSA cryogel, is anticipated to increase the probability of collisional contact with the bacterial cells that would lead to high disinfection efficacies.

.

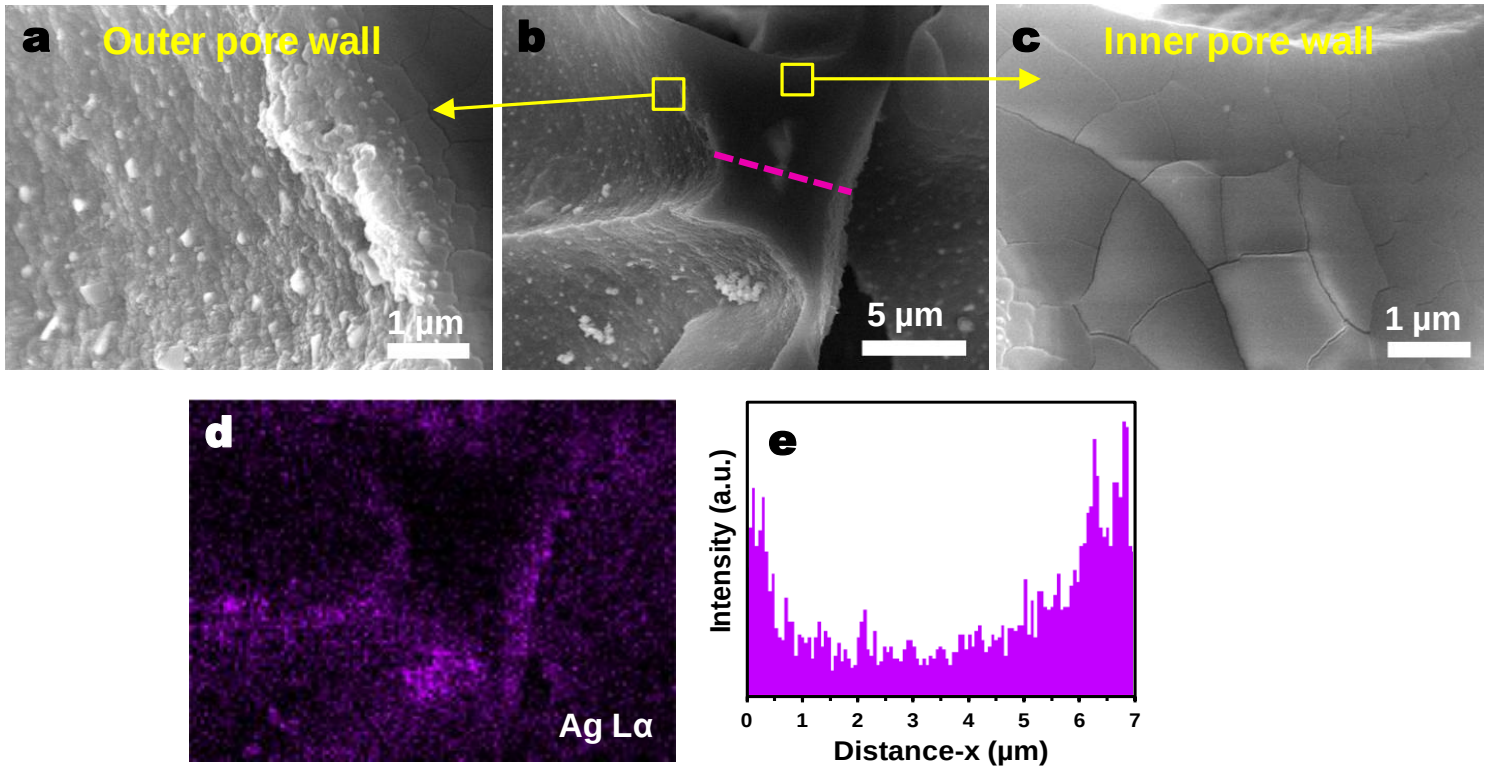

Figure 6.5 Distribution of AgNPs in the AgNC-170. (b) FESEM image of the cross-section of a pore strut that reveals the morphology of its inner wall, which is the star-shaped middle region. High-magnification FESEM images of the (a) outer and (c) inner pore walls. (d) Ag elemental mapping corresponding to the FESEM image shown in (b). (e) EDX line-scan showing the distribution of Ag along the cross-section of the pore strut as indicated by the purple line in (b).

.

XPS analyses were conducted to ascertain the chemical states of Ag in the cryogel nanocomposites. Fig. 6.6a shows the high-resolution XPS spectra at the Ag 3d core level of the PSA/Ag cryogels. Distinct doublet peaks centered at 367.6 and 373.6 eV, which are the peaks for Ag $3d_{3/2}$ and Ag $3d_{5/2}$, respectively, were observed. A spin-orbit splitting energy of 6.0 eV for the 3d doublet of Ag indicates the formation of metallic AgNPs (Moulder et al., 1992). Furthermore, Fig. 6.6b shows that the three nanocomposites had diffraction peaks at 2θ angles of 38.1, 44.3, 64.5, and 77.4°, which are the characteristic peaks of face-centered-cubic Ag (JCPDS card no. 4-783). The major crystal plane in the nanocomposites was (111), a high atom-density facet, which has been found to be highly effective for disinfection (Fig. 6.6b) (Morones et al., 2005; Pal et al., 2007). The selected area electron diffraction (SAED) pattern confirms the results from the XRD analyses (Fig. 6.6c, inset). The lattice fringes of the major crystal planes can be observed in the high-resolution transmission electron (HRTEM) images of the AgNPs (Fig. 6.6c).

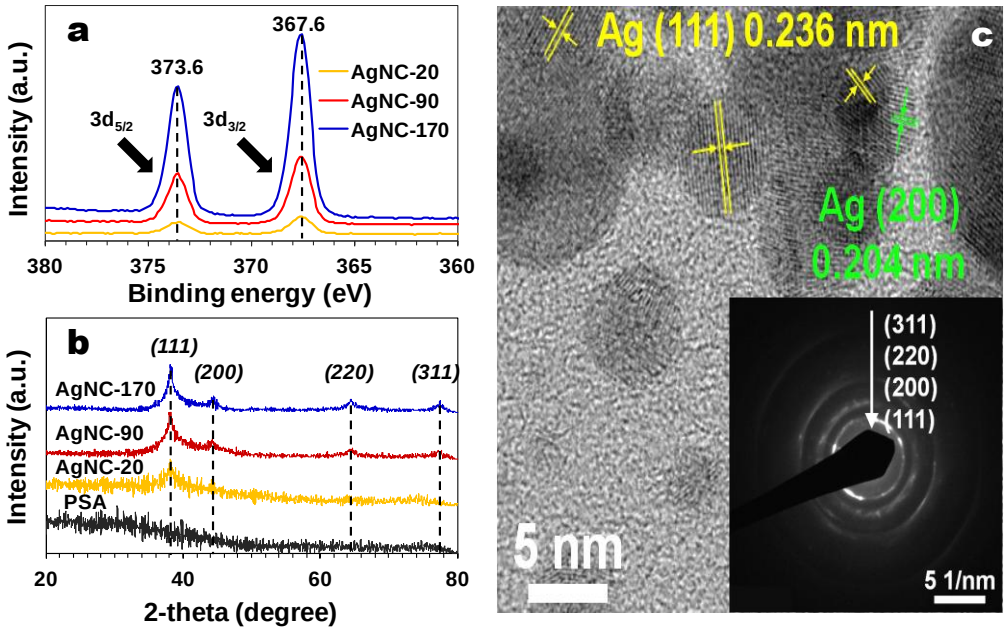

Figure 6.6 (a) XPS and (b) XRD spectra of PSA cryogels with different Ag loadings. (c) HRTEM image and with SAED pattern of AgNC-170 shown in the inset.

Fig. 6.7 shows the dynamic swelling profile of the PSA/AgNP cryogels; the nanocomposites took less than 10 s to reach their equilibrium swollen state. As shown in the inset of Fig. 6.7, an increase in the Ag loading generally led to a decrease in the swelling degree of the nanocomposites as a result of an increase in the non-swellable component, Ag (Mohan et al., 2006). However, this effect may be less important at low Ag loading since the AgNC-20 had a higher swelling degree than that of the PSA cryogel. The enhanced swelling degree at low Ag loading may be ascribed to an increased permeability of the cryogel network as a result of the interaction between the electron-dense AgNPs that causes a free volume expansion (Mohan et al., 2006; Park et al., 2011). This also explains the higher swelling rate of PSA/AgNP cryogels loaded with a higher Ag content (Fig. 6.7).

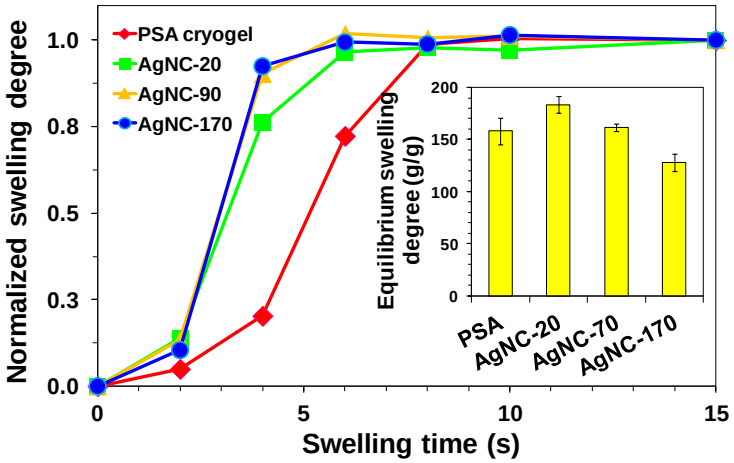

Figure 6.7 Dynamic swelling profiles of cryogels. The swelling degrees were normalized with respected to their respective equilibrium swelling degrees, which are shown in the inset.

PSA cryogels loaded with AgNPs not only showed better swelling behavior but also showed improved mechanical properties. None of the PSA/AgNP cryogels synthesized in this study failed at the end of the compression test (Table 6.1). Moreover, AgNPs loading into the PSA cryogels further improved their mechanical properties since it resulted in stronger and more rigid nanocomposites as indicated by the increase in the Young's modulus (Table 6.1). The PSA/AgNP cryogels are highly robust because they can repeatedly sorb and desorb water for over 1000 cycles with little change in their morphology and mechanical properties (Figs. 6.8

.

and 6.9). The water recovery efficiencies of the PSA/AgNP cryogels were not compromised as a result of their excellent mechanical properties and high pore-interconnectivity. About 85% of the absorbed water could be recovered via low-pressure vacuum filtration or manual hand squeezing (Table 6.1).

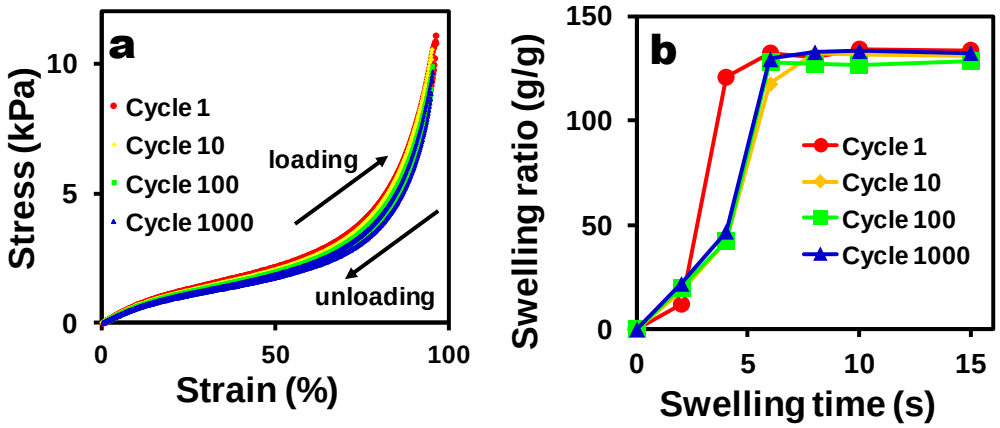

Figure 6.8 (a) Stress-strain profiles of the PSA/AgNP cryogels recorded during fatigue tests. (b) Dynamic swelling profiles of PSA/AgNP cryogels after fatigue tests; the swelling ratios at various times t were computed by taking the ratio of the mass of the swollen gel at time t relative to that of the initial dry mass of gel.

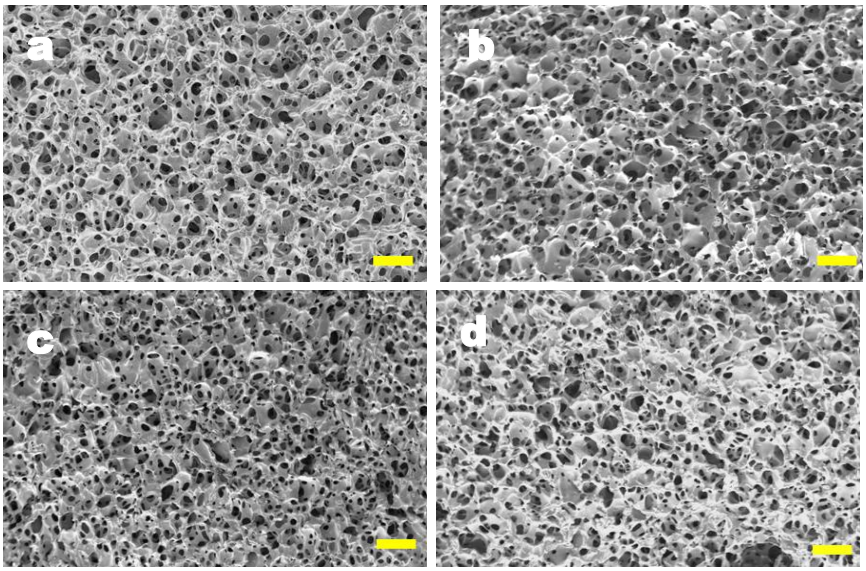

Figure 6.9 Morphology of the PSA/AgNP cryogels (a) before, (b) after 10 cycles, (c) after 100 cycles, and (d) after 1000 cycles of compression; the scale bar denotes 100 µm.

.

6.2.2 Ag release into the treated water

A particular issue with the use of AgNPs as antimicrobial agents is the potential release of significant levels of Ag into the treated water that may occur via (i) uncontrolled dissolution of AgNPs into the water in the form of Ag^+ ions, and (ii) dislodgement of the AgNPs from the polymer matrix. Significant Ag release into the treated water is undesirable since it may reduce the reusability of the nanocomposites and pose health risks. The PSA/AgNP cryogels displayed excellent stability because the total Ag loss after a 24-h Ag-release test was lower than 2% (Table 6.1). The high stability of the nanocomposites may be due to the coordination capacity of the carboxylate groups ($–COO^-$) in PSA that is responsible for anchoring the fine AgNPs within its network; PSA has been shown to be an effective stabilizing agent for AgNPs (Falletta et al., 2008). Furthermore, excess Ag^+ ions released from the AgNPs can be efficiently captured by the free $–COO^-$ functionalities in the PSA/AgNP cryogels (Liang et al., 2012). Interestingly, lower Ag leaching was observed for cryogels with a higher Ag loading (Table 6.1). This may be due to aggregation of some AgNPs in the AgNC-90 and AgNC-170 that could have reduced the available surface area for the dissolution reaction. Similar observations were made by other researchers (Sotiriou and Pratsinis, 2010; Dankovich and Gray, 2011). The total Ag concentrations in the squeezed water for all nanocomposites did not exceed 100 µg/L, the WHO's recommended limit for total Ag concentration in drinking water (Table 6.1). An Ag speciation study revealed that free Ag^+ ions constitute 45-56% of the total Ag in the squeezed water. The remaining Ag constituents may be attributed to other Ag domains not detectable by an ion-selective electrode such as Ag complexes or AgNPs. A more detailed Ag speciation study is discussed in Section 7.2.2. The results also revealed that cryogels with a lower Ag content showed a higher fraction of Ag^+ in the squeezed water (Table 6.1).

.

6.2.3 Disinfection efficacies of the cryogel nanocomposites

The PSA/AgNP cryogels were used to disinfect water using the approach shown in Fig. 1.1. They were found to show significantly higher disinfection efficacies for the squeezed water relative to that of the bulk water (p-value < 0.05; Fig. 6.10a). Note that "squeezed water" refers to the absorbed water recovered via squeezing the cryogel, while the term "bulk water" refers to the excess water outside the cryogel (see Fig. 1.1b and c). This supports the proposed rationale of using them as sorbents because the results suggests that they work better as sorbents than being dispersed in raw water. Notably, even the PSA/AgNP cryogels having the lowest Ag content (i.e., AgNC-20) could inactivate more than 5 logs of viable bacteria in the squeezed water after being allowed to swell in the bacterial suspension for 15 s (Fig. 6.10a). Furthermore, the PSA/AgNP cryogels were highly reusable as indicated by the relatively consistent disinfection efficacies over five cycles of operation (Fig. 6.10b). The extent of disinfection of *E. coli* was not statistically different between the five operating cycles (p-value > 0.05). The good reusability of PSA/AgNP cryogels may be attributed to the high stability of the AgNPs in the PSA cryogel matrices.

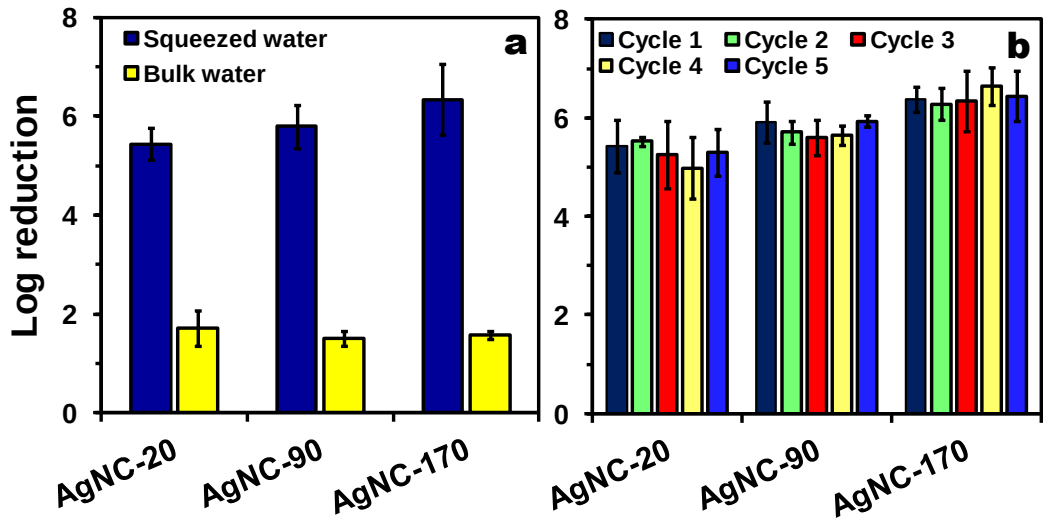

Figure 6.10 (a) Comparison of the *E. coli* disinfection efficacies in the squeezed and bulk waters. (b) Reusability of PSA/AgNP cryogels over five cycles of operation.

As shown in Fig. 6.11, the cryogels are also effective in disinfecting other types of bacteria including *Salmonella typhimurium (S. Typhimurium), Bacillus subtilis (B. subtilis),* and *Staphylococcus aureus (S. aureus)* besides *E. coli.*

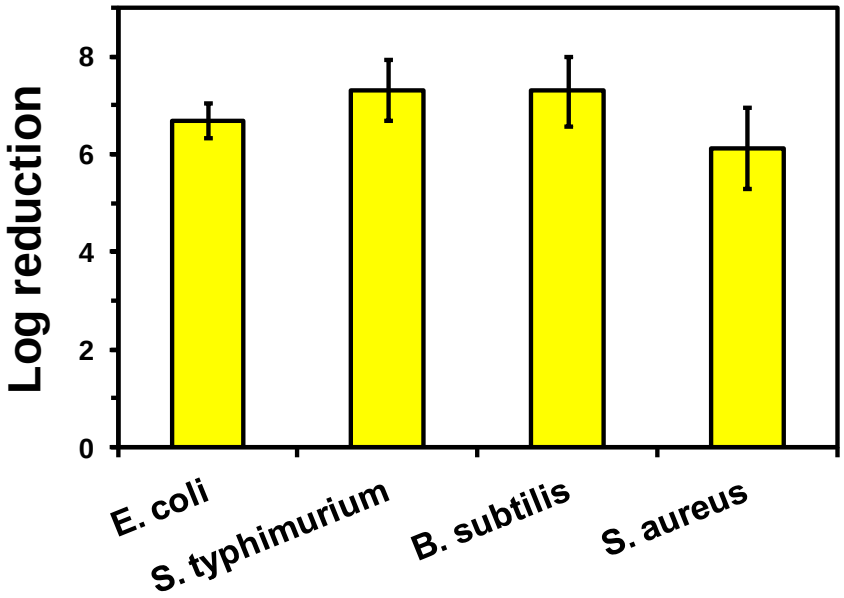

Figure 6.11 The disinfection efficacies of the cryogels toward various types of bacteria.

Although the PSA/AgNP cryogels have been shown to have excellent bactericidal activity using synthetic microbiologically contaminated water, their ability to disinfect natural water samples needs to be studied due to potential complications owing to a more complex solution chemistry. Two types of water samples namely, pond water and tap water were used to represent turbid and clear water in the natural environment. Both the raw water samples were spiked with 10^4 cfu/mL of *E. coli* to study the disinfection efficacies of the PSA/AgNP cryogels in the two water samples under high bacterial loadings. Water quality characteristics of the two water samples can be found in Table 6.2.

.

Table 6.2 Summary of water quality metrics of the two raw water samples

Water quality metric	Turbid water[a]	Clear water[b]
Turbidity (NTU)	36.9 ± 4.6	0.5 ± 0.2
Dissolved organic carbon (mg-C/L)	3.3 ± 0.3	1.6 ± 0.1
pH	6.3 ± 0.2	6.6 ± 0.2
Bacterial count (cfu/mL)	260 ± 70	Not detectable

Note: [a]Water sample collected from a freshwater pond on the campus of Nanyang Technological University; [b]Dechlorinated water sample collected from the laboratory water tap.

Fig. 6.12a shows that the PSA/AgNP cryogels, after being allowed to swell in the contaminated water for 15 s, could achieve more than 2 logs (99%) of bacterial inactivation for both raw water samples. The reusability of the PSA/AgNP cryogels was tested over ten disinfection cycles. Indeed, the cryogels showed stable disinfection performance over ten repetitions that indicates their high reusability (Fig. 6.12b). This shows that the PSA/AgNP cryogels are very promising for water disinfection.

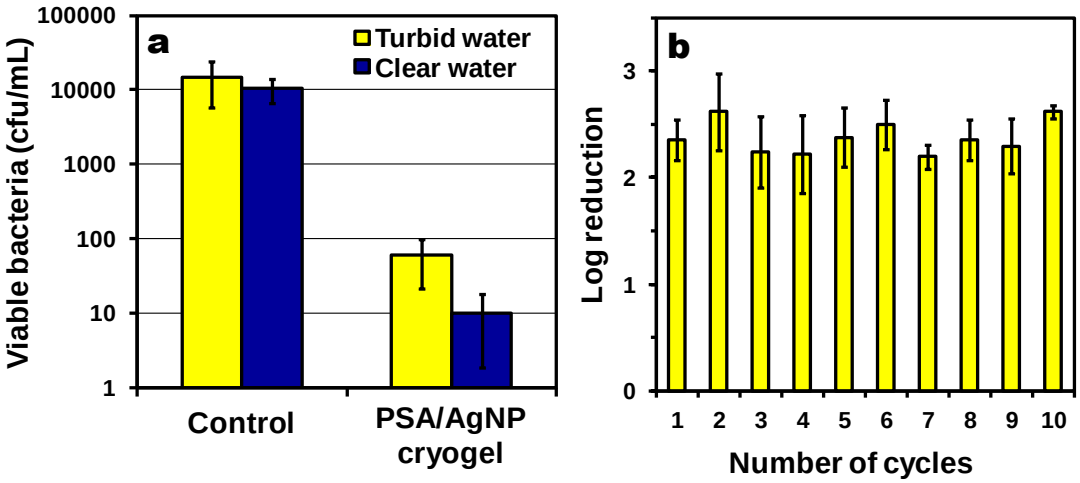

Figure 6.12 (a) Bacterial inactivation in turbid and clear water samples. (b) Disinfection of turbid water samples by PSA/Ag cryogels over ten cycles.

The results revealed that the presence of natural organic matter (NOM) and suspended solids apparently had an adverse effect on the antibacterial activity of the cryogel as evidenced by the lower bacterial inactivation in the turbid water relative to the clear water (Fig. 6.12a). Note that in addition to having a higher turbidity, the "turbid water" also has a higher dissolved organic carbon (DOC) value indicating the presence of a greater amount of NOM (Table 6.1). The reduced disinfection efficacies in the presence of NOM and suspended solids is probably due to their interactions with the bioactive Ag species (both AgNPs and Ag^{+}) that consequently limit the contact between bacterial cells and the Ag species, thereby preventing the inactivation of the bacterial cells to take effect (Fabrega et al., 2009; Gao et al., 2009; Xiu et al., 2011; Zhang et al., 2012). It is envisaged that deactivation of the Ag species in the presence of NOM and suspended solids occur via: (i) shielding of the pathogenic microbes from the Ag species due to sorption of the NOM or suspended solids on the surface of the bacterial cells, (ii) sorption of NOM and suspended solids on the surface of the AgNPs that would lower the reactivity of the nanoparticle surface to a variety of reactions (e.g., ROS generation, oxidative dissolution of Ag^{+}, or specific interaction with bacterial cells) that are believed to be the possible biocidal mechanisms of AgNPs, and/or (iii) adsorption or partitioning of Ag^{+} by NOM that reduces the amount of Ag that is bio-available to the bacterial cells in the solution. The effect of solution chemistry on the antibacterial properties of the PSA/AgNP cryogels will be discussed in greater detail in Chapter 8.

The mechanisms by which free AgNPs exert toxicity have been studied; however, there is no general consensus as to whether the toxicity of the AgNPs was due to the release of Ag^{+} ions (Kittler et al., 2010; Xiu et al., 2012) or to the intrinsic properties specific to the particles (primarily Ag^{0}) (Sondi and Salopek-Sondi, 2004; Morones et al., 2005; Fabrega et al., 2009). Ag^{+} ions are toxic to bacteria due to various mechanisms including binding to thiols in proteins and disrupting the bacterial respiratory chain, thereby generating reactive oxygen species (ROS) that can lead to oxidative stress and cell damage (Holt and Bard, 2005; AshaRani et al., 2008). On the other hand, the toxicity effects of AgNPs have been suggested to arise from: (i) physical processes that involve disruption of the cell membrane and/or

.

penetration of the AgNPs into the cell (Sondi and Salopek-Sondi, 2004; Morones et al., 2005), (ii) particle-surface reactions that generate ROS, which catalyzes the oxidation of cellular contents (Holt and Bard, 2005; AshaRani et al., 2008), and/or (iii) direct interaction with enzyme sites that changes the conformation resulting in impaired metabolism (Wigginton et al., 2010).

However, the bactericidal mechanism of bulk materials functionalized with AgNPs is rarely discussed in the literature. The biocidal action of PSA/AgNP cryogels is hypothesized to be dominated by surface-controlled mechanisms that are dependent on direct contact of the interface of the PSA/AgNP cryogels with the bacterial cells. This is supported by the fact that PSA/AgNP cryogels showed a significantly higher disinfection of the squeezed water than that of the bulk water (Fig. 6.10a). This indicates that the bacterial cells need to come into close contact with the PSA/AgNP cryogels to significantly reduce their viability. The large difference in the disinfection efficacies between the bulk and squeezed waters would not have been observed if the Ag species in the solution were responsible for bacterial inactivation. In particular, the concentrations of Ag^+ (and toxicity levels) in the bulk and absorbed waters should be the same because it can efficiently diffuse from the porous PSA/AgNP cryogels into the solution (both absorbed and bulk waters). It has been shown that for an AgNPs suspension, the diffusion rate of Ag^+ ions into the bulk solution is much faster than their dissolution from the AgNPs (Kittler et al., 2010).

It is envisaged that the water-absorbing cryogels bring water and bioactive Ag species into close proximity for disinfection to take effect within the micrometer-sized pore spaces, which are densely decorated with AgNPs. At this juncture, the toxicity pathways of PSA/AgNP cryogels to the bacterial cells are thought to involve three mechanisms as illustrated in Fig. 6.13.

.

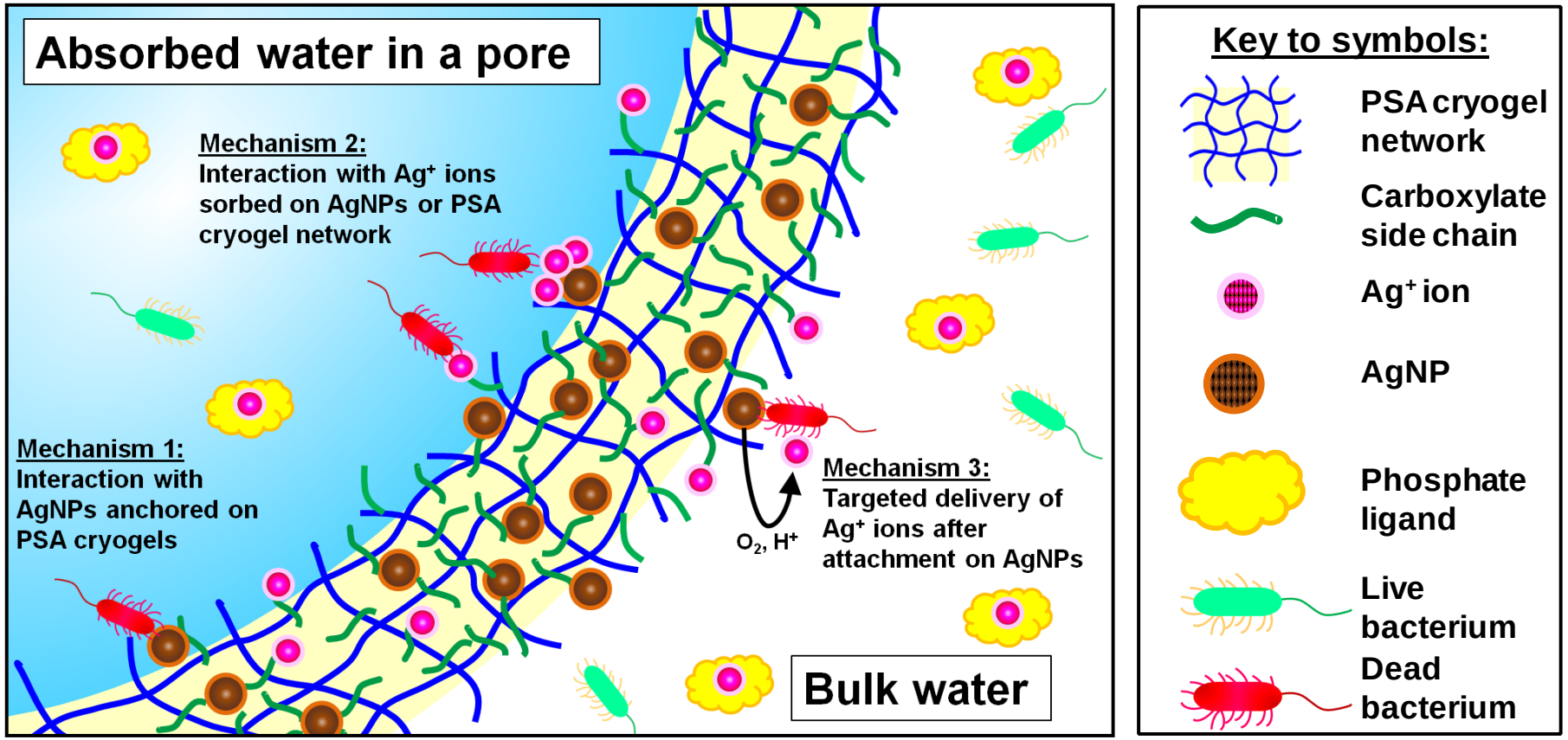

Figure 6.13 Illustration that summarizes the possible mechanisms of biocidal action of PSA/AgNP cryogel nanocomposites.

One possible mechanism involves direct contact between the bacterial cells and the AgNPs anchored on the PSA cryogels (Mechanism 1 in Fig. 6.13). Another plausible mechanism involves Ag^+ ions that are associated with the PSA/AgNP cryogels via chemical/physical sorption on the surface of the AgNPs or the PSA cryogel network (Mechanism 2 in Fig. 6.13). Note that there is evidence that Ag^+ ions can be chemisorbed on the AgNP surface (Henglein, 1998; Lok et al., 2007; Liu and Hurt, 2010). In addition, the cryogels developed in this study contained O and to a lesser extent N functional groups that can bind Ag^+ ions. Such polymeric materials can control the release of bound Ag^+ ions via a reversible adsorption-desorption mechanism (Liu et al., 2010a). PSA/AgNP cryogels with Ag^+ ions bound to their polymeric network or to the AgNP surface can associate directly with the bacterial cells in close proximity to provide a targeted delivery of Ag^+ ions directly to the bacteria. Targeted delivery of Ag^+ ions may also occur via oxidative dissolution of Ag^0 after attachment of the AgNPs to biomolecules on the bacterial cells (Mechanism 3 in Fig. 6.13) (Lok et al., 2007; Navarro et al., 2008). Detailed investigation to elucidate the toxicity pathways involved in the bactericidal action of the PSA/AgNP cryogels will be elaborated in Chapter 7.

6.2.4 Perspectives on using PSA/AgNP cryogels for onsite water treatment in emergencies

PSA/AgNP cryogels have been demonstrated to have excellent bactericidal efficacy after a brief swelling time (i.e., 15 seconds) whereby over a 2-log reduction could be achieved when used to disinfect natural water samples. Furthermore, in Chapter 4, the cryogels were found to significantly improve the visual quality of the water. Due to its substantial water absorption and high disinfection efficacy, only 4 g of AgNC-170 are sufficient to rapidly produce 500 mL of disinfected drinking water in one cycle of operation. Furthermore, they are highly reusable due to their high elasticity and stability of the AgNPs. The AgNPs in the cryogels are highly stable that prevents uncontrolled release of Ag species into the treated water; the total Ag consumed in one disinfection cycle was estimated to be 0.1% of the Ag content in a

.

fresh cryogel (further details can be found in Fig. 7.3). As such, a mass-balance analysis indicates that the cryogel can be used up to 1000 cycles provided that there is no mechanical degradation during squeezing to recover the treated water. As shown in Figs. 6.8 and 6.9, the cryogels were sufficiently robust to be repeatedly compressed for over 1000 cycles. This is equivalent to 150 L/g production capacity. Disposal of the used PSA/AgNP cryogels should be avoided both because Ag is a precious metal and to avoid the potential of an ecotoxicological impact on the environment. The limiting factor for repeated use of the cryogels may be either deterioration in the bacterial inactivation as a result of Ag loss or physical damage during squeezing. The disinfection efficacies of the cryogels can be restored by re-loading them with AgNPs if they remain mechanically robust. However, for physically damaged cryogels the residual Ag can be recovered by burning off the polymer scaffolds. Based on these results, the PSA/AgNP cryogels are thought to offer a simple approach for potable water production in disaster-relief applications. Furthermore, these cryogels are lightweight and highly portable allowing them to be easily deployed for emergency response.

6.3 Concluding remarks

The study presented in this chapter has demonstrated the successful application of PSA/AgNP cryogels for enhanced water disinfection using the approach shown in Fig. 1.1. The PSA/AgNP cryogels combine the high porosity, excellent mechanical and water absorption properties of cryogels, and uniform dispersion of fine AgNPs on the cryogel pore surface for rapid disinfection with minimal Ag release (< 100 µg/L). Their antibacterial performance was evaluated based on the disinfection efficacies of *E. coli*, *S. typhimurium*, *B. subtilis, and S. aureus*. The PSA/AgNP cryogels had excellent disinfection efficacies showing over a 5-log reduction of viable bacteria after a brief 15-s swelling time. In addition, the cryogels were also effective in disinfecting natural water samples for which more than a 2-log reduction of viable bacteria could be achieved. They were highly reusable since there was no significant difference in the disinfection efficacies over five cycles of

.

operation; moreover, they can be repeated compressed for over 1000 cycles. The bactericidal action of the PSA/AgNP cryogels is believed to be dominated by surface-controlled mechanisms that are dependent on direct contact of the interface of PSA/AgNP cryogels with the bacterial cells. The PSA/AgNP cryogels are thought to offer a simpler approach for drinking-water disinfection in disaster-relief applications.

.

CHAPTER 7 Bactericidal mechanisms revealed for rapid water disinfection by superabsorbent cryogels decorated with silver nanoparticles[†]

The cryogels prepared in Chapter 6 have been found to demonstrate remarkable bactericidal efficacy. The study reported in this chapter aimed to systematically investigate the involvement of various possible pathways in the bactericidal mechanism of AgNPs, both generally and in the specific context of PSA/AgNP cryogels.

7.1 Experimental details

The syntheses, characterization, and experimental procedure in this chapter can be found in Chapter 3. Unless otherwise stated, all the tests were conducted using the AgNC-170 cryogel. To compare the bactericidal action of AgNPs to that of Ag^+, PSA cryogels bound with Ag^+ were also prepared. The method used to fabricate PSA/Ag^+ is the same as that for PSA/AgNP except that the $NaBH_4$ reduction step is omitted for synthesis of the former. Note that after equilibration of the cryogels in Ag^+, precautionary steps were taken to avoid light exposure to minimize photo-reduction of Ag^+ to Ag^0 in the cryogels.

[†]This chapter has been published as 'Bactericidal Mechanisms Revealed for Rapid Water Disinfection by Superabsorbent Cryogels Decorated with Silver Nanoparticles' in *Environmental Science and Technology* (49) 2310–2318. Please see Appendix A for reuse permission.

7.2 Results and discussion

7.2.1 Rapid and irreversible bactericidal action of PSA/AgNP cryogels

In Chapter 6, PSA/AgNP cryogels have been shown to achieve over a 5 log reduction in viable bacteria after a brief swelling time of 15 s. However, the disinfection could have occurred over the span of the 24-h incubation. To verify that this did not occur, the kinetics of the bactericidal action of AgNC-170 was studied by adding quenching agent once the water was squeezed out to deactivate the Ag species (in the bacteria or solution phase) to suppress its bactericidal effects during the 24-h incubation period. It was found that part of the disinfection (2.7±0.3 logs) could take place immediately during the 15-s contact time (Fig. 7.1a). Close to 6 logs could be achieved by increasing the contact time to 5 min (Fig. 7.1a). This means that 20 mg of the cryogel (containing less than 4 mg silver) can inactivate 3×10^6 *E. coli* per second in the first 30 s of contact (Fig. 7.1a). Note that such an unprecedented rapid water disinfection was achieved without any external energy input unlike methods such as electroporation (Schoen et al., 2010; Liu et al., 2013). Furthermore, the cryogels are so effective that the *E. coli* contacted with the gels for 3 minutes or longer cannot be revived even after 5 h of incubation in a nutrient-rich medium (Fig. 7.1b).

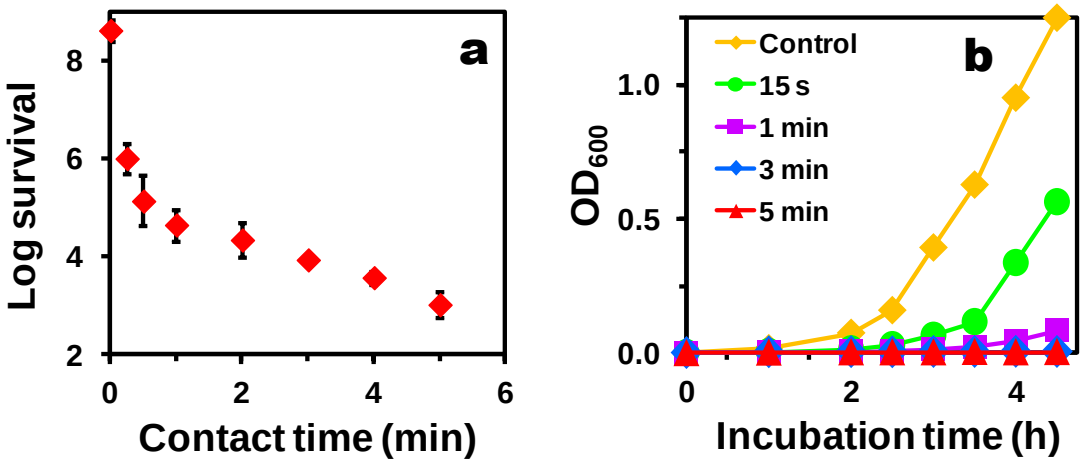

Figure 7.1 Time course of *E. coli* death determined by the addition of a quenching agent. (b) Re-growth test of *E. coli* cells exposed to the cryogels for various contact times.

.

7.2.2 Contact-killing action of PSA/AgNP cryogels via targeted Ag^+ delivery

To understand the mode of action of the PSA/AgNP cryogels, the disinfection efficacies of the PSA/AgNP cryogels that are either directly or indirectly exposed to bacterial cells were also conducted. Fig. 7.2a shows the procedure involved in the experiment comparing the disinfection efficacies of the cryogels via direct and indirect contact.

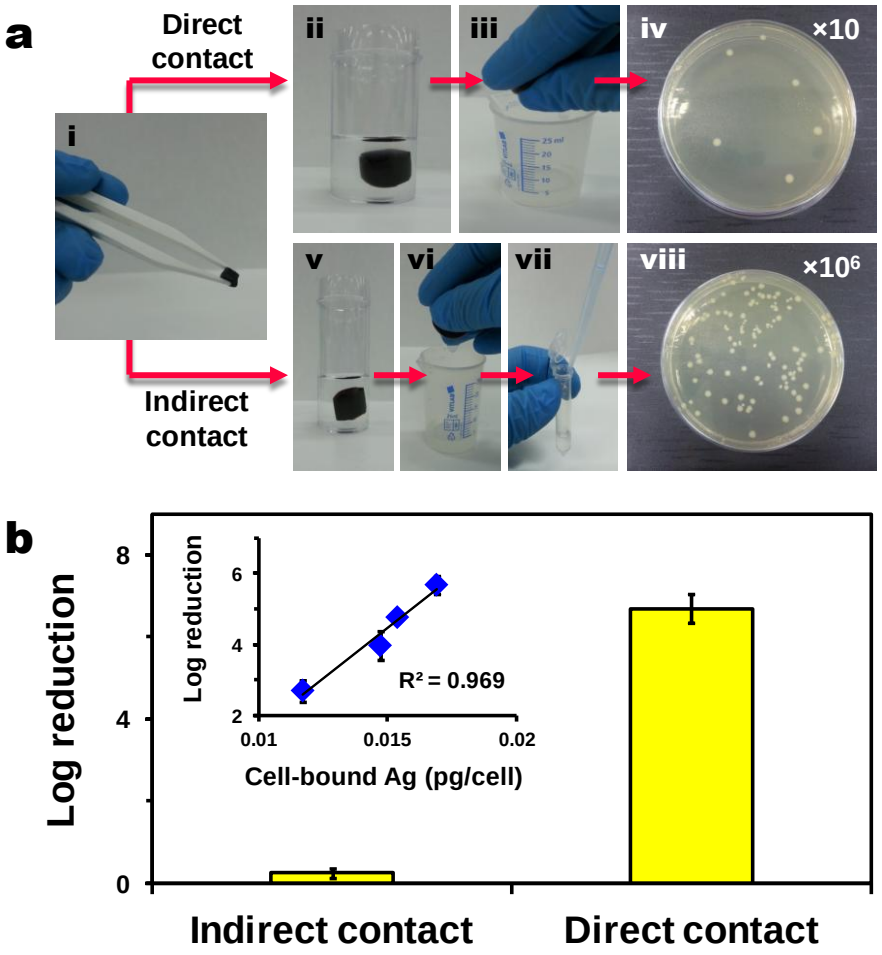

Figure 7.2 (a) Summary of the procedure used to compare the disinfection efficacies of the cryogels via direct and indirect contact. For direct contact, the PSA/AgNP cryogel was allowed to swell in a bacterial suspension (for 5 min) after which the absorbed water was squeezed out and directly plated (i-iv). For indirect contact, the PSA/AgNP cryogel first was allowed to swell in PBS for 5 min (v). Then 1 mL of the PBS squeezed from the gel was added to a bacterial pellet and thoroughly mixed for another 5 min before it was plated (vi-vii). (b) Comparison of the disinfection efficacies of the cryogels via direct or indirect contact with *E. coli* cells.

The indirect approach, which involves exposing the absorbed water, which was squeezed from the PSA/AgNP cryogels (that contains dissolved Ag^+), did not result in any significant bactericidal activity (Fig. 7.2b). This indicates that the bacterial cells need to interact with the Ag species on the cryogels for disinfection to take place, which corroborates the findings reported in Section 6.3. One possible mechanism involving direct contact advanced in the literature attributes cell death to injury inflicted from physical interaction with sharp surfaces of the AgNPs (Sondi and Salopek-Sondi, 2004; Morones et al., 2005; Taglietti et al., 2012). However, this contradicts recent reports that found fully reduced AgNPs have no antibacterial effect when the experiments were conducted under anaerobic conditions (that precludes the formation of Ag^+), which underscores the importance of Ag^+ ions (Lok et al., 2007; Navarro et al., 2008; Xiu et al., 2012). In fact, it was found that there is a close correlation between disinfection efficacy and the cell-bound Ag concentration (Fig. 7.2b, inset). However, no such correlation was observed for the dissolved Ag concentration.

A detailed Ag speciation study revealed that most of the Ag species released from the AgNPs (about 95%) was taken up by the bacteria (Fig. 7.3). Only a small fraction (< 100 µg/L) ends up in the dissolved phase. Because the free Ag^+ concentration in the extracellular solution was very low (i.e., below the detection limit of the Ag ion-selective electrode), the dissolved Ag probably was mainly in the form of dissolved complexes bound to the phosphate ligands or bacterial exudates (Junkins and Doyle, 1992; Eboigbodin and Biggs, 2008). Note that the extracellular total organic carbon (TOC) concentration was determined to be 6.2±0.6 mg/L. This explains the lack of antibacterial activity using the indirect contact approach since the majority of the Ag^+ ions in the solution are bound to ligands that reduce their bioavailability to the bacterial cells (Fig. 7.2b). As shown in Fig. 7.3, the concentration of extracellular Ag^0 was negligible (< 10 µg/L). This is further verified by the absence of a surface plasmon resonance peak in the extracellular solutions (data not shown).

.

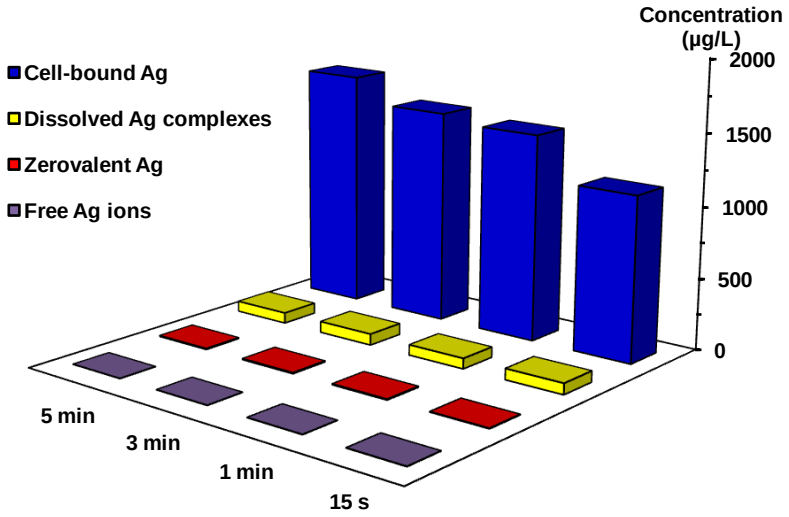

Figure 7.3 Distribution of Ag species of bacterial suspension exposed to PSA/AgNP cryogels at various contact times.

7.2.3 The differential disinfection mode of AgNPs and Ag^+ ions

Most of the Ag delivered to the cells should be in the form of Ag^+ ions (or other labile Ag complexes) because bacterial porins only allow passive diffusion of molecules smaller than 600 Da (Denyer and Stewart, 1998), thereby preventing cellular internalization of the AgNPs (or commonly known as the Trojan horse mechanism). Uptake of the Ag^+ can cause a myriad of adverse effects on the cellular metabolic functions of the bacteria. For example, a rapid drop in the cellular adenosine triphosphate (ATP) content (by 69-86%) was observed following the exposure to PSA/AgNP cryogels (data not shown). In order to distinguish the specific functions of the Ag domains, comparative tests using PSA cryogels impregnated with bound Ag^+ ions (or PSA/Ag^+ cryogels without reducing Ag^+ to Ag^0) were performed. Interestingly, for bacterial cells exposed to PSA/Ag^+ cryogels, a substantial portion (about 30%) of the Ag consumed dissolves into the bulk solution that may result in waste and potential hazards (Fig. 7.4a). This is in stark constrast to the PSA/AgNP cryogels for which the majority of Ag consumed (>95%) is attributed to cell uptake, thereby displaying a higher cell partition ratio (Fig. 7.4).

.

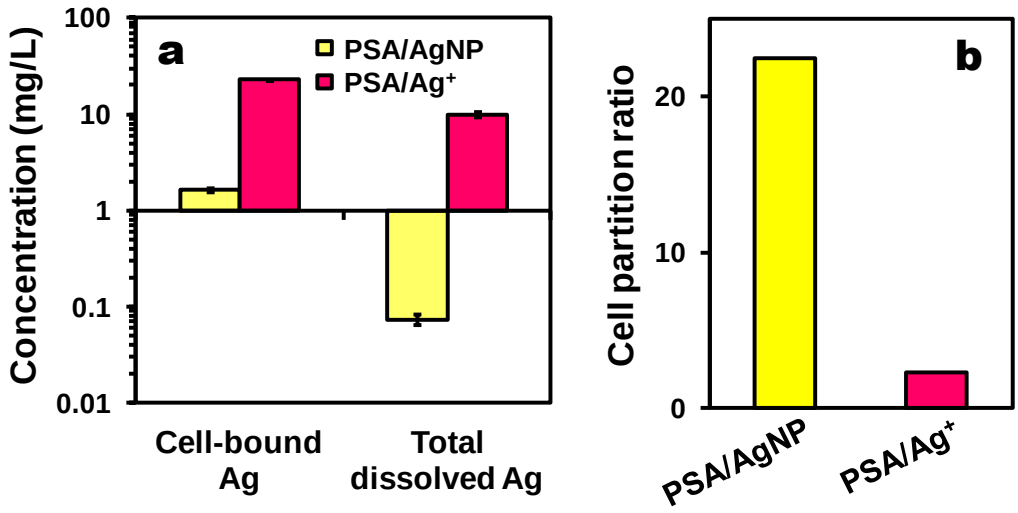

Figure 7.4 Comparison of (a) the cell-bound and total dissolved Ag concentrations, and (b) cell partition ratios of *E. coli* exposed to PSA/AgNP and PSA/Ag^+ cryogels. Note that the cell partition ratio was computed by taking the ratio of the cell-bound Ag concentration to that of the dissolved Ag.

Furthermore, although the PSA/AgNP cryogels led to a substantially lower concentration of cell-bound Ag and poorer ATP inhibition than did the PSA/Ag^+ cryogels, the PSA/AgNP cryogels surprisingly caused severe cell-membrane lesions to the majority of the cells (Fig. 7.5). In contrast, bacteria contacted with the PSA/Ag^+ cryogels did not show any cell-membrane damage but the presence of a few elongated cells could indicate stress and disturbed cell division (Fig. 7.5b). These puzzling results imply that the mechanism may be more complex than just the toxicity caused by intracellular Ag^+ ions alone.

.

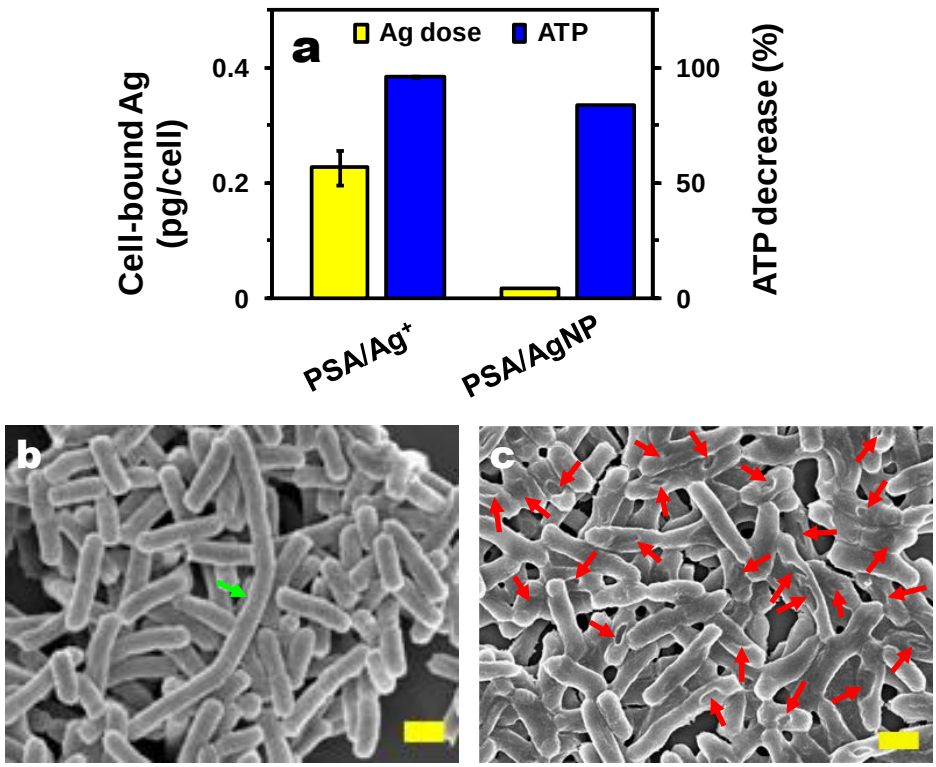

Figure 7.5 (a) Comparison of the cell-bound Ag concentration, and the extent of ATP reduction in cells exposed to PSA/Ag^+ (116.0 ± 7.9 mg/g) and PSA/AgNP cryogels (Ag content of 166.7 ± 15.0 mg/g). FESEM images of *E. coli* after a 5-min exposure to (b) PSA/Ag^+ cryogels and (c) PSA/AgNP cryogels. Note: the scale bars represent 0.5 µm. The green arrow in (c) points to a cell that appears to be elongated indicative of stress, while the red arrows in (d) point to the holes in the cells.

7.2.4 Role of ROS in mediating cell lesions

The time-dependent nature of the cell-membrane damage as shown in Fig. 7.6 suggests that the lesions on the cells exposed to the PSA/AgNP cryogels are caused by chemical reaction rather than physical interaction. Furthermore, if the membrane damage were due to physical puncturing of the cell walls by the Ag^0, random pits would be present all over the cells. The chemical reaction is probably a self-propagating one since sustained exposure of the cells to PSA/AgNP cryogels caused the indentations on the cells to develop into holes, which were localized mainly at the mid-point of most injured cells (Fig. 7.6a). Such damage was also observed in other bacterial strains exposed to PSA/AgNP cryogels (Fig. 7.7).

.

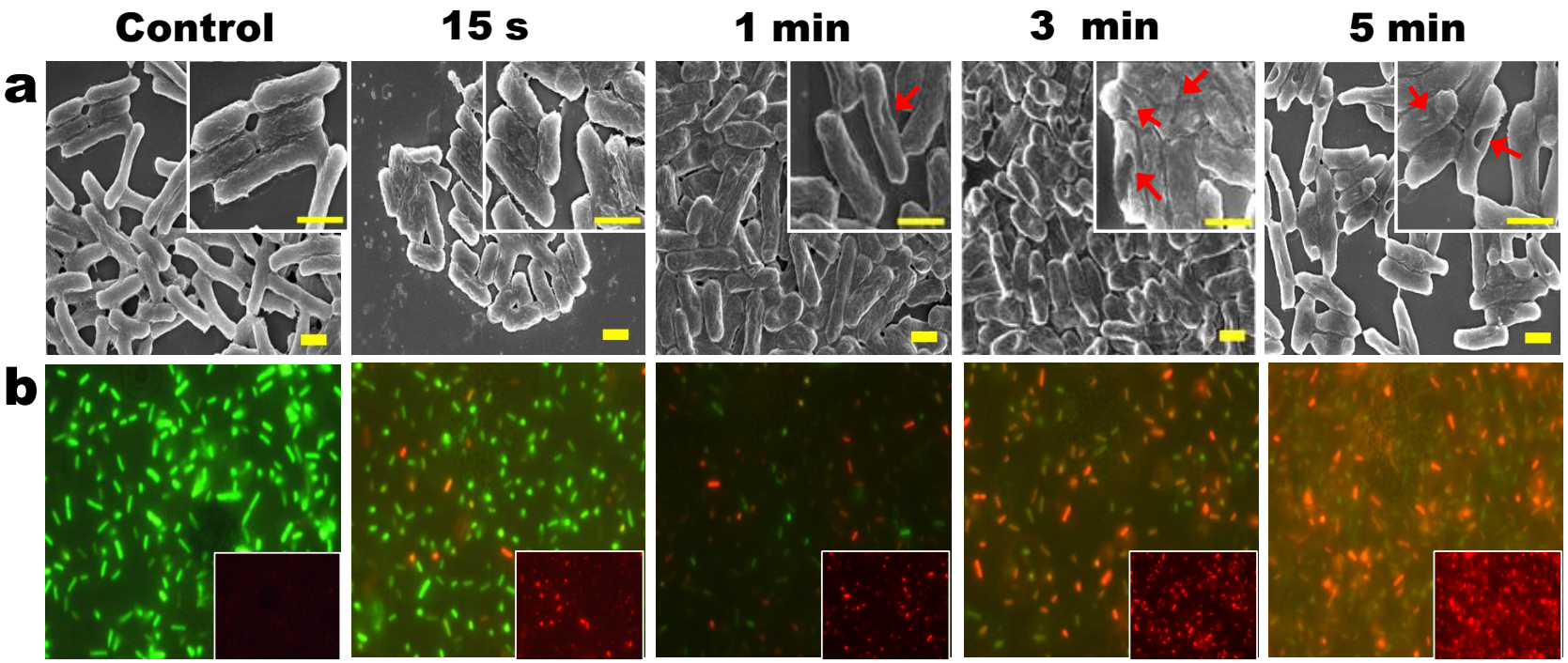

Figure 7.6 (a) FESEM images, and (b) Fluorescence images (recorded using dual color channels) of *E. coli* cells contacted with the cryogels for various times. The inset of (b) shows the corresponding fluorescence images recorded using the red channel. The scale bars in (a) represent 1 µm.

.

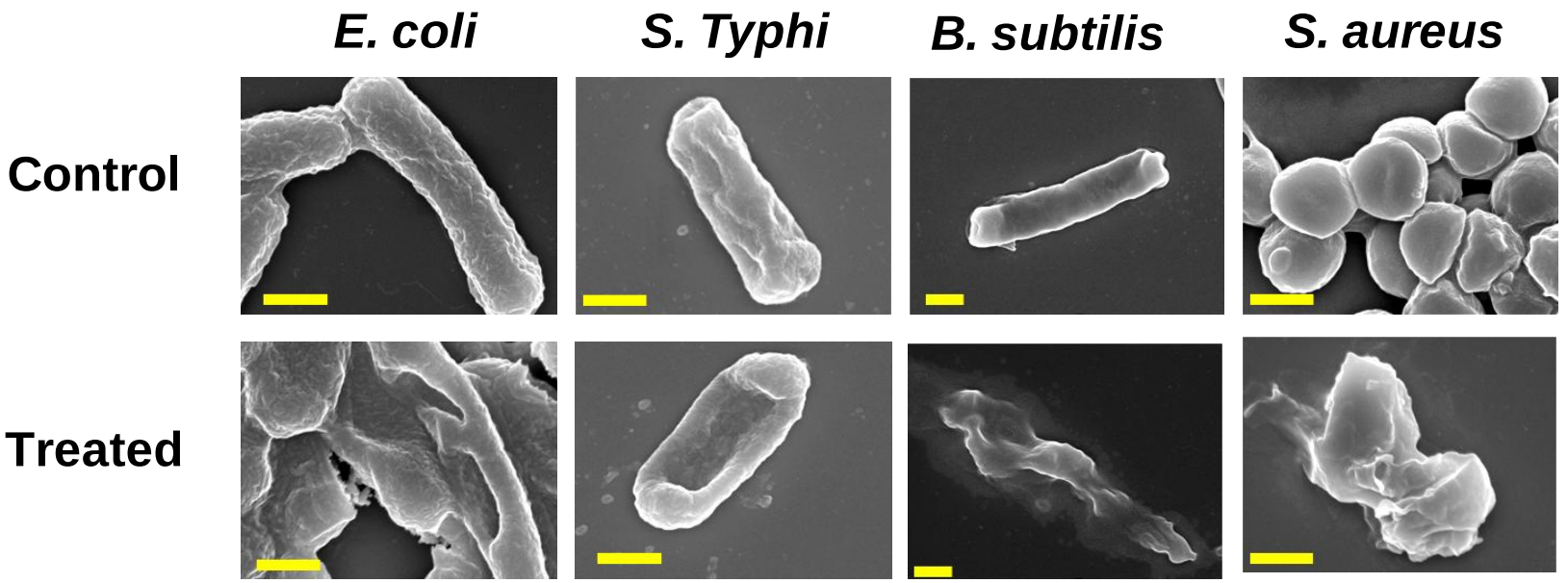

Figure 7.7 FESEM images of various types of bacteria before and after exposure to the PSA/AgNP cryogels for a 5-min contact time; the scale bars denote 0.5 µm length.

.

It is postulated that such damage is likely exacerbated by reactive oxygen species (ROS) whose presence could initiate a chain reaction. Indeed, the results from a ROS scavenging test confirm the involvement of ROS ($\cdot O_2^-$, H_2O_2, and $\cdot OH$) in the bactericidal action of the PSA/AgNP cryogels (Fig. 7.8); it is known that $\cdot O_2^-$ and H_2O_2 are precursors to the more reactive $\cdot OH$ species.

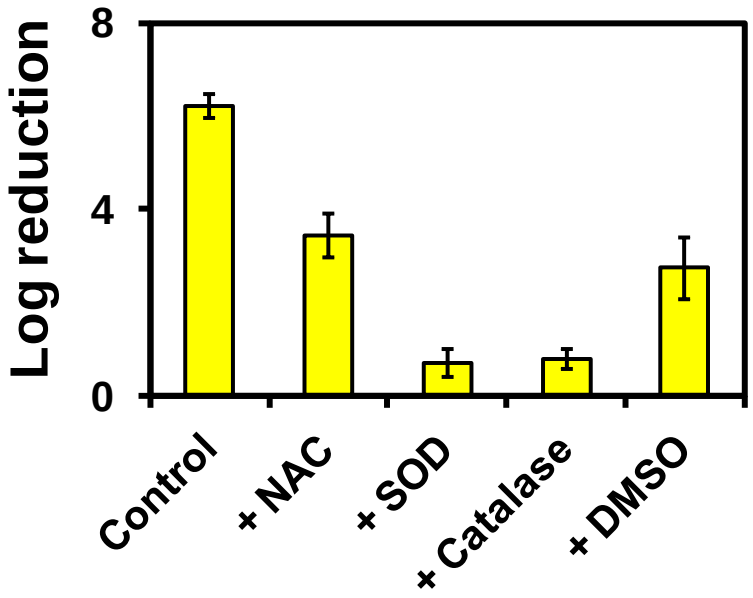

Figure 7.8 Antibacterial activity of PSA/AgNP cryogels towards *E. coli* in the presence of different ROS scavengers. Note that the scavengers were added at different concentrations. Hence, the extent of reduction in the antibacterial activities is not proportional to the contribution of the specific ROS quenched by the scavenger. Note: NAC increases the production of glutathione, which is an antioxidant; SOD catalyzes dismutation of $\cdot O_2^-$ to H_2O_2; catalase scavenges H_2O_2; DMSO scavenges $\cdot OH$.

In addition, both PSA/AgNP and PSA/Ag^+ cryogels were found to induce the formation of intracellular ROS albeit to different extents (Fig. 7.9). This observation was again perplexing because, even though the PSA/Ag^+ cryogels had a higher Ag content and delivered more Ag^+ into the cells than the PSA/AgNP cryogels (AgNC-90 and AgNC-170), the amount of ROS generated by the PSA/Ag^+ cryogels was significantly lower (Fig. 7.9a). This observation suggested the critical role of AgNPs in ROS formation.

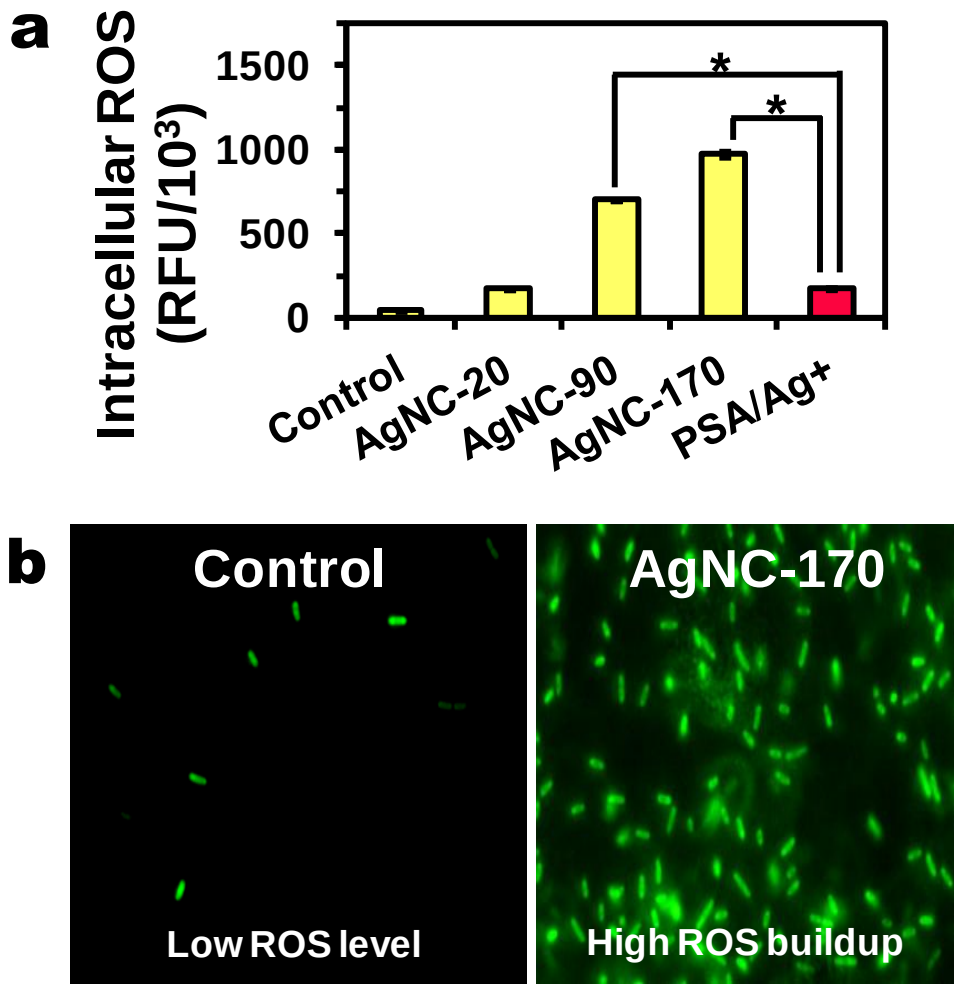

Figure 7.9 (a) Fluorescence measurement of intracellular ROS generation using PSA/AgNP cryogels with different Ag content, and PSA/Ag^{+} cryogels (120 mg Ag/g). Significant differences between the fluorescence intensity of the exposed cells are denoted by asterisks: (*) $p<0.01$ (Student's t test, n = 3). Note that RFU denotes relative fluorescence unit. (b) Intracellular ROS fluorescence images of the control cells and those exposed to the PSA/AgNP cryogels; increased fluorescence indicates an enhanced buildup of intracellular ROS.

The resultant ROS, especially ·OH, can subsequently injure cells by reacting with various biomolecules. One possible route for ROS-mediated cell injury is via lipid peroxidation of the cellular membrane as indicated by the results from the TBARS (thiobarbituric acid reactive substances) assay (Fig. 7.10); an enhanced TBARS level was assumed to be indicative of the presence of lipid peroxidation. As noted earlier, both *E. coli* and *B. subtilis* cells that were exposed to PSA/AgNP cryogels show an elevated level of TBARS (Fig. 7.10). A higher concentration of TBARS

was detected for cells exposed to cryogels with a higher Ag content that may be attributed to the formation of more ROS (especially ·OH) (Figs. 7.9a and 7.10) Increased TBARS levels in bacteria has also been observed when exposed to other ROS-generating materials such as Cu-based materials, graphene oxide, and TiO_2 among others (Maness et al., 1999; Applerot et al., 2012; Hong et al., 2012; Krishnamoorthy et al., 2012). These studies also provide evidence that although the level of polyunsaturated fatty acids (PUFAs) in bacterial membranes is low, ROS-mediated injury can proceed via a lipid peroxidation mechanism; note that PUFA is the preferred substrate for lipid peroxidation because it forms a radical that is stabilized by molecular rearrangement to form a conjugated diene. Furthermore, overexpression of yqhD, the gene responsible for aldehyde reductase activity for cell defence against the harmful effects of aldehydes derived from lipid peroxidation, in *E. coli* when exposed to ROS-generating compounds provides further evidence of the occurrence of lipid peroxidation in bacterial membranes (Pérez et al., 2008). The injury sustained by the bacterial cells exposed to the PSA/AgNP cryogels was severe as indicated by the leakage of cytoplasmic contents detected via spectrophotometric detection (data not shown).

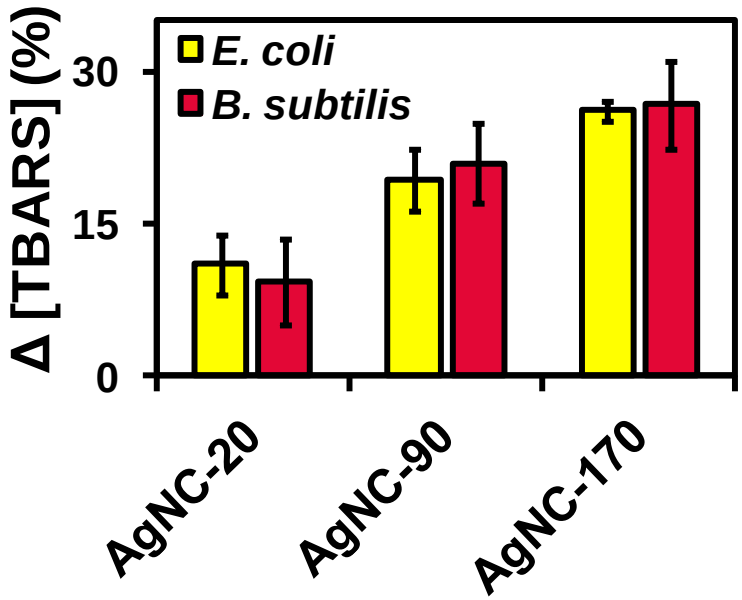

Figure 7.10 Comparison of TBARS (thiobarbituric acid reactive substances) level in healthy bacterial cells versus those exposed to PSA/AgNP cryogels.

7.2.5 Bactericidal mechanism of PSA/AgNP cryogels

Based on the evidence gathered, it is proposed that there are two concerted pathways that enable the PSA/AgNP cryogels to achieve a virtually instantaneous bacterial disinfection (Fig. 7.11).

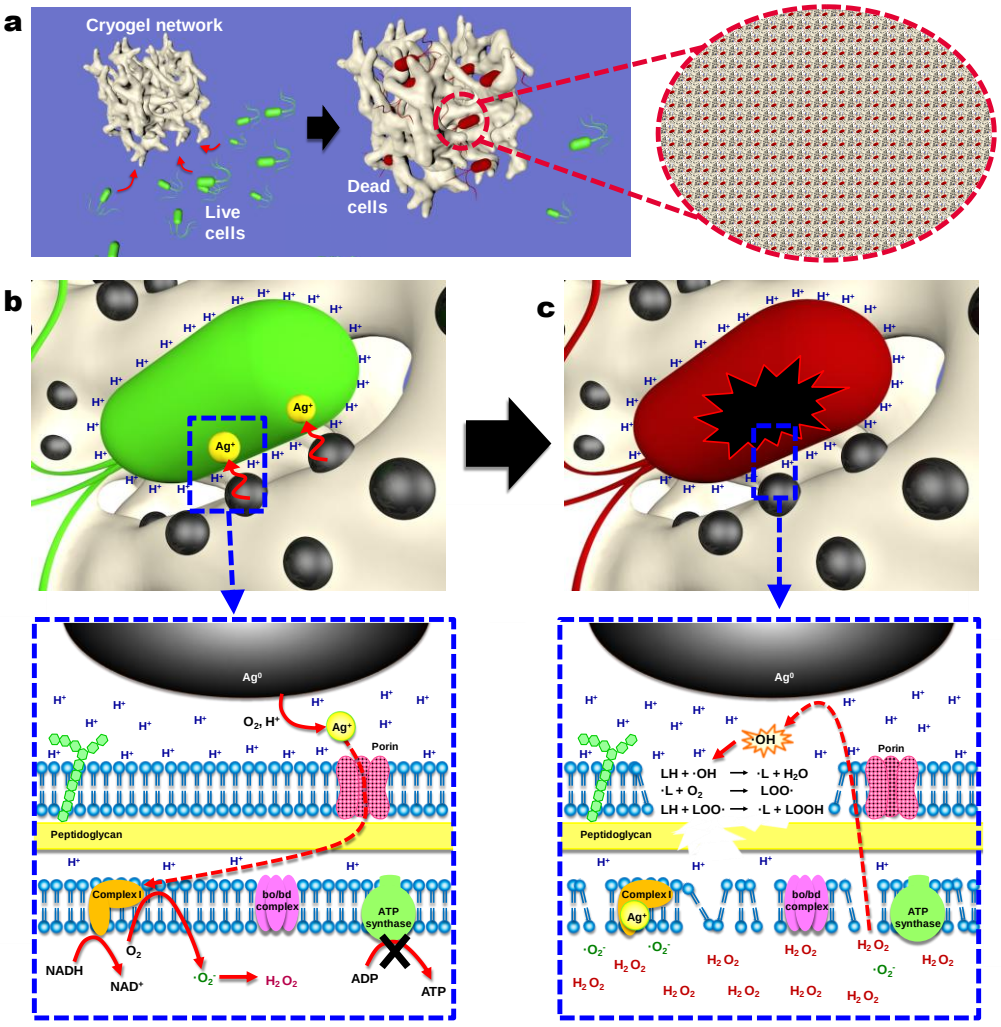

Figure 7.11 Illustration summarizing the proposed bactericidal mechanism of PSA/AgNP cryogels. (a) Rapid water absorption draws an immediate flow of bacteria into the microchannels of the cryogels allowing frequent encounters with the anchored AgNPs . (b) pH-lowering effect as the cell approaches the AgNP interface triggers the release of Ag^+. The Ag^+ is instantaneously taken up by the cell and subsequently inhibits ATP synthesis and the electron transport chain. The latter process results in the indirect formation of ROS ($\cdot O_2^-$ and H_2O_2). (c) In an acidic environment, AgNPs can form ·OH by causing the decomposition of H_2O_2. The resultant ·OH can initiate a peroxidative sequence that inevitably results in cell death by destroying the cell membrane (Gutteridge and Halliwell, 1990). Note: ·L and LOO· denote a carbon-centered radical and a peroxyl radical, respectively.

The cryogels provide a conducive physical pathway (which is densely decorated with AgNPs) for cell-AgNP interaction due to their unique micro-architecture and swelling behavior. The large number of fine and well-dispersed AgNPs anchored on the PSA cryogel surface combined with the highly porous network of cryogels exposes a large surface area of bioactive Ag species to bacterial cells in a confined environment. In addition, the ability of the cryogels to rapidly imbibe water essentially drives an instant flow of bacterial cells into the tortuous microchannels of the cryogels within which the cells can interact with the exposed AgNPs (anchored on the cryogel pore surface) within a short diffusional distance (Fig. 7.11a); note that these interactions with the AgNPs can happen again during the 1-s water recovery or expulsion step. While in the microchannels, close proximity between the AgNPs and the cells is assured due to comparable size scales (of the microchannels and cells). Besides bringing the bacterial suspension into close contact with the biocidal Ag species located on the pore surfaces, the fast water absorption ability of cryogels also played a crucial role in exposing the bacterial suspension to Ag species in a timely manner to allow rapid disinfection.

Close proximity between the AgNPs and cells is just one of the prerequisites to triggering a cascade of events. It is known that a narrow region outside the bacterial cell wall is acidified due to proton extrusion under the influence of a proton motive force (Koch, 1986; Xiu et al., 2012) (Fig. 7.12). Furthermore, the high surface-charge of the PSA/AgNP cryogels (due to the presence of numerous carboxylate groups) could lower the interfacial pH as a cell approaches the surface (O'Reilly et al., 2005; Hong and Brown, 2009). Consequently, Ag^0 dissolution at the cell-AgNP interface is substantially accelerated due to rapid oxidation under low-pH conditions. The enhanced Ag^0 dissolution at the cell-AgNP interface translates into a unique "on-demand" Ag^+-release behaviour (i.e., triggered in the presence of bacteria), which is an interesting new insight into the bactericidal action of AgNPs. This hypothesis is supported by the Ag speciation data that revealed PSA/AgNP but not PSA/Ag^+ cryogels demonstrate the on-demand release behavior as shown by their significantly higher cell partition ratio (Fig. 7.4b). The triggered-Ag^+-release for targeted delivery of toxic Ag^+ to the contacted cell is essentially Mechanism 3 in the proposed toxicity pathways discussed in Section 6.3. The new insights on the

triggered-Ag^+-release provide a plausible explanation for the enhanced disinfection with improved AgNP contact and excellent disinfection efficacies despite the observed low Ag leaching for PSA/AgNP cryogels (that was discussed in Chapter 6) and other Ag nanohybrids that were previously not understood (Balogh et al., 2000; Su et al., 2009; Dankovich and Gray, 2011; Alonso et al., 2013; Zhang et al., 2013).

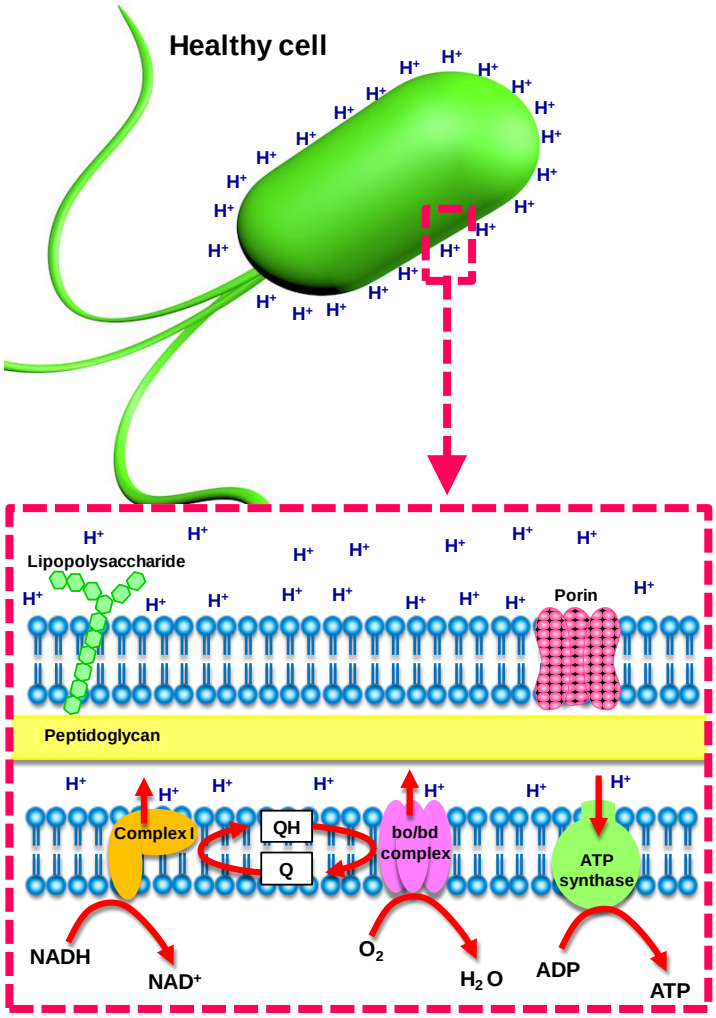

Figure 7.12 Illustration depicting the metabolic processes occurring at the bacterial cytoplasmic membrane, which serves as the oxidative phosphorylation site. In healthy cells, protons are continuously pumped out of the cells (via coupling proteins) using the energy generated by the transfer of electrons from electron donors (NADH) to electron acceptors (O_2) via redox reactions. This creates an electrochemical gradient for chemiosmosis of a proton back into the cell that generates ATP via phosphorylation of ADP.

Cellular uptake of the Ag^+ results in a chain of events in the subsequent metabolic pathway (Fig. 7.11b). First, the cells are almost instantaneously inactivated due to metabolic arrest as a consequence of a drastic drop in the ATP level. Note that Ag^+ has been found to inhibit ATP formation by either behaving like a protonophore (Dibrov et al., 2002) or by inhibiting enzymes in the respiratory chain (Holt and Bard, 2005; Park et al., 2009) to dissipate the proton motive force. In addition, the interaction between Ag^+ and coupling enzymes (bearing cysteine groups with a strong affinity to Ag^+ such as NADH and succinate dehydrogenase) impedes the electron-shuttling process causing the increased intracellular production and buildup of $\cdot O_2^-$ and H_2O_2 (Liau et al., 1997; Messner and Imlay, 1999; Holt and Bard, 2005; Jung et al., 2008). Ag^+ also enhances the susceptibility of the bacterial cells to ROS by depleting intracellular antioxidants such as glutathione (Avalos et al., 2014).

Note that the *E. coli* membrane shows substantial permeability (16 μm/s) towards H_2O_2 (Seaver and Imlay, 2001). Therefore, when H_2O_2 persists long enough, which is the case when the ROS defence mechanism is compromised, it can efflux from the cell to react with the AgNPs (primarily Ag^0) forming ·OH (Fig. 7.11c). In fact, a recent study has shown that AgNPs can form ·OH in the presence of H_2O_2, but only under acidic conditions (He et al., 2012c). Although the proposed Fenton-like pathway (He et al., 2012c) for the AgNP-induced formation of ·OH requires further validation, other corroborative studies shed some insight into the reaction mechanisms (He et al., 2012a; He et al., 2012b). Hence, effective decomposition of H_2O_2 to ·OH in this case is anticipated since the close proximity between the cell and the exposed AgNPs provides the prerequisite acidic conditions. The resultant ·OH can react with the cell membrane causing severe structural distortion resulting in impaired cell functions that culminate in irreversible cell death due to leakage of the cytoplasmic contents (Fig. 7.11c). Evidently, both Ag^+ and AgNPs work together to effect disinfection; ·OH would not have been formed if either Ag^+ or the AgNPs were absent.

7.3 Concluding remarks

The proposed mechanism provides a conceptual framework to better understand the bactericidal action of AgNPs in general and in the specific case of the PSA/AgNP cryogels studied here. The elusive mechanism can be unraveled because the cryogels provide a conducive environment to elicit the intricacies of the bactericidal action mode of AgNPs; they not only provide a large surface-area platform for cell-AgNP interaction in the microchannels, but the rapid swelling of the cryogels also provides the driving force for the bacterial cells to approach the AgNPs. The intimate contact between the AgNPs and the cells within a confined environment ensures their interaction to be biologically significant. This enables the manifestation of triggered-Ag^+ release that reveals the interaction of the protons in the cell-AgNP interface (generated from cell metabolism and to a lesser extent the high surface-charge of the cryogel) with the Ag^0 resulting in efficient uptake of Ag^+ by the contacting bacteria. This new insight can guide future design of environmentally safe Ag-based disinfectants that will exhibit excellent disinfection with very low Ag leaching. Furthermore, the use of cryogels impregnated with either Ag^0 or Ag^+ allows the discovery of their differential bactericidal action whilst minimizing confounding effects due to solution chemistry (e.g., aggregation and complexation) when the AgNPs or Ag^+ are directly dispersed in the exposure medium. As a result, the disparity in the cell injury caused by the Ag^+ alone versus that of the AgNPs (that show the combined effect of Ag^0 and Ag^+) can be clearly distinguished. Most importantly, it was found that both Ag^+ and Ag^0 are involved in the bactericidal mechanism of AgNPs in the cryogels. This may ultimately resolve the long debate over the disinfection mechanism of AgNPs. Although most mechanistic studies reported in this study were on *E. coli*, PSA/AgNP cryogels have been shown to work with both Gram-negative and Gram-positive bacteria. The mechanistic understanding developed herein could be extended to other bacteria although this requires further study.

CHAPTER 8 Impact of solution chemistry on the toxicity and properties of silver nanoparticles decorated on superabsorbent cryogels[†]

The study reported herein aimed to understand the effects of environmental matrix species on the properties of AgNPs decorated on cryogels. Specifically, dissolved organic matter (DOM with Suwannee River humic acid as a surrogate) and various electrolytes commonly found in environmental matrices (i.e., Cl^-, HCO_3^-, SO_4^{2-}, Na^+, K^+, Ca^{2+}, and Mg^{2+}) of varying concentrations under circum-neutral conditions were employed to investigate their impact on the physicochemical properties of the AgNPs and their corresponding bactericidal efficacy.

8.1 Experimental details

The relevant syntheses, characterization, and experimental procedure employed in the study reported here can be found in Chapter 3. Note that the disinfection test reported in this chapter were conducted using an *E. coli* suspension having a cell density of 10^6 cfu/mL. The following describes the preparation of the test solutions used in this study.

In this study the effect of solution chemistry was investigated by using two series of environmentally relevant freshwater matrices. One contained varying concentrations of DOM while the other contained different concentrations of multiple monovalent and divalent inorganic ions. The DOM-containing matrices were prepared by dissolving a well-characterized humic acid, Suwannee River Humic Acid (SRHA) Standard I obtained from International Humic Substances Society, in DI water followed by filtration through a 0.45 µm pore-size Millipore filter. The DOM concentration was varied from 0.5 to 25 mg-C/L (pH value range:

[†] Impact of solution chemistry on the properties and bactericidal activity of silver nanoparticles decorated on superabsorbent cryogels' in *Journal of Colloid and Interface Science* 461, 104-113. Please see Appendix A for reuse permission.

6-7). The total organic carbon (TOC) concentration in the filtered samples was verified using a TOC analyzer (TOC-V_{CSH}, Shimadzu).

The concentration range was selected because DOM concentrations in surface water usually range from 0.1 mg-C/L (for springs and small mountain streams) to 25 mg-C/L (for water originating from moors and wetlands) (Thurman, 1985; Kramer et al., 2004). Hereafter, solutions containing DOM will be referred to as DOM water with their concentration specified, when necessary. Reconstituted water (pH 7-8) solutions containing the major ions present in natural water (i.e., Cl^-, HCO_3^-, SO_4^{2-}, Na^+, K^+, Ca^{2+}, and Mg^{2+}) (Nikanorov and Brazhnikova, 2009) with varying concentrations (and hardness) were prepared according to a method described by USEPA. The nomenclature (based on the solution hardness) and composition of the reconstituted water are given in Table 8.1.

Table 8.1 Composition and characteristics of the reconstituted water

Water sample	Composition (mg/L)				Water-quality characteristics		
	$NaHCO_3$	$CaSO_4.2H2O$	$MgSO_4$	KCl	pH	Hardness[a]	Alkalinity[a]
Very Soft	12	7.5	7.5	0.5	6.4-6.8	10-13	10-13
Soft	48	30	30	2	7.2-7.6	40-48	30-35
Moderately Hard	96	60	60	4	7.4-7.8	80-100	57-64
Hard	192	120	120	8	7.6-8.0	160-180	110-120
Very hard	384	240	240	16	8.0-8.4	280-320	225-245

Note: [a] As mg-$CaCO_3$/L

8.2 Results and discussion

8.2.1 Effect on the physicochemical properties of immobilized AgNPs

To assess the impact of different solution chemistries on the particle morphology, powdered samples of the PSA/AgNP cryogels were dispersed in the test solutions for a prolonged duration before they were subjected to XPS and XRD analyses, and TEM imaging. While the XRD spectra of the exposed samples showed a negligible difference (Fig. 8.1), XPS analyses revealed that most exposed samples contained a

significantly higher amount of oxidized Ag species (Fig. 8.2). Note that the presence of Ag_2O in the exposed samples is indicated by the presence of a peak at 367.5 eV while the predominance of Ag^0 is also indicated by the intense peak centered at 368.2 eV (Hoflund et al., 2000; Morales et al., 2004; Prieto et al., 2012). Fresh PSA/AgNP cryogels contained 1.4% of Ag_2O that increased to 4.0% and 5.3% upon exposure to DI water and DOM water (25 mg-C/L), respectively (Fig. 8.2). In the presence of the electrolytes, however, the amount of the Ag_2O layer was only 1.1% (Fig. 8.2). The significant enhancement in surface oxidation of the AgNPs in the presence of DOM, which was even higher than that in DI water despite their low redox potential, may be ascribed to the photoreactivity of the SRHA that can generate reactive intermediates and reactive oxygen species (ROS) such as H_2O_2, $\bullet O_2^-$, •OH and $^1O_2$ among others (Cooper and Zika, 1983; Cooper et al., 1988; Mopper and Zhou, 1990; Sandvik et al., 2000; Scully et al., 2003; Latch and McNeill, 2006; Aiken et al., 2011).

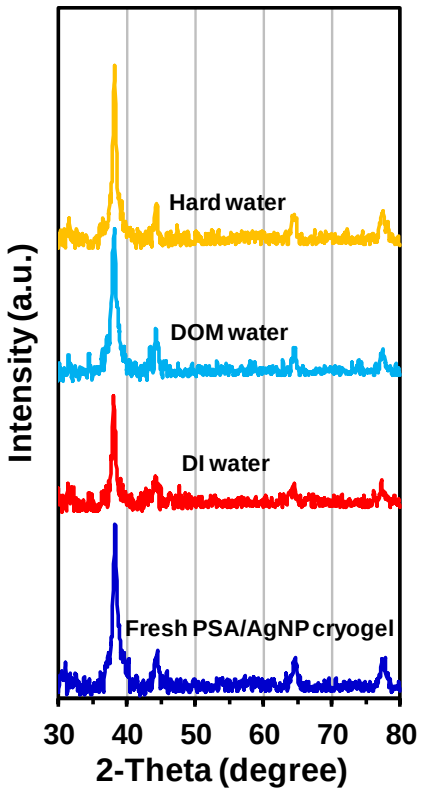

Figure 8.1 XRD spectra of powdered samples of PSA/AgNP cryogels before and after exposure to DI water, DOM water (25 mg-C/L), and hard water.

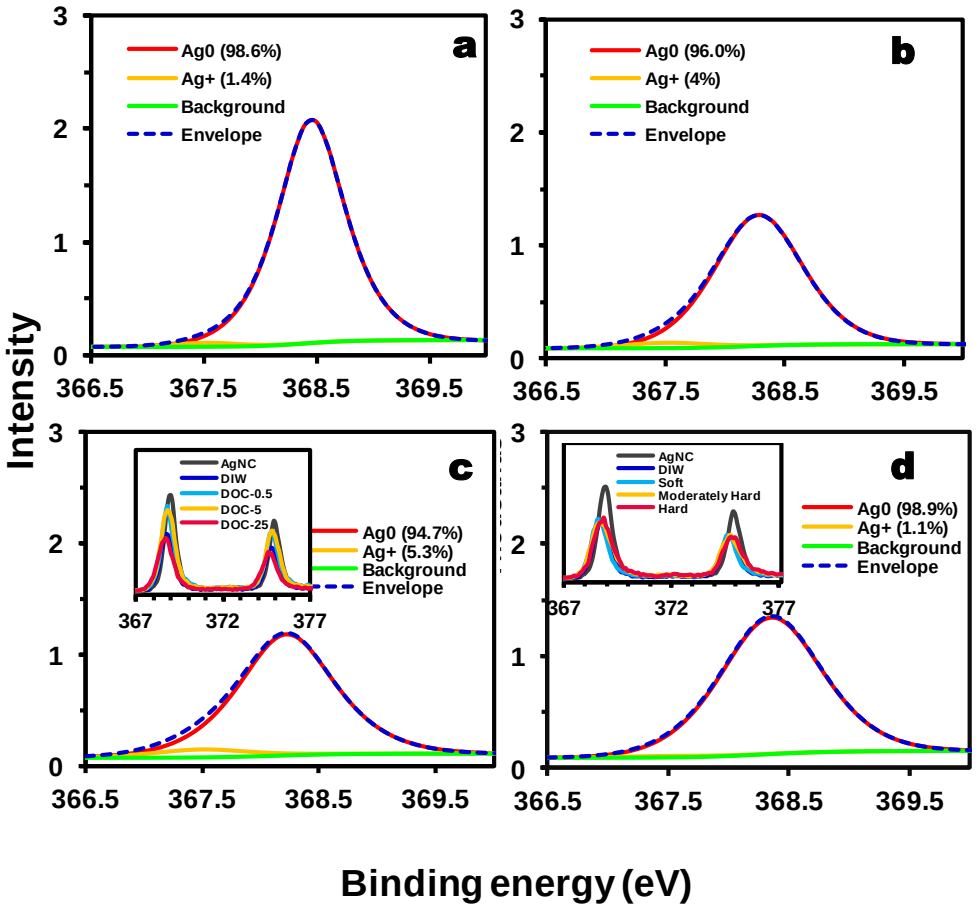

Figure 8.2 XPS spectra of the PSA/AgNP cryogel (a) before and after exposure to (b) DI water, (c) DOM water, and (d) EPA water. Note that the insets in (c) and (d) provide a comparison of the XPS spectra of the control and cryogel samples exposed to varying concentrations of (c) DOM or (d) electrolytes.

Besides changes in their chemical states, the AgNPs in exposed samples also displayed morphological transformations (Fig. 8.3). In the fresh PSA/AgNP cryogel samples, the AgNPs were well-dispersed in the PSA matrix with a relatively uniform particle-size diameter ranging from 5-15 nm with a few AgNP clusters with a diameter of 20-30 nm (Fig. 8.3a); the mean AgNP diameter for this sample was 8.6±3.8 nm. However, prolonged exposure of the PSA/AgNP cryogels to various types of solutions resulted in the coarsening and broadening of the AgNP-size distribution (Fig. 8.4). For example, the mean AgNP diameters for samples exposed to DI water, DOM water, and hard water were 30.5±24.5, 21.7±15.3, and 89.9±28.9 nm, respectively. The increase in the AgNP particle diameter of the exposed samples is not necessarily due to aggregation of the existing particles *per se* owing

to their strong anchoring on the PSA matrix. The broad size distribution in the exposed samples indicates that the AgNP-size increase might be attributed to particle growth due to Ostwald ripening where small AgNPs dissolve followed by re-deposition of the newly formed AgNPs on the large particles in order to minimize the surface energy (Peretyazhko et al., 2014).

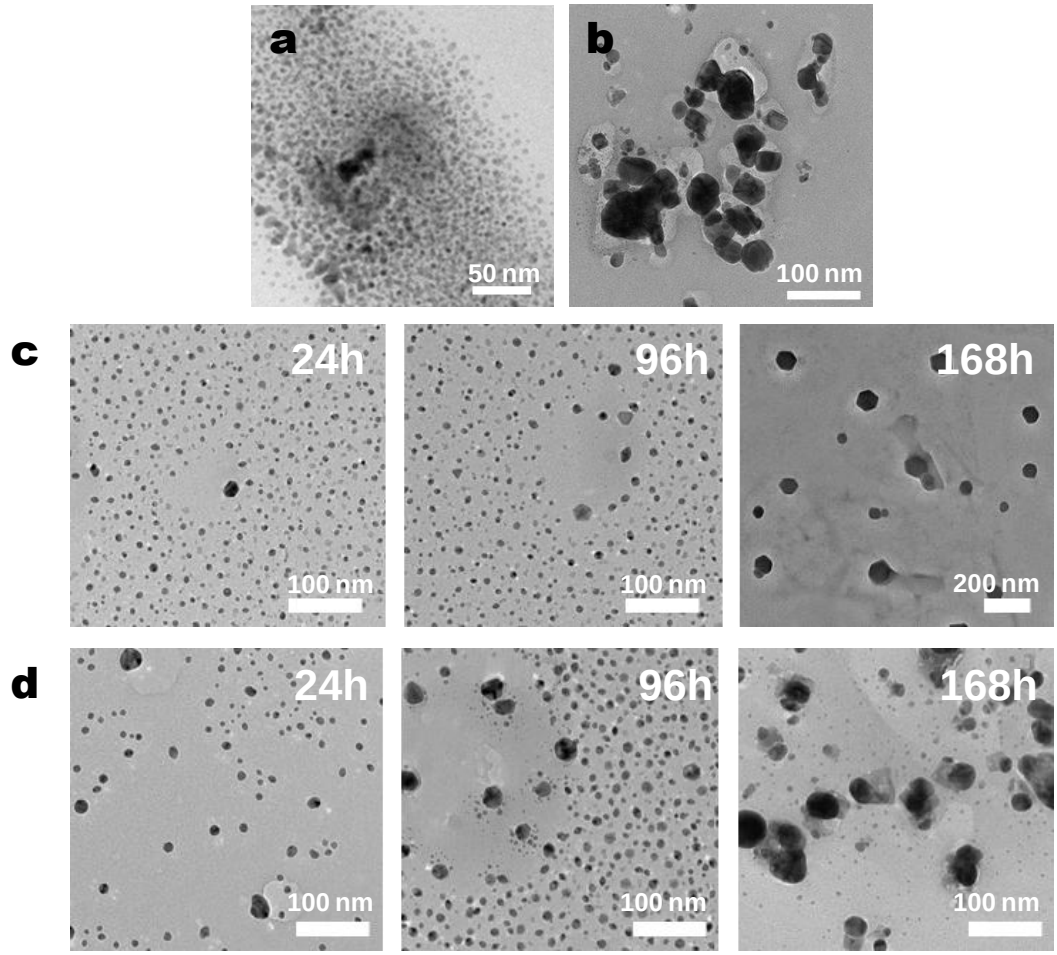

Figure 8.3 Representative TEM images of PSA/Ag cryogels before exposure (a) and after prolonged exposure to deionized water for 168h (b), hard water (c), and 25 mg-C/L of DOM (d).

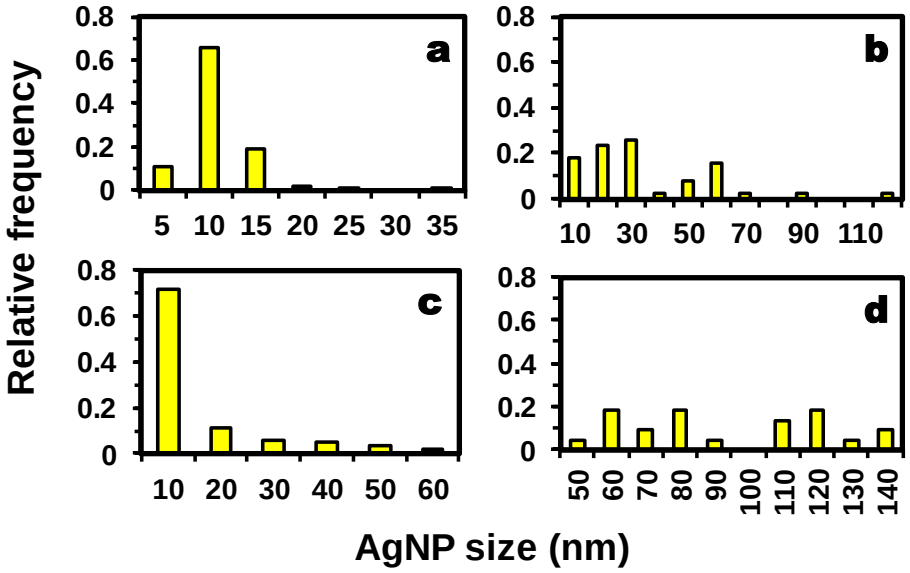

Figure 8.4 AgNP-size distribution of PSA/AgNP cryogels (a) before and after exposure to (b) DI water, (c) DOM water (25 mg-C/L), and (d) hard water for 168h.

Despite the increase in the AgNP size, exposure to DOM water and DI water did not significantly change the shape of the particles (Fig. 8.3b and d); they retained a somewhat quasi-spherical shape (sphericity factor >0.88). However, the AgNPs in the sample exposed to the hard water showed a significant change in the AgNP shape such that most of them had truncated edges forming quasi-hexagonal structures (Fig. 8.3c). The hexagonally shaped particles are probably not due to precipitation of AgCl since there was no evidence of AgCl formation seen in either the XRD spectrum or the XPS survey scan (Figs. 8.1 and 8.2). Other researchers have also observed such changes to spherical AgNPs in the presence of anionic ligands (e.g., chloride, sulfate, and nitrate) (Jin et al., 2001; Wiley et al., 2004; Yang et al., 2007; Tejamaya et al., 2012). It has been proposed that such a shape transformation is due to the selective removal of twinned particles, which are thought to have a much higher solubility than that of single crystal particles due to the presence of defects, through a chloride-mediated oxidative etching process (Wiley et al., 2004). The role of Cl^- in the proposed mechanism is unclear, but it is possible that sorption of anionic ligands on the surface of a nanoparticle could enhance its sensitivity towards oxidation (Henglein, 1993; Wiley et al., 2007). This

hypothesis is also supported by the fact that the TEM image shows the absence of any twinned particles in the sample (Fig. 8.3c).

Interestingly, a comparison between samples exposed to DOM water (Fig. 8.3d) with those exposed to DI water (Fig. 8.3b) indicates that a large number of fine particles (mostly smaller than 10 nm) surrounding the larger clusters can be observed in the former. It can be argued that the fine AgNPs may well be the original AgNPs; however, this is unlikely because small AgNPs would have been preferentially oxidized especially in the presence of DOM, which was found to increase the extent of oxidation of the AgNP surface as indicated by the XPS analysis (Fig. 8.1c). The smaller particles surrounding the large clusters may be the new particles formed from reduction of the dissolved Ag^{+}. It should be noted that, although SRHAs enhances oxidation of AgNPs due to photogeneration of ROS, the presence of functional groups such as phenolic –OH, quinones, hydroxyls, methoxyls, aldehydes, ketones, and enolic –OH on SRHAs can also create an ideal reductive compartment for Ag^{+} reduction to Ag^{0} (Stevenson, 1994). In fact, there is growing evidence that DOM in general can form AgNPs from Ag^{+}, a process that can be accelerated in the presence of sunlight (Akaighe et al., 2011; Yin et al., 2012; Hou et al., 2013). Because DOM can increase particle stability via electrosteric effects, the presence of DOM could have enhanced the mobility of the as-formed particles that decreases their propensity to deposit on the existing particles. The resultant particles may be transported over substantial distances before they are deposited on the surface of the cryogel. The lower deposition tendency of the reformed particles that retarded the AgNP growth might also explain the smaller mean AgNP size for samples exposed to DOM water (Fig. 8.3c) relative to those exposed to DI water (Fig. 8.3b) and hard water (Fig. 8.3d).

8.2.2 Effect on the Ag-release behavior and subsequent cell-uptake

Fig. 8.5 shows the effect of the solution chemistry on the Ag leaching and partitioning behavior.

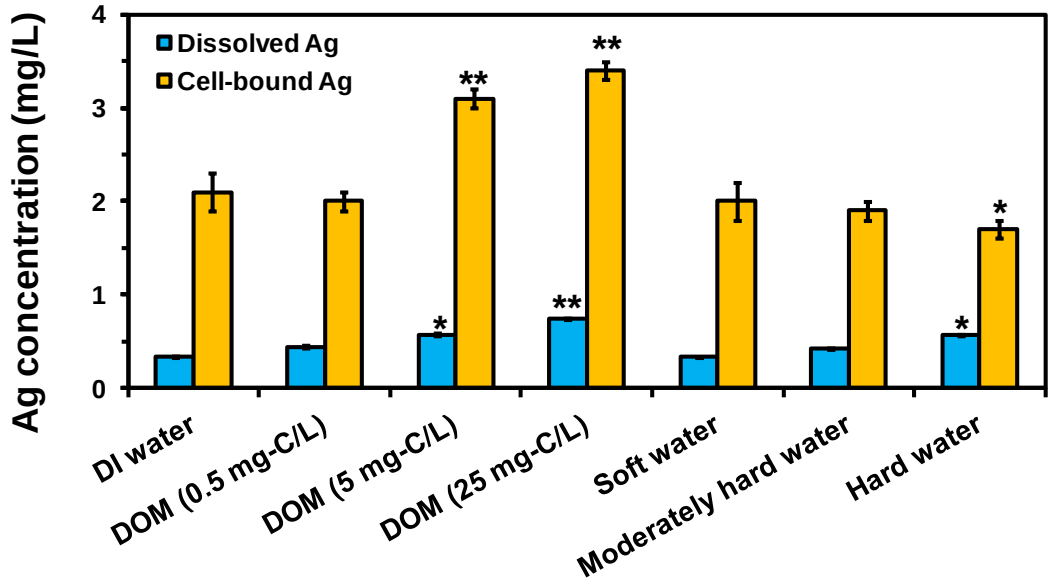

Figure 8.5 Impact of solution chemistry on the Ag release and uptake by cell. Note: Statistically significant results compared to the control (i.e., samples exposed to DI water) at 95% and 99% confidence level are denoted by (*) and (**), respectively (Student's *t* test, n = 3).

The presence of DOM and electrolytes generally increased the release of Ag from the PSA/AgNP cryogels into the dissolved phase. Nonetheless, the total Ag loss remained less than 0.2% for all types of solution chemistry (Fig. 8.5). Despite the increase in dissolved Ag with solution hardness, the concentration of cell-bound Ag apparently showed the opposite trend (Fig. 8.5). The increase of dissolved Ag may be attributed to either (i) formation of dissolved Ag complexes with anions in the reconstituted water or (ii) sequestration of surface chemisorbed Ag^+ by the anions that can cause instability to the NP structure and induce further dissolution (Li et al., 2010; Huynh and Chen, 2011; Adegboyega et al., 2012). The reduced uptake of dissolved Ag might be explained by the lower bioavailability of the Ag complexes with the ionorganic anions (Gupta et al., 1998; Behra et al., 2013). Notably, as discussed in Chapter 7, cell-bound Ag is thought to result from the uptake of dissolved Ag species rather than direct internalization of the AgNPs because passive diffusion across bacterial membranes is limited to solutes smaller than 600 Da and the majority of the Ag species released from the cryogels is dissolved Ag^+. Besides the lower bioavailability of the resultant Ag complexes with the inorganic anions, the reduction in cell-bound Ag could be also attributed to competitive

sorption of cations (Ag^+ versus Mg^{2+} and Ca^{2+}) onto bacterial binding sites (Anderson et al., 2014).

Increasing the DOM content in the solution was found to increase the concentration of cell-bound Ag as well as the amount of dissolved Ag. Enhanced Ag dissolution in the presence of DOM was previously reported in some studies (Chappell et al., 2011; Ivask et al., 2013; Pokhrel et al., 2013; 2014). In contrast, other studies reported reduced Ag dissolution attributable to surface passivation by the DOM layer (Gao et al., 2009; Ostermeyer et al., 2013). Enhanced Ag dissolution in the presence of DOM has usually been ascribed to ligand-assisted Ag dissolution. It is also possible that the ROS generated by SRHA via photochemical reactions cause further oxidative dissolution of the AgNPs. This would enhance Ag dissolution at the cell-AgNP interface that would increase the Ag concentration gradient and induces back-diffusion into the bulk solution or for direct cell-uptake. It has been determined that the interaction between SRHA and Ag^+ is weak (Chen et al., 2013). This suggests that the resultant Ag-SRHA complexes should be sufficiently labile for bacterial uptake. Moreover, it has been found that the toxicity of Ag^+ in the presence of SRHA was not significantly reduced (Fabrega et al., 2009; Kennedy et al., 2012). Even if the SRHA is initially biologically refractory, it may also be subsequently degraded into smaller molecules via the action of reactive oxygen species (ROS) or photolysis, thereby forming labile Ag-SRHA complexes that are more bio-available, especially in systems with high DOM levels (Mopper et al., 1991; Scully et al., 2003; Anesio et al., 2005).

8.2.3 Effect on the acute toxicity of immobilized AgNPs

AgNPs disinfect by disrupting multiple bacterial cellular processes via the release of Ag^+ and particle-specific reactions. For example, uptake of Ag^+ ions can disrupt the bacterial respiratory chain that causes indirect generation of (intracellular) ROS (Liau et al., 1997; Messner and Imlay, 1999; Holt and Bard, 2005; Jung et al., 2008) and cell damage as well as metabolic perturbation because of ATP loss (Holt and Bard, 2005; Park et al., 2009). On the other hand, AgNPs can damage cell

membranes via physical interactions (Sondi and Salopek-Sondi, 2004; Morones et al., 2005) or particle surface reactions that generate ROS (Su et al., 2009). In view of the multifaceted bactericidal action of AgNPs, the impact of solution chemistry on the toxicity was systematically investigated by assessing the extent of cell topological destruction, metabolic perturbation through ATP depletion, and ROS-mediated damage as well as alterations in the disinfection efficacies to measure different biological outcomes.

FESEM images of the *E. coli* before and after exposure to test solutions of different chemistries can provide a qualitative assessment of the extent of cell damage (Fig. 8.6). The images revealed that *E. coli* exposed to PSA/AgNP cryogels under different solution chemistries sustained severe cell-membrane lesions to varying extents (Fig. 8.6). This suggests that the changes in the solution chemistry did not completely diminish the acute bactericidal effects of the cryogels.

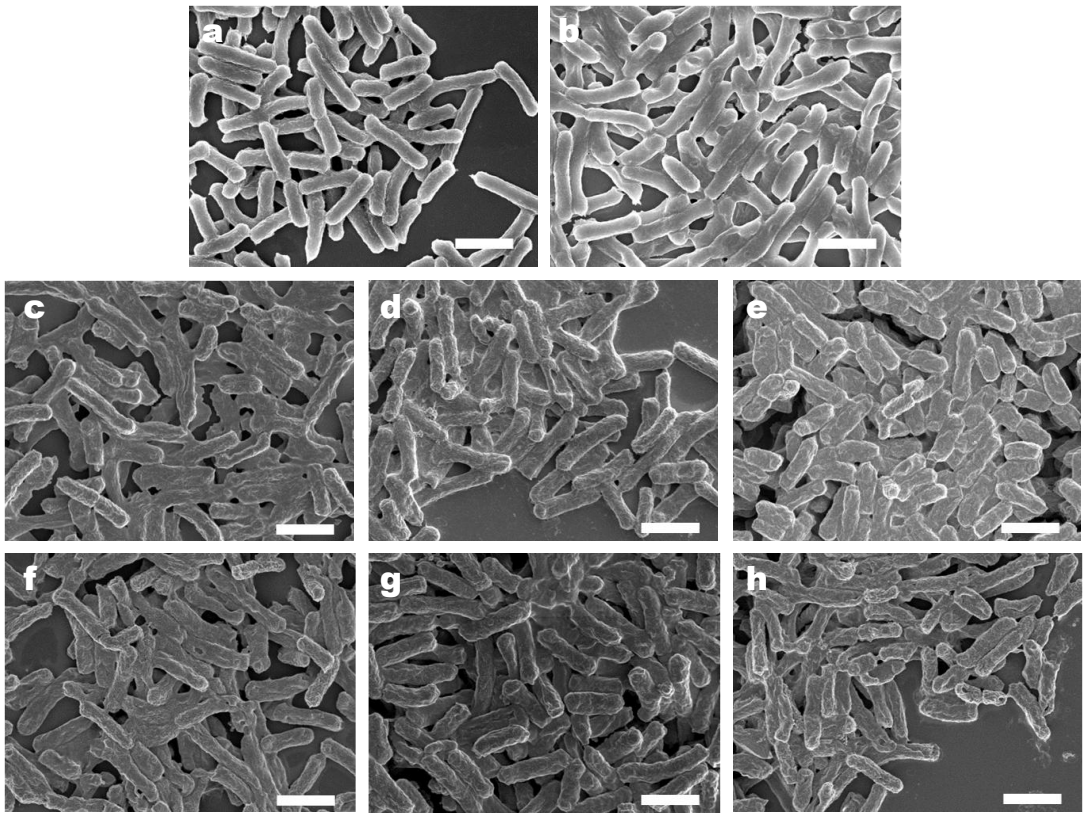

Figure 8.6 FESEM images of *E. coli* (a) before and after exposure to PSA/AgNP cryogels in (b) DI water, (c) 0.5 mg-C/L DOM, (d) 5 mg-C/L DOM, (e) 25 mg-C/L DOM, (f) soft water, (g) moderately hard water, and (h) hard water. Note: all the scale bars represent 2 μm.

In fact, the presence of electrolytes (in the concentration range studied) did not cause a significant reduction in toxicity ($p>0.05$) (Fig. 8.7a). This is in contrast to free AgNPs that usually showed a reduction in their toxicity in the presence of elevated electrolyte concentration (and hence increased ionic strength) that induced particle aggregation (Jin et al., 2010; Zhang and Oyanedel-Craver, 2012; Liu et al., 2014). The strong anchoring of the AgNPs on the PSA cryogel (Fig. 7.3) prevented such aggregation behavior. Although there is no observable effect on the toxicity, the extent of intracellular ATP depletion seems to decrease slightly with increasing concentration of ions (Fig. 8.7b). The observation that the disinfection efficacy is maintained in spite of a reduction in the ATP depletion indicates that there are other toxicity routes besides metabolic perturbation.

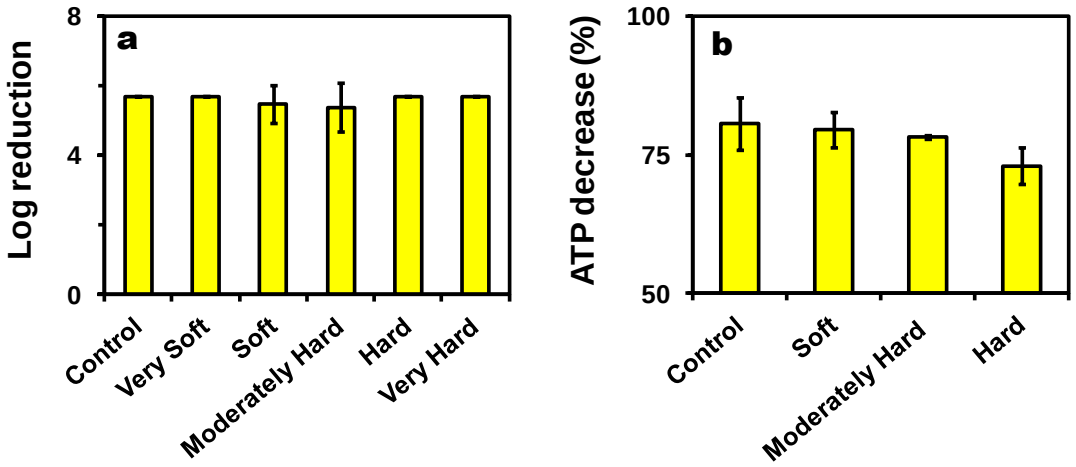

Figure 8.7 Effect of electrolytes on (a) bactericidal efficacy of PSA/AgNP cryogels and (b) extent of ATP depletion in exposed cells.

On the other hand, the DOM had a significant impact on the acute toxicity of the AgNPs with respect to their bactericidal action. Although the initial increase of DOM to 2.5 mg-C/L mitigated the toxicity of the AgNPs, a further increase in the DOM concentration beyond 5 mg-C/L led to a toxicity enhancement (Fig. 8.8a). A FESEM image of the bacterial cells exposed to a high DOM concentration (25 mg-C/L) shows more severe damage. The observations that the cells appear more shriveled and apparently developed larger holes corroborate the toxicity results (Figs. 8.6b-d and 8.8a). This is rather surprising because several prior studies found

that DOM attenuated the toxicity of AgNPs towards bacteria (Fabrega et al., 2009; Liu and Hurt, 2010; Zhang et al., 2012; Pokhrel et al., 2014). Note that the aforementioned studies conducted their toxicity tests using free AgNP suspensions. In contrast, the enhanced toxicity of immobilized AgNPs in the presence of DOM has also been observed by others (Dankovich, 2012; Diagne et al., 2012). These conflicting observations suggest that free and immobilized AgNPs may interact differently with DOM. For the toxicity attenuation, it has been suggested that DOM may act as a physical barrier to cell-AgNP interactions (due to charge repulsion) by decreasing the binding of AgNPs to proteins, membrane pitting or decreasing the dissolution of Ag (Fabrega et al., 2009). However, in the present study, the presence of DOM enhanced the Ag dissolution and subsequent cell uptake of Ag leading to the enhanced depletion of the intracellular ATP level (Figs. 8.6 and 8.8b). Although the increased toxicity of AgNPs in the presence of DOM concentrations beyond 5 mg-C/L may be ascribed to the reduction of intracellular ATP levels, the initial reduction of toxicity at low DOM concentrations and the drastic enhancement in toxicity at high DOM concentrations cannot be solely explained by the depletion of intracellular ATP.

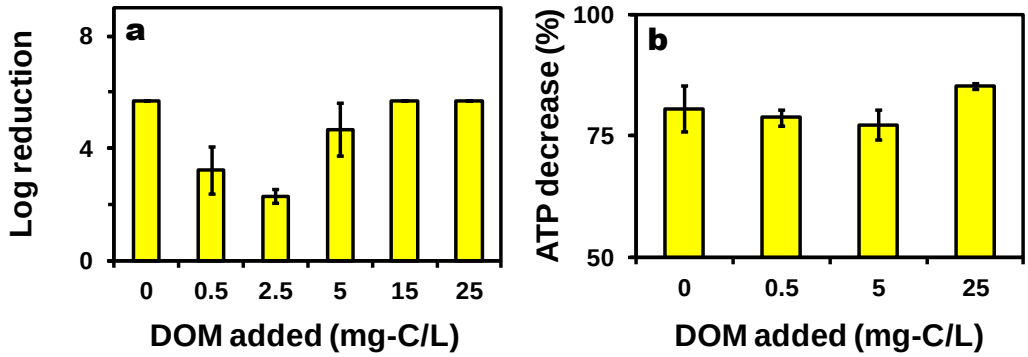

Figure 8.8 Effect of DOM on (a) bactericidal efficacy of PSA/AgNP cryogels, (b) extent of ATP depletion in exposed cells.

In Chapter 7 it was found that the formation of ROS plays a critical role in the bactericidal action of AgNPs that can subsequently initiate an autocidal process. In view of the severity of the cell-membrane damage (at 25 mg-C/L) and the ability of DOM to form and consume radicals, ROS might have a role in modulating the toxicity. To test this hypothesis, the enhancement of intracellular ROS levels of

exposed bacterial cells relative to unexposed samples was determined. The experiment was conducted under illuminated (with ambient lighting) and non-illuminated conditions to discern the ROS formed as a result of the photoreactivity of the DOM. The data obtained under both non-illuminated and illuminated conditions showed that in the presence of DOM, the cells generally have a lower intracellular ROS other than at a DOM concentration of 25 mg-C/L (Fig. 8.9). The initial reduction (for both illuminated and non-illuminated conditions) may be due to scavenging of ROS (and its intermediates) by DOM. The slightly higher intracellular ROS level at 25 mg-C/L, in the absence of illumination, might be due enhanced indirect ROS generation as a consequence of increased cell-bound Ag. Interestingly, the results obtained under illumination conditions show a trend that is broadly consistent with the acute toxicity data (Figs. 8.8a and 8.9). Notably, significant enhancement in the intracellular ROS level was observed at 25 mg-C/L.

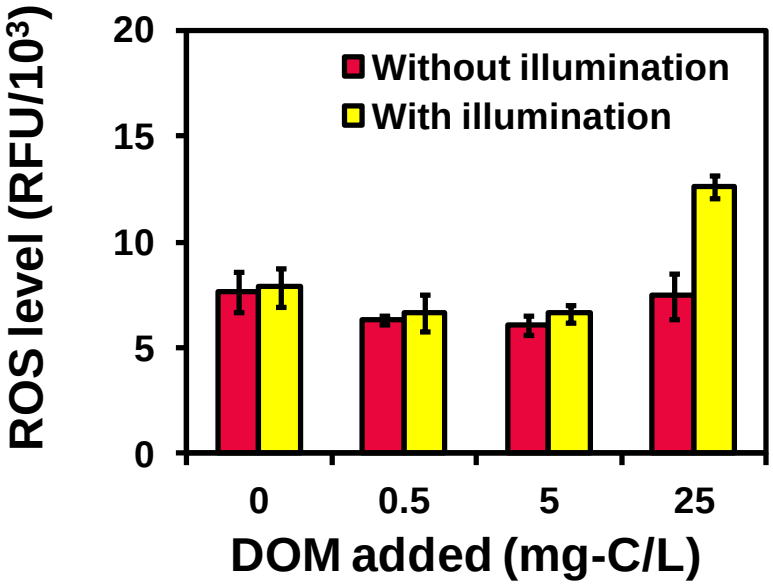

Figure 8.9 Effect of DOM on intracellular ROS level in exposed cells.

At a high DOM concentration level, the increased photochemical production of ROS may overcome ROS scavenging effect on toxicity reduction. As mentioned earlier, photodecomposition of DOM produces several types of ROS, which are mostly short-lived with the exception of H_2O_2 whose half-life in water ranges from

1 to 8 h (Cooper and Zepp, 1990). In this case the lifetime of the ROS is important because they exist as diffusing species in the bulk solution whereby the majority of them are not in immediate vicinity of the bacterial cells. Because H_2O_2 is more stable, it may diffuse to the AgNP surface as the concentration of (extracellularly) generated H_2O_2 accumulates in the bulk solution. H_2O_2 by itself is not very effective against microbes, but it has been shown to possess bactericidal properties, especially in the presence of a transition metal that could generate toxic •OH radicals (Juven and Pierson, 1996). Furthermore, there is growing evidence that AgNP can induce the decomposition of of H_2O_2, especially under acidic conditions (He et al., 2012a; 2012b; 2012c; He et al., 2014):

$$Ag^0 + H_2O_2 + H^+ \rightarrow Ag^+ + \cdot OH + H_2O \quad (1)$$

This hypothesis is consistent with the toxicity data shown in Fig. 8.8a that show no significant inactivation of bacteria in the presence of DOM (and illumination) without the AgNPs. Furthermore, Fig. 8.10 shows that the addition of H_2O_2 (up to 10 mM) without exposing the bacteria to PSA/AgNP cryogel did not result in any significant bacterial inactivation ($p>0.05$; *t*-test; n=6). Labas et al. (2008) found that H_2O_2 showed little disinfection effect when exposed to *E. coli* at 100 ppm (about 3 mM) even when a long reaction time was used.

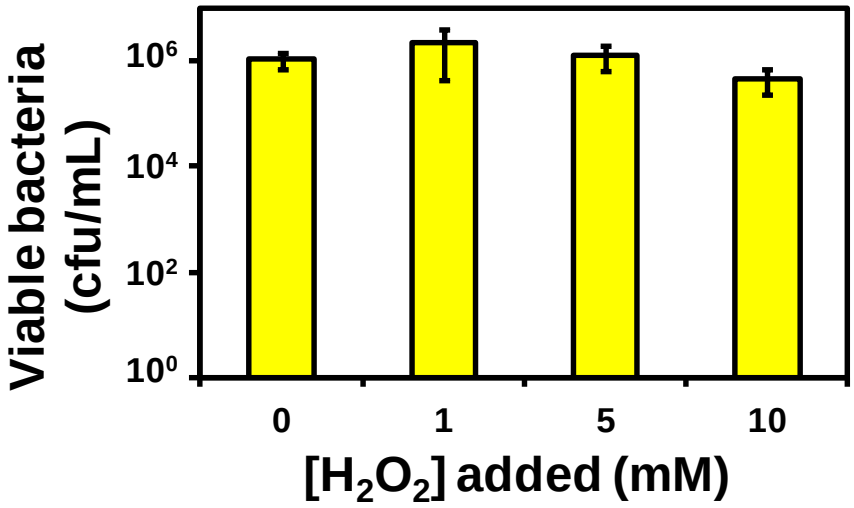

Figure 8.10 The effect of H_2O_2 addition to cell viability in DOM water (25 mg-C/L).

A narrow region outside the bacterial cell wall that is acidified due to proton extrusion under the influence of a proton motive force can provide the requisite acidic condition (Koch, 1986; Xiu et al., 2012). Therefore, it is postulated that the decomposition of H_2O_2 most likely occurs at the cell-AgNP interface. Because the immobilized AgNPs allow enhanced contact with bacterial cells (Mukherji et al., 2013), it leads to a more efficient generation of •OH radicals that in turn has a more significant biological effect due to the proximity of the cells to the as-formed short-lived radical. This might explain the discrepancy of the influence of the DOM on the toxicity of AgNPs observed in free suspension versus immobilized on support materials.

8.3 Concluding remarks

Fig. 8.10 summarizes all the major processes that occur in exposure media containing either electrolytes or DOM based on the findings of this study. This study found that the presence of an additional component in solution can present a highly complex chemistry with the occurrence of many competing processes that might enhance or decrease the toxicity of AgNPs. For example, the presence of DOM alone can present a complicated situation where it can have conflicting effects due to its ability to quench and generate ROS at the same time. Therefore, this study underscores the importance of solution chemistry in assessing the bactericidal efficacy of Ag-based antimicrobial agents. Furthermore, this study found that immobilization of the AgNPs can overcome some physical changes such as aggregation when they are exposed to different environmental media. This significantly ameliorates the effect of the solution chemistry on their bactericidal efficacy. As such, immobilizing the AgNPs can be a good strategy to preserve their efficacy for disinfection in various solution matrices. More importantly, the findings from this study implicate that the current understanding drawn from studies using free AgNPs may not be applicable to immobilized AgNPs.

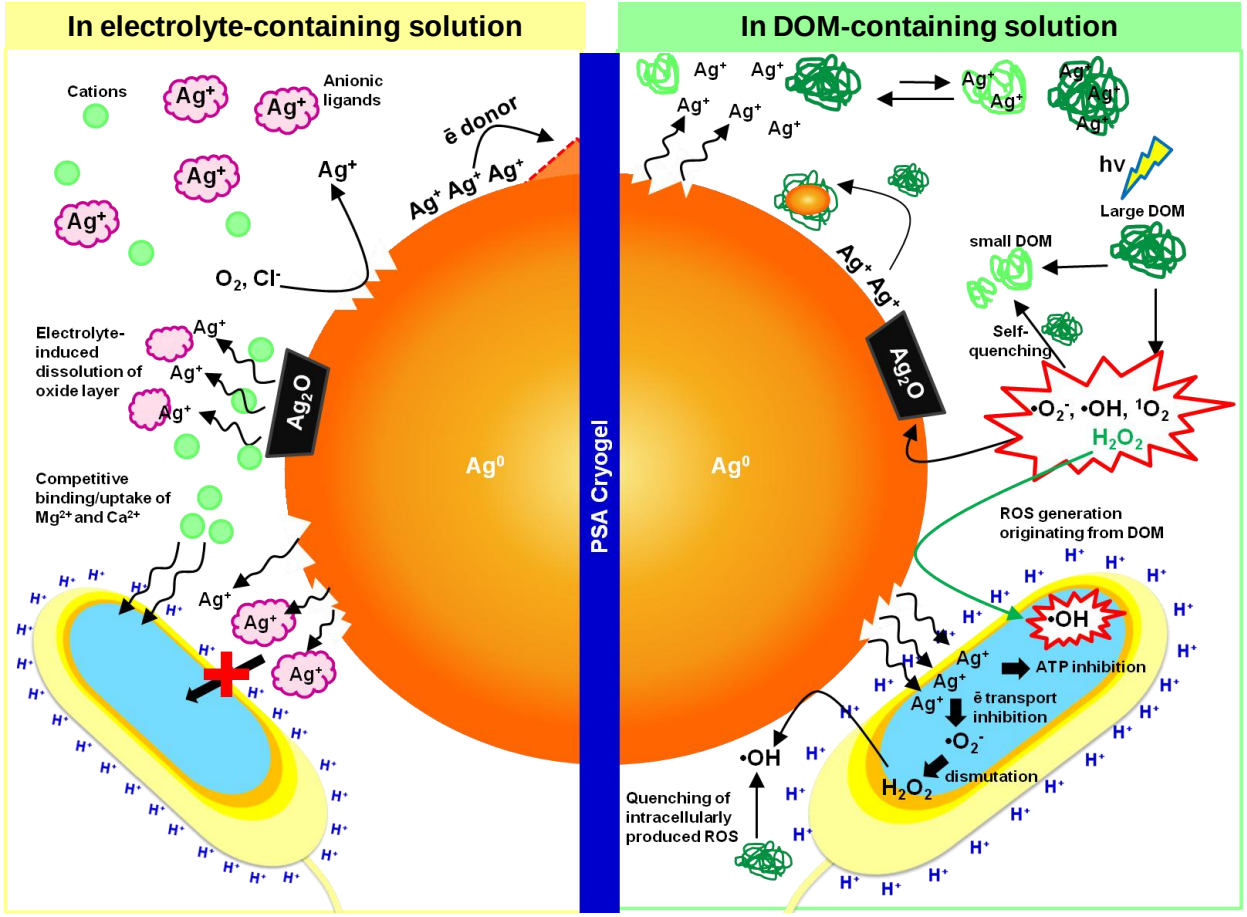

Figure 8.11 Illustration summarizing the important processes that occur in exposure solutions due to the presence of electrolytes (left panel) and DOM (right panel).

CHAPTER 9 Conclusions and recommendations

This chapter provides a summary of the conclusions drawn from this research followed by a brief overview of possible future research directions with immediate relevance. These suggestions may serve as technical springboard to facilitate further development and commercialization of the cryogels prepared in this research.

9.1 Overall conclusions

Contaminated water is a major problem in many parts of the world especially in the aftermath of natural disasters in which case power outages, and limited resources and abilities pose significant challenges. Current emergency water technologies are limited by their low efficiency, inadequate ease of deployment, and their high energy requirement. This thesis presents an in-depth investigation on the feasibility of using cryogels for emergency water treatment. The major findings and conclusions from this research are summarized as follows:

- Controlling the T_{prep} in the cryogel preparation protocol is instrumental in achieving the desired pore morphology since pore formation results from ice crystallization. However, it is also important to control the initial monomer and initiator concentrations in order to tune the polymerization rate such that ice crystallization occurs prior to gelation. The crosslinker ratio can be varied to tune the swelling degree of the PSA cryogels although it did not have a substantive effect on the morphology.
- PSA cryogels with open interconnected pores and high porosity are desired for water-treatment applications because they had a higher rate and degree of swelling, and could withstand large deformation. In addition, the pore size of the PSA cryogels should be sufficiently small in order to achieve satisfactory separation and mechanical properties, although there could be a compromise in the swelling rate.

- PSA cryogels can be used as integral membranes for turbidity removal whereby a relatively high water recovery and particulate removal efficiency were achieved. In addition, the turbidity removal efficiency was found to increase with operating cycles due to pore-size reduction as the particulates in the raw water become deposited in the cryogel pores.
- AgNP-incorporated cryogels prepared using three different synthesis approaches resulted in distinctly different spatial distributions of the AgNPs; i.e., only on the pore surface or embedded throughout the polymer matrix or a mixture of both. Furthermore, the AgNP-incorporated cryogels prepared via different methods have varying AgNP size, pore morphology, swelling and mechanical behavior. The three types of cryogel nanocomposites were found to be effective in disinfecting the *E. coli* to different extents. Specifically, synthesis routes that formed more AgNPs on the exterior surface of the cryogels displayed enhanced bactericidal efficacy.
- The PSA/AgNP cryogels (prepared via the intermatrix synthesis method) displayed excellent disinfection efficacies showing over a 5-log reduction of viable bacteria. In addition, the cryogels were also effective in disinfecting the natural water samples for which more than 2 logs reduction could be achieved. They were highly reusable as there was no significant difference in the disinfection efficacies over five cycles of operation and they can be repeated compressed for over 1000 cycles. They show good promise for potable-water disinfection in disaster-relief applications.
- The PSA/AgNP cryogels show rapid disinfection whereby AgNC-170 has been demonstrated to inactivate close to 3 logs of bacteria during the 15-s contact time. Increasing the contact time to 5 min allows irreversible inactivation of close to 6 logs of bacteria.
- Direct contact between the PSA/AgNP cryogel interface and the bacterial cells is required to effect disinfection. Specifically, the disinfection efficacy is closely correlated to the cell-bound Ag concentration, which constitutes >90% of the Ag released. Cells exposed to PSA/AgNP cryogels show a significant depletion of intracellular adenosine triphosphate (ATP) content and cell-membrane lesions. A positive ROS scavenging test and

enhanced level of TBARS in the exposed cells implicate the occurrence of cell-membrane peroxidation mediated by ROS.

- Both Ag^{+} and Ag^{0} are involved in the bactericidal mechanism of AgNPs, but each has a different mode of action.
- Significantly, bacterial cells exposed to PSA/Ag^{+} cryogels did not show any cell-membrane damage even though the former had a higher cell-bound Ag concentration than that of the PSA/AgNP cryogels, thus indicating the differential action of Ag^{+} and Ag^{0}.
- PSA/AgNP cryogels exposed to solutions of various chemistries show changes in the amount of oxidized Ag species and display some physical transformations in the AgNP morphology. The AgNPs in exposed samples generally have larger mean diameters. In particular, samples exposed to a DOM-containing solution show the formation of fine AgNPs surrounding larger clusters, while those exposed to electrolytes transformed into truncated and hexagonally shaped particles.
- The presence of DOM and electrolytes generally increased the Ag leaching. However, the biological uptake of Ag species is increased in the presence of DOM, but decreased in the presence of electrolytes.
- Apparently, the toxicity of the AgNPs anchored on the cryogels is less sensitive to changes in solution chemistry. The presence of electrolytes did not result in any significant reduction in the bactericidal activity. Although the initial increase of DOM to 2.5 mg-C/L mitigated the toxicity of the AgNPs, a further increase in the DOM concentration beyond 5 mg-C/L led to toxicity enhancement.

9.2. Recommendations for future research

Building on the findings presented in this thesis, the following three research areas are of recommended to facilitate further development and commercialization of the cryogels prepared in this project:

9.2.1 Optimization of materials syntheses

As a proof-of-concept study, the cryogels prepared in this study were in the form of small cylindrical disks (i.e., 5×5 mm). Larger sized cryogels — about 4 g that may be in the form a cylinder 1.5 cm in diameter and 9 cm long that would be capable of purifying a half liter of water in one operating cycle — need to be synthesized to increase the water production rate of cryogels. Because this would affect the volume of the reaction mixture and heat transfer across the mold in which the cryogels are formed, the freezing and gelation rates would be significantly altered. As discussed in Chapter 4, it is crucial that the cryogelation occurs in the "freezing before gelation" mode to ensure the cryogels have a well-interconnected porous network. As such, a systematic study is required to optimize the synthesis conditions. The development of a cryogel synthesis procedure should also consider scalability of the method in order to mass-produce the cryogels efficiently.

In Chapter 5, cryogels with a higher concentration of surface Ag displayed superior bactericidal efficacy. Therefore, to further improve the bactericidal activity of the PSA/AgNP cryogels (prepared via the IMS method), a reducing agent of higher charge density should be used during the second step whereby the AgNPs are formed on the cryogels via *in situ* reduction. The use of reductants of higher charge density amplifies the Donnan exclusion effect that further restricts their diffusion into the cryogels and thereby limits the formation AgNPs on the outer surface of cryogel pore walls. One such reducing agent that may be explored in future studies is the dithionite ($S_2O_4^{2-}$) ion.

Even though this research has shown that AgNPs can achieve high bactericidal efficacy with minimal Ag release, it is relatively expensive and there is still inevitable loss of Ag with repeated use. Also, as discussed in Section 2.4, antimicrobial resistance to Ag could be an issue in the future. Nonetheless, cryogels provide a versatile platform for modifications with other antimicrobial agents. As such, future research should be directed at exploring alternative inorganic or organic-based disinfectants to either replace or be used in tandem with AgNPs. In particular, non-leaching antimicrobial polymers are advantageous due to their potential low-cost and high stability that minimizes the release of harmful species

into the treated water (Daels et al., 2011; Zhang and Oyanedel-Craver, 2013). There is a vast range of antimicrobial polymers, but they are mostly polycations bearing quarternary ammonium or pyridinium groups (Ferreira and Zumbuehl, 2009). The bactericidal activity of the polycations can be further enhanced by optimizing the balance of charge and hydrophobicity to improve the extent of cell interaction by minimizing electrostatic repulsion and interchain aggregation (Klibanov, 2007).

9.2.2 Long-term performance testing

In this research, the disinfection efficacy of PSA/AgNP cryogels was tested using bacteria as model pathogens. However, in real water samples, there may be a multiplicity of microbes that also could include viruses and protozoa. Fig. 9.1 provides a summary of the waterborne pathogens commonly found in untreated water that can lead to gastrointestinal diseases. Therefore, future studies should assess the ability of the PSA/AgNP cryogels to inactivate viruses and protozoa as well.

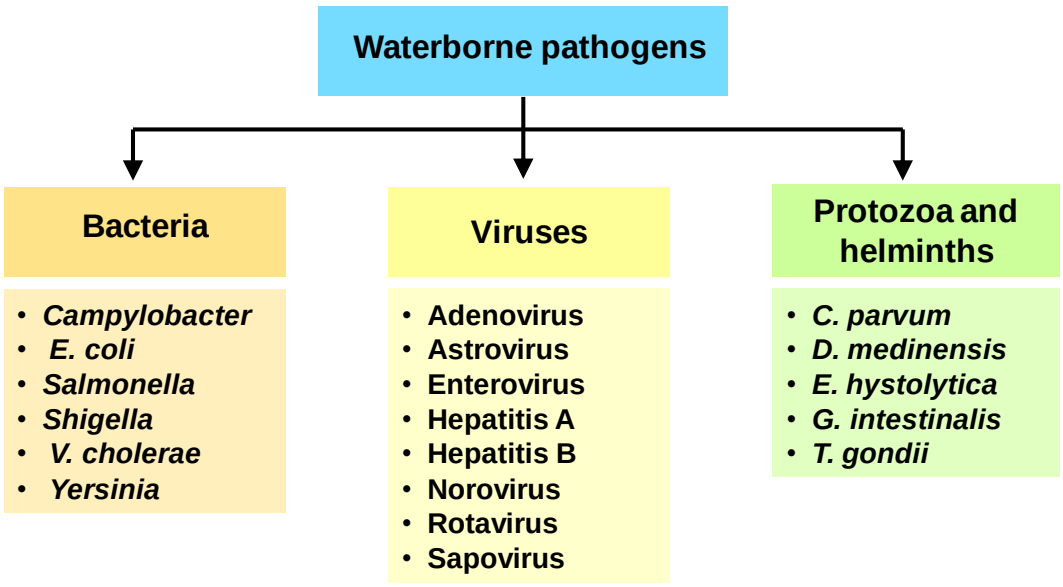

Figure 9.1 Summary of common waterborne pathogens (WHO, 2011).

In Chapter 8, the exposure media used was an idealized solution compared to actual environmental water samples for which a mixture of DOM and electrolytes may be

concurrently present. Therefore, further exploration of the behavior of the PSA/AgNP cryogels in more complex systems is warranted. Besides SRHA, there are other DOM surrogates such as alginate and albumin that have different molecular structures. Therefore, their interaction with the PSA/AgNP cryogels may be substantially different compared to that of SRHA. Thus, comparison of the effects of different types of DOM on the toxicity and properties of PSA/AgNP cryogels merits future study. Furthermore, a detailed investigation on the interplay between Ag and the various types of DOM as redox couple should be conducted. In particular, characterization techniques such as X-ray absorption spectroscopy can be employed to characterize the redox state of the Ag species anchored on the PSA cryogel in greater detail. One important parameter that was not studied in Chapter 8 was the pH effects. This should also be included in future study to better understand the disinfection mechanism as well as to determine the optimal operating conditions.

The PSA/AgNP cryogels have been shown to display stable disinfection efficacy over multiple cycles of use. However, the time frame for the assessment (i.e., in hours rather than weeks or months) is relatively short to gauge the long-term performance of the cryogels. As such, future studies should include toxicity assessment of the PSA/AgNP cryogels over an extended time frame. In addition, comparisons should be made on the impact of storing the PSA/AgNP cryogels in solution or dried form on their long-term bactericidal efficacy.

9.2.3 Design of a portable device incorporating PSA/AgNP cryogels for point-of-use water treatment

For practical applications these cryogels can be incorporated into a portable and simple device that can be used for efficient recovery of treated water. One possible configuration is in the form of a bottle as illustrated in Fig. 9.2. The prototype is basically a bottle casing incorporated with an optimized nanofiber-reinforced cryogel composite membrane as the functional unit (Fig. 9.2). On one end of the bottle casing is the movable piston while the other end of the bottle is the potable water outlet.

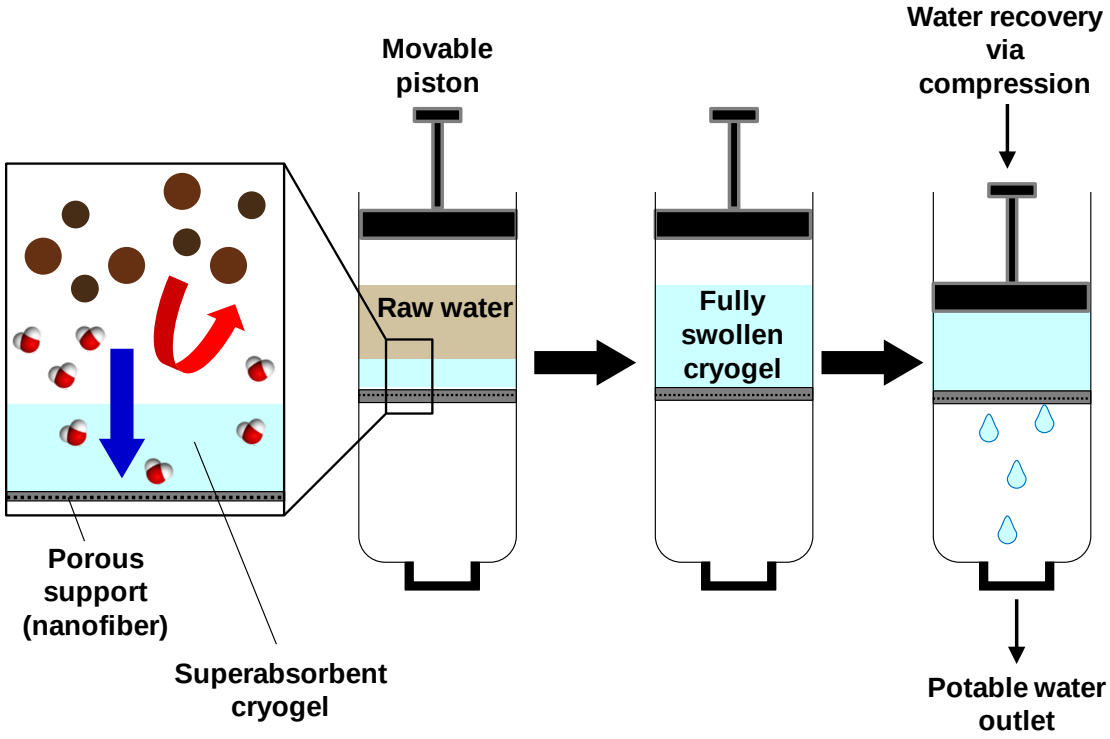

Figure 9.2 Schematic diagram of the cross-section of a possible configuration of the portable device incorporating cryogels.

In this configuration, one side of the cryogel is exposed to raw water while the other side remains unexposed to contaminants in the raw water. Due to the swelling pressure of cryogels, particulate-free water is drawn into the cryogel. AgNPs in the cryogel provide disinfection in case harmful microbes enter the cryogels. After the cryogel has fully swollen, the absorbed water can be subsequently recovered by pushing the piston. The porous support material on the other side of the cryogel provides additional mechanical support during compression. A nanofiber membrane may be a suitable porous support material due to its high porosity (ca. 90%) and ease of fabrication. A preliminary study has shown that a layer of PSA cryogel can be formed on a nanofiber membrane (Fig. 9.2). Nonetheless, the adherence of the cryogel layer on the nanofiber can be further improved.

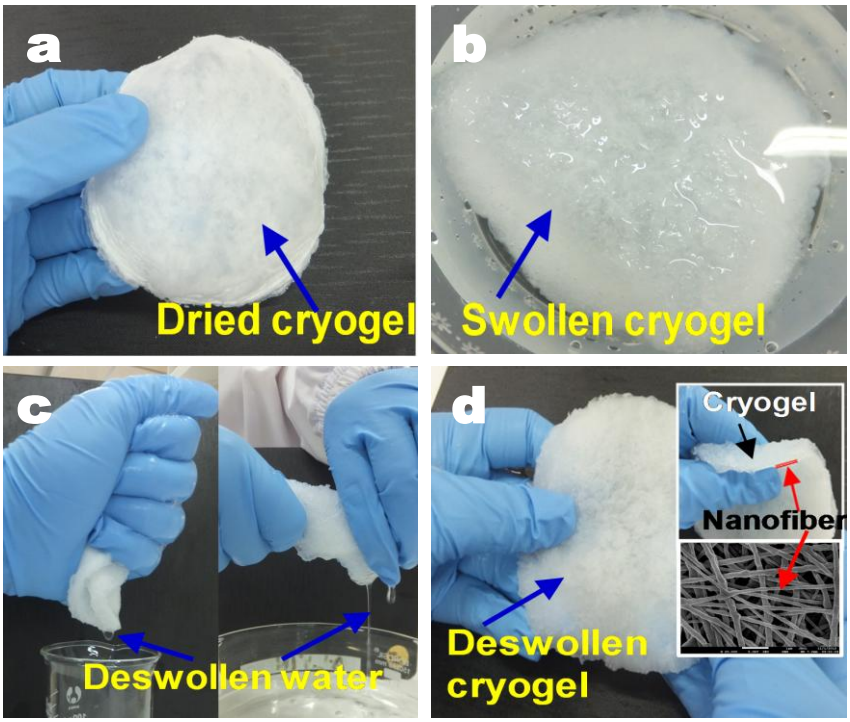

Figure 9.3 Photographs depicting a (a) dried and (b) swollen cryogel/nanofiber composite membrane. Photographs showing (c) recovery of the absorbed water via mechanical means and (d) the composite membrane remains intact after squeezing and twisting that suggests mechanical robustness of the cryogel/nanofiber membrane.

APPENDIX A Reuse permission

The contents in Chapter 2 are reproduced from *Water Research* [2012 (46) 3125-3151] with permission of Elsevier (License number: 3011681334189). Hyperlink to article: http://www.sciencedirect.com/science/article/pii/S0043135412001935

The contents in Chapter 4 are reproduced from *Soft Matter* [2013 (9) 224-234] with permission of The Royal Society of Chemistry. Hyperlink to article: http://pubs.rsc.org/en/content/articlelanding/2012/SM/C2SM26859K

The contents in Chapter 5 are reproduced from *RSC Advances* [2015 (x) xx] with permission of The Royal Society of Chemistry. Hyperlink to article: http://pubs.rsc.org/en/content/articlelanding/2015/ra/c5ra08449k

The contents in Chapter 6 are reproduced from *Environmental Science and Technology* [2013 (47) 9363-9371] with permission of The American Chemical Society. Hyperlink to article: http://pubs.acs.org/doi/abs/10.1021/es401219s and *Desalination and Water Treatment* [2015 (53) 1506-1515] with permission of Taylor and Francis (Reference number: LA/TDWT/P3070). Hyperlink to article: http://www.tandfonline.com/doi/abs/10.1080/19443994.2014.943064#.VaYc6CuUd4A

The contents in Chapter 7 are reproduced from *Environmental Science and Technology* [2015 (49) 2310–2318] with permission of The American Chemical Society. Hyperlink to article: http://pubs.acs.org/doi/abs/10.1021/es5048667

The contents in Chapter 8 are reproduced from *Journal of Colloids and Interface Science* [2016 (61) 104-113] with permission of Elsevier (License number: 3814751410777). Hyperlink to article: http://www.sciencedirect.com/science/article/pii/S0021979715301788

APPENDIX B Water-technology selection for emergency relief[†]

Providing drinking water is probably one of the most challenging aspects of an emergency response for which there is no panacea. Due to the varying scenarios for different disasters, it is not feasible to adopt the same solution for every disaster. The WT selection process is not straightforward. It depends on the emergency characteristics, quality of the water source, and the technical aspects of the WT. A major consideration is readily available energy, whose absence precludes using certain WTs. A methodology for emergency water-technology evaluation and selection is described here. In Section B.1, mutually independent evaluation criteria are established. Subsequently, a novel methodology for WT selection based on compensatory multi-criteria analysis that has been developed in this research will be discussed in Section B.2.

[†]The selection methodology presented in this chapter has been published as 'Emergency Water Supply: A Review of Potential Technologies and Selection Criteria' in *Water Research* (46) 3125-3151. Please see Appendix A for reuse permission.

B.1 Establishment of criteria and evaluation of water technologies

Several sets of criteria for evaluation of emergency WTs have been proposed. Quinn (1997) suggested that the criteria set should include the speed of deployment, quantity and quality of treated water, and the cost of the treatment unit. Steele and Clarke (2008) suggested that the criteria should not be limited only to the performance-related characteristics, but should include the emergency characteristics. They suggested the criteria set should include the throughput, quality improvement, reliability, maintenance required, rate and ease of deployment, capital and operational costs, system complexity, required operator skill and knowledge, and the required consumables. Clarke and Steele (2009) suggested that the evaluation criteria of WTs used by relief agencies include their versatility to treat a wide range of feedwater, durability and reliability of operation, costs and size, ability to meet water demand and quality, ease of deployment, and ease of operation and maintenance.

This review suggests that the criteria set used to evaluate the appropriateness of a WT for a given emergency include the throughput, performance, capital and operating costs, ease of use and deployment, and the required maintenance. However, there are several important criteria missing. One criterion is the energy requirement that is highly relevant in WT evaluation for emergency relief since access to electrical power is usually absent after a disaster. In addition, potential acceptance by the affected population (AP) should also be considered because there were reported failures of WTs due to a lack of social acceptance. Environmental impact and the supply chain requirement of the WT should be also included. Hence, a new set of criteria is proposed and redefined in Table B.1. The scoring system will be used as a basis in developing the decision matrix that will be discussed in the following section.

Table B.1 Evaluation criteria of water technologies and their definition of scores

Evaluation criteria	Definition of scores				
	1	**2**	**3**	**4**	**5**
Costs	Very high cost per liter (>1.00 US$/L)	Moderate cost per liter (0.10-1.00 US$/L)	Low cost per liter (0.01- 0.10 US$/L)	Low cost per liter (< 0.01 US$/L)	Only one-time cost is required (< 10 US$ /unit)
Ease of deployment	Large and heavy; require construction and assembly of the whole system onsite	Large and heavy; require relatively extensive assembly of parts of the system	Moderately large and heavy; require some simple set-up of the WT	Light and small sized; require some simple household materials for set-up	Light and small sized; no set-up required
Ease of use	Very complicated process design; can only be operated by skilled operator	Difficult to be operated by unskilled personnel; require determination of proper dosage of chemicals	Require some simple training to user; long treatment time (> 1 h)	Simple training is required to start using; short treatment time (< 1 h)	Essentially no training required to start using; short treatment time (< 1 h)
Environmental impact	Produces large quantity environmentally malign byproducts; toxic	Produce small quantity environmentally malign byproducts; toxic	Produce small quantity environmentally malign byproducts; mild effect	Does not produce any environmentally malign byproducts; use non-biodegradable materials	Does not produce any environmentally malign byproducts; does not use any non-biodegradable materials
Maintenance	Complicated maintenance; done regularly; time-consuming	Complicated maintenance; done regularly; not time-consuming	Slightly complicated activities; done regularly; not time-consuming	Simple maintenance; done occasionally; not time-consuming	No maintenance required
Performance	Modest microbe removal; treatment performance is affected by variations in source water quality; cannot remove turbidity	Modest microbe removal; treatment performance is affected by variations in source water quality; can remove turbidity	Excellent microbe removal; treatment performance is not affected by variations in source water quality; cannot remove turbidity	Excellent microbe removal; treatment performance is not affected by variations in source water quality; can remove turbidity	Excellent microbe removal; treatment performance is not affected by variations in source water quality; can remove a wide range of contaminants (either chemicals or salt)
Energy requirement	Uses large amount of energy and cannot be powered by renewable energy	Uses a large amount of energy but can be powered by renewable energy	Can be powered by small hand pump or bicycle	Requires energy/fuel for operation but does not involve additional use of energy	No power requirement (gravity fed or mouth suction)
Supply chain requirement	Requires continuous supply of consumables; consumables are only available from specific vendors	Periodic replacement of damaged parts; replacement parts are only available from specific vendors	Requires continuous supply of consumables; consumables are off-the-shelf materials	Periodic replacement of damaged parts; uses off-the-shelf materials	No supply chain required
Water throughput	Very low yield (< 3 L/d)	Low yield; depends on meteorological conditions	Moderate yield	High yield; can serve a small community of people or household	High yield; can be used to serve a large community of people

B.2 Water technology selection methodology

Owing to the differences between emergencies, each scenario will require a well-chosen solution that also considers the local conditions. There are various competing factors that influence the selection of the most appropriate WT. Hence, a structured selection process that considers the various influencing factors is needed.

Fig. B.1 summarizes the steps involved in the emergency WT selection process. In Step 1 a smaller set of feasible WTs is identified based on the local conditions. A decision tree (Fig. B.2) based on the following deliberations can help to eliminate non-feasible WTs for the next level of assessment:

(i) Access to road links;
(ii) Meteorological conditions such as the solar radiation intensity, wind velocity, and availability of an alternative source of energy;
(iii) Quality of the available water source, including turbidity, salinity and level of pollution;
(iv) The desired level of intervention.

The first consideration implies the possibility of using a land-based mobile water-treatment system. In the event road links cannot be accessed, a land-based mobile water-treatment system cannot be delivered. The second consideration can indicate the type of potential renewable energy that can be harnessed onsite assuming that access to energy from the electric grid is not available. In the absence of utilizable renewable energy, a WT that does not require the use of a plug-in energy supply should be used. Alternatively, if an energy-intensive WT needs to be used, it should be equipped at least with an electric generator. The third consideration, which is the quality of the source water, dictates the extent of treatment required for removal of turbidity, pathogens, taste and odor, or harmful chemicals. The last consideration is the level of intervention. It determines the required capacity of the WT.

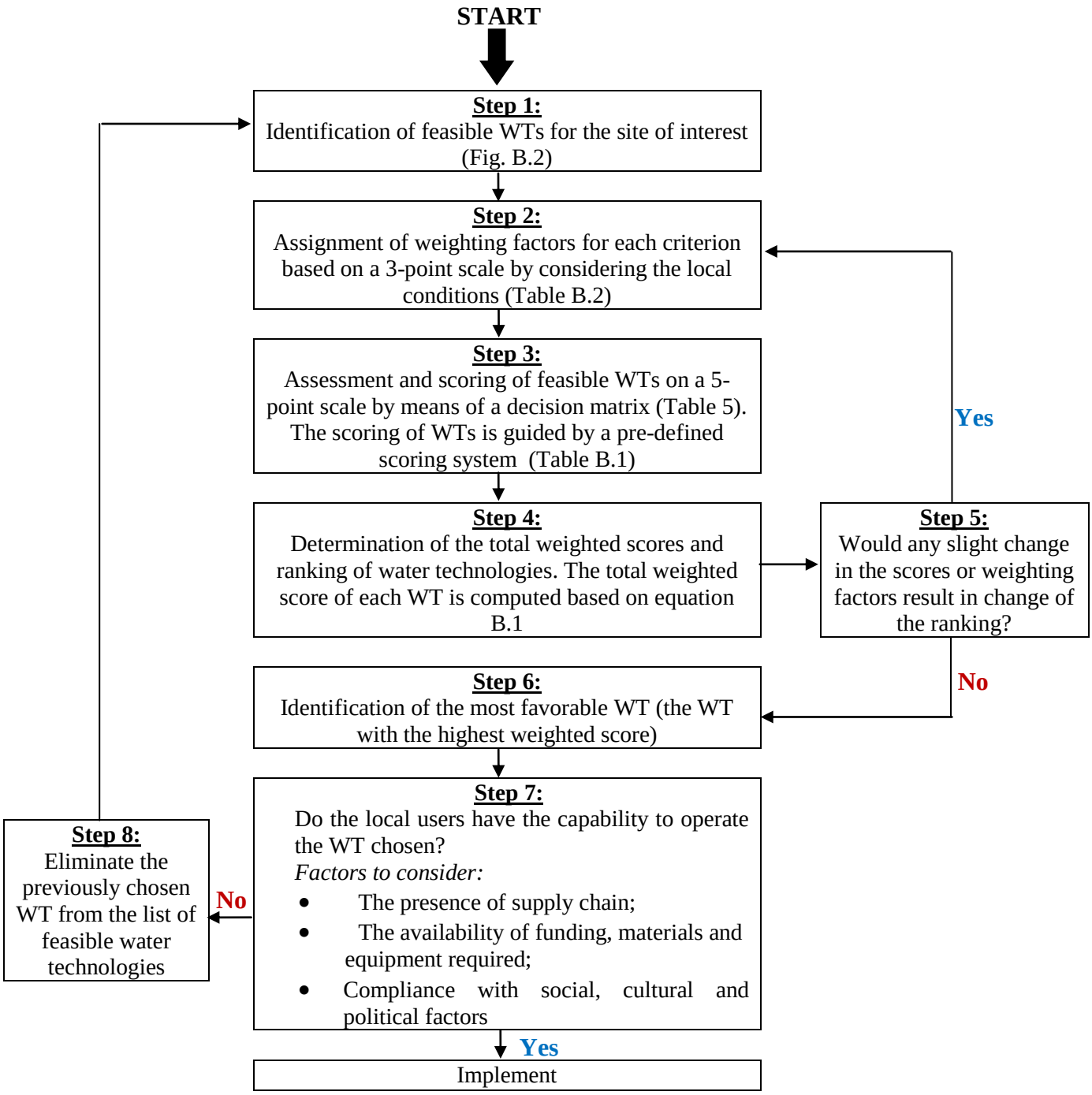

Figure B.1 Flow chart summarizing the water technology selection process.

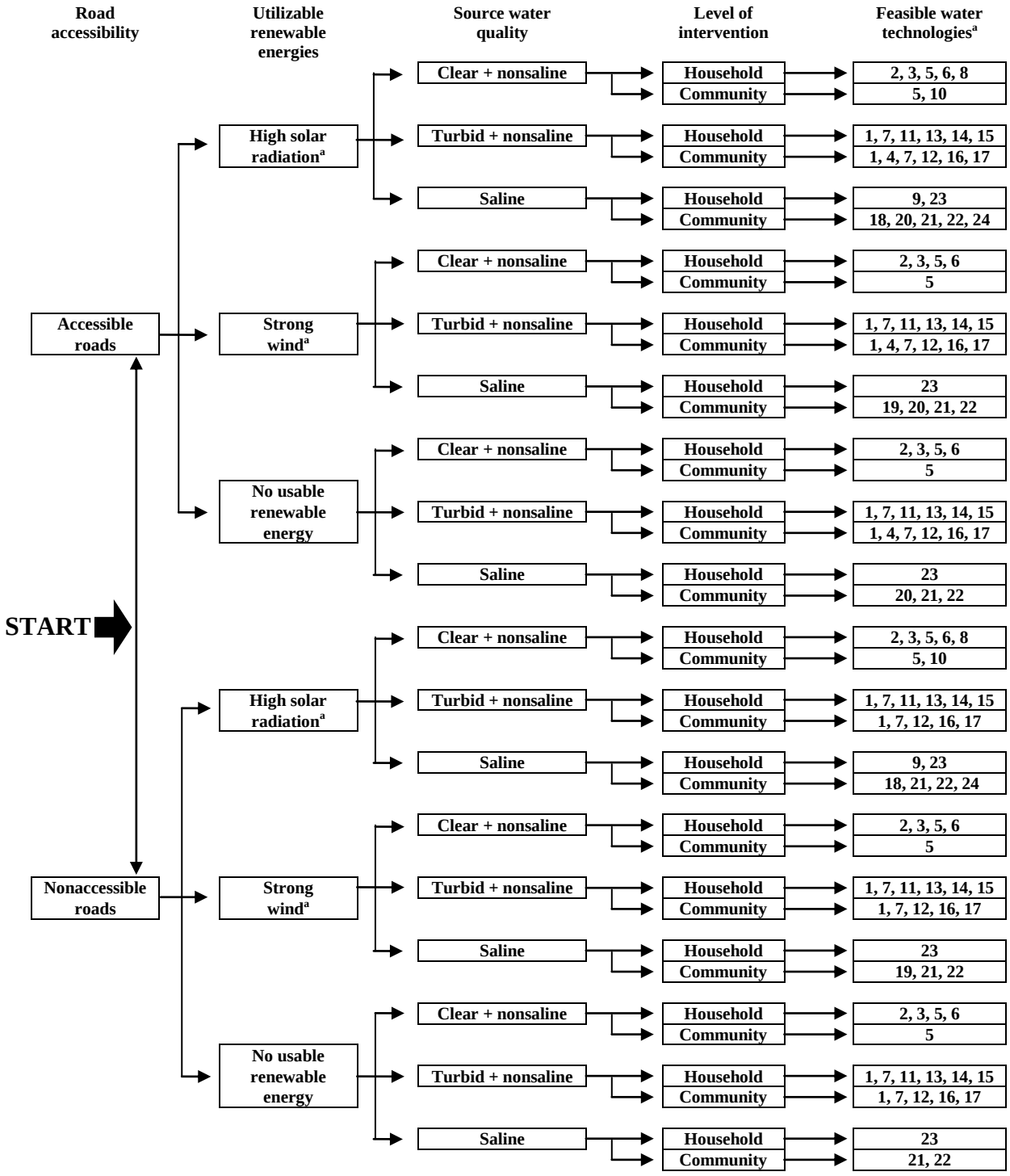

Note: 1= Biosand filter; 2= Boiling; 3= Thermal pasteurizer; 4= Land-based mobile water treatment plant; 5= NADCC tablets; 6= UV disinfection (portable); 7= PUR® sachet; 8= SODIS; 9= Solar still; 10= Solar water heater; 11= Structured matrix filter; 12= Upflow clarifier; 13= Household ceramic filter; 14= Portable MF; 15= Portable UF;16= Modular UF; 17= Bicycle-powered NF; 18= Modular PV-RO; 19= Modular wind-powered RO; 20= Land-based mobile RO plant (generator); 21= Mobile floating RO (generator); 22= Modular RO (generator); 23= FO filter pouch; 24= solar MD.

[a]The list of feasible water technologies also includes those powered by non-renewable energy sources such as electrical generator, fossil fuels, etc.

Figure B.2 Decision tree for identification of feasible emergency water technologies.

In Step 2 feasible WTs are scored and in Step 3 they are ranked by means of a decision matrix (Table B.2). The assignment of scores is conducted based on the scoring system mentioned earlier (Table B.2). A weighting factor is assigned to each criterion to adjust its relative importance based on the needs of the AP and the local conditions of the affected area. For example, in the immediate emergency stage, the speed of deployment, stability of the system, acceptance by the AP, and throughput might be more important than other factors. In Step 4 the total weighted scores of each WT are calculated and compared. The total weighted score of a WT, S_i, is determined from the following:

$$S_i = \sum_{j=1}^{n} w_j \cdot x_{ij} \; ; i = 1, 2, 3..., m \tag{B.1}$$

where w_j and x_{ij} are the weighting factor and score of the i^{th} WT for the j^{th} criterion, respectively. In Step 5 a sensitivity analysis is conducted to ascertain whether slight changes in the scores and the weighting factors would change the ranking of the WTs. If any slight change in the score or weighting factor results in alteration of the ranking, Steps 2-5 need to be repeated until a sensible ranking of WTs is obtained. Step 6 involves identifying the most favorable WT, which is usually the one with the highest S_i. In Step 7 the assessors must ensure that they have the funding, materials and equipment required to implement the WT. In addition, the assessors should ensure that there are suitable site personnel to operate the WT. If the implementation is not possible, the selection process needs to be reiterated omitting the previously selected WT.

Table B.2 Decision matrix for comparing emergency water technologies

No.	Weighting factor[a] / Technologies	Evaluation criteria scores[a]										Scores	
		Costs	Ease of deployment	Ease of use	Environmental impact	Maintenance	Performance	Potential acceptance	Energy requirement	Supply chain requirement	Water through-put	Nominal	Weighted
		1	3	3	1	2	2	3	3	1	3		
1	Biosand filter	5	1	4	5	3	2	4	5	5	4	38	79
2	Boiling	4	4	5	3	4	3	5	1	3	4	36	81
3	*Chulli* purifier/WADIS	5	1	5	3	4	3	4	4	4	4	37	80
4	Land-based mobile water treatment plant[b]	3	3	1	2	1	4	3	1	2	5	25	56
5	NADCC tablets	3	4	2	3	4	1	1	5	1	4	28	65
6	UV disinfection (portable)	2	5	5	5	4	1	2	3	2	4	33	76
7	PuR® sachets[b]	3	5	4	1	4	5	3	5	1	4	35	86
8	SODIS	5	5	3	4	4	1	2	5	4	2	35	74
9	Solar stills[b]	3	3	3	3	4	5	2	2	4	2	31	64
10	Solar water heater	3	3	3	5	5	1	2	5	4	2	33	69
11	Structured matrix filter[b]	2	5	5	5	4	2	4	3	2	3	35	81
12	Upflow clarifier	3	1	2	1	2	2	3	1	1	5	21	49
13	Household ceramic filter	5	1	3	5	4	2	4	5	4	2	35	71
14	Portable MF	2	5	5	5	4	4	4	3	2	2	36	82
15	Portable UF	3	5	5	5	4	4	4	5	2	4	41	95
16	Modular UF	4	3	5	5	3	4	4	5	2	5	40	91
17	Bicycle-powered NF[a]	3	3	1	3	3	5	4	3	2	5	32	72
18	Modular PV-RO systems[b]	3	3	1	3	2	5	4	2	2	2	27	58
19	Modular wind-powered RO[b]	3	3	1	3	2	5	4	2	2	2	27	58
20	Mobile RO plant on bus[a]	3	3	1	3	2	5	4	1	2	5	29	64
21	Mobile floating RO[b]	3	2	1	3	2	5	4	1	2	5	28	61
22	Modular RO (generator)[b]	2	3	1	3	2	5	4	1	2	5	28	63
23	FO filter pouch[b]	1	5	5	4	5	5	1	5	1	1	33	77
24	Compact SMADES (MD)[b]	3	3	1	3	2	5	4	2	2	2	27	64

Note:
[a]May vary from case-to-case.
[b]Can be used to treat chemically-contaminated water.

Weighting factors

3	Most important
2	
1	Least important

Scores

5	Most favorable
4	
3	
2	
1	Least favorable

REFERENCES

Abbaszadegan, M., Hasan, M. N., Gerba, C. P., Roessler, P. F., Wilson, B. R., Kuennen, R. and Van Dellen, E. (1997). "The disinfection efficacy of a point-of-use water treatment system against bacterial, viral and protozoan waterborne pathogens." Water Research 31(3): 574-582.

Aboabboud, M. M., Horvath, L., Szépvölgy, J., Mink, G., Radhika, E. and Kudish, A. I. (1997). "The use of a thermal energy recycle unit in conjunction with a basin-type solar still for enhanced productivity." Energy 22(1): 83-91.

Adegboyega, N. F., Sharma, V. K., Siskova, K., Zbořil, R., Sohn, M., Schultz, B. J. and Banerjee, S. (2012). "Interactions of aqueous Ag^{+} with fulvic acids: Mechanisms of silver nanoparticle formation and investigation of stability." Environmental Science & Technology 47(2): 757-764.

Agnihotri, S., Mukherji, S. and Mukherji, S. (2012). "Antimicrobial chitosan–PVA hydrogel as a nanoreactor and immobilizing matrix for silver nanoparticles." Applied Nanoscience 2(3): 179-188.

Agnihotri, S., Mukherji, S. and Mukherji, S. (2013). "Immobilized silver nanoparticles enhance contact killing and show highest efficacy: Elucidation of the mechanism of bactericidal action of silver." Nanoscale 5(16): 7328-7340.

Ahammed, M. M. and Davra, K. (2011). "Performance evaluation of biosand filter modified with iron oxide-coated sand for household treatment of drinking water." Desalination 276(1-3): 287-293.

Ahmed, A. E.-S. I. (2011). "Hydrogels for water filters: Preparation and antibacterial evaluation." Journal of Applied Polymer Science 122 (2): 1162-1167.

Aiken, G. R., Hsu-Kim, H. and Ryan, J. N. (2011). "Influence of dissolved organic matter on the environmental fate of metals, nanoparticles, and colloids." Environmental Science & Technology 45(8), 3196-3201.

Akaighe, N., MacCuspie, R.I., Navarro, D. A., Aga, D. S., Banerjee, S., Sohn, M. and Sharma, V. K. (2011). "Humic acid-induced silver nanoparticle formation under environmentally relevant conditions." Environmental Science & Technology 45(9): 3895-3901.

Alonso, A., MacAnás, J., Shafir, A., Muñoz, M., Vallribera, A., Prodius, D., Melnic, S., Turta, C. and Muraviev, D. N. (2010). "Donnan-exclusion-driven distribution of catalytic ferromagnetic nanoparticles synthesized in polymeric fibers." Dalton Transactions 39(10): 2579-2586.

Alonso, A., Muñoz-Berbel, X., Vigués, N., Macanás, J., Muñoz, M., Mas, J. and Muraviev, D. N. (2011a). "Characterization of fibrous polymer silver/cobalt nanocomposite with enhanced bactericide activity." Langmuir 28(1): 783-790.

Alonso, A., Munoz-Berbel, X., Vigues, N., Rodriguez-Rodriguez, R., Macanas, J., Mas, J., Munoz, M. and Muraviev, D. N. (2012a). "Intermatrix synthesis of monometallic and magnetic metal/metal oxide nanoparticles with bactericidal activity on anionic exchange polymers." RSC Advances 2(11): 4596-4599.

Alonso, A., Muñoz-Berbel, X., Vigués, N., Rodríguez-Rodríguez, R., MacAnás, J., Muñoz, M., Mas, J. and Muraviev, D. N. (2013). "Superparamagnetic Ag@Co-nanocomposites on granulated cation exchange polymeric matrices with enhanced antibacterial activity for the environmentally safe purification of water." Advanced Functional Materials 23(19): 2450-2458.

Alonso, A., Shafir, A., MacAnás, J., Vallribera, A., Muñoz, M. and Muraviev, D. N. (2012b). "Recyclable polymer-stabilized nanocatalysts with enhanced accessibility for reactants." Catalysis Today 193(1): 200-206.

Alonso, A., Vigues, N., Munoz-Berbel, X., Macanas, J., Munoz, M., Mas, J. and Muraviev, D. N. (2011b). "Environmentally-safe bimetallic Ag@Co magnetic nanocomposites with antimicrobial activity." Chemical Communications 47(37): 10464-10466.

Amin, M. T. and Han, M. Y. (2011). "Improvement of solar based rainwater disinfection by using lemon and vinegar as catalysts." Desalination 276: 416-424.

Amin, T. and Han, M. (2009). "Roof-harvested rainwater for potable purposes: Application of solar disinfection (SODIS) and limitations." Water Science & Technology 60(2): 419-431.

Anderson, J.W., Semprini, L. and Radniecki, T. S. (2014). "Influence of water hardness on silver ion and silver nanoparticle fate and toxicity toward *Nitrosomonas europaea*." Environmental Engineering Science 31(7): 403-409.

Anesio, A.M., Granéli, W., Aiken, G. R., Kieber, D. J. and Mopper, K. (2005). "Effect of humic substance photodegradation on bacterial growth and respiration in lake water." Applied and Environmental Microbiology 71(10), 6267-6275.

Aoustin, E., Schäfer, A. I., Fane, A. G. and Waite, T. D. (2001). "Ultrafiltration of natural organic matter." Separation and Purification Technology 22-23): 63-78.

Apopei, D. F., Dinu, M. V., Trochimczuk, A. W. and Dragan, E. S. (2012). "Sorption isotherms of heavy metal ions onto semi-interpenetrating polymer network cryogels based on polyacrylamide and anionically modified potato starch" Industrial and Engineering Chemistry Research 51 (31): 10462-10471.

Applerot, G., Lellouche, J., Lipovsky, A., Nitzan, Y., Lubart, R., Gedanken, A. and Banin, E. (2012). "Understanding the antibacterial mechanism of CuO nanoparticles: Revealing the route of induced oxidative stress." Small 8(21): 3326-3337.

Archer, A. and Elmore, A. C. (2010). "Use of ceramic pot filters for drinking water disinfection in Guatemala." World Environmental and Water Resources Congress 2010: Challenges of change ASCE) 545-558.

Arnal Arnal, J. M., Sancho Fernández, M., Martín Verdú, G. and Lora García, J. (2001). "Design of a membrane facility for water potabilization and its application to third world countries." Desalination 137(1-3): 63-69.

Arnal, J. M., García-Fayos, B., Sancho, M., Verdú, G. and Lora, J. (2010). "Design and installation of a decentralized drinking water system based on ultrafiltration in Mozambique." Desalination 250(2): 613-617.

Arnal, J. M., Garcia-Fayos, B., Verdu, G. and Lora, J. (2009). "Ultrafiltration as an alternative membrane technology to obtain safe drinking water from surface water: 10 years of experience on the scope of the AQUAPOT project." Desalination 248(1-3): 34-41.

Arnal, J. M., Garcia-Fayos, B., Verdu, G., Lora, J. and Sancho, M. (2008). "AQUAPOT: Study of the causes in reduction of permeate flow in spiral wound uf membrane. Simulation of a non-rigorous cleaning protocol in a drinkable water treatment facility." Desalination 222(1-3): 513-518.

Arnal, J. M., Sancho, M., García Fayos, B., Lora, J. and Verdú, G. (2007). "Aquapot: UF real applications for water potabilization in developing countries. Problems, location and solutions adopted." Desalination 204(1-3): 316-321.

Arnal, J. M., Sancho, M., Verdú, G., Campayo, J. M. and Gozálvez, J. M. (2003a). "Treatment of ^{137}Cs liquid wastes by reverse osmosis part II. Real application." Desalination 154(1): 35-42.

Arnal, J. M., Sancho, M., Verdú, G., Campayo, J. M. and Villaescusa, J. I. (2003b). "Treatment of ^{137}Cs liquid wastes by reverse osmosis part I. Preliminary tests." Desalination 154(1): 27-33.

Arnal, J. M., Sancho, M., Verdú, G., Lora, J., Marín, J. F. and Cháfer, J. (2004). "Selection of the most suitable ultrafiltration membrane for water disinfection in developing countries." Desalination 168): 265-270.

Arvidsson, P., Plieva, F. M., Savina, I. N., Lozinsky, V. I., Fexby, S., Bülow, L., Yu. Galaev, I. and Mattiasson, B. (2002). "Chromatography of microbial cells using continuous supermacroporous affinity and ion-exchange columns." Journal of Chromatography A 977(1): 27-38.

AshaRani, P. V., Low K. M., G., Hande, M. P. and Valiyaveettil, S. (2008). "Cytotoxicity and genotoxicity of silver nanoparticles in human cells." ACS Nano 3(2): 279-290.

Atkinson, S. (2006). "Membranes help US military produce clean drinking water." Membrane Technology 2006(2): 7-8.

Avalos, A., Haza, A. I., Mateo, D. and Morales, P. (2014). "Cytotoxicity and ROS production of manufactured silver nanoparticles of different sizes in hepatoma and leukemia cells." Journal of Applied Toxicology 34(4): 413-423.

Badawy, A. M. E., Luxton, T. P., Silva, R. G., Scheckel, K. G., Suidan, M. T. and Tolaymat, T. M. (2010). "Impact of environmental conditions (pH, ionic strength, and electrolyte type) on the surface charge and aggregation of silver nanoparticles suspensions." Environmental Science & Technology 44(4): 1260-1266.

Bagwell, T. H., Shalewitz, B. and Coleman, A. (1994). "The army water supply program: An overview." Desalination 99(2-3): 423-445.

Balogh, L., Swanson, D. R., Tomalia, D. A., Hagnauer, G. L. and McManus, A. T. (2000). "Dendrimer−silver complexes and nanocomposites as antimicrobial agents." Nano Letters 1(1), 18-21.

Banat, F. and Jwaied, N. (2008). "Economic evaluation of desalination by small-scale autonomous solar-powered membrane distillation units." Desalination 220(1–3): 566-573.

Banat, F., Jumah, R. and Garaibeh, M. (2002). "Exploitation of solar energy collected by solar stills for desalination by membrane distillation." Renewable Energy 25(2): 293-305.

Banat, F., Jwaied, N., Rommel, M., Koschikowski, J. and Wieghaus, M. (2007). "Desalination by a "compact SMADES" autonomous solarpowered membrane distillation unit." Desalination 217(1-3): 29-37.

Barbot, E., Carretier, E., Wyart, Y., Marrot, B. and Moulin, P. (2009). "Transportable membrane process to produce drinking water." Desalination 248(1-3): 58-63..

Barrow, M., Eltmimi, A., Ahmed, A., Myers, P. and Zhang, H. (2012). "Frozen polymerization for aligned porous structures with enhanced mechanical stability, conductivity, and as stationary phase for HPLC." Journal of Materials Chemistry 22(23): 11615-11620.

Behra, R., Sigg, L., Clift, M. J. D., Herzog, F., Minghetti, M., Johnston, B., Petri-Fink, A. and Rothen-Rutishauser, B. (2013). "Bioavailability of silver nanoparticles and ions: From a chemical and biochemical perspective." Journal of the Royal Society Interface 10(87): 20130396.

Bell Jr, F. A., Perry, D. L., Smith, J. K. and Lynch, S. C. (1984). "Studies on home water treatment systems." Journal of American Water Works Association 76(Compendex): 126-130.

Bennett, D. J., Burford, R. P., Davis, T. P. and Tilley, H. J. (1995). "Synthesis of porous hydrogel by polymerizing the continuous phase of a microemulsion." Polymer International 36: 219-226.

Berg, P. A. (2010) "A new water treatment product for the urban poor in the developing world", Providence, Rhode Island, pp. 210-210.

Berillo, D., Mattiasson, B., Galaev, I. Y. and Kirsebom, H. (2012). "Formation of macroporous self-assembled hydrogels through cryogelation of Fmoc–Phe–Phe." Journal of Colloid and Interface Science 368(1): 226-230.

Berney, M., Weilenmann, H. U., Simonetti, A. and Egli, T. (2006). "Efficacy of solar disinfection of *Escherichia coli, Shigella flexneri, Salmonella typhimurium and Vibrio cholerae*." Journal of Applied Microbiology 101(4): 828-836.

Bielefeldt, A. R., Kowalski, K., Schilling, C., Schreier, S., Kohler, A. and Scott Summers, R. (2010). "Removal of virus to protozoan sized particles in point-of-use ceramic water filters." Water Research 44(5): 1482-1488.

Bilici, C., Karayel, S., Demir, T. T. and Okay, O. (2010). "Self-oscillating pH-responsive cryogels as possible candidates of soft materials for generating mechanical energy." Journal of Applied Polymer Science 118(5): 2981-2988.

Blacher, S., Maquet, V., Pirard, R., Pirard, J. P. and Jérôme, R. (2001). "Image analysis, impedance spectroscopy and mercury porosimetry characterisation of freeze-drying porous materials." Colloids and Surfaces A: Physicochemical and Engineering Aspects 187–188: 375-383.

Blacher, S., Maquet, V., Pirard, R., Pirard, J.P. and Jérôme, R. (2001). "Image analysis, impedance spectroscopy and mercury porosimetry characterisation of freeze-drying porous materials." Colloids and Surfaces A: Physicochemical and Engineering Aspects 187–188(0): 375-383.

Blanco Gálvez, J., García-Rodríguez, L. and Martín-Mateos, I. (2009). "Seawater desalination by an innovative solar-powered membrane distillation system: The MEDESOL project." Desalination 246(1-3): 567-576.

Boisson, S., Kiyombo, M., Sthreshley, L., Tumba, S., Makambo, J. and Clasen, T. (2010). "Field assessment of a novel household-based water filtration device: A randomised, placebo-controlled trial in the democratic Republic of Congo." PLoS ONE 5(9): e12613.

Bondarenko, O., Ivask, A., Käkinen, A., Kurvet, I. and Kahru, A. (2013). "Particle-cell contact enhances antibacterial activity of silver nanoparticles." PLoS ONE 8(5): e64060.

Bouchekima, B., Gros, B., Ouahes, R. and Diboun, M. (1998). "Performance study of the capillary film solar distiller." Desalination 116(2-3): 185-192.

Bouguecha, S., Hamrouni, B. and Dhahbi, M. (2005). "Small scale desalination pilots powered by renewable energy sources: Case studies." Desalination 183(1-3): 151-165.

Brown, J. and Sobsey, M. D. (2010). "Microbiological effectiveness of locally produced ceramic filter for drinking water treatment in Cambodia." Journal of Water and Health. 8(1): 1-10.

Brown, J., Sobsey, M. D. and Loomis, D. (2008). "Local drinking water filters reduce diarrhea disease in cambodia: A randomized, controlled trial of the ceramic water purifier." American Journal of Tropical Medicine and Hygiene 79(3): 394-400.

Burch, J. D. and Thomas, K. E. (1998). "Water disinfection for developing countries and potential for solar thermal pasteurization." Solar Energy 64(1–3): 87-97.

Butler, R. (2009). "Skyjuice technology impact on the U.N. MDG outcomes for safe affordable potable water." Desalination 248(1-3): 622-628.

Calvert, P., 2009. Hydrogels for soft machines. Advanced Materials 21(7), 743-756.

Caroli, G., Levre, E., Armani, G., Biffi-Gentili, S. and Molinari, G. (1985). "Search for acid-fast *bacilli* in bottled mineral waters." Journal of Applied Microbiology 58(5): 461-463.

Cath, T. Y., Childress, A. E. and Elimelech, M. (2006). "Forward osmosis: principles, applications, and recent developments." Journal of Membrane Science 281(1-2): 70-87.

Caykara, T., Küçüktepe, S. and Turan, E. (2006). "Thermosensitive poly[(2-(diethylamino)ethyl methacrylate)-co-(n,n-dimethylacrylamide)] cryogels prepared by a two-step polymerization method." Macromolecular Materials and Engineering 291(10): 1278-1286.

CDC (2008). "Household water treatment options in developing countries: solar disinfection (sodis). Available from: www.cdc.gov/safewater/publications_pages/options-sodis.pdf.

Ceylan, D. and Okay, O. (2007). "Macroporous polyisobutylene gels: A novel tough organogel with superfast responsivity." Macromolecules 40(24): 8742-8749.

Ceylan, D., Can, V. and Okay, O. (2006). "Phase transition of acrylamide-based polyampholyte gels in water." Journal of Macromolecular Science, Part A: Pure and Applied Chemistry 43(10): 1635-1649.

Ceylan, D., Dogu, S., Karacik, B., Yakan, S. D., Okay, O. S. and Okay, O. (2009). "Evaluation of butyl rubber as sorbent material for the removal of oil and polycyclic aromatic hydrocarbons from seawater." Environmental Science and Technology 43(10): 3846-3852.

Ceylan, D., Ozmen, M. M. and Okay, O. (2006). "Swelling-deswelling kinetics of ionic poly(acrylamide) hydrogels and cryogels." Journal of Applied Polymer Science 99(1): 319-325.

Chalal, M., Ehrburger-Dolle, F. O., Morfin, I., Vial, J.-C., Aguilar de Armas, M.-R., San Roman, J., Bölgen, N., Pişkin, E., Ziane, O. and Casalegno, R. (2009). "Imaging the structure of macroporous hydrogels by two-photon fluorescence microscopy." Macromolecules 42(7): 2749-2755.

Chambers, B. A., Afrooz, A. R. M. N., Bae, S., Aich, N., Katz, L., Saleh, N. B. and Kirisits, M. J. (2013). "Effects of chloride and ionic strength on physical morphology, dissolution, and bacterial toxicity of silver nanoparticles." Environmental Science & Technology 48(1): 761-769.

Chanda, M., Pillay, S. A., Sarkar, A. and Modak, J. M. (2009). "A thermally regenerable composite sorbent of crosslinked poly(acrylic acid) and ethoxylated polyethyleneimine for water desalination by sirotherm process." Journal of Applied Polymer Science 111(6): 2741-2750.

Chanda, M., Pillay, S. A., Sarkar, A. and Modak, J. M. (2010). "Interpenetrating networks of cross-linked poly(acrylic acid) and cross-linked polyethyleneimine (80% ethoxylated) for desalination of brackish water by thermoreversible sorption." Industrial and Engineering Chemistry Research 49(16): 7136-7146.

Chappell, M. A., Miller, L. F., George, A. J., Pettway, B. A., Price, C. L., Porter, B. E., Bednar, A. J., Seiter, J. M., Kennedy, A. J. and Steevens, J. A. (2011). "Simultaneous dispersion–dissolution behavior of concentrated silver nanoparticle

suspensions in the presence of model organic solutes." Chemosphere 84(8): 1108-1116.

Charley R. C. and Bull A. T. (1979). "Bioaccumulation of silver by a multispecies community of bacteria." Archives of Microbiology **123**(3): 239-244.

Chauhan, G. S. and Lal, H. (2003). "Novel grafted cellulose-based hydrogels for water technologies." Desalination 159(2): 131-138.

Chen, C. Z. S. and Cooper, S. L. (2002). "Interactions between dendrimer biocides and bacterial membranes." Biomaterials 23: 3359-3368.

Chen, K. L. and Bothun, G. D. (2013). "Nanoparticles meet cell membranes: Probing nonspecific interactions using model membranes." Environmental Science & Technology 48(2): 873-880.

Chen, Y., Worley, S. D., Kim, J., Wei, C.-I., Chen, T.-Y., Santiago, J. I., Williams, J. F. and Sun, G. (2003). "Biocidal poly(styrenehydantoin) beads for disinfection water." Industrial and Engineering Chemistry Research 42: 280-284.

Chen, Z., Porcher, C., Campbell, P. G. C. and Fortin, C. (2013). "Influence of humic acid on algal uptake and toxicity of ionic silver." Environmental Science & Technology 47(15): 8835-8842.

Chen, Z., Xu, L., Liang, Y., Wang, J., Zhao, M. and Li, Y. (2008). "Polyethylene glycol diacrylate-based supermacroporous monolithic cryogel as high-performance liquid chromatography stationary phase for protein and polymeric nanoparticle separation." Journal of Chromatography A 1182(1): 128-131.

Choi, O. and Hu, Z. (2008). "Size dependent and reactive oxygen species related nanosilver toxicity to nitrifying bacteria." Environmental Science & Technology 42(12): 4583-4588.

Chopra. I. (2007). "The increasing use of silver-based products as antimicrobial agents: a useful development or a cause for concern?" Journal of Antimicrobial Chemotherapy 59: 587–590.

Choudhury P. and Kumar R. (1998). "Multidrug- and metal-resistant strains of *Klebsiella pneumoniae* isolated from *Penaeus monodon* of the coastal waters of deltaic Sundarban." Canadian Journal of Microbiology 44: 186–189.

Christen, A., Navarro, C. M. and Mäusezahl, D. (2009). "Safe drinking water and clean air: An experimental study evaluating the concept of combining household water treatment and indoor air improvement using the water disinfection stove (WADIS)." International Journal of Hygiene and Environmental Health 212(5): 562-568.

Clarke, B. A. and Steele, A. (2009). "Water treatment systems for relief agencies: The on-going search for the 'silver bullet'." Desalination 248(1-3): 64-71.

Clasen, T. and Boisson, S. (2006). "Household-based ceramic water filters for the treatment of drinking water in disaster reponse: An assessment of a pilot programme in the Dominican Republic." Water Practice and Technology 1(2).

Clasen, T. and Edmondson, P. (2006). "Sodium dichloroisocyanurate (NADCC) tablets as an alternative to sodium hypochlorite for the routine treatment of drinking water at the household level." International Journal of Hygiene and Environmental Health 209(2): 173-181.

Clasen, T. F. and Cairncross, S. (2004). "Editorial: Household water management: Refining the dominant paradigm." Tropical Medicine and International Health 9(2): 187-191.

Clasen, T. F., Brown, J., Collin, S., Suntura, O. and Cairncross, S. (2004b). "Reducing diarrhea through the use of household-based ceramic water filters: A randomized,

controlled trial in rural Bolivia." The American Journal of Tropical Medicine and Hygiene 70(6): 651-657.

Clasen, T. F., Do, H. T., Boisson, S. and Shipin, O. (2008b). "Microbiological effectiveness and cost of boiling to disinfect drinking water in rural Vietnam." Environmental Science and Technology 42(12): 4255-4260.

Clasen, T., Brown, J., Suntura, O. and Collin, S. (2004a). "Safe household water treatment and storage using ceramic drip filters: A randomised controlled trial in Bolivia." Water Science and Technology 50(1): 111-115.

Clasen, T., McLaughlin, C., Nayaar, N., Boisson, S., Gupta, R., Desai, D. and Shah, N. (2008a). "Microbiological effectiveness and cost of disinfecting water by boiling in semi-urban India." American Journal of Tropical Medicine and Hygiene 79(3): 407-413.

Clasen, T., Naranjo, J., Frauchiger, D. and Gerba, C. (2009). "Laboratory assessment of a gravity-fed ultrafiltration water treatment device designed for household use in low-income settings." American Journal of Tropical Medicine and Hygiene 80(5): 819-823.

Clasen, T., Saeed, T., Boisson, S., Edmonson, P. and Shipin, O. (2007). "Household water treatment using sodium dichloroisocyanurate (NADCC) tablets: A randomized, controlled trial to assess microbiological effectiveness in Bangladesh." American Journal of Tropical Medicine and Hygiene 76(1): 187-192.

Colindres, R. E., Jain, S., Bowen, A., Domond, P. and Mintz, E. (2007). "After the flood: An evaluation of in-home drinking water treatemnt with combined flocculent-disinfectant following tropical storm Jeanne - Gonaives, Haiti, 2004." Journal of Water and Health 5(3): 367-374.

Conroy, R. M., Elmore-Meegan, M., Joyce, T., McGuigan, K. G. and Barnes, J. (1996). "Solar disinfection of drinking water and diarrhoea in Maasai children: A controlled field trial." The Lancet 348(9043): 1695-1697.

Conroy, R., Meegan, M. E., Joyce, T., McGuigan, K. and Barnes, J. (1999). "Solar disinfection of water reduces diarrhoeal disease: An update." Archive of Disease in Childhood 81(4): 337-338.

Cooper, W. J. and Zepp, R. G. (1990). "Hydrogen peroxide decay in waters with suspended soils: Evidence for biologically mediated processes." Canadian Journal of Fisheries and Aquatic Sciences 47(5): 888-893.

Cooper, W. J. and Zika, R. G. (1983). "Photochemical formation of hydrogen peroxide in surface and ground waters exposed to sunlight." Science 220(4598): 711-712.

Cooper, W. J., Zika, R. G., Petasne, R. G. and Plane, J. M. C. (1988). "Photochemical formation of hydrogen peroxide in natural waters exposed to sunlight." Environmental Science & Technology 22(10): 1156-1160.

Copello, G. J., Mebert, A. M., Raineri, M., Pesenti, M. P. and Diaz, L. E. (2011). "Removal of dyes from water using chitosan hydrogel/ SiO_2 and chitin hydrogel/SiO_2 hybrid materials obtained by the sol-gel method." Journal of Hazardous Materials 186(1): 932-939.

Cordelires, F. and Jackson, J., 2007. 3D object counter, http://rsb.info.nih.gov/ij/plugins/track/objects.html (accessed 27/02/2014).

Dabrowski, A., Podkoscielny, P., Hubicki, Z. and Barczak, M. (2005). "Adsorption of phenolic compounds by activated carbon — A critical review." Chemosphere 58(8): 1049-1070.

Daels, N., De Vrieze, S., Sampers, I., Decostere, B., Westbroek, P., Dumoulin, A., Dejans, P., De Clerck, K. and Van Hulle, S. W. H. (2011). "Potential of a

functionalised nanofibre microfiltration membrane as an antibacterial water filter." Desalination 275(1–3): 285-290.

Dallas, P., Sharma, V.K. and Zboril, R. (2011). "Silver polymeric nanocomposites as advanced antimicrobial agents: Classification, synthetic paths, applications, and perspectives." Advances in Colloid and Interface Science 166(1–2): 119-135.

Dankovich, T. A. and Gray, D. G. (2011). "Bactericidal paper impregnated with silver nanoparticles for point-of-use water treatment." Environmental Science and Technology 45(5): 1992-1998.

Dankovich, T. (2012). "Bactericidal paper containing silver nanoparticles for water treatment." Chapter 5: Impact of the influent water composition on bacterial inactivation by a silver nanoparticle paper. pp 127-149. Phd thesis, McGill University, Available from: http://digitool.library.ccgill.ca/webclient/streamgate?folder_id=0&dvs=1417413811669~411.

Darling, A. L. and Sun, W. (2004). "3D microtomographic characterization of precision extruded poly-e-caprolactone scaffolds." Journal of Biomedical Materials Research Part B: Applied Biomaterials 70B: 311-317.

Davis I. J, Richards H. and Mullany P. (2005). "Isolation of silver- and antibiotic-resistant *Enterobacter cloacae* from teeth." Oral Microbiology and Immunology 20: 191–194

Deng, S., Wang, R., Xu, H., Jiang, X. and Yin, J. (2012). "Hybrid hydrogels of hyperbranched poly(ether amine)s (HPEAs) for selective adsorption of guest molecules and separation of dyes." Journal of Materials Chemistry 22(19): 10055-10061.

Denyer, S. P. and Stewart, G. S. A. B. (1998). "Mechanisms of action of disinfectants." International Biodeterioration & Biodegradation 41(3–4): 261-268.

Deville, S., Saiz, E., Nalla, R. K. and Tomsia, A. P. (2006). "Freezing as a path to build complex composites." Science 311(5760): 515-518.

Diagne, F., Malaisamy, R., Boddie, V., Holbrook, R. D., Eribo, B. and Jones, K. L. (2012). "Polyelectrolyte and silver nanoparticle modification of microfiltration membranes to mitigate organic and bacterial fouling." Environmental Science & Technology 46(7): 4025-4033.

Dibrov, P., Dzioba, J., Gosink, K. K. and Häse, C. C. (2002). "Chemiosmotic mechanism of antimicrobial activity of Ag^{+} in *Vibrio cholerae*." Antimicrobial Agents and Chemotherapy 46(8), 2668-2670.

Dinu, M. V., Ozmen, M. M., Dragan, E. S. and Okay, O. (2007). "Freezing as a path to build macroporous structures: Superfast responsive polyacrylamide hydrogels." Polymer 48(1): 195-204.

Dinu, M. V., Perju, M. M. and Drăgan, E. S. (2011b). "Composite IPN ionic hydrogels based on polyacrylamide and dextran sulfate." Reactive and Functional Polymers 71(8): 881-890.

Dinu, M. V., Perju, M. M., Cazacu, M. and Dragan, E. S. (2011a). "Polyacrylamide-dextran polymeric networks: Effect of gel preparation of their morphology and swelling properties." Cellulose Chemical Technology 45): 197-203.

Domotenko, L. V., Lozinskii, V. I., Vainerman, Y. S. and Rogozhin, S. V. (1988). "Effect of freezing conditions of dilute solutions of polyvinyl alcohol and conditions of defreezing samples on properties of cryogels obtained." Polymer Science U.S.S.R. 30(8): 1758-1764.

Doocy, S. and Burnham, G. (2006). "Point-of-use water treatment and diarrhoea reduction in the emergency context: An effectiveness trial in Liberia." Tropical Medicine and International Health 11(10): 1542-1552.

Dorea, C. C. (2009). "Coagulant-based emergency water treatment." Desalination 248(1-3): 83-90.

Dorea, C. C., Bertrand, S. and Clarke, B. A. (2006). "Particle separation options for emergency water treatment." Water Science and Technology 53(Compendex): 253-260.

Dorea, C. C. and Clarke, B. A. (2006). "Performance of a water clarifier in Gonaives (Haiti)." Waterlines 24, 22-24.

Dorea, C. C., Bertrand, S. and Clarke, B. A. (2006). "Particle separation options for emergency water treatment." Water Science and Technology 53(Compendex): 253-260.

Doria-Serrano, M. C., Riva-Palacio, G., Ruiz-Treviño, F. A. and Hernández-Esparza, M. (2002). "Poly(n-vinyl pyrrolidone)−calcium alginate (PVP−Va-Alg) composite hydrogels: Physical properties and activated sludge immobilization for wastewater treatment." Industrial and Engineering Chemistry Research 41(13): 3163-3168.

Doube, M., Kłosowski, M. M., Arganda-Carreras, I., Cordelières, F. P., Dougherty, R. P., Jackson, J. S., Schmid, B., Hutchinson, J. R. and Shefelbine, S. J. (2010). "BoneJ: Free and extensible bone image analysis in ImageJ." Bone 47(6): 1076-1079.

Downing, E. A., Coleman, A. J. and Bagwell, T. H. (1994). "US army reverse osmosis membrane research programs." Desalination 99(2-3): 401-408.

Doyle, J. P., Giannouli, P., Martin, E. J., Brooks, M. and Morris, E. R. (2006). "Effect of sugars, galactose content and chainlength on freeze-thaw gelation of galactomannans." Carbohydrate Polymers 64(3): 391-401.

Dragan, E. S. and Apopei, D. F. (2011). "Synthesis and swelling behavior of pH-sensitive semi-interpenetrating polymer network composite hydrogels based on native and modified potatoes starch as potential sorbent for cationic dyes" Chemical Engineering Journal 178: 252-263.

Dragan, E. S., Lazar, M. M., Dinu, M. V. and Doroftei, F. (2012). "Macroporous composite IPN hydrogels based on poly(acrylamide) and chitosan with tuned swelling and sorption of cationic dyes" Chemical Engineering Journal 204-205: 198-209.

Du Preez, M., McGuigan, K. G. and Conroy, R. M. (2010). "Solar disinfection of drinking water in the prevention of dysentery in South African children aged under 5 years: The role of participant motivation." Environmental Science and Technology 44: 8744-8749.

Duffy, E. F., Al Touati, F., Kehoe, S. C., McLoughlin, O. A., Gill, L. W., Gernjak, W., Oller, I., Maldonado, M. I., Malato, S., Cassidy, J., Reed, R. H. and McGuigan, K. G. (2004). "A novel TiO_2-assisted solar photocatalytic batch-process disinfection reactor for the treatment of biological and chemical contaminants in domestic drinking water in developing countries." Solar Energy 77(5): 649-655.

Duke, W., Nordin, R., Baker, D. and Mazumder, A. (2006). "The use and performance of biosand filters in the Artibonite valley of Haiti: A field study of 107 households." Rural and Remote Health 6: Art. 570.

Eboigbodin, K. E. and Biggs, C. A. (2008). "Characterization of the extracellular polymeric substances produced by *Escherichia coli* using infrared spectroscopic, proteomic, and aggregation studies." Biomacromolecules 9(2): 686-695.

Eckhardt, S., Brunetto, P. S., Gagnon, J., Priebe, M., Giese, B. and Fromm, K. M. (2013). "Nanobio silver: Its interactions with peptides and bacteria, and its uses in medicine." Chemical Reviews 113(7): 4708-4754.

Elfil, H., Hamed, A. and Hannachi, A. (2007). "Technical evaluation of a small-scale reverse osmosis desalination unit for domestic water." Desalination 203(1-3): 319-326.

Elliott, M. A., Stauber, C. E., Koksal, F., DiGiano, F. A. and Sobsey, M. D. (2008). "Reductions of *E. coli, Echovirus* type 12 and bacteriophages in an intermittently operated household-scale slow sand filter." Water Research 42(10-11): 2662-2670.

EMDAT (2009). "Disaster trends- trends and relationship period 1900-2010." Available from: http://www.emdat.be/natural-disasters-trends (accessed on 21 July 2011).

Estevez, L., Kelarakis, A., Gong, Q., Da'as, E. H. and Giannelis, E. P. (2011). "Multifunctional graphene/platinum/nafion hybrids via ice templating." Journal of the American Chemical Society 133(16): 6122-6125.

Fabrega, J., Fawcett, S. R., Renshaw, J. C. and Lead, J. R. (2009). "Silver nanoparticle impact on bacterial growth: Effect of pH, concentration, and organic matter." Environmental Science & Technology 43(19): 7285-7290.

Falletta, E., Bonini, M., Fratini, E., Lo Nostro, A., Pesavento, G., Becheri, A., Lo Nostro, P., Canton, P. and Baglioni, P. (2008). "Clusters of poly(acrylates) and silver nanoparticles: Structure and applications for antimicrobial fabrics." The Journal of Physical Chemistry C 112(31): 11758-11766.

Fane, A. G. (1996). "Membranes for water production and wastewater reuse." Desalination 106(1-3): 1-9.

Faruque, S. M., Naser, I. B., Islam, M. J., Faruque, A. S. G., Ghosh, A. N., Nair, G. B., Sack, D. A. and Mekalanos, J. J. (2005). "Seasonal epidemics of cholera inversely correlate with the prevalence of environmental cholera phages." Proceedings of the National Academy of Sciences of the United States of America 102(5): 1702-1707.

Fath, H. E. S., Elsherbiny, S. M., Hassan, A. A., Rommel, M., Wieghaus, M., Koschikowski, J. and Vatansever, M. (2008). "PV and thermally driven small-scale, stand-alone solar desalination systems with very low maintenance needs." Desalination 225(1-3): 58-69.

Fauss, E.K., MacCuspie, R.I., Oyanedel-Craver, V., Smith, J.A. and Swami, N.S. (2014). "Disinfection action of electrostatic versus steric-stabilized silver nanoparticles on *E. coli* under different water chemistries." Colloids and Surfaces B: Biointerfaces 113(0): 77-84.

Feachem, R. E., Bradley, D. J., Garelick, H. and Mara, D. D. (1983), Sanitation and disease: Health aspects excreta and wastewater management, ed., Wiley, New York.

Ferreira, L. and Zumbuehl, A. (2009). "Non-leaching surfaces capable of killing microorganisms on contact." Journal of Materials Chemistry 19(42): 7796-7806.

Fisher, S. and Kunin, R. (1955). "Routine exchange capacity determinations of ion exchange resins." Analytical Chemistry 27(7): 1191-1194.

Foo, K. Y. and Hameed, B. H. (2009). "An overview of landfill leachate treatment via activated carbon adsorption process." Journal of Hazardous Materials 171(1-3): 54-60.

Foo, K. Y. and Hameed, B. H. (2010). "Detoxification of pesticide waste via activated carbon adsorption process." Journal of Hazardous Materials 175(1-3): 1-11.

Frechen, F. B., Exler, H., Romaker, J. and Schier, W. (2011). "Long-term behaviour of a gravity-driven dead end membrane filtration unit for potable water supply in cases of disasters." Water Science and Technology: Water Supply 11(1): 39-44.

Frist, W. H. (2005). "Recovering from the tsunami." New England Journal of Medicine 352(5): 438-438.

Gadgil, A. (1998). "Drinking water in developing countries." Annual Review of Energy and the Environment 23(1): 253-286.

Gangadharan, D., Harshvardan, K., Gnanasekar, G., Dixit, D., Popat, K. M. and Anand, P. S. (2010). "Polymeric microspheres containing silver nanoparticles as a bactericidal agent for water disinfection." Water Research 44(18): 5481-5487.

Gao, J., Youn, S., Hovsepyan, A., Llaneza, V. L., Wang, Y., Bitton, G. and Bonzongo, J.-C. J. (2009). "Dispersion and toxicity of selected manufactured nanomaterials in natural river water samples: Effects of water chemical composition." Environmental Science & Technology 43(9): 3322-3328.

Garsadi, R., Salim, H. T., Soekarno, I., Doppenberg, A. F. J. and Verberk, J. Q. J. C. (2009). "Operational experience with a micro hydraulic mobile water treatment plant in indonesia after the "tsunami of 2004"." Desalination 248(1-3): 91-98.

Gelover, S., Gómez, L. A., Reyes, K. and Teresa Leal, M. (2006). "A practical demonstration of water disinfection using TiO_2 films and sunlight." Water Research 40(17): 3274-3280.

Gerba, C. P. and Naranjo, J. E. (2000). "Microbiological water purification without the use of chemical disinfection." Wilderness Environmental Medicine 11(1): 12-16.

Gerba, C. P., Naranjo, J. E. and Jones, E. L. (2008). "Virus removal from water by a portable water treatment device." Wilderness and Environmental Medicine 19(1): 45-49.

Ghoneyem, A. and Ileri, A. (1997). "Software to analyze solar stills and an experimental study on the effects of the cover." Desalination 114(1): 37-44.

Giannouli, P. and Morris, E. R. (2003). "Cryogelation of xanthan." Food Hydrocolloids 17(4): 495-501.

Gopishetty, V., Tokarev, I. and Minko, S. (2012). "Biocompatible stimuli-responsive hydrogel porous membranes via phase separation of polyvinyl alcohol and alginate intermolecular complex." Journal of Materials Chemistry 22: 19482-19487.

Greenlee, L. F., Lawler, D. F., Freeman, B. D., Marrot, B. and Moulin, P. (2009). "Reverse osmosis desalination: Water sources, technology, and today's challenges." Water Research 43(9): 2317-2348.

Groendijk, L. and de Vries, H. E. (2009). "Development of a mobile water maker, a sustainable way to produce safe drinking water in developing countries." Desalination 248(1-3): 106-113.

Gupta, A., Maynes, M. and Silver, S. (1998). "Effects of halides on plasmid-mediated silver resistance in *Escherichia coli*." Applied and Environmental Microbiology 64(12): 5042-5045.

Gupta, S. K., Islam, M. S., Johnston, R., Ram, P. K. and Luby, S. P. (2008). "The Chulli water purifier: Acceptability and effectiveness of an innovative strategy for household water treatment in Bangladesh." The American Journal of Tropical Medicine and Hygiene 78(6): 979-984.

Gupta, S., Suantio, A., Gray, A., Widyastuti, E., Jain, N., Rolos, R., Hoekstra, R. and Quick, R. (2007). "Factors associated with the *E. coli* contamination of household drinking water among tsunami and earthquake survivors, Indonesia." The American Journal of Tropical Medicine and Hygiene 76(6): 1158-1162.

Gupta, S. K., Islam, M. S., Johnston, R., Ram, P. K. and Luby, S. P. (2008). "The Chulli water purifier: Acceptability and effectiveness of an innovative strategy for household water treatment in Bangladesh." The American Journal of Tropical Medicine & Hygiene 78(6): 979-984.

Gutiérrez, M. C., Ferrer, M. L. and del Monte, F. (2008). "Ice-templated materials: Sophisticated structures exhibiting enhanced functionalities obtained after unidirectional freezing and ice-segregation-induced self-assembly." Chemistry of Materials 20(3): 634-648.

Gutiérrez, M. C., García-Carvajal, Z. Y., Jobbágy, M., Rubio, F., Yuste, L., Rojo, F., Ferrer, M. L. and Del Monte, F. (2007). "Poly(vinyl alcohol) scaffolds with tailored morphologies for drug delivery and controlled release." Advanced Functional Materials 17(17): 3505-3513.

Gutteridge, J. M. C. and Halliwell, B. (1990). "The measurement and mechanism of lipid peroxidation in biological systems." Trends in Biochemical Sciences 15(4), 129-135.

Haefeli C., Franklin C. and Hardy K. (1984). "Plasmid-determined silver resistance in *Pseudomonas stutzeri* isolated from a silver mine." Journal of Bacteriology **158**: 389-392.

Hajizadeh, S., Kirsebom, H. and Mattiasson, B. (2010). "Characterization of macroporous carbon-cryostructured particle gel, an adsorbent for small organic molecules." Soft Matter 6(21): 5562-5569.

Hamthamrongwit, M., Wilkinson, R., Osborne, C., Reid, W. H. and Grant, M. H. (1996). "Confocal laser-scanning microscopy for determining the structure of and keratinocyte infiltration through collagen sponges." Journal of Biomedical Materials Research 30): 331-339.

Hanson, A., Zachritz, W., Stevens, K., Mimbela, L., Polka, R. and Cisneros, L. (2004). "Distillate water quality of a single-basin solar still: Laboratory and field studies." Solar Energy 76(5): 635-645.

Harris, C. (2000). "Modular desalting for specialized applications." Desalination 132(1-3): 269-274.

He, D., Dorantes-Aranda, J. J. and Waite, T. D. (2012a). "Silver nanoparticle—algae interactions: Oxidative dissolution, reactive oxygen species generation and synergistic toxic effects." Environmental Science & Technology 46(16): 8731-8738.

He, D., Garg, S. and Waite, T. D. (2012b). "H_2O_2-mediated oxidation of zero-valent silver and resultant interactions among silver nanoparticles, silver ions, and reactive oxygen species." Langmuir 28(27): 10266-10275.

He, D., Ikeda-Ohno, A., Boland, D. D. and Waite, T. D. (2013). "Synthesis and characterization of antibacterial silver nanoparticle-impregnated rice husks and rice husk ash." Environmental Science & Technology 47(10): 5276-5284.

He, D., Miller, C. J. and Waite, T. D. (2014). "Fenton-like zero-valent silver nanoparticle-mediated hydroxyl radical production." Journal of Catalysis 317(0), 198-205.

He, W., Zhou, Y.-T., Wamer, W. G., Boudreau, M. D. and Yin, J.-J. (2012c). "Mechanisms of the pH dependent generation of hydroxyl radicals and oxygen induced by Ag nanoparticles." Biomaterials 33(30): 7547-7555.

He, X., Yao, K., Shen, S. and Yun, J. (2007). "Freezing characteristics of acrylamide-based aqueous solution used for the preparation of supermacroporous cryogels via cryo-copolymerization." Chemical Engineering Science 62(5): 1334-1342.

He, Y. (2009). "Transportable membrane system produces drinking water." Membrane Technology 2009(8): 8-9.

Hedström, M., Plieva, F., Galaev, I. and Mattiasson, B. (2008). "Monolithic macroporous albumin/chitosan cryogel structure: A new matrix for enzyme immobilization." Analytical and Bioanalytical Chemistry 390(3): 907-912.

Henglein, A. (1993). "Physicochemical properties of small metal particles in solution: "Microelectrode" reactions, chemisorption, composite metal particles, and the atom-to-metal transition." The Journal of Physical Chemistry 97(21): 5457-5471.

Henglein, A. (1998). "Colloidal silver nanoparticles: Photochemical preparation and interaction with O_2, CCl_4, and some metal ions." Chemistry of Materials 10(1), 444-450.

Hernández, R., Sarafian, A., López, D. and Mijangos, C. (2004). "Viscoelastic properties of poly(vinyl alcohol) hydrogels and ferrogels obtained through freezing-thawing cycles." Polymer 45(16): 5543-5549.

Herold, D. and Neskakis, A. (2001). "A small PV-driven reverse osmosis desalination plant on the island of Gran Canaria." Desalination 137(1-3): 285-292.

Herold, D., Horstmann, V., Neskakis, A., Plettner-Marliani, J., Piernavieja, G. and Calero, R. (1998). "Small scale photovoltaic desalination for rural water supply - demonstration plant in Gran Canaria." Renewable Energy 14(1-4): 293-298.

Hindiyeh, M. and Ali, A. (2010). "Investigating the efficiency of solar energy system for drinking water disinfection." Desalination 259(1-3): 208-215.

Ho, M.-H., Kuo, P.-Y., Hsieh, H.-J., Hsien, T.-Y., Hou, L.-T., Lai, J.-Y. and Wang, D.-M. (2004). "Preparation of porous scaffolds by using freeze-extraction and freeze-gelation methods." Biomaterials 25(1): 129-138.

Ho, S. T. and Hutmacher, D. W. (2006). "A comparison of microCT with other techniques used in the characterization of scaffolds." Biomaterials 27(8): 1362-1376.

Hoflund, G., Hazos, Z. and Salaita, G. (2000). "Surface characterization study of Ag, AgO, and Ag_2O using X-ray photoelectron spectroscopy and electron energy-loss spectroscopy." Physical Review B 62(16): 11126-11133.

Holland S. L., Dyer P. S., Bond C. J., James S. A. , Roberts I. N. and Avery S. V. (2011). *Candida argentea* sp. nov., a copper and silver resistant yeast species. Fungal Biology 115: 909–918.

Holloway, R. W., Childress, A. E., Dennett, K. E. and Cath, T. Y. (2007). "Forward osmosis for concentration of anaerobic digester centrate." Water Research 41(17): 4005-4014.

Holt, K. B. and Bard, A. J. (2005). "Interaction of silver(i) ions with the respiratory chain of *Escherichia coli*: An electrochemical and scanning electrochemical microscopy study of the antimicrobial mechanism of micromolar Ag^+." Biochemistry 44(39): 13214-13223.

Hong, R., Kang, T. Y., Michels, C. A. and Gadura, N. (2012). "Membrane lipid peroxidation in copper alloy-mediated contact killing of *Escherichia coli*." Applied and Environmental Microbiology 78(6): 1776-1784.

Hong, Y. and Brown, D.G. (2009). "Variation in bacterial ATP level and proton motive force due to adhesion to a solid surface." Applied and Environmental Microbiology 75(8): 2346-2353.

Höpfner, J., Klein, C. and Wilhelm, M. (2010). "A novel approach for the desalination of seawater by means of reusable poly(acrylic acid) hydrogels and mechanical force." Macromolecular Rapid Communications 31(15): 1337-1342.

Hou, W.-C., Stuart, B., Howes, R. and Zepp, R. G. (2013). "Sunlight-driven reduction of silver ions by natural organic matter: Formation and transformation of silver nanoparticles." Environmental Science & Technology 47(14): 7713-7721.

Hsieh, C.-Y., Tsai, S.-P., Ho, M.-H., Wang, D.-M., Liu, C.-E., Hsieh, C.-H., Tseng, H.-C. and Hsieh, H.-J. (2007). "Analysis of freeze-gelation and cross-linking processes for preparing porous chitosan scaffolds." Carbohydrate Polymers 67(1): 124-132.

Hsiue, G.-H., Pung, L.-S., Chu, M.-L. and Shieh, M.-C. (1989). "Treatment of uranium effluent by reverse osmosis membrane." Desalination 71(1): 35-44.

HTI (2010a). "Hydropack: The simplest way to prepare water for emergencies." Available from: http://www.htiwater.com/hydropack.html?Vl=6&tp=2 (accessed on 9 April 2011).

Huang, Y., Zeng, M., Ren, J., Wang, J., Fan, L. and Xu, Q. (2012). "Preparation and swelling properties of graphene oxide/poly(acrylic acid-co-acrylamide) super-absorbent hydrogel nanocomposites." Colloids and Surfaces A: Physicochemical and Engineering Aspects 401: 97-106.

Huikuri, P., Salonen, L. and Raff, O. (1998). "Removal of natural radionuclides from drinking water by point of entry reverse osmosis." Desalination 119(1-3): 235-239.

Huynh, K.A. and Chen, K.L. (2011). "Aggregation kinetics of citrate and polyvinylpyrrolidone coated silver nanoparticles in monovalent and divalent electrolyte solutions." Environmental Science & Technology 45(13): 5564-5571.

Hwang, T., Sangaj, N. and Varghese, S. (2010). "Interconnected macroporous poly(ethylene glycol) cryogels as a cell scaffold for cartilage tissue engineering." Tissue Engineering: Part A 16: 3033-3041.

Hwang, Y., Zhang, C. and Varghese, S. (2010). "Poly(ethylene glycol) cryogels as potential cell scaffolds: Effect of polymerization conditions on cryogel microstructure and properties." Journal of Materials Chemistry 20(2): 345-351.

I. Lozinsky, V. (1998). "Cryotropic gelation of poly(vinyl alcohol) solutions." Russian Chemical Reviews 67(7): 573-586.

I. Lozinsky, V. (2002). "Cryogels on the basis of natural and synthetic polymers: Preparation, properties and application." Russian Chemical Reviews 71(6): 489-511.

Islam, M. F. and Johnston, R. B. (2006). "Household pasteurization of drinking-water: The chulli water-treatment system." Journal of Health Population and Nutrition 24(3): 356-362.

Ivask, A., ElBadawy, A., Kaweeteerawat, C., Boren, D., Fischer, H., Ji, Z., Chang, C. H., Liu, R., Tolaymat, T., Telesca, D., Zink, J. I., Cohen, Y., Holden, P. A. and Godwin, H. A. (2013). "Toxicity mechanisms in *Escherichia coli* vary for silver nanoparticles and differ from ionic silver." ACS Nano 8(1): 374-386.

Ives, K. (1968). "Theory of operation of sludge blanket clarifiers." Proceedings Institution of Civil Engineers 39: 243-260.

Jain, E., Srivastava, A. and Kumar, A. (2009). "Macroporous interpenetrating cryogel network of poly(acrylonitrile) and gelatin for biomedical applications." Journal of Materials Science: Materials in Medicine 20: S173-S179.

Jain, P. and Pradeep, T. (2005). "Potential of silver nanoparticle-coated polyurethane foam as an antibacterial water filter." Biotechnology and Bioengineering 90(1): 59-63.

Jain, S., Sahanoon, O. K., Blanton, E., Schmitz, A., Wannemuehler, K. A., Hoekstra, R. M. and Quick, R. E. (2010). "Sodium dichloroisocyanurate tablets for routine treatment of household drinking water in periurban Ghana: A randomized

controlled trial." The American Journal of Tropical Medicine and Hygiene 82(1): 16-22.

Jana, N.R., Gearheart, L. and Murphy, C.J. (2001). "Wet chemical synthesis of silver nanorods and nanowires of controllable aspect ratio." Chemical Communications (7): 617-618.

Jelenko C. (1969). "Silver nitrate resistant *E. coli*: report of case." Annual Surgery 170: 296–299.

Jill, B., Susan, M. and Majid, E. (2007). "Reconsidering 'appropriate technology': The effects of operating conditions on the bacterial removal performance of two household drinking-water filter systems." Environmental Research Letters 2(2): 024003.

Jin, R., Cao, Y., Mirkin, C. A., Kelly, K. L., Schatz, G. C. and Zheng, J. G. (2001). "Photoinduced conversion of silver nanospheres to nanoprisms." Science 294(5548), 1901-1903.

Jin, X., Li, M., Wang, J., Marambio-Jones, C., Peng, F., Huang, X., Damoiseaux, R. and Hoek, E. M. V. (2010). "High-throughput screening of silver nanoparticle stability and bacterial inactivation in aquatic media: Influence of specific ions." Environmental Science & Technology 44(19): 7321-7328.

John A Crump, P. O. O., Laurence Slutsker, Bruce H Keswick, Daniel H Rosen, R Michael Hoekstra, John M Vulule, Stephen P Luby (2005). "Household based treatment of drinking water with flocculant-disinfectant for preventing diarrhoea in areas with turbid source water in rural western Kenya: Cluster randomised controlled trial. BMJ, doi:10.1136/bmj.38512.618681.E0. Available online from http://www.bmj.com/content/331/7515/478.long.").

Johnson, W., Makame, Y. M. M. and Mkayula, L. L. (2011). "Monolithic hydrophilic poly(epoxy-acrylamide) cryogels: Effect of monomer concentration on cryogel's pore structure and properties." Tanzania Journal of Natural and Applied Sciences 2: 238-250.

Johnston, M. D., Johnston, R. J. W., Hanlon, G. W. and Denyer, S. P. (2002). "A rapid method for assessing the suitability of quenching agents for individual biocides as well as combinations." Journal of Applied Microbiology 92(4): 784-789.

Jung, W. K., Koo, H. C., Kim, K. W., Shin, S., Kim, S. H. and Park, Y. H. (2008). "Antibacterial activity and mechanism of action of the silver ion in *Staphylococcus aureus* and *Escherichia coli*." Applied and Environmental Microbiology 74(7): 2171-2178.

Junkins, A. and Doyle, M. (1992). "Demonstration of exopolysaccharide production by *Enterohemorrhagicescherichia coli*." Current Microbiology 25(1): 9-17.

Juven, B.J. and Pierson, M.D. (1996). "Antibacterial effects of hydrogen peroxide and methods for its detection and quantitation." Journal of Food Protection 59(11): 1233-1241.

Kabeel, A. E. and El-Agouz, S. A. (2011). "Review of researches and developments on solar stills." Desalination 276(1-3): 1-12.

Kabiri, K., Omidian, H., Hashemi, S. A. and Zohuriaan-Mehr, M. J. (2003). "Synthesis of fast-swelling superabsorbent hydrogels: Effect of crosslinker type and concentration on porosity and absorption rate." European Polymer Journal 39(7): 1341-1348.

Kahveci, M. U., Beyazkilic, Z. and Yaggi, Y. (2010). "Polyacrylamide cryogels by photoinitiated free radical polymerization." Journal of Polymer Science: Part A: Polymer Chemistry 48): 4989-4994.

Kang, G., Roy, S. and Balraj, V. (2006). "Appropriate technology for rural India - solar decontamination of water for emergency settings and small communities." Transactions of the Royal Society of Tropical Medicine and Hygiene 100(9): 863-866.

Karakutuk, I. and Okay, O. (2010). "Macroporous rubber gels as reusable sorbents for the removal of oil from surface waters." Reactive and Functional Polymers 70(9): 585-595.

Katadyn (2011). "Katadyn mini." Available from: http://www.Katadyn.Com/sgen/katadyn-products/products/katadynshopconnect/katadyn-wasserfilter-ultralight-series-produkte/katadyn-mini/ (accessed on 13 April 2011).

Kathuria, N., Tripathi, A., Kar, K. K. and Kumar, A. (2009). "Synthesis and characterization of elastic and macroporous chitosan-gelatin cryogels for tissue engineering." Acta Biomaterialia 5(1): 406-418.

Kaushal, A. and Varun (2010). "Solar stills: A review." Renewable and Sustainable Energy Reviews 14(1): 446-453.

Kemal, E., Adesanya, K. O. and Deb, S. (2011). "Phosphate based 2-hydroxyethyl methacrylate hydrogels for biomedical applications." Journal of Materials Chemistry 21(7): 2237-2245.

Kennedy, A. J., Chappell, M. A., Bednar, A. J., Ryan, A. C., Laird, J. G., Stanley, J. K. and Steevens, J. A. (2012). "Impact of organic carbon on the stability and toxicity of fresh and stored silver nanoparticles." Environmental Science & Technology 46(19), 10772-10780.

Kirsebom, H. and Mattiasson, B. (2011). "Cryostructuration as a tool for preparing highly porous polymer materials." Polymer Chemistry 2(5): 1059-1062.

Kirsebom, H., Aguilar, M. R., San Roman, J., Fernandez, M., Prieto, M. A. and Bondar, B. (2007). "Macroporous scaffolds based on chitosan and bioactive molecules." Journal of Bioactive and Compatible Polymers 22(6): 621-636.

Kirsebom, H., Mattiasson, B. and Galaev, I. Y. (2009a). "Building macroporous materials from microgels and microbes via one-step cryogelation." Langmuir 25(15): 8462-8465.

Kirsebom, H., Rata, G., Topgaard, D., Mattiasson, B. and Galaev, I. Y. (2008). "In situ ^{1}H NMR studies of free radical cryopolymerization." Polymer 49(18): 3855-3858.

Kirsebom, H., Rata, G., Topgaard, D., Mattiasson, B. and Galaev, I. Y. (2009b). "Mechanism of cryopolymerization: Diffusion-controlled polymerization in a nonfrozen microphase. An NMR study." Macromolecules 42(14): 5208-5214.

Kirsebom, H., Topgaard, D., Galaev, I. Y. and Mattiasson, B. (2010). "Modulating the porosity of cryogels by influencing the nonfrozen liquid phase through the addition of inert solutes." Langmuir 26(20): 16129-16133.

Kittler, S., Greulich, C., Diendorf, J., Köller, M. and Epple, M. (2010). "Toxicity of silver nanoparticles increases during storage because of slow dissolution under release of silver ions." Chemistry of Materials 22(16): 4548-4554.

Klibanov, A. M. (2007). "Permanently microbiocidal materials coatings." Journal of Materials Chemistry 17(24): 2479-2482.

Koch, A. L. (1986). "The pH in the neighborhood of membranes generating a proton motive force." Journal of Theoretical Biology 120(1): 73-84.

Konieczny, K. and Klomfas, G. (2002). "Using activated carbon to improve natural water treatment by porous membranes." Desalination 147(1-3): 109-116.

Kostova, B., Momekova, D., Petrov, P., Momekov, G., Toncheva-Moncheva, N., Tsvetanov, C. B. and Lambov, N. (2011). "Poly(ethoxytriethyleneglycol acrylate)

cryogels as novel sustained drug release systems for oral application." Polymer 52(5): 1217-1222.

Kozlovskaya, V., Kharlampieva, E., Chang, S., Muhlbauer, R. and Tsukruk, V.V. (2009). "pH-responsive layered hydrogel microcapsules as gold nanoreactors." Chemistry of Materials 21(10): 2158-2167.

Kramer, K. J. M., Jak, R. G., van Hattum, B., Hooftman, R. N. and Zwolsman, J. J. G. (2004). "Copper toxicity in relation to surface water-dissolved organic matter: Biological effects to *Daphnia magna*." Environmental Toxicology and Chemistry 23(12): 2971-2980.

Krasner, S. W. and Wright, J. M. (2005). "The effect of boiling water on disinfection by-product exposure." Water Research 39(5): 855-864.

Kremer A. N. and Hoffmann H. (2012). "Subtractive hybridization yields a silver resistance determinant unique to nosocomial pathogens in the Enterobacter cloacae complex." Journal of Clinical Microbiology 50: 3249–3257.

Krishnamoorthy, K., Veerapandian, M., Zhang, L.-H., Yun, K. and Kim, S. J. (2012). "Antibacterial efficiency of graphene nanosheets against pathogenic bacteria via lipid peroxidation." The Journal of Physical Chemistry C 116(32): 17280-17287.

Kueseng, P., Thammakhet, C., Thavarungkul, P. and Kanatharana, P. (2010). "Multiwalled carbon nanotubes/cryogel composite, a new sorbent for determination of trace polycyclic aromatic hydrocarbons." Microchemical Journal 96(2): 317-323.

Kwon, S.-M., Kim, H.-S. and Jin, H.-J. (2009). "Multiwalled carbon nanotube cryogels with aligned and non-aligned porous structures." Polymer 50(13): 2786-2792.

Labas, M. D., Zalazar, C. S., Brandi, R. J. and Cassano, A. E., 2008. Reaction kinetics of bacteria disinfection employing hydrogen peroxide. Biochemical Engineering Journal 38(1), 78-87.

Lai, H. L., Abu'Khalil, A. and Craig, D. Q. M. (2003). "The preparation and characterisation of drug-loaded alginate and chitosan sponges." International Journal of Pharmaceutics 251(1-2): 175-181.

Laîné, J. M., Vial, D. and Moulart, P. (2000). "Status after 10 years of operation -- overview of UF technology today." Desalination 131(1-3): 17-25.

Lambert, R. J., Johnston, M. D., and Simons, E. A. (1998). "Disinfectant testing: Use of the bioscreen microbiological growth analyser for laboratory biocide screening." Letters in Applied Microbiology 26(4): 288-292.

Lampe, H., Altmann, T. and Gätjens, H. J. (1997). "PCS - Preussag conversion system® mobile floating seawater desalination plant." Desalination 114(2): 145-151.

Lantagne, D. S. and Clasen, T. (2009). "Point of use water treatment in emergency response. London school of hygience and tropical medicine. London, UK." Available from: www.ehproject.org/pdf/ehkm/lantagne-pou_emergencies2009.pdf.

Lantagne, D. S., B.C, B., Cardinali, F. and Quick, R. (2008). "Disinfection by-product formation and mitigation strategies in point-of-use chlorination of turbid and non-turbid waters in western Kenya." Journal of Water and Health 6(1): 6782.

Lantagne, D. S., Cardinali, F. and Blount, B. C. (2010). "Disinfection by-product formation and mitigation strategies in point-of-use chlorination with sodium dichloroisocyanurate in Tanzania." The American Journal of Tropical Medicine and Hygiene 83(1): 135-143.

Latch, D. E. and McNeill, K. (2006). "Microheterogeneity of singlet oxygen distributions in irradiated humic acid solutions." Science 311(5768): 1743-1747.

Lazaridou, A. and Biliaderis, C. G. (2004). "Cryogelation of cereal β-glucans: Structure and molecular size effects." Food Hydrocolloids 18(6): 933-947.

Lazaridou, A., Vaikousi, H. and Biliaderis, C. G. (2008). "Effects of polyols on cryostructurization of barley β -glucans." Food Hydrocolloids 22(2): 263-277.

Le Noir, M., Plieva, F., Hey, T., Guieysse, B. and Mattiasson, B. (2007). "Macroporous molecularly imprinted polymer/cryogel composite systems for the removal of endocrine disrupting trace contaminants." Journal of Chromatography A 1154(1–2): 158-164.

LeChevallier, M. W., Evans, T. M. and Seidler, R. J. (1981). "Effect of turbidity on chlorination efficiency and bacterial persistence in drinking water." Applied Environmental Microbioliology 42(1): 159-167.

Lee, E. K., Chen, V. and Fane, A. G. (2008). "Natural organic matter (NOM) fouling in low pressure membrane filtration - Effect of membranes and operation modes." Desalination 218(1-3): 257-270.

Lee, J. and Deng, Y. (2011). "The morphology and mechanical properties of layer structured cellulose microfibril foams from ice-templating methods." Soft Matter 7(13): 6034-6040.

Lee, W.-F. and Huang, Y.-C. (2007). "Swelling and antibacterial properties for the superabsorbent hydrogels containing silver nanoparticles." Journal of Applied Polymer Science 106(3): 1992-1999.

Lemire, J. A., Harrison, J. J. and Turner, R. J. (2013). "Antimicrobial activity of metals: Mechanisms, molecular targets and applications." Nature Reviews Microbiology 11(6): 371-384.

Levard, C., Hotze, E. M., Lowry, G. V. and Brown, G. E. (2012). "Environmental transformations of silver nanoparticles: Impact on stability and toxicity." Environmental Science & Technology 46(13): 6900-6914.

Levard, C., Mitra, S., Yang, T., Jew, A. D., Badireddy, A. R., Lowry, G. V. and Brown, G. E. (2013). "Effect of chloride on the dissolution rate of silver nanoparticles and toxicity to *E. coli*." Environmental Science & Technology 47(11): 5738-5745.

Li, D., Zhang, X., Yao, J., Simon, G. P. and Wang, H. (2011a). "Stimuli-responsive polymer hydrogels as a new class of draw agent for forward osmosis desalination." Chemical Communications 47(6): 1710-1712.

Li, D., Zhang, X., Yao, J., Zeng, Y., Simon, G. P. and Wang, H. (2011b). "Composite polymer hydrogels as draw agents in forward osmosis and solar dewatering." Soft Matter 7(21): 10048-10056.

Li, Q., Mahendra, S., Lyon, D. Y., Brunet, L., Liga, M. V., Li, D. and Alvarez, P. J. J. (2008). "Antimicrobial nanomaterials for water disinfection and microbial control: Potential applications and implications." Water Research 42(18): 4591-4602.

Li, X., Lenhart, J. J. and Walker, H. W. (2010). "Dissolution-accompanied aggregation kinetics of silver nanoparticles." Langmuir 26(22): 16690-16698.

Liang, Y. N., Hu, J., Tam, M. K. C. and Hu, X. (2012). "CuO_x nanotubes via an unusual complexation induced block copolymer-like self-assembly of poly(acrylic acid)." RSC Advances 2(25): 9531-9537.

Liau, S. Y., Read, D. C., Pugh, W. J., Furr, J. R. and Russell, A. D. (1997). "Interaction of silver nitrate with readily identifiable groups: Relationship to the antibacterial action of silver ions." Letters in Applied Microbiology 25(4): 279-283.

LifeStraw (2007). "Summary of test data received from the University of North Carolina School of Public Health, Department of Environmental Sciences and Engineering."Available from: http://www.lifestraw.com.br/ls-p-testresult.pdf.

Lin, A. S. P., Barrows, T. H., Cartmell, S. H. and Guldberg, R. E. (2003). "Microarchitectural and mechanical characterization of oriented porous polymer scaffolds." Biomaterials 24(3): 481-489.

Lin, S., Huang, R., Cheng, Y., Liu, J., Lau, B. L. T. and Wiesner, M. R. (2013). "Silver nanoparticle-alginate composite beads for point-of-use drinking water disinfection." Water Research 47(12): 3959-3965.

Liu, C., Wei, N., Wang, S. and Xu, Y. (2009). "Preparation and characterization superporous hydroxypropyl methylcellulose gel beads." Carbohydrate Polymers 78(1): 1-4.

Liu, C., Xie, X., Zhao, W., Liu, N., Maraccini, P. A., Sassoubre, L. M., Boehm, A. B. and Cui, Y. (2013). "Conducting nanosponge electroporation for affordable and high-efficiency disinfection of bacteria and viruses in water." Nano Letters 13(9): 4288-4293.

Liu, J. and Hurt, R. H. (2010). "Ion release kinetics and particle persistence in aqueous nano-silver colloids." Environmental Science & Technology 44(6): 2169-2175.

Liu, J., Sonshine, D. A., Shervani, S. and Hurt, R. H. (2010a). "Controlled release of biologically active silver from nanosilver surfaces." ACS Nano 4(11): 6903-6913.

Liu, J., Wang, Z., Liu, F. D., Kane, A. B. and Hurt, R. H. (2012). "Chemical transformations of nanosilver in biological environments." ACS Nano 6(11): 9887-9899.

Liu, R., Liang, S., Tang, X.-Z., Yan, D., Li, X. and Yu, Z.-Z. (2012). "Tough and highly stretchable graphene oxide/polyacrylamide nanocomposite hydrogels." Journal of Materials Chemistry 22(28): 14160-14167.

Liu, S., Wei, L., Hao, L., Fang, N., Chang, M. W., Xu, R., Yang, Y. and Chen, Y. (2009b). "Sharper and faster "nano darts" kill more bacteria: A study of antibacterial activity of individually dispersed pristine single-walled carbon nanotube." ACS Nano 3(12): 3891-3902.

Liu, X., Jin, X., Cao, B. and Tang, C.Y. (2014). "Bactericidal activity of silver nanoparticles in environmentally relevant freshwater matrices: Influences of organic matter and chelating agent." Journal of Environmental Chemical Engineering 2(1): 525-531.

Liu, Y., Chidambaram, D., Collazo, L., Grella, R., Anyene, I., Genova, W., Herrera, L. and Rafailovich, M. (2010). "Functional polymer hydrogels for water purification applications." NSTI-Nanotech 3: 520-523.

Livermore D. M. (1992). "Interplay of impermeability and chromosomal betalactamase activity in imipenem-resistant *Pseudomonas aeruginosa*." Antimicrobial Agents and Chemotherapy **36(9)**: 2046-2048.

Lok, C.-N., Ho, C.-M., Chen, R., He, Q.-Y., Yu, W.-Y., Sun, H., Tam, P.-H., Chiu, J.-F. and Che, C.-M. (2007). "Silver nanoparticles: Partial oxidation and antibacterial activities." JBIC Journal of Biological Inorganic Chemistry 12(4): 527-534.

Lougheed, T. (2006). "A clear solution for dirty water." Environment Health Perspectives 114(7): A424-A427.

Lozinsky, V. I. (2008). "Polymeric cryogels as a new family of macroporous and supermacroporous materials for biotechnological purposes." Russian Chemical Bulletin 57(5): 1015-1032.

Lozinsky, V. I. (1998). "Cryotropic gelation of poly(vinyl alcohol) solutions." Russian Chemical Reviews 67): 573-586.

Lozinsky, V. I. (2002). "Cryogels on the basis of natural and synthetic polymers: Preparation, properties and applications." Russian Chemical Reviews 71(6): 489-511.

Lozinsky, V. I. (2014). "Polymeric cryogels: Macroporous gels with remarkable properties." Okay, O. (ed), pp. 1-48, Springer International Publishing, Cham.

Lozinsky, V. I. and Damshkaln, L. G. (2003). "Polymeric composition for the preparation of poly(vinyl alcohol) cryogel. Russia patent (application number 2003-131705).

Lozinsky, V. I., Galaev, I. Y., Plieva, F. M., Savina, I. N., Jungvid, H. and Mattiasson, B. (2003). "Polymeric cryogels as promising materials of biotechnological interest." Trends in Biotechnology 21(10): 445-451.

Lozinsky, V. I., Zubov, A. L. and Titova, E. F. (1996). "Swelling behavior of poly(vinyl alcohol) cryogels employed as matrices for cell immobilization." Enzyme and Microbial Technology 18(8): 561-569.

Lozinsky, V., Plieva, F., Galaev, I. and Mattiasson, B. (2001). "The potential of polymeric cryogels in bioseparation." Bioseparation 10(4): 163-188.

Madaeni, S. S. (1999). "The application of membrane technology for water disinfection." Water Research 33(2): 301-308.

Madani, A. A. and Zaki, G. M. (1995). "Yield of solar stills with porous basins." Applied Energy 52(2-3): 273-281.

Magrí, A., Vanotti, M. B. and Szögi, A. A. (2012). "Anammox sludge immobilized in polyvinyl alcohol (PVA) cryogel carriers." Bioresource Technology 114(0): 231-240.

Mahmood, Q., Baig, S. A., Nawab, B., Shafqat, M. N., Pervez, A. and Zeb, B. S. (2011). "Development of low cost household drinking water treatment system for the earthquake affected communities in northern Pakistan." Desalination 273(2-3): 316-320.

Malik, A. L. A., Younan, N. G., Rao, B. J. R. and Mousa, K. M. (1989). "Skid mounted mobile brackish water reverse osmosis plants at different sites in Kuwait." Desalination 75: 341-361.

Maness, P.-C., Smolinski, S., Blake, D.M., Huang, Z., Wolfrum, E.J. and Jacoby, W.A. (1999). "Bactericidal activity of photocatalytic TiO_2 reaction: Toward an understanding of its killing mechanism." Applied and Environmental Microbiology 65(9): 4094-4098.

Masson, L., Richards, B. S. and Schäfer, A. I. (2005). "System design and performance testing of a hybrid membrane -- photovoltaic desalination system." Desalination 179(1-3): 51-59.

Mather, M. L., Morgan, S. P., White, L. J., Tai, H., Kockenberger, W., Howdle, S. M., Shakesheff, K. M. and Crowe, J. A. (2008). "Image-based characterization of foamed polymeric tissue scaffolds." Biomedical Materials 3: 1-11.

Matsumoto, M. and Inoue, K. (2011). "Editorial: Earthquake, tsunami, radiation leak, and crisis in rural health in japan." Rural and Remote Health 11(1759): 1-3.

Mäusezahl, D., Christen, A., Pacheco, G. D., Tellez, F. A., Iriarte, M., Zapata, M. E., Cevallos, M., Hattendorf, J., Cattaneo, M. D., Arnold, B., Smith, T. A. and Colford, J. M., Jr. (2009). "Solar drinking water disinfection (SODIS) to reduce childhood diarrhoea in rural Bolivia: A cluster-randomized, controlled trial." PLoS Med 6(8): e1000125.

Mazumdar, N., Chikindas, M. L. and Uhrich, K. (2010). "Slow release polymer-iodine tablets for disinfection of untreated surface water." Journal of Applied Polymer Science 117): 329-334.

McBean, E. A. (2009). "Evaluation of a bicycle-powered filtration system for removing 'clumped' coliform bacteria as a low-tech option for water treatment." Desalination 248(1-3): 138-143.

McCarthy, J. J., Canziani, O. F., Leary, N. A., Dokken, D. J. and White, K. S. (2001). "Climate change 2001: Impacts, adaptation, and vulnerability. Contribution of working group II to the third assessment report of the intergovernmental panel on climate change." Cambridge University Press. Available from: http://www.grida.no/publications/other/ipcc_tar/.

McGuigan, K. G., Méndez-Hermida, F., Castro-Hermida, J. A., Ares-Mazás, E., Kehoe, S. C., Boyle, M., Sichel, C., Fernández-Ibáñez, P., Meyer, B. P., Ramalingham, S. and Meyer, E. A. (2006). "Batch solar disinfection inactivates oocysts of *Cryptosporidium Parvum* and cysts of *Giardia Muris* in drinking water." Journal of Applied Microbiology 101(2): 453-463.

McLennan, S. D., Peterson, L. A. and Rose, J. B. (2009). "Comparison of point-of-use technologies for emergency disinfection of sewage-contaminated drinking water." Applied Environmental Microbiology 75(22): 7283-7286.

Meierhofer, R. and Landolt, G. (2009). "Factors supporting the sustained use of solar water disinfection -- experiences from a global promotion and dissemination programme." Desalination 248(1-3): 144-151.

Mendez-Hermida, F., Castro-Hermida, J. A., Ares-Mazas, E., Kehoe, S. C. and McGuigan, K. G. (2005). "Effect of batch-process solar disinfection on survival of *Cryptosporidium parvum* oocysts in drinking water." Applied Environmental Microbiology 71(3): 1653-1654.

Messner, K. R. and Imlay, J. A. (1999). "The identification of primary sites of superoxide and hydrogen peroxide formation in the aerobic respiratory chain and sulfite reductase complex of *Escherichia coli*." Journal of Biological Chemistry 274(15): 10119-10128.

Meyer, V. and Reed, R. H. (2001). "SOLAIR disinfection of coliform bacteria in hand-drawn drinking water." Water South Africa 27(1): 49-52.

Mikhalovsky, S.V., Savina, I.N., Dainiak, M., Ivanov, A.E. and Galaev, I.Y. (2011) Comprehensive biotechnology (second edition). Editor-in-Chief: Murray, M.-Y. (ed), pp. 11-22, Academic Press, Burlington.

Mohan, D. and Pittman Jr, C. U. (2006). "Activated carbons and low cost adsorbents for remediation of tri- and hexavalent chromium from water." Journal of Hazardous Materials 137(2): 762-811.

Mopper, K. and Zhou, X. (1990). "Hydroxyl radical photoproduction in the sea and its potential impact on marine processes." Science 250(4981): 661-664.

Mopper, K., Zhou, X., Kieber, R. J., Kieber, D. J., Sikorski, R. J. and Jones, R. D. (1991). "Photochemical degradation of dissolved organic carbon and its impact on the oceanic carbon cycle." Nature 353(6339): 60-62.

Morales, J., Sánchez, L., Martín, F., Ramos-Barrado, J. R. and Sánchez, M. (2004). "Synthesis, characterization, and electrochemical properties of nanocrystalline silver thin films obtained by spray pyrolysis." Journal of The Electrochemical Society 151(1): A151-A157.

Morones, J. R., Elechiguerra, J. L., Camacho, A., Holt, K., Kouri, J. B., Ramírez, J. T. and Yacaman, M. J. (2005). "The bactericidal effect of silver nanoparticles." Nanotechnology 16(10): 2346.

Moulder, J. F., Stickle, W. F., Sobol, P. E. and Bomben, K. D. (1992) Handbook of X-ray photoelectron spectroscopy Eden Prairie, MN Perkin Elmer.

Mthombeni, N. H., Mpenyana-Monyatsi, L., Onyango, M. S. and Momba, M. N. B. (2012). "Breakthrough analysis for water disinfection using silver nanoparticles coated resin beads in fixed-bed column." Journal of Hazardous Materials 217–218(0): 133-140.

Mukherji, S., Agnihotri, S. and Mukherji, S. (2013). "Immobilized silver nanoparticles enhance contact killing and show highest efficacy: Elucidation of the mechanism of bactericidal action of silver." Nanoscale 5(16): 7328-7340.

Mulder, M. (2000). "Basic principles of membrane technology. Kluwer Academic Publishers, Dordrecht, the Netherlands."

Muller, R., Matter, S., Neuenschwander, P., Suter, U. V. and Ruegsegger, P. (1997). "3D micro-tomographic imaging and quantitative morphometry for the nondestructive evaluation of porous biomaterials." Materials Research Society Symposium Proceedings 461: 217-222.

Murinda, S. and Kraemer, S. (2008). "The potential of solar water disinfection as a household water treatment method in peri-urban Zimbabwe." Physics and Chemistry of the Earth, Parts A/B/C 33(8-13): 829-832.

Murphy, H. M., McBean, E. A. and Farahbakhsh, K. (2010). "A critical evaluation of two point-of-use water treatment technologies: Can they provide water that meets WHO drinking water guidelines?" Journal of Water and Health 8(4): 611-630.

Murphy, H. M., Sampson, M., McBean, E. and Farahbakhsh, K. (2009). "Influence of household practices on the performance of clay pot water filters in rural Cambodia." Desalination 248(1-3): 562-569.

Murthy, P. S. K., Murali Mohan, Y., Varaprasad, K., Sreedhar, B. and Mohana Raju, K. (2008). "First successful design of semi-IPN hydrogel–silver nanocomposites: A facile approach for antibacterial application." Journal of Colloid and Interface Science 318(2): 217-224.

Murthy, P. S. K., Murali Mohan, Y., Varaprasad, K., Sreedhar, B. and Mohana Raju, K. (2008). "First successful design of semi-IPN hydrogel–silver nanocomposites: A facile approach for antibacterial application." Journal of Colloid and Interface Science 318(2): 217-224.

Navarro, E., Piccapietra, F., Wagner, B., Marconi, F., Kaegi, R., Odzak, N., Sigg, L. and Behra, R. (2008). "Toxicity of silver nanoparticles to *Chlamydomonas reinhardtii*." Environmental Science & Technology 42(23): 8959-8964.

Ndabigengesere, A. and Subba Narasiah, K. (1998). "Quality of water treated by coagulation using *Moringa Oleifera* seeds." Water Research 32(3): 781-791.

Nel, A., Xia, T., Mädler, L. and Li, N. (2006). "Toxic potential of materials at the nanolevel." Science 311(5761), 622-627.

Nel, A. E., Madler, L., Velegol, D., Xia, T., Hoek, E. M. V., Somasundaran, P., Klaessig, F., Castranova, V. and Thompson, M. (2009). "Understanding biophysicochemical interactions at the nano-bio interface." Nature Materials 8(7): 543-557.

Nieto, M., Nardecchia, S., Peinado, C., Catalina, F., Abrusci, C., Gutierrez, M. C., Ferrer, M. L. and del Monte, F. (2010). "Enzyme-induced graft polymerization for preparation of hydrogels: Synergetic effect of laccase-immobilized-cryogels for pollutants adsorption." Soft Matter 6(15): 3533-3540.

Nikaido H. and Takatsuka Y. (2009). "Mechanisms of RND multidrug efflux pumps." Biochimica et Biophysica Acta **1794**: 769-81.

Nikanorov, A. M. and Brazhnikova, L. V. (2009). "Water chemical composition of rives, lakes and wetlands, in: M.G. Khublaryan (Ed.), types and properties of water" Volume 2, EOLSS Co Ltd **2009**, pp. 42–80. Available from: http://www.eolss.net/sample-chapters/c07/e2-03.pdf

Northcott, K. A., Woodberry, P., Snape, I. and Stevens, G. W. (2007). "Water treatment to prevent contaminant dispersal during remediation of cold regions contaminated sites." Cold Regions Science and Technology 48(2): 92-104.

Oh, J. I., Yamamoto, K., Kitawaki, H., Nakao, S., Sugawara, T., Rahman, M. M. and Rahman, M. H. (2000). "Application of low-pressure nanofiltration coupled with a bicycle pump for the treatment of arsenic-contaminated groundwater." Desalination 132(1-3): 307-314.

Okay, O. (2000). "Macroporous copolymer networks." Progress in Polymer Science 25(6): 711-779.

Omidian, H., Rocca, J. G. and Park, K. (2005). "Advances in superporous hydrogels." Journal of Controlled Release 102(1): 3-12.

Önnby, L., Pakade, V., Mattiasson, B. and Kirsebom, H. (2012). "Polymer composite adsorbents using particles of molecularly imprinted polymers or aluminium oxide nanoparticles for treatment of arsenic contaminated waters." Water Research, 46(13): 4111-4120.

Orakdogen, N., Karacan, P. and Okay, O. (2011). "Macroporous, responsive DNA cryogel beads." Reactive and Functional Polymers 71(8): 782-790.

O'Reilly, J. P., Butts, C. P., I'Anso, I. A. and Shaw, A. M. (2005). "Interfacial pH at an isolated silica−water surface." Journal of the American Chemical Society 127(6): 1632-1633.

Ostermeyer, A.-K., Kostigen Mumuper, C., Semprini, L. and Radniecki, T. (2013). "Influence of bovine serum albumin and alginate on silver nanoparticle dissolution and toxicity to *Nitrosomonas europaea*." Environmental Science & Technology 47(24): 14403-14410.

Oswald, W. E., Lescano, A. G., Bern, C., Calderon, M. M., Cabrera, L. and Gilman, R. H. (2007). "Fecal contamination of drinking water within peri-urban households, Lima, Peru." The American Journal of Tropical Medicine and Hygiene 77(4): 699-704.

Oyanedel-Craver, V. A. and Smith, J. A. (2007). "Sustainable colloidal-silver-impregnated ceramic filter for point-of-use water treatment." Environmental Science & Technology 42(3): 927-933.

Ozmen, M. and Okay, O. (2008). "Formation of macroporous poly(acrylamide) hydrogels in DMSO/water mixture: Transition from cryogelation to phase separation copolymerization." Reactive and Functional Polymers 68(10): 1467-1475.

Ozmen, M. M. and Okay, O. (2005). "Superfast responsive ionic hydrogels with controllable pore size." Polymer 46(19): 8119-8127.

Ozmen, M. M. and Okay, O. (2006b). "Superfast responsive ionic hydrogels: Effect of the monomer concentration." Journal of Macromolecular Science Part A: Pure and Applied Chemistry 43: 1215-1225.

Ozmen, M. M., Dinu, M. V., Dragan, E. S. and Okay, O. (2007). "Preparation of macroporous acrylamide-based hydrogels: Cryogelation under isothermal conditions." Journal of Macromolecular Science Part A: Pure and Applied Chemistry 44: 1195-1202.

Pal, S., Tak, Y.K. and Song, J.M. (2007). "Does the antibacterial activity of silver nanoparticles depend on the shape of the nanoparticle? A study of the gram-negative bacterium *Escherichia coli*." Applied and Environmental Microbiology 73(6): 1712-1720.

Palmateer, G., Manz, D., Jurkovic, A., McInnis, R., Unger, S., Kwan, K. K. and Dutka, B. J. (1999). "Toxicant and parasite challenge of Manz intermittent slow sand filter." Environmental Toxicology 14(2): 217-225.

Pan, G., Kurumada, K.-I. and Yamada, Y. (2008). "Application of hydrogel for the removal of pollutant phenol in water." Journal of the Chinese Institute of Chemical Engineers 39(4): 361-366.

Panáček, A., Kvítek, L., Prucek, R., Kolář, M., Večeřová, R., Pizúrová, N., Sharma, V.K., Nevěčná, T.j. and Zbořil, R. (2006). "Silver colloid nanoparticles: Synthesis, characterization, and their antibacterial activity." The Journal of Physical Chemistry B 110(33): 16248-16253.

Park, H. H., Park, S., Ko, G. and Woo, K. (2013). "Magnetic hybrid colloids decorated with Ag nanoparticles bite away bacteria and chemisorb viruses." Journal of Materials Chemistry B 1: 2701-2709.

Park, H.-J., Kim, J. Y., Kim, J., Lee, J.-H., Hahn, J.-S., Gu, M. B. and Yoon, J. (2009). "Silver-ion-mediated reactive oxygen species generation affecting bactericidal activity." Water Research 43(4): 1027-1032.

Park, S., Murthy, P. S. K., Park, S., Mohan, Y. M. and Koh, W.-G. (2011). "Preparation of silver nanoparticle-containing semi-interpenetrating network hydrogels composed of pluronic and poly(acrylamide) with antibacterial property." Journal of Industrial and Engineering Chemistry 17(2): 293-297.

Peretyazhko, T. S., Zhang, Q. and Colvin, V. L. (2014). "Size-controlled dissolution of silver nanoparticles at neutral and acidic pH conditions: Kinetics and size changes." Environmental Science & Technology 48(20): 11954-11961.

Pérez, J. M., Arenas, F. A., Pradenas, G. A., Sandoval, J. M. and Vásquez, C. C. (2008). "*Escherichia coli* yqhd exhibits aldehyde reductase activity and protects from the harmful effect of lipid peroxidation-derived aldehydes." Journal of Biological Chemistry 283(12): 7346-7353.

Peter-Varbanets, M., Gujer, W. and Pronk, W. (2012). "Intermittent operation of ultra-low pressure ultrafiltration for decentralized drinking water treatment." Water Research 46(10): 3272-3282.

Peter-Varbanets, M., Hammes, F., Vital, M. and Pronk, W. (2010). "Stabilization of flux during dead-end ultra-low pressure ultrafiltration." Water Research 44(12): 3607-3616.

Petrov, P. D. and Georgiev, G. L. (2011). "Ice-mediated coating of macroporous cryogels by carbon nanotubes: A concept towards electrically conducting nanocomposites." Chemical Communications 47(20): 5768-5770.

Petrov, P. D. and Georgiev, G. L. (2012). "Fabrication of super-macroporous nanocomposites by deposition of carbon nanotubes onto polymer cryogels." European Polymer Journal 48(8): 1366-1373.

Petrov, P., Petrova, E. and Tsvetanov, C. B. (2009). "UV-assisted synthesis of super-macroporous polymer hydrogels." Polymer 50(5): 1118-1123.

Petrov, P., Petrova, E., Stamenova, R., Tsvetanov, C. B. and Riess, G. (2006). "Cryogels of cellulose derivatives prepared via UV irradiation of moderately frozen systems." Polymer 47(19): 6481-6484.

Petrov, P., Petrova, E., Tchorbanov, B. and Tsvetanov, C. B. (2007). "Synthesis of biodegradable hydroxyethylcellulose cryogels by UV irradiation." Polymer 48(17): 4943-4949.

Petrov, P., Utrata-Wesolek, A., Trzebicka, B., Tsvetanov, C. B., Dworak, A., Aniol, J. and Sieron, A. (2011). "Biocompatible cryogels of thermosensitive polyglycidol derivatives with ultra-rapid swelling properties." European Polymer Journal 47(5): 981-988.

Plieva, F. M. and Mattiasson, B. (2008). "Macroporous gel particles as novel sorbent materials: Rational design." Industrial and Engineering Chemistry Research 47(12): 4131-4141.

Plieva, F. M., Ekstrom, P., Galaev, I. Y. and Mattiasson, B. (2008a). "Monolithic cryogels with open porous structure and unique double-continuous macroporous networks." Soft Matter 4(12): 2418-2428.

Plieva, F. M., Galaev, I. Y. and Mattiasson, B. (2007). "Macroporous gels prepared at subzero temperature as novel materials for chromatography of particulate-containing fluids and cell culture applications." Journal of Separation Science 30): 1657-1671.

Plieva, F. M., Galaev, I. Y., Noppe, W. and Mattiasson, B. (2008b). "Cryogel applications in microbiology." Trends in Microbiology 16(11): 543-551.

Plieva, F. M., Karlsson, M., Aguilar, M.-R., Gomez, D., Mikhalovsky, S. and Galaev, I. Y. (2005). "Pore structure in supermacroporous polyacrylamide based cryogels." Soft Matter 1(4): 303-309.

Plieva, F. M., Savina, I. N., Deraz, S., Andersson, J., Galaev, I. Y. and Mattiasson, B. (2004). "Characterization of supermacroporous monolithic polyacrylamide based matrices designed for chromatography of bioparticles." Journal of Chromatography B 807(1): 129-137.

Plieva, F., Huiting, X., Galaev, I. Y., Bergenstahl, B. and Mattiasson, B. (2006). "Macroporous elastic polyacrylamide gels prepared at subzero temperatures: Control of porous structure." Journal of Materials Chemistry 16(41): 4065-4073..

Plieva, F. M. and Mattiasson, B. (2008). "Macroporous gel particles as novel sorbent materials: Rational design." Industrial & Engineering Chemistry Research 47(12): 4131-4141.

Plieva, F. M., Ekstrom, P., Galaev, I. Y. and Mattiasson, B. (2008). "Monolithic cryogels with open porous structure and unique double-continuous macroporous networks." Soft Matter 4(12): 2418-2428.

Plieva, F. M., Galaev, I. V. and Mattiasson, B. (2007). "Macroporous gels prepared at subzero temperatures as novel materials for chromatography of particulate-containing fluids and cell culture applications." Journal of Separation Science 30(11), 1657-1671.

Plieva, F. M., Galaev, I. Y., Noppe, W. and Mattiasson, B. (2008c). "Cryogel applications in microbiology." Trends in Microbiology 16(11): 543-551.

Plieva, F. M., Karlsson, M., Aguilar, M.-R., Gomez, D., Mikhalovsky, S. and Galaev, I. Y. (2005). "Pore structure in supermacroporous polyacrylamide based cryogels." Soft Matter 1(4): 303-309.

Plieva, F. M., Kumar, A., Galaev, I. Y. and Mattiasson, B. (2009a) Advanced biomaterials : Fundamentals, processing, and applications. Basu, B., Katti, D.S. and Kumar, A. (eds), pp. 499-531, The American Ceramic Society.

Plieva, F. M., Savina, I. N., Deraz, S., Andersson, J., Galaev, I. Y. and Mattiasson, B. (2004). "Characterization of supermacroporous monolithic polyacrylamide based matrices designed for chromatography of bioparticles." Journal of Chromatography B 807(1): 129-137.

Plieva, F. M., Seta, E. D., Galaev, I. Y. and Mattiasson, B. (2009b). "Macroporous elastic polyacrylamide monolith columns: Processing under compression and scale-up." Separation and Purification Technology 65(1): 110-116.

Podorozhko, E. A., Korlyukov, A. A. and Lozinsky, V. I. (2010). "Cryostructuring of polymer systems. XXX. Poly(vinyl alcohol)-based composite cryogels filled with small disperse oil droplets: A gel system capable of mechanically induced

releasing of the lipophilic constituents." Journal of Applied Polymer Science 117(3): 1332-1349.

Podorozhko, E. A., Kurskaya, E. A., Kulakova, V. K. and Lozinsky, V. I. (2000). "Cryotropic structuring of aqueous dispersions of fibrous collagen: Influence of the initial pH values." Food Hydrocolloids 14(2): 111-120.

Pokhrel, L. R., Dubey, B. and Scheuerman, P. R. (2013). "Impacts of select organic ligands on the colloidal stability, dissolution dynamics, and toxicity of silver nanoparticles." Environmental Science & Technology 47(22): 12877-12885.

Pokhrel, L. R., Dubey, B. and Scheuerman, P. R. (2014). "Natural water chemistry (dissolved organic carbon, pH, and hardness) modulates colloidal stability, dissolution, and antimicrobial activity of citrate functionalized silver nanoparticles." Environmental Science: Nano 1(1): 45-54.

Přádnýa, M., Lesný, P., Fialab, J., Vacíka, J., Šloufa, M., Micháleka, J. and Sykováb, E. (2003). "Macroporous hydrogels based on 2-hydroxyethyl methacrylate. Part 1. Copolymers of 2-hydroxyethyl methacrylate with methacrylic acid." Collection of Czechoslovak Chemical Communications 68: 812-822.

Prieto, P., Nistora, V., Nouneh, K., Oyama, M., Abd-Lefdil, M. and Díaz, R. (2012). "XPS study of silver, nickel and bimetallic silver–nickel nanoparticles prepared by seed-mediated growth." Applied Surface Science 258: 8807– 8813.

Pritchard, M., Craven, T., Mkandawire, T., Edmondson, A. S. and O'Neill, J. G. (2010). "A comparison between *Moringa Oleifera* and chemical coagulants in the purification of drinking water - an alternative sustainable solution for developing countries." Physics and Chemistry of the Earth, Parts A/B/C 35(13-14): 798-805.

Pritchard, M., Mkandawire, T., Edmondson, A., O'Neill, J. G. and Kululanga, G. (2009). "Potential of using plant extracts for purification of shallow well water in Malawi." Physics and Chemistry of the Earth, Parts A/B/C 34(13-16): 799-805.

Pryor, M. J., Jacobs, E. P., Botes, J. P. and Pillay, V. L. (1998). "A low pressure ultrafiltration membrane system for potable water supply to developing communities in South Africa." Desalination 119(1-3): 103-111.

Psutka, R., Peletz, R., Michelo, S., Kelly, P. and Clasen, T. (2011). "Assessing the microbiological performance and potential cost of boiling drinking water in urban Zambia." Environmental Science and Technology 45: 6095-6101.

Pumpel T and Schinner F. (1986). "Silver tolerance and silver accumulation of microorganisms from soil materials of a silver mine." Applied Microbiology and Biotechnology **24**: 244-247.

Purifier, 2011. Structured matrix : how does it work ? Available from: http://www.purifiersaustralia.com.au/menu.php?id=21 (accessed on 29 January 2012).

Qian, L., Ahmed, A., Foster, A., Rannard, S. P., Cooper, A. I. and Zhang, H. (2009). "Systematic tuning of pore morphology and pore volumes in macroporous materials by freezing." Journal of Materials Chemistry 19: 5212-5219.

Qiblawey, H. M. and Banat, F. (2008). "Solar thermal desalination technologies." Desalination 220(1-3): 633-644.

Qu, X., Alvarez, P. J. J. and Li, Q. (2013). "Applications of nanotechnology in water and wastewater treatment." Water Research 47: 3931-3946.

Quang, D. V., Sarawade, P. B., Hilonga, A., Kim, J.-K., Chai, Y. G., Kim, S. H., Ryu, J.-Y. and Kim, H. T. (2011). "Preparation of silver nanoparticle containing silica micro beads and investigation of their antibacterial activity." Applied Surface Science 257(15), 6963-6970.

Quang, D. V., Sarawade, P. B., Jeon, S. J., Kim, S. H., Kim, J.-K., Chai, Y. G. and Kim, H. T. (2013). "Effective water disinfection using silver nanoparticle containing silica beads." Applied Surface Science 266(0): 280-287.

Quinn, L. (1997). "Reverse osmosis systems in military or emergency operations." Desalination 113(2-3): 297-301.

Rangel, J. M., Lopez, B., Mejia, M. A., Mendoza, C. and Luby, S. (2003). "A novel technology to improve drinking water quality: A microbiological evaluation of in-home flocculation and chlorination in rural Guatemala." Journal of Water and Health 1(1): 15-22.

Reller, M. E., Carlos, C. E., Lopez, M. B., Alvarez, M., Hoekstra, R. M., Olson, C. A., Baier, K. G., Keswick, B. H. and Luby, S. P. (2003). "A randomized controlled trial of household-based flocculant-disinfectant drinking water treatment for diarrhea prevention in rural Guatemala " The American Journal of Tropical Medicine and Hygiene 69(4): 411-419.

Remoundaki, E., Hatzikioseyian, A. and Tsezos, M. (2007). "A systematic study of chromium solubility in the presence of organic matter: Consequences for the treatment of chromium-containing wastewater." Journal of Chemical Technology & Biotechnology 82(9): 802-808.

Richards, B. S. and Schäfer, A. I. (2002). "Design considerations for a solar-powered desalination system for remote communities in Australia." Desalination 144(1-3): 193-199.

Richards, B. S. and Schäfer, A. I. (2003). "Photovoltaic-powered desalination system for remote Australian communities." Renewable Energy 28(13): 2013-2022.

Rizzello, L. and Pompa, P. P. (2014). "Nanosilver-based antibacterial drugs and devices: Mechanisms, methodological drawbacks, and guidelines." Chemical Society Reviews 43(5): 1501-1518.

Rizzieri, R., Baker, F. S. and Donald, A. M. (2003). "A study of the large strain deformation and failure behaviour of mixed biopolymer gels via in situ ESEM." Polymer 44(19): 5927-5935.

Robinson, R., Ho, G. and Mathew, K. (1992). "Development of a reliable low-cost reverse osmosis desalination unit for remote communities." Desalination 86(1): 9-26.

Roig, B., Delpla, I., Baurès, E., Jung, A. V. and Thomas, O. (2011). "Analytical issues in monitoring drinking-water contamination related to short-term, heavy rainfall events." TrAC Trends in Analytical Chemistry 30(8): 1243-1251.

Roig, B., Delpla, I., Baurès, E., Jung, A.V. and Thomas, O. (2011). "Analytical issues in monitoring drinking-water contamination related to short-term, heavy rainfall events." TrAC Trends in Analytical Chemistry 30(8): 1243-1251.

Romeo, H. E., Hoppe, C. E., Lopez-Quintela, M. A., Williams, R. J. J., Minaberry, Y. and Jobbagy, M. (2012). "Directional freezing of liquid crystalline systems: From silver nanowire/PVA aqueous dispersions to highly ordered and electrically conductive macroporous scaffolds." Journal of Materials Chemistry 22(18): 9195-9201.

Rosa, G., Miller, L. and Clasen, T. (2010). "Microbiological effectiveness of disinfecting water by boiling in rural Guatemala." The American Journal of Tropical Medicine and Hygiene 83(3): 473-477.

Rose, A., S Roy, Abraham, V., Holmgren, G., George, K., Balraj, V., Abraham, S., J Muliyil, Joseph, A. and Kang, G. (2006). "Solar disinfection of water for diarrhoeal prevention in Southern India." Archive Disease of Childhood 91(139-141).

Ruiz, P., Muñoz, M., Macanás, J. and Muraviev, D. N. (2010). "Intermatrix synthesis of polymer−copper nanocomposites with tunable parameters by using copper comproportionation reaction." Chemistry of Materials 22(24): 6616-6623.

Sampathkumar, K., Arjunan, T. V., Pitchandi, P. and Senthilkumar, P. (2010). "Active solar distillation - A detailed review." Renewable and Sustainable Energy Reviews 14(6): 1503-1526.

Sandvik, S. L. H., Bilski, P., Pakulski, J. D., Chignell, C. F. and Coffin, R. B. (2000). "Photogeneration of singlet oxygen and free radicals in dissolved organic matter isolated from the Mississippi and Atchafalaya river plumes." Marine Chemistry 69(1–2): 139-152.

Savina, I. N., Cnudde, V., D'Hollander, S., Van Hoorebeke, L., Mattiasson, B., Galaev, I. Y. and Du Prez, F. (2007). "Cryogels from poly(2-hydroxyethyl methacrylate): Macroporous, interconnected materials with potential as cell scaffolds." Soft Matter 3(9): 1176-1184.

Savina, I. N., English, C. J., Whitby, R. L. D., Zheng, Y., Leistner, A., Mikhalovsky, S. V. and Cundy, A. B. (2011a). "High efficiency removal of dissolved As(III) using iron nanoparticle-embedded macroporous polymer composites." Journal of Hazardous Materials 192(3): 1002-1008.

Savina, I. N., Galaev, I. Y. and Mattiason, B. (2006). "Ion-exchange macroporous hydrophilic gel monolith with grafter polymer brushes." Journal of Molecular Recognition 19): 313-321.

Savina, I. N., Gun'ko, V. M., Turov, V. V., Dainiak, M., Phillips, G. J., Galaev, I. Y. and Mikhalovsky, S. V. (2011b). "Porous structure and water state in cross-linked polymer and protein cryo-hydrogels." Soft Matter 7(9): 4276-4283.

Savina, I. N., Hanora, A., Plieva, F. M., Galaev, I. Y., Mattiasson, B. and Lozinsky, V. I. (2005a). "Cryostructuration of polymer systems. XXIV. Poly(vinyl alcohol) cryogels filled with particles of a strong anion exchanger: Properties of the composite materials and potential applications." Journal of Applied Polymer Science 95(3): 529-538.

Savina, I. N., Mattiasson, B. and Galaev, I. Y. (2005b). "Graft polymerization of acrylic acid onto macroporous polyacrylamide gel (cryogel) initiated by potassium diperiodatocuprate." Polymer 46(23): 9596-9603.

Savina, I., Tomlins, P., Mikhalovsky, S. and Galaev, I. (2009) Macroporous polymers, pp. 211-235, CRC Press.

Savina, I.N., Cnudde, V., D'Hollander, S., Van Hoorebeke, L., Mattiasson, B., Galaev, I.Y. and Du Prez, F. (2007). "Cryogels from poly(2-hydroxyethyl methacrylate): Macroporous, interconnected materials with potential as cell scaffolds." Soft Matter 3(9): 1176-1184.

Savina, I. N., English, C. J., Whitby, R. L. D., Zheng, Y., Leistner, A., Mikhalovsky, S. V. and Cundy, A. B. (2011a). "High efficiency removal of dissolved As(III) using iron nanoparticle-embedded macroporous polymer composites." Journal of Hazardous Materials 192(3): 1002-1008.

Savina, I. N., Galaev, I. Y. and Mattiason, B. (2006). "Ion-exchange macroporous hydrophilic gel monolith with grafter polymer brushes." Journal of Molecular Recognition 19: 313-321.

Savina, I. N., Gun'ko, V. M., Turov, V. V., Dainiak, M., Phillips, G. J., Galaev, I. Y. and Mikhalovsky, S. V. (2011b). "Porous structure and water state in cross-linked polymer and protein cryo-hydrogels." Soft Matter 7(9): 4276-4283.

Savina, I. N., Hanora, A., Plieva, F. M., Galaev, I. Y., Mattiasson, B. and Lozinsky, V. I. (2005). "Cryostructuration of polymer systems. XXIV. Poly(vinyl alcohol)

cryogels filled with particles of a strong anion exchanger: Properties of the composite materials and potential applications." Journal of Applied Polymer Science 95(3): 529-538.

Schäfer, A. I., Fane, A. G. and Waite, T. D. (1998). "Nanofiltration of natural organic matter: Removal, fouling and the influence of multivalent ions." Desalination 118(1-3): 109-122.

Schäfer, A. I., Schwicker, U., Fischer, M. M., Fane, A. G. and Waite, T. D. (2000). "Microfiltration of colloids and natural organic matter." Journal of Membrane Science 171(2): 151-172.

Schlosser, O., Robert, C., Bourderioux, C., Rey, M. and de Roubin, M. R. (2001). "Bacterial removal from inexpensive portable water treatment systems for travelers." Journal of Travel Medicine 8(1): 12-018.

Schmid, P., Kohler, M., Meierhofer, R., Luzi, S. and Wegelin, M. (2008). "Does the reuse of PET bottles during solar water disinfection pose a health risk due to the migration of plasticisers and other chemicals into the water?" Water Research 42(20): 5054-5060.

Schoen, D. T., Schoen, A. P., Hu, L., Kim, H. S., Heilshorn, S. C. and Cui, Y. (2010). "High speed water sterilization using one-dimensional nanostructures." Nano Letters 10(9): 3628-3632.

Schwab, P., Zhu, D. and Banks, M. K. (2007). "Heavy metal leaching from mine tailings as affected by organic amendments." Bioresource Technology 98(15): 2935-2941.

Scully, N. M., Cooper, W. J. and Tranvik, L. J. (2003). "Photochemical effects on microbial activity in natural waters: The interaction of reactive oxygen species and dissolved organic matter." FEMS Microbiology Ecology 46(3): 353-357.

Seaver, L. C. and Imlay, J. A. (2001). "Hydrogen peroxide fluxes and compartmentalization inside growing *Escherichia coli*." Journal of Bacteriology 183(24): 7182-7189.

Seidel, A. (1953) Solubilities of inorganic and metal organic compounds, New York: Van Nostrand.

Seidel, A. (1953), Solubilities of inorganic and metal organic compounds, ed.

Seo, S. Y., Lee, G. H., Lee, S. G., Jung, S. Y., Lim, J. O. and Choi, J. H. (2012). "Alginate-based composite sponge containing silver nanoparticles synthesized in situ." Carbohydrate Polymers 90(1): 109-115.

Shah, V. J., Kava, R. M., Rao, A. V. and Taquikhan, M. M. (1988). "A mobile reverse osmosis demonstration plant." Desalination 69(2): 161-169.

Shawky, H. A., El-Sayed, M. H., Ali, A. E.-H. and Abdel Mottaleb, M. S. (2006). "Treatment of polluted water resources using reactive polymeric hydrogel." Journal of Applied Polymer Science 100(5): 3966-3973.

Skoog, D. A., Holler, F. J. and Nieman, T. A. (1998) Principles of instrumental analysis.

Snyder, J. W., Craig, J. R., Anderson, R. E. and Bisonnette, G. K. (1995). "Effect of point-of-use, activated carbon filters on the bacteriology quality of rural groundwater supplies." Applied Environmental Microbioliology 61(12): 4291-4295.

Sobsey, M. (2002). "Managing water in the home: accelerated health gains from improved water supply." World Health Organization, Geneva.

Sobsey, M. D., Stauber, C. E., Casanova, L. M., Brown, J. M. and Elliott, M. A. (2008). "Point of use household drinking water filtration: A practical, effective solution for providing sustained access to safe drinking water in the developing world." Environmental Science & Technology 42(12): 4261-4267.

Sondi, I. and Salopek-Sondi, B. (2004). "Silver nanoparticles as antimicrobial agent: A case study on *E. coli* as a model for Gram-negative bacteria." Journal of Colloid and Interface Science 275(1): 177-182.

Sotiriou, G. A. and Pratsinis, S. E. (2010). "Antibacterial activity of nanosilver ions and particles." Environmental Science & Technology 44(14): 5649-5654.

Souter, P. F., Cruickshank, G. D., Tankerville, M. Z., Keswick, B. H., Ellis, B. D., Langworthy, D. E., Metz, K. A., Appleby, M. R., Hamilton, N., Jones, A. L. and Perry, J. D. (2003). "Evaluation of a new water treatment for point-of-use household applications to remove microorganism and arsenic from drinking water." Journal of Water and Health 1(2): 74-84.

Sphere (2004). "The sphere project: Humanitarian charter and minimum standards in disaster response." Available from: http;//ocw/jhsph.edu/courses/refugeehealthcare/PDFs/SphereProjectHandbook.pdf.

Srinivas, H. and Nakagawa, Y. (2008). "Environmental implications for disaster preparedness: Lessons learnt from the Indian Ocean tsunami." Journal of Environmental Management 89(1): 4-13.

Srinivasan, N. R., Shankar, P. A. and Bandyopadhyaya, R. (2013). "Plasma treated activated carbon impregnated with silver nanoparticles for improved antibacterial effect in water disinfection." Carbon 57(0): 1-10.

Srivastava, A., Jain, E. and Kumar, A. (2007). "The physical characterization of supermacroporous poly(*n*-isopropylacrylamide) cryogel: Mechanical strength and swelling/de-swelling kinetics." Materials Science and Engineering: A 464(1-2): 93-100.

Stauber, C. E., Elliott, M. A., Koksal, F., Ortiz, G. M., DiGiano, F. A. and Sobsey, M. D. (2006). "Characterisation of the biosand filter for *E. coli* reductions from household drinking water under controlled laboratory and field use conditions." Water Science and Technology 54(3): 1-7.

Stauber, C. E., Ortiz, G. M., Loomis, D. P. and Sobsey, M. D. (2009). "A randomized controlled trial of the concrete biosand filter and its impact on diarrheal disease in Bonao, Dominican Republic." The American Journal of Tropical Medicine and Hygiene 80(2): 286-293.

Steele, A. and Clarke, B. (2008). "Problems of treatment process selection for relief agency water supplies in an emergency." Journal of Water and Health 6(4): 483-489.

Stevenson, F.J., Humic chemistry: Genesis, composition, reactions. Wiley: New york, 1994.

Su, F., Luo, M., Zhang, F., Li, P., Lou, K. and Xing, X. (2009). "Performance of microbiological control by a point-of-use filter system for drinking water purification." Journal of Environmental Sciences 21(9): 1237-1246.

Su, H.-L., Chou, C.-C., Hung, D.-J., Lin, S.-H., Pao, I.C., Lin, J.-H., Huang, F.-L., Dong, R.-X. and Lin, J.-J. (2009). "The disruption of bacterial membrane integrity through ROS generation induced by nanohybrids of silver and clay." Biomaterials 30(30): 5979-5987.

Su, Y., Zhao, Q., Sun, J. and Wu, J. (2012). "Synthesis and characterization of biodegradable macroporous cryogels crosslinked by chitosan oligosaccharide-graft-acrylic acid." Soft Matter 8(16): 4382-4389.

Summers A. O., Jacoby G. A., Swartz M. N., Mchugh G. and Sutton L. (1978). "Metal cation and oxyanion resistances in plasmids of gram-negative bacteria." in Microbiology, Schlessinger D., Editor, American Society for Microbiology.

Sun, S., Tang, Y., Fu, Q., Liu, X., Guo, L. a., Zhao, Y. and Chang, C. (2012). "Monolithic cryogels made of agarose–chitosan composite and loaded with agarose beads for purification of Immunoglobulin G." International Journal of Biological Macromolecules 50(4): 1002-1007.

Sun, X.-L., He, W.-D., Pan, T.-T., Ding, Z.-L. and Zhang, Y.-J. (2010). "RAFT cryopolymerizations of acrylamides and acrylates in dioxane at −5 °C." Polymer 51(1): 110-114.

Suresh, A. K., Pelletier, D. A. and Doktycz, M. J. (2013). "Relating nanomaterial properties and microbial toxicity." Nanoscale 5(2): 463-474.

Susanto, H. (2011). "Towards practical implementations of membrane distillation." Chemical Engineering and Processing: Process Intensification 50(2): 139-150.

Suwanchawalit, C., Patil, A. J., Kumar, R. K., Wongnawa, S. and Mann, S. (2009). "Fabrication of ice-templated macroporous TiO_2-chitosan scaffolds for photocatalytic applications." Journal of Materials Chemistry 19(44): 8478-8483.

Tagami, K. and Uchida, S. (2011) "Can we remove iodine-131 from tap water in Japan by boiling? - Experimental testing in response to the Fukushima Daiichi nuclear power plant accident." Chemosphere 84: 1282-1284.

Taglietti, A., Diaz Fernandez, Y. A., Amato, E., Cucca, L., Dacarro, G., Grisoli, P., Necchi, V., Pallavicini, P., Pasotti, L. and Patrini, M. (2012). "Antibacterial activity of glutathione-coated silver nanoparticles against Gram positive and Gram negative bacteria." Langmuir 28(21): 8140-8148.

Tejamaya, M., Römer, I., Merrifield, R. C. and Lead, J. R. (2012). "Stability of citrate, PVP, and PEG coated silver nanoparticles in ecotoxicology media." Environmental Science & Technology 46(13): 7011-7017.

Thomas, V., Yallapu, M. M., Sreedhar, B. and Bajpai, S. K. (2007). "A versatile strategy to fabricate hydrogel-silver nanocomposites and investigation of their antimicrobial activity." Journal of Colloid and Interface Science 315(1): 389-395.

Thurman, E. M. (1985). Organic geochemistry of natural waters. Martinus Nijhoff/Junk Publishers, The Netherlands.

Tiwari, G. N., Singh, H. N. and Tripathi, R. (2003). "Present status of solar distillation." Solar Energy 75(5): 367-373.

Tiwari, S.-S. K., Schmidt, W.-P., Darby, J., Kariuki, Z. G. and Jenkins, M. W. (2009). "Intermittent slow sand filtration for preventing diarrhoea among children in Kenyan households using unimproved water sources: Randomized controlled trial." Tropical Medicine and International Health 14(11): 1374-1382.

Tobin, R. S., Smith, D. K. and Lindsay, J. A. (1981). "Effects of activated carbon and bacteriostatic filters on microbiological quality of drinking water." Applied and Environmental Microbiology 41(3): 646-651.

Toole, M. J. and Waldman, R. J. (1990). "Prevention of excess mortality in refugee and displaced populations in developing countries." Journal of American Medical Association 263(24): 3296-3302.

Topuz, F. and Okay, O. (2009). "Macroporous hydrogel beads of high toughness and superfast responsivity." Reactive and Functional Polymers 69(5): 273-280.

Tripathi, A. and Kumar, A. (2011). "Multi-featured macroporous agarose–alginate cryogel: Synthesis and characterization for bioengineering applications." Macromolecular Bioscience 11(1): 22-35.

Tripathi, A., Kathuria, N. and Kumar, A. (2008). "Elastic and macroporous agarose-gelatin cryogels with isotropic and anisotropic porosity for tissue engineering." Journal of Biomedical Materials Research Part A 90A(3): 680-694.

Tripathi, A., Kathuria, N. and Kumar, A. (2008). "Elastic and macroporous agarose-gelatin cryogels with isotropic and anisotropic porosity for tissue engineering." Journal of Biomedical Materials Research Part A 90A(3): 680-694.

Tsarik, N. (1993). "Supplying water and treating sewage in Kiev after the chernobyl accident." Journal of American Water Works Association 85: 42-45.

Tzen, E., Perrakis, K. and Baltas, P. (1998). "Design of a stand alone PV - desalination system for rural areas." Desalination 119(1-3): 327-333.

United States Environmental Protection Agency (2007). "Dilution water." Available from:http://water.epa.gov/scitech/methods/cwa/wet/upload/2007_07_10_methods_wet_disk2_atx7-10.pdf .

Uygun, M., Kahveci, M. U., Odaci, D., Timur, S. and Yagci, Y. (2009). "Antibacterial acrylamide hydrogels containing silver nanoparticles by simultaneous photoinduced free radical polymerization and electron transfer processes." Macromolecular Chemistry and Physics 210(21): 1867-1875.

van Halem, D., Heijman, S. G. J., Soppe, A. I. A., van Dijk, J. C. and Amy, G. L. (2007). "Ceramic silver-impregnated pot filters for household drinking water treatment in developing countries: Materials characterization nad performance study." Water Science and Technololgy: Water Supply 7(5-6): 9-17.

van Halem, D., van der Laan, H., Heijman, S. G. J., van Dijk, J. C. and Amy, G. L. (2009). "Assessing the sustainability of the silver-impregnated ceramic pot filter for low-cost household drinking water treatment." Physics and Chemistry of the Earth, Parts A/B/C 34(1-2): 36-42.

Velickova, E., Winkelhausen, E., Kuzmanova, S., Cvetkovska, M. and Tsvetanov, C. (2009). "Hydroxyethylcellulose cryogels used for entrapment of *Saccharomyces Cerevisiae* cells." Reactive and Functional Polymers 69(9): 688-693.

Velmurugan, V. and Srithar, K. (2011). "Performance analysis of solar stills based on various factors affecting the productivity - a review." Renewable and Sustainable Energy Reviews 15(2): 1294-1304.

Vestergaard The Lifestraw® concept. Available from: http://www.vestergaard-frandsen.com/lifestraw (accessed 4 april 2011).

Vijaya, Y., Popuri, S. R., Boddu, V. M. and Krishnaiah, A. (2008). "Modified chitosan and calcium alginate biopolymer sorbents for removal of nickel (ii) through adsorption." Carbohydrate Polymers 72(2): 261-271.

Vimala, K., Samba Sivudu, K., Murali Mohan, Y., Sreedhar, B. and Mohana Raju, K. (2009). "Controlled silver nanoparticles synthesis in semi-hydrogel networks of poly(acrylamide) and carbohydrates: A rational methodology for antibacterial application." Carbohydrate Polymers 75(3): 463-471.

Violette, S., Boulicot, G. and Gorelick, S. M. (2009). "Tsunami-induced groundwater salinization in Southeastern India." Comptes Rendus Geosciences 341(4): 339-346.

Walczyk, D., Bombelli, F. B., Monopoli, M. P., Lynch, I. and Dawson, K. A. (2010). "What the cell "sees" in bionanoscience." Journal of the American Chemical Society 132(16): 5761-5768.

Wallace, M., Cui, Z. and Hankins, N. P. (2008). "A thermodynamic benchmark for assessing an emergency drinking water device based on forward osmosis." Desalination 227(1-3): 34-45.

Wallis, C., Stagg, C. H. and Melnick, J. L. (1974). "The hazards of incorporating charcoal filters into domestic water systems." Water Research 8(2): 111-113.

Wang, F., Shor, L., A. Darling, Khalil, S., Sun, W., Guceri, S. and Lau, A. (2004). "Precision extruding deposition and characterization of cellular poly-ε-caprolactone tissue scaffolds." Rapid Prototyping Journal 10: 42-49.

Wassouf, P., Peska, T., Singh, R. and Akbarzadeh, A. (2011). "Novel and low cost designs of portable solar stills." Desalination 276(1-3): 294-302.

Wegelin, M., Canonica, S., Mechsner, K., Fleischmann, T., Pesaro, F. and Metzler, A. (1994). "Solar water disinfection: Scope of process and analysis of radiation experiments." Journal of Water Supply Research and Technology 43: 154-169.

Wei, C., Lin, W. Y., Zainal, Z., Williams, N. E., Zhu, K., Kruzic, A. P., Smith, R. L. and Rajeshwar, K. (1994). "Bactericidal activity of TiO_2 photocatalyst in aqueous media: Toward a solar-assisted water disinfection system." Environmental Science and Technology 28(5): 934-938.

WHO (2008) "Guidelines for Drinking-Water Quality. Third Edition Incorporating the First and Second Addenda. Volume 1. Recommendations." World Health Organization, Geneva.

Wigginton, N. S., Titta, A. D., Piccapietra, F., Dobias, J., Nesatyy, V. J., Suter, M. J. F. and Bernier-Latmani, R. (2010). "Binding of silver nanoparticles to bacterial proteins depends on surface modifications and inhibits enzymatic activity." Environmental Science & Technology 44(6): 2163-2168.

Wiley, B., Herricks, T., Sun, Y. and Xia, Y. (2004). "Polyol synthesis of silver nanoparticles: Use of chloride and oxygen to promote the formation of single-crystal, truncated cubes and tetrahedrons." Nano Letters 4(9): 1733-1739.

Wiley, B., Sun, Y. and Xia, Y. (2007). "Synthesis of silver nanostructures with controlled shapes and properties." Accounts of Chemical Research 40(10): 1067-1076.

Wirth, S. M., Lowry, G. V. and Tilton, R. D. (2012). "Natural organic matter alters biofilm tolerance to silver nanoparticles and dissolved silver." Environmental Science & Technology 46(22): 12687-12696.

Wolfe, J., Bryant, G. and Koster, K. L. (2002). "What is 'unfreezable water', how unfreezable is it and how much is there?" Cryo-Letters 23(3): 157-166.

Wu, J., Zhao, Q., Sun, J. and Zhou, Q. (2012). "Preparation of poly(ethylene glycol) aligned porous cryogels using a unidirectional freezing technique." Soft Matter 8(13): 3620-3626.

Xiu, Z., Liu, Y., Mathieu, J., Wang, J., Zhu, D. and Alvarez, P. J. J. (2014). "Elucidating the genetic basis for *Escherichia coli* defense against silver toxicity using mutant arrays." Environmental Toxicology and Chemistry 33(5): 993-997.

Xiu, Z.-M., Ma, J. and Alvarez, P. J. J. (2011). "Differential effect of common ligands and molecular oxygen on antimicrobial activity of silver nanoparticles versus silver ions." Environmental Science & Technology 45(20): 9003-9008.

Xiu, Z.-M., Zhang, Q.-B., Puppala, H. L., Colvin, V. L. and Alvarez, P. J. J. (2012). "Negligible particle-specific antibacterial activity of silver nanoparticles." Nano Letters 12(8): 4271-4275.

Xu, P., Yao, Y., Shen, S., Yun, J. and Yao, K. (2010). "Preparation of supermacroporous composite cryogel embedded with SiO_2 nanoparticles." Chinese Journal of Chemical Engineering 18(4): 667-671.

Xue, W., Champ, S., Huglin, M. B. and Jones, T. G. J. (2004). "Rapid swelling and deswelling in cryogels of crosslinked poly(*n*-isopropylacrylamide-*co*-acrylic acid)." European Polymer Journal 40(3): 467-476.

Xue, Z., Wang, S., Lin, L., Chen, L., Liu, M., Feng, L. and Jiang, L. (2011). "A novel superhydrophilic and underwater superoleophobic hydrogel-coated mesh for oil/water separation." Advanced Materials 23(37): 4270-4273.

Yang, J., Zhang, Q., Lee, J.Y. and Too, H.-P. (2007). "Dissolution–recrystallization mechanism for the conversion of silver nanospheres to triangular nanoplates." Journal of Colloid and Interface Science 308(1): 157-161.

Yang, X., Jiang, C., Hsu-Kim, H., Badireddy, A. R., Dykstra, M., Wiesner, M., Hinton, D. E. and Meyer, J. N. (2014). "Silver nanoparticle behavior, uptake, and toxicity in *Caenorhabditis Elegans*: Effects of natural organic matter." Environmental Science & Technology 48(6): 3486-3495.

Yao, K., Shen, S., Yun, J., Wang, L., Chen, F. and Yu, X. (2007). "Protein adsorption in supermacroporous cryogels with embedded nanoparticles." Biochemical Engineering Journal 36(2): 139-146.

Yao, K., Shen, S., Yun, J., Wang, L., He, X. and Yu, X. (2006). "Preparation of polyacrylamide-based supermacroporous monolithic cryogel beds under freezing-temperature variation conditions." Chemical Engineering Science 61(20): 6701-6708.

Yao, K., Yun, J., Shen, S., Wang, L., He, X. and Yu, X. (2006b). "Characterization of a novel continuous supermacroporous monolithic cryogel embedded with nanoparticles for protein chromatography." Journal of Chromatography A 1109(1): 103-110.

Yin, L., Cheng, Y., Espinasse, B., Colman, B. P., Auffan, M., Wiesner, M., Rose, J., Liu, J. and Bernhardt, E. S. (2011). "More than the ions: The effects of silver nanoparticles on *Lolium Multiflorum*." Environmental Science & Technology 45(6): 2360-2367.

Yin, Y., Liu, J. and Jiang, G. (2012). "Sunlight-induced reduction of ionic Ag and Au to metallic nanoparticles by dissolved organic matter." ACS Nano 6(9): 7910-7919.

Yoshida, R., Takahashi, T., Yamaguchi, T. and Ichijo, H. (1997). "Self-oscillating gels." Advanced Materials 9(2): 175-178.

Young, S., Balluz, L. and Malilay, J. (2004). "Natural and technologic hazardous material releases during and after natural disasters: A review." Science of The Total Environment 32: 3-20.

Yuan, N.-Y., Lin, Y.-A., Ho, M.-H., Wang, D.-M., Lai, J.-Y. and Hsieh, H.-J. (2009). "Effects of the cooling mode on the structure and strength of porous scaffolds made of chitosan, alginate, and carboxymethyl cellulose by the freeze-gelation method." Carbohydrate Polymers 78(2): 349-356.

Zargar, B. and Hatamie, A. (2012). "Colorimetric determination of resorcinol based on localized surface plasmon resonance of silver nanoparticles." Analyst 137(22): 5334-5338.

Zhang, H. and Cooper, A. I. (2007). "Aligned porous structures by directional freezing." Advanced Materials 19(11): 1529-1533.

Zhang, H. and Oyanedel-Craver, V. (2012). "Evaluation of the disinfectant performance of silver nanoparticles in different water chemistry conditions." Journal of Environmental Engineering 138(1): 58-66.

Zhang, H. and Oyanedel-Craver, V. (2013). "Comparison of the bacterial removal performance of silver nanoparticles and a polymer based quaternary amine functionalized silsesquioxane coated point-of-use ceramic water filters." Journal of Hazardous Materials 260: 272-277.

Zhang, H., Hussain, I., Brust, M., Butler, M. F., Rannard, S. P. and Cooper, A. I. (2005). "Aligned two- and three-dimensional structures by directional freezing of polymers and nanoparticles." Nature Materials 4(10): 787-793.

Zhang, H., Smith, J.A. and Oyanedel-Craver, V. (2012). "The effect of natural water conditions on the anti-bacterial performance and stability of silver nanoparticles capped with different polymers." Water Research 46(3): 691-699.

Zhang, M., Xie, X., Tang, M., Criddle, C. S., Cui, Y. and Wang, S. X. (2013). "Magnetically ultraresponsive nanoscavengers for next-generation water purification systems." Nature Communications 4: 1866.

Zhang, X., Chang, D., Liu, J. and Luo, Y. (2010). "Conducting polymer aerogels from supercritical CO_2 drying PEDOT-PSS hydrogels." Journal of Materials Chemistry 20(24): 5080-5085.

Zhang, X.-Z. and Chu, C.-C. (2003a). "Synthesis of temperature sensitive PNIPAAM cryogels in organic solvent with improved properties." Journal of Materials Chemistry 13(10): 2457-2464.

Zhang, X.-Z. and Chu, C.-C. (2003b). "Thermosensitive PNIPAAM cryogel with superfast and stable oscillatory properties." Chemical Communications (12): 1446-1447.

Zhang, X.-Z. and Zhuo, R.-X. (1999a). "A novel method to prepare a fast responsive, thermosensitive poly(*n*-isopropylacrylamide) hydrogel." Macromolecular Rapid Communications 20(4): 229-231.

Zhang, X.-Z. and Zhuo, R.-X. (1999b). "Preparation of fast responsive, temperature-sensitive poly(*n*-isopropylacrylamide) hydrogel." Macromolecular Chemistry and Physics 200(12): 2602-2605.

Zhang, X.-Z., Yang, Y.-Y. and Chung, T.-S. (2002). "The influence of cold treatment on properties of temperature-sensitive poly(*n*-isopropylacrylamide) hydrogels." Journal of Colloid and Interface Science 246(1): 105-111.

Zhao, Q., Sun, J., Wu, X. and Lin, Y. (2011). "Macroporous double-network cryogels: Formation mechanism, enhanced mechanical strength and temperature/pH dual sensitivity." Soft Matter 7(9): 4284-4293.

Zhu, Z.-Q., Sun, H.-X., Qin, X.-J., Jiang, L., Pei, C.-J., Wang, L., Zeng, Y.-Q., Wen, S.-H., La, P.-Q., Li, A. and Deng, W.-Q. (2012). "Preparation of poly(acrylic acid)-graphite oxide superabsorbent nanocomposites." Journal of Materials Chemistry 22(11): 4811-4817.